



HAL
open science

Dissection électrophysiologique et fonctionnelle des propriétés du réseau des ganglions de la base

Corinne Beurrier

► **To cite this version:**

Corinne Beurrier. Dissection électrophysiologique et fonctionnelle des propriétés du réseau des ganglions de la base. Neurobiologie. Aix Marseille Université, 2018. tel-02348409

HAL Id: tel-02348409

<https://hal.science/tel-02348409>

Submitted on 5 Nov 2019

HAL is a multi-disciplinary open access archive for the deposit and dissemination of scientific research documents, whether they are published or not. The documents may come from teaching and research institutions in France or abroad, or from public or private research centers.

L'archive ouverte pluridisciplinaire **HAL**, est destinée au dépôt et à la diffusion de documents scientifiques de niveau recherche, publiés ou non, émanant des établissements d'enseignement et de recherche français ou étrangers, des laboratoires publics ou privés.

Habilitation à Diriger des Recherches

Corinne Beurrier

Chargée de Recherche au CNRS

Dissection électrophysiologique et fonctionnelle des propriétés
du réseau des ganglions de la base

Soutenue le 14 décembre 2018 devant le jury composé de :

Pr. Valéry Matarazzo	Président
Pr. Stéphane Charpier	Rapporteur
Dr. Catherine Le Moine	Rapportrice
Dr. Paul Apicella	Rapporteur
Dr. Hélène Marie	Examinatrice
Dr. Lydia Kerkerian Le-Goff	Examinatrice

SOMMAIRE

I. Curriculum Vitae

II. Travaux antérieurs

III.1 Les propriétés intrinsèques des neurones du noyau subthalamique et l'effet de la stimulation à haute fréquence

III.2 La plasticité à long terme dans le noyau accumbens est un support neuronal de la sensibilisation à la cocaïne

III.3 L'ablation génétiquement ciblée des neurones striato-nigraux révèle des fonctions très diverses de ces neurones

III.4 Les interneurones cholinergiques du striatum sont des acteurs essentiels dans la pathophysiologie de la maladie de Parkinson

III. Projet de recherche

IV. Références

V. Articles

I. CURRICULUM VITAE

Née le 28 avril 1971 à Libourne (33), France, nationalité française.

Adresse professionnelle:

Institut de Biologie du Développement de Marseille (IBDM),
UMR CNRS 7288 - Aix Marseille Université,
Parc scientifique de Luminy, Case 907, 13288 Marseille cedex 9.
Tél: +33(0)4 91 26 92 50; Fax: +33(0)4 91 26 92 44
e-mail: corinne.beurrier@univ-amu.fr

Situation actuelle:

Chargé de Recherche de 1ère classe CNRS à l'IBDM dirigé par le Dr. A Le Bivic, commission 25 :
"Neurobiologie moléculaire et cellulaire, neurophysiologie".

GRADES UNIVERSITAIRES ET PARCOURS SCIENTIFIQUE

- **1993 : Maîtrise de Psychologie Expérimentale, Université de Bordeaux II.**

Ces quatre années d'étude en psychologie ont été très enrichissantes d'un point de vue personnel. Cependant, ne me projetant pas dans une carrière professionnelle en tant que psychologue, j'ai décidé de changer d'orientation. L'université de Bordeaux offrant l'opportunité aux étudiants en psychologie de s'inscrire dans un cursus neuroscientifique, j'ai saisi cette occasion.

- **1994 : Diplôme d'Etudes Approfondies de Neurosciences et Pharmacologie, Universités de Bordeaux I et II.**

- **1994-1998 : Doctorat Sciences biologiques et médicales, Université de Bordeaux II.**

J'ai effectué ma thèse dans le laboratoire de Neurophysiologie dirigé par le Dr. B. Bioulac, UMR CNRS 5543. Après mon stage de DEA effectué dans le même laboratoire où j'ai travaillé sur l'effet de la stimulation à haute fréquence du noyau subthalamique chez le singe, j'ai décidé, pour une raison qui m'échappe encore, de faire de l'électrophysiologie *in vitro* sur des tranches de cerveau. Le noyau subthalamique est resté mon centre d'intérêt et j'ai décortiqué au cours de ma thèse les propriétés intrinsèques de ces neurones par des enregistrements intracellulaires et en patch-clamp. L'électrophysiologie *in vitro* sur tranches étant une approche nouvelle dans le laboratoire, je dois remercier ici plusieurs personnes sans lesquelles mon parcours scientifique aurait pu s'arrêter là ... Particulièrement : Jean-Marc Israel, chercheur travaillant sur les neurones de l'hypothalamus dans le laboratoire de D. Poulain, qui m'a appris l'électrophysiologie ; Jacques Audin, électronicien dans le laboratoire, qui m'a apporté une aide technique (et amicale) inestimable et enfin Constance Hammond qui a co-encadré ma thèse avec Bernard Bioulac. J'ai soutenu mon travail de thèse en novembre 1998.

- **1999-2002 : Post-doctorat, Stanford University** dans le Nancy Pritzker laboratory dirigé par le Dr. Robert.C. Malenka, Department of Psychiatry and Behavioral Sciences, School of Medicine.

J'ai décidé d'explorer le monde de la synapse que je n'avais pas du tout abordé au cours de ma thèse chez Robert C. Malenka qui venait de s'installer à l'université de Stanford après avoir travaillé de nombreuses années dans le laboratoire de Roger Nicoll. J'ai travaillé principalement sur l'effet de la cocaïne sur la transmission glutamatergique dans le noyau accumbens. Nous avons montré que la dépression à long terme entre les synapses du cortex pré-frontal et les neurones de projection du noyau accumbens pouvait être un des substrats neuronaux de la sensibilisation à la cocaïne.

- **2002-2003 : Post-doctorat, Institut de Neurobiologie de la Méditerranée (INMED)** dirigé par le Dr. Y. Ben-Ari, INMED - INSERM U29, Marseille. Après mon post-doc, j'ai décidé d'intégrer l'équipe de Constance Hammond avec qui j'avais travaillé pendant ma thèse. J'ai ainsi rejoint l'INMED qui venait tout juste de s'installer à Marseille. J'ai développé au cours de ces années une préparation permettant de conserver le réseau des ganglions de la base *in vitro*.
- **2003 : Recrutée au CNRS en tant que chargé de recherche de 2^{ième} classe** par la commission 24 "Interactions cellulaires". Affectée à l'Institut de Neurosciences de la Méditerranée (INMED) dirigé par le Dr. Y. Ben-Ari, INSERM U29, Marseille.
- **2003-2006** : J'ai poursuivi le travail entamé pendant mon post-doc toujours dans l'équipe de Constance Hammond à l'INMED.
- **2006 - présent** : en 2006, Lydia Kerkerian m'a accueillie dans son équipe "Interactions Cellulaires, Neurodégénérescence et Neuroplasticité" installée depuis peu à l'Institut de Biologie du Développement de Marseille (IBDM, UMR CNRS 6216 - Aix Marseille Université) dirigé à l'époque par le Dr. Geneviève Rougon et actuellement par le Dr. André Le Bivic. En 2007, j'ai été promue au grade de chargé de recherche de 1^{ère} classe. La thématique de l'équipe se focalise sur la fonction des ganglions de la base dans un contexte normal et pathologique, particulièrement la maladie de Parkinson. A mon arrivée, j'ai travaillé en étroite collaboration avec Paolo Gubellini sur des projets en cours dans le laboratoire s'attachant à décrire le rôle des transporteurs et des récepteurs métabotropiques du glutamate dans un contexte parkinsonien. Depuis quelques années, je développe ma propre thématique au sein du laboratoire que j'exposerai plus en détail dans ce manuscrit.

ENCADREMENT

- Delphine Révy : Master 2 Biologie des Eucaryotes, Aix-Marseille Université, 2007-2008. Delphine a caractérisé les effets d'un nouvel agoniste orthostérique des récepteurs mGlu4 au niveau de la synapse striato-pallidale. Ce travail s'inscrivait dans une collaboration plus large impliquant J-P Pin, F. Acher et M. Amalric sur le potentiel thérapeutique de nouvelles molécules agissant sur les récepteurs mGlu dans la maladie de Parkinson.
- Delphine Révy : Thèse de doctorat Aix-Marseille Université, Spécialité : Neurosciences, 2008-2012. Delphine a décidé de rester faire sa thèse dans le laboratoire après avoir obtenu une bourse du ministère de l'Enseignement Supérieur et de la Recherche et a été ma première étudiante en thèse. Elle a caractérisé d'un point de vue cellulaire et comportemental un modèle de souris transgénique que j'ai créé en collaboration avec le Dr. Hélène Marie permettant l'ablation spécifique des neurones striato-nigraux.
- Latéfa Yekhlif : Master 2 Neurosciences Aix-Marseille Université, Spécialité : cellulaire et moléculaire, 2011-2012. Latéfa est arrivée au laboratoire au moment où je développais l'optogénétique. Elle a testé les effets de deux types d'opsines, la channelrhodopsine (activation) et l'halorhodopsine (inhibition), sur l'activité électrique de la population que nous voulions cibler : les interneurons cholinergiques du striatum.
- Florence Jaouen : Ingénieur de recherche en CDD de 2011 à 2016. Nous avons recruté Florence grâce à l'ANR que nous avons obtenu en 2011. Florence a énormément contribué à la mise en place de la technique d'optogénétique grâce à ses compétences en biologie moléculaire et cellulaire.
- Marion Deroche : Etudiante en Licence 3 Sciences de la vie, Aix-Marseille Université, 2012-2013. Marion a été co-encadrée par Florence et moi-même et a participé à la caractérisation du modèle optogénétique.

- Dorian Chabbert : Master 2 Neurosciences Aix-Marseille Université, Spécialité : Neurobiologie, Neurophysiologie, Neuropathologie, 2012-2013. Dorian a repris la suite du travail de thèse de Delphine et a approfondi les relations entre les neurones striato-nigraux et les interneurons cholinergiques. Il a obtenu une bourse du ministère de l'Enseignement Supérieur et de la Recherche à l'issue de son master 2 et a poursuivi sa thèse dans le laboratoire sous la direction de P. Gubellini.
- Gwenaëlle Laverne : Master 2 Biologie Santé, Sciences du médicament de l'Université de Poitiers, Spécialité : Recherche et Ingénierie et Bio-santé, 2015-2016. Gwenaëlle effectuait son Master à Poitiers et a voulu faire son stage dans le laboratoire pour se former aux techniques d'électrophysiologie et d'optogénétique. Elle a caractérisé le patron induit par l'activation de la channelrhodopsine sur l'activité électrique des interneurons cholinergiques.
- Gwenaëlle Laverne : Thèse de doctorat Aix-Marseille Université, Spécialité : Neurosciences, 2016 - présent. Bien qu'ayant obtenu une bourse à l'université de Poitiers, Gwenaëlle a décidé de faire sa thèse avec moi sur les effets de la manipulation optogénétique des interneurons cholinergiques sur la plasticité cortico-striée à long terme. Elle est financée par un contrat que j'ai obtenu à la Fondation de France.

BOURSES DE RECHERCHE ET PRIX

- **1994-1997** : Bourse de thèse du ministère de la recherche et de l'éducation nationale, Université de Bordeaux II.
- **1998** : Bourse de thèse de l'Institut Lilly, Université de Bordeaux II.
- **1999-2000** : Bourse de post-doctorat attribuée par la Fondation pour la Recherche Médicale, Université de Stanford, USA.
- **2000** : Prix du jeune post-doctorant attribué par la Société Française des Neurosciences.
- **2000-2002** : CDD de 2 ans comme post-doctorante à l'Université de Stanford, USA.
- **2002** : Bourse candidat INSERM/CNRS attribuée par la Fondation pour la Recherche Médicale, INSERM U29, Marseille.
- **2003** : CDD du CNRS comme post-doctorante, CNRS UMR 5543, Bordeaux.
- **2005** : Financement de la Ville de Marseille pour l'aide à l'installation de chercheurs extérieurs.

TRAVAUX D'EXPERTISE

- Evaluation de demande de financement pour :
 - Fondation de France, comité Parkinson (depuis 2015)
 - Dystonia Foundation
 - Fonds de la Recherche Scientifique, Belgique
 - Fédération pour la Recherche sur le Cerveau.
- Revues scientifiques : Journal of Neurophysiology, Neurobiology of Disease, PlosOne, The Journal of Neuroscience, Cell Reports.
- Jurys de thèse

FINANCEMENTS POUR LA RECHERCHE

Financements demandés et obtenus :

- **2007 : Fondation de France, programme "Physiopathologie de la maladie de Parkinson", PI.**
 - Titre: "Contrôle de l'équilibre GABA/glutamate dans le réseau des ganglions de la base par les voies directe et indirecte en situation normale et pathologique".
 - Partenaire : Dr. H. Marie, European Brain Research Institute, Rome, Italie.
 - Montant : 2 ans, 70 000 €.
- **2007 : Fédération pour la Recherche sur le Cerveau, PI.**
 - Titre : "Characterization of the GABAergic and glutamatergic drives in the basal ganglia network in physiological and pathological conditions".
 - Partenaire : Dr. H. Marie, European Brain Research Institute, Rome, Italie.
 - Montant : 2 ans, 30 000 €.
- **2010 : Association France Parkinson, PI.**
 - Titre: "Plasticity and role of cholinergic-driven striatal microcircuits in basal ganglia pathophysiological functioning".
 - Durée et montant : 2 ans, 25 000 €.
- **2010 : ANR, programme blanc (comité d'évaluation : SVSE 4 Neurosciences), partenaire.**
 - Titre : "Plasticity and role of cholinergic-driven striatal microcircuits in basal ganglia pathophysiological functioning".
 - Acronyme : OptoChAT-Park.
 - Partenaires : Equipe du Dr. Marianne Amalric, Laboratoire de Neurobiologie de la Cognition (UMR6155 CNRS/Aix-Marseille Université), France.
 - Durée et montant : 3 ans, 455 918 €.
- **2016 : Fondation de France (comité d'évaluation : Parkinson), PI.**
 - Titre : "Modulation de la plasticité corticostriatale par les interneurons cholinergiques du striatum en situation normale et parkinsonienne".
 - Durée et montant : 2 ans, 102 600 €.
- **2017 : Association France Parkinson, co-PI.**
 - Titre : "Investigating the expression of miR-124, miR-128 and miR-132 in specific striatal neuronal subsets and their changes in a mouse model of Parkinson disease".
 - Partenaire et co-PI : Dr. Eduardo Gascon, Institut de Neurosciences de la Timone, Marseille.
 - Durée et montant : 2 ans, 35 000 € (20 000 € et 15 000 € après évaluation de l'avancement du projet au bout d'un an).

Financements demandés et non-obtenus :

- **2006 : Association France Parkinson, PI.**
 - Titre: "Contrôle de l'équilibre GABA/glutamate dans le réseau des ganglions de la base par les voies directe et indirecte en situation normale et pathologique".
 - Partenaire : Dr. H. Marie, European Brain Research Institute, Rome, Italie.
 - Montant : 2 ans, 35 000 €.
- **2008 : Appel PEPS CNRS/INSB, Projets exploratoires / Premier soutien, PI.**
 - Titre : "Plasticité du réseau cholinergique dans la maladie de Parkinson : une approche anatomo-fonctionnelle par la méthode d'optogénétique".
 - Acronyme : OptoPark.
 - Montant : 15 000 €.

- **2015-2016 : Projet de Recherche Collaborative soumis à l'ANR (Défi sociétal 4 : Vie, santé et bien-être), partenaire.** Ce projet a été pré-sélectionné et n'a pas été retenu en phase finale.
 - Titre: "Function of the coxsackievirus & adenovirus receptor (CAR) in adult neurogenesis".
 - Acronyme : CAR-LOF.
 - PI : Eric Kremer, Institut de Génétique Moléculaire de Montpellier. Autre partenaire : H Cremer, Institut de Biologie du Développement de Marseille.
 - Durée et montant : 4 ans, 640 920 €.
- **2015-2016 : Projet de Recherche Collaborative soumis à l'ANR (Défi sociétal 4 : Vie, santé et bien-être), PI.** Ce projet a été pré-sélectionné et n'a pas été retenu en phase finale.
 - Titre : "Gating of long-term corticostriatal plasticity by cholinergic interneurons in normal and parkinsonian conditions".
 - Acronyme : CholGATE.
 - Partenaires : Nicolas Mallet, Institute of Neurodegenerative Diseases (UMR5293 CNRS/University of Bordeaux), France.
 - Durée et montant : 3 ans, 650 522 €.
- **2016-2017 : Projet de Recherche Collaborative soumis à l'ANR (Défi sociétal : Vie, santé et bien-être), PI.** Ce projet a été pré-sélectionné et n'a pas été retenu en phase finale.
 - Titre : "Gating of long-term corticostriatal plasticity by cholinergic interneurons in normal and parkinsonian conditions".
 - Acronyme : CholGATE.
 - Partenaires : Nicolas Mallet, Institute of Neurodegenerative Diseases (UMR5293 CNRS/University of Bordeaux), France.
 - Durée et montant : 3 ans, 689 741 €.
- **2016-2017 : A*MIDEX, Initiative d'excellence Aix-Marseille, appel à projets Interdisciplinarité, PI.** En cours d'évaluation.
 - Titre : "Cholinergic interneurons: key players in striatal plasticity and reward-based learning".
 - Acronyme : ChoPPY.
 - Partenaires : Emmanuel Daucé, Institut de Neurosciences des Systèmes (UMR Aix-Marseille University/Inserm 1106), France.
 - Durée et montant : 3 ans, 300 448 €.

PUBLICATIONS

Liste des publications durant ma thèse :

- **Beurrier C**, Bézard E, Bioulac B, Gross C.
Subthalamic stimulation elicits hemiballismus in normal monkey. *NeuroReport*, 1997, 8:1625-1629.
- **Beurrier C**, Congar P, Bioulac B, Hammond C.
Subthalamic nucleus neurons switch from single spike activity to burst firing mode. *Journal of Neuroscience*, 1999, 19:599-609.
- **Beurrier C**, Bioulac B, Hammond C.
The slowly inactivating sodium current (I_{NaP}) underlies single-spike activity in rat subthalamic neurons. *Journal of Neurophysiology*, 2000, 83:1951-1957.
- **Beurrier C**, Bioulac B, Audin J, Hammond C.
High frequency stimulation produces a transient blockade of voltage-gated currents in subthalamic neurons. *Journal of Neurophysiology*, 2001, 85:1351-1356.

Liste des publications durant mes stages post-doctoraux :

- Thomas MJ, **Beurrier C**, Bonci A, Malenka RC.

Long-term depression in the nucleus accumbens: a neural correlate of behavioral sensitization to cocaine. *Nature Neuroscience*, 2001, 4:1217-1223.

- **Beurrier C**, Malenka RC.

Enhanced inhibition of synaptic transmission by dopamine in the nucleus accumbens during behavioral sensitization to cocaine. *Journal of Neuroscience*, 2002, 22:5817-5822.

- **Beurrier C**, Garcia L, Bioulac B, Hammond C.

Subthalamic nucleus: a clock inside basal ganglia? *Thalamus & Related Systems*, 2002, 1:1-8. (Article de revue)

Liste des publications depuis mon recrutement au CNRS :

- **Beurrier C**, Ben-Ari Y, Hammond C.

Preservation of the direct and indirect pathways in an *in vitro* preparation of the mouse basal ganglia. *Neuroscience*, 2006, 140:77-86.

- **Beurrier C**, Bonvento G, Kerkerian-Le Goff L, Gubellini P.

Role of glutamate transporters in corticostriatal synaptic transmission. *Neuroscience*, 2009, 158:1608-1615.

- Cuomo D, Martella G, Barabino E, Platania P, Vita D, Madeo G, Selvam C, Goudet C, Oueslati N, Pin J-P, Acher F, Pisani A, **Beurrier C**, Melon C, Kerkerian-Le Goff L, Gubellini P.

Metabotropic glutamate receptor subtype 4 selectively modulates both glutamate and GABA transmission in the striatum: implications for Parkinson's disease treatment. *Journal of Neurochemistry*, 2009, 109:1096-1105.

- **Beurrier C**, Lopez S, Revy D, Selvam C, Goudet C, Lherondel M, Gubellini P, Kerkerian-LeGoff L, Acher F, Pin J-P, Amalric M.

Electrophysiological and behavioral evidence that modulation of metabotropic glutamate receptor 4 with a new agonist reverses experimental parkinsonism. *The FASEB Journal*, 2009, 23(10):3619-3628.

- **Beurrier C**, Faideau M, Bennouar KE, Escartin C, Kerkerian-Le Goff L, Bonvento G, Gubellini P.

Ciliary neurotrophic factor protects striatal neurons against excitotoxicity by enhancing glial glutamate uptake, *PLoS ONE*, 2010, 5(1): e8550.

- Révy D*, Jaouen F*, Salin P, Melon C, Chabbert D, Tafi E, Concetta L, Langa F, Amalric M, Kerkerian-Le Goff L, Marie H, **Beurrier C**.

Cellular and behavioral outcomes of dorsal striatonigral neuron ablation: new insights into striatal functions, *Neuropsychopharmacology*, 2014, 39(11): 2662-2672.

- Reynders A, Mantilleri A, Malapert P, Rialle S, Nidelet S, Laffray S, **Beurrier C**, Bourinet E, Moqrich A. Transcriptional Profiling of Cutaneous MRGPRD Free Nerve Endings and C-LTMRs, *Cell Rep.*, 2015, 10(6):1007-1019.

- Maurice N, Liberge M, Jaouen F, Ztaou S, Hanini M, Camon J, Deisseroth K, Amalric M, Kerkerian-Le Goff L, **Beurrier C**.

Striatal Cholinergic Interneurons Control Motor Behavior and Basal Ganglia Function in Experimental Parkinsonism, *Cell Rep.*, 2015, 13(4):657-666.

- Martin HG, Bernabeu A, Lassalle O, Bouille C, **Beurrier C**, Pelissier-Alicot AL, Manzoni OJ.

Endocannabinoids Mediate Muscarinic Acetylcholine Receptor-Dependent Long-Term Depression in the Adult Medial Prefrontal Cortex, *Front Cell Neurosci.*, 2015, 1(9):457.

- Wei ZB, Yuan YF, Jaouen F, Ma MS, Hao CJ, Zhang Z, Chen Q, Yuan Z, Yu L, **Beurrier C**, Li W.

SLC35D3 increases autophagic activity in midbrain dopaminergic neurons by enhancing BECN1-ATG14-PIK3C3 complex formation, *Autophagy*, 2016, 12(7):1168-79.

- Tiveron MC, **Beurrier C**, Céni C, Andriambao N, Combes A, Koehl M, Maurice N, Gatti E, Abrous DN, Kerkerian-Le Goff L, Pierre P, Cremer H.

LAMP5 fine-tunes GABAergic synaptic transmission in defined circuits of the mouse brain, *PLoS One*, 2016, 11(6): e0157052.

- Ztaou S, Maurice N, Camon J, Guiraudie-Capraz G, Kerkerian-Le Goff L, **Beurrier C**, Liberge M, Amalric M.

Involvement of Striatal Cholinergic Interneurons and M1 and M4 Muscarinic Receptors in Motor Symptoms of Parkinson's Disease, *The Journal of Neuroscience*, 2016, 36(35):9161-9172.

Chapitres de livre

- Charpier S, **Beurrier C**, Paz J.

The Subthalamic Nucleus: From *In Vitro* to *In Vivo* Mechanisms, in **Handbook of basal ganglia structure and function**, 2010, ed. H. Steiner and K. Tseng, 259-273, Elsevier.

COMMUNICATIONS ORALES (SEMINAIRES - CONGRES)

- 2012 : Laboratoire de Neurosciences Cognitives, Marseille, France. *Optogenetics: principles and applications*.
- 2014 : European winter conference on brain research, Brides-les-bains, France. *Striatal cholinergic interneurons control motor function and basal ganglia outflow in the parkinsonian condition*.
- 2015 : 9th Japanese-French Frontiers of Science (JFFoS) Symposium, Kyoto, Japan. *Understanding the role of specific neuronal populations with light: the optogenetics contribution to neuroscience*.
- 2017 : 2nd Basal Ganglia and Parkinson's disease Day organized by Centre of excellence on Neurodegenerative diseases (DHUNE), Marseille. *Striatal cholinergic interneurons control motor behavior and basal ganglia function in experimental parkinsonism*.
- 2017 : NeuroFrance 2017, Annual meeting of the French Neuroscience Society, Bordeaux, France. *Striatal cholinergic interneurons control motor behavior and basal ganglia function in experimental parkinsonism*
- 2017 : Co-organization of the symposium "Cholinergic signal dynamics in physiopathological conditions" for the annual meeting of the French Neuroscience Society, Bordeaux, France.

II. TRAVAUX ANTERIEURS

Etant donné ma décision tardive à soutenir mon HDR, je ne vais pas développer dans ce manuscrit l'ensemble des travaux que j'ai menés au cours de ma carrière scientifique. Cela serait un exercice pénible, tant pour la rédactrice que pour les lecteurs ! J'ai donc décidé de développer 4 parties qui, je pense, illustrent particulièrement mes intérêts scientifiques. Ces travaux ont été réalisés à différentes étapes de mon parcours : durant ma thèse (II.1), mon post-doc (II.2) et depuis mon intégration dans l'équipe du Dr. Lydia Kerkerian (II.3 et 4), qui m'a laissée la liberté de développer des thématiques qui me tiennent particulièrement à cœur. Les articles se référant aux travaux que j'ai choisi d'exposer sont insérés à la fin du manuscrit et s'accompagnent, pour chaque article, d'un résumé.

Mon travail s'est toujours focalisé sur le réseau des ganglions de la base en condition normale ou en condition de dysfonctionnement dopaminergique (hypo-dopaminergie : maladie de Parkinson ou hyper-dopaminergie : addiction à la cocaïne). J'ai disséqué les propriétés intrinsèques ou synaptiques dans plusieurs structures du réseau en utilisant une approche d'électrophysiologie *in vitro* sur tranches de cerveau. Le fil conducteur est de comprendre le normal pour mieux comprendre la pathologie et de relier, dans la mesure du possible, fonctions cellulaires et comportements. Des outils tels que les souris transgéniques, l'optogénétique et la chémogénétique, issus des avancées de la biologie moléculaire et de la génétique, ont rendu possible pour les neurosciences l'élucidation du rôle fonctionnel de circuits neuronaux spécifiques. Ainsi, pour pouvoir utiliser ces outils j'ai décidé quand je suis arrivée dans l'équipe de L. Kerkerian d'introduire la souris comme modèle. J'ai pu bénéficier de la nouvelle animalerie de l'IBDM et je remercie à cet égard Aziz Moqrich qui s'est investi dans la construction et la gestion du personnel de l'animalerie, indispensables pour gérer les différentes lignées transgéniques nécessaires à mes projets. Avant de rentrer dans le vif du sujet, voici un bref rappel sur l'organisation anatomo-fonctionnelle du réseau des ganglions de la base.

Les ganglions de la base sont constitués d'un ensemble de structures sous-corticales impliquées dans le contrôle de la motricité extrapyramidale ainsi que dans la régulation de processus cognitifs et limbiques. Le principe de fonctionnement du réseau, décrit il y a plus de vingt ans, repose sur un équilibre fonctionnel entre des influences inhibitrices et excitatrices (Albin et al., 1989; DeLong, 1990). Selon ce modèle, le striatum, considéré comme la structure d'entrée du réseau recevant des informations de l'ensemble des aires corticales, contrôle les structures de sortie [la substance noire pars reticulata (SNr) et le globus pallidus interne (GPi)] via deux voies : une voie directe inhibitrice monosynaptique et une voie indirecte excitatrice polysynaptique qui contacte d'abord le globus pallidus externe (GPe) puis le noyau subthalamique (NST) avant d'atteindre les structures de sortie (fig. 1). Les neurones de projection du striatum (95% de la population striatale, aussi appelés Medium Spiny Neurons, MSNs) exprimant le récepteur dopaminergique D2 sont à l'origine de la voie indirecte (MSNs D2) alors que les MSNs exprimant le récepteur dopaminergique D1 (MSNs D1) constituent la voie directe. Dans la maladie de Parkinson, l'absence de dopamine due à la dégénérescence des neurones de la substance noire pars compacta (SNc), entraîne une perturbation de l'activité de l'ensemble du réseau et notamment un déséquilibre entre les voies directe et indirecte en faveur de l'excitation. On constate une hyperactivité des MSNs D2 à l'origine de la voie indirecte et une hypoactivité des MSNs D1 à l'origine de la voie directe. Un des grands défis dans le domaine des mouvements anormaux est de comprendre les mécanismes à l'origine de ce déséquilibre. Il faut cependant souligner que des données récentes suggèrent que les voies directe et indirecte fonctionneraient plus en synergie qu'en opposition pour contrôler les différentes fonctions associées aux ganglions de la base. Il n'est pas

impossible que les deux modes de fonctionnement, opposition et synergie, cohabitent selon la tâche engagée (Calabresi et al., 2014; Cui et al., 2013).

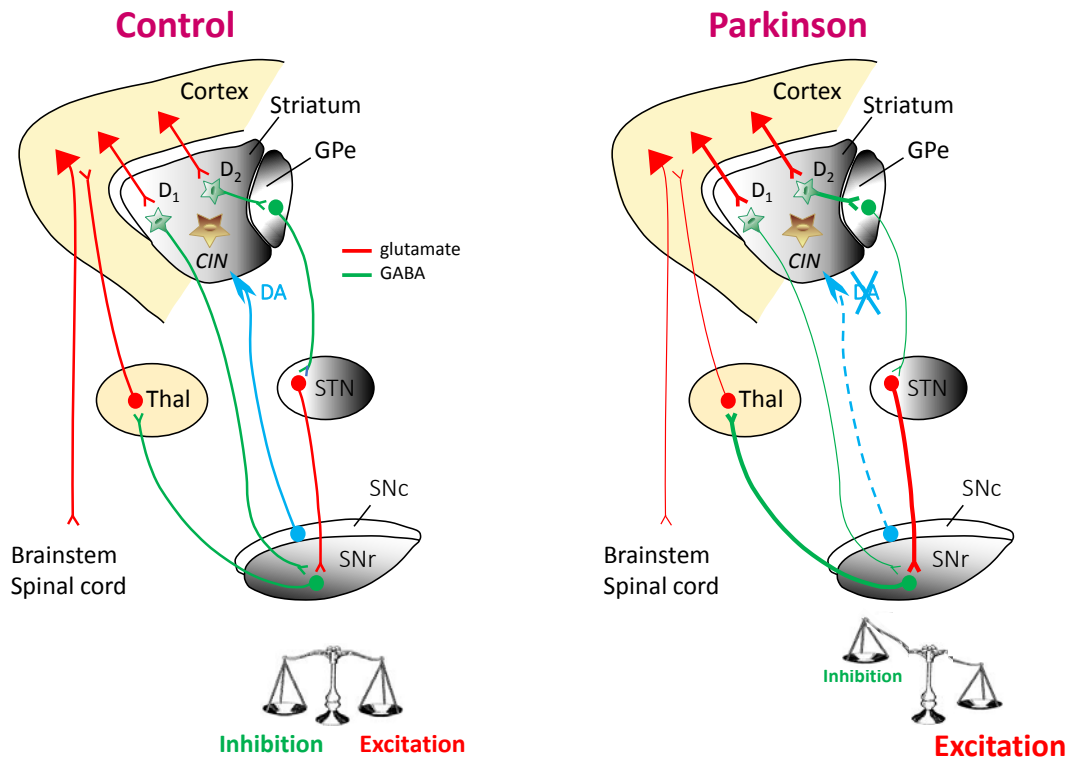


Figure 1. Schéma simplifié du réseau des ganglions de la base. Les flèches représentent les connexions synaptiques entre les différentes structures.

GPe: globus pallidus externe; STN: noyau subthalamique; SNc/SNr: substance noire pars compacta/reticulata; Thal: thalamus, DA: dopamine; CIN: interneurons cholinergiques. D₁ et D₂: récepteurs dopaminergiques de type 1 et 2.

II.1 LES PROPRIETES INTRINSEQUES DES NEURONES DU NOYAU SUBTHALAMIQUE ET L'EFFET DE LA STIMULATION A HAUTE FREQUENCE

Le noyau subthalamique (NST) occupe une position particulière au sein des ganglions de la base. Ce noyau est la seule structure glutamatergique et joue un rôle fondamental dans le maintien d'une activité tonique excitatrice au niveau des structures de sortie du réseau, la SNr et le GPi (Robledo and Féger, 1990). Les projections du NST sont loin d'être limitées au GPi et à la SNr et il reçoit également de nombreuses afférences des autres structures du réseau, ainsi que du cortex, du thalamus et de la SNc. Ces entrées et sorties multiples placent le STN comme une véritable «structure clef» intervenant en différents points du réseau pour réguler le flot d'informations qui y circule (Parent and Hazrati, 1995).

Le modèle physiopathologique de la maladie de Parkinson met en avant l'hyperactivité des neurones du NST qui retentit de façon drastique sur les structures de sortie (figure 9A). Chez le rat présentant une déplétion du système monoaminergique ou une lésion du système dopaminergique nigro-strié par la 6-hydroxydopamine (6-OHDA), les neurones du NST augmentent leur fréquence de décharge, mais ils ont surtout tendance à décharger en bouffées de potentiels d'action (Hassani et al., 1996; Hollerman

and Grace, 1992; Kreiss et al., 1997; Robledo and Féger, 1990) de façon synchrone (Ryan et al., 1992). Cette activité en bouffées a également été rapportée chez le singe traité au 1-méthyl-4-phényl-1,2,3,6-tétrahydropyridine (MPTP) (Bergman et al., 1994) et chez les malades parkinsoniens (Benazzouz et al., 2002; Rodriguez-Oroz et al., 2001). Ce patron de décharge en bouffées des neurones du STN est donc une caractéristique des états parkinsoniens. Ces modifications qualitatives de l'activité électrique des neurones jouent sans doute un rôle essentiel dans la genèse des symptômes. La mise en évidence, dans les années 90, d'une amélioration des symptômes parkinsoniens suite à la lésion ou à la stimulation à haute fréquence de ce noyau conforte définitivement cette idée. La stimulation à haute fréquence du NST reste actuellement une option thérapeutique pour les malades parkinsoniens. Si les effets cliniques de la stimulation à haute fréquence sont incontestables, son mode d'action au niveau neuronal était (et est encore en partie) totalement inconnu au moment où je commençais ma thèse. Ceci nous a amené à développer un modèle adapté permettant d'aborder les mécanismes cellulaires de la stimulation à haute fréquence : l'électrophysiologie sur tranches de cerveau de rat. Il était en effet indispensable, dès lors qu'on applique cette technique en pathologie humaine, de préciser comment elle pouvait interagir sur l'activité même des neurones du NST. Mais là encore, il survenait une autre question fondamentale : les caractéristiques électrophysiologiques des neurones du NST étaient en effet fort mal connues. Les mécanismes ioniques sous-tendant l'activité électrique de ces neurones n'avaient jamais été abordés de manière approfondie. Il semblait pourtant essentiel de bien comprendre ces propriétés vu l'importance des neurones du STN dans la régulation de la motricité normale et dans un contexte parkinsonien. J'ai donc réalisé au cours de ma thèse (i) une étude approfondie des propriétés intrinsèques des neurones du NST et, (ii) une analyse des effets de la stimulation à haute fréquence sur ces propriétés intrinsèques. L'ensemble de ce travail peut être résumé en trois points principaux.

II.1.1 Les neurones du STN présentent deux modes de décharge : une activité tonique et en bouffées

Tous les neurones du NST que nous avons enregistré présentent une activité tonique (potentiels d'action émis à intervalle régulier). Parmi eux, 48% ont aussi la capacité de générer des bouffées de potentiels d'action rythmiques en réponse à une hyperpolarisation de la membrane (activité en bouffées). Les neurones qui présentent les deux patrons de décharge passent de l'un à l'autre selon la valeur de leur potentiel membranaire : une légère hyperpolarisation déclenche une décharge en bouffées alors qu'une dépolarisation favorise plutôt l'activité tonique. Le neurone illustré dans la figure 2 présente d'abord une activité tonique lorsque aucun courant n'est injecté puis une activité en bouffées lorsque la membrane est hyperpolarisée. L'augmentation de l'intensité du courant négatif supprime tout type d'activité. L'application d'un agoniste des récepteurs glutamatergiques métabotropiques du groupe I et II, l'ACPD, favorise l'activité en bouffées.

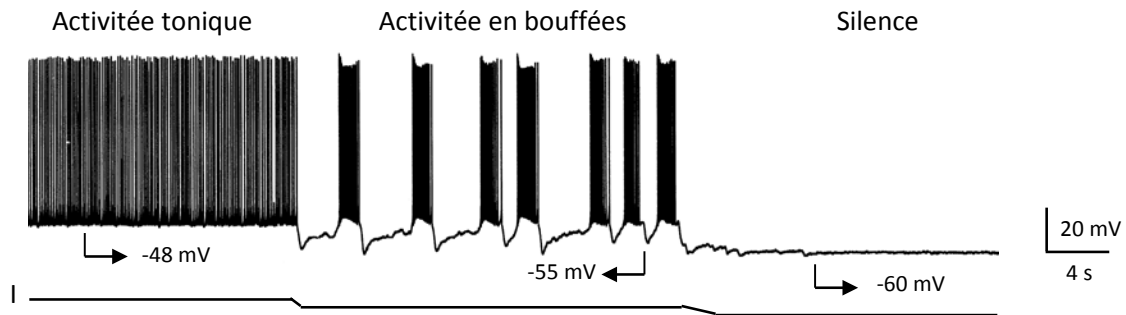


Figure 2. Changement d'activité en fonction du potentiel membranaire.

Les neurones du NST peuvent passer d'une activité tonique à une activité en bouffées sous l'effet d'une légère hyperpolarisation membranaire par injection d'un courant négatif continu. Les potentiels d'action constituant l'activité tonique sont tronqués.

II.1.2 L'activité tonique et en bouffées résulte d'une cascade de courants sensibles au voltage

Les résultats de nos expériences pharmacologiques et les caractéristiques de sensibilité au voltage de l'activité en bouffées nous ont permis d'établir que l'activité en bouffées est une propriété membranaire intrinsèque due à l'activation d'une cascade de courants sensibles au voltage. Nous pouvons distinguer plusieurs étapes dans cette activité, chacune étant caractérisée par la présence de courants sous-liminaires particuliers. Les oscillations du potentiel de membrane sous-jacentes aux bouffées de potentiels d'action peuvent être décomposées en trois phases (fig. 3) : dépolarisation (b-c), plateau (c-d) et repolarisation (d-a) qui dépendent toutes des ions Ca^{2+} . Ces oscillations sont séparées par des dépolarisations lentes de la membrane (dépolarisations inter-bouffées a-b). La phase de dépolarisation (b-c) résulte de l'activation d'un courant Ca^{2+} de type T (I_T) qui dépolarise la membrane jusqu'au seuil d'activation d'un courant Ca^{2+} de type L (I_L). Ce courant serait, avec le courant cationique non spécifique (I_{CAN}), responsable de la phase plateau des oscillations sur lesquelles se greffent les potentiels d'action sodiques (c-d). L'augmentation de la concentration intracellulaire en ions Ca^{2+} qui en résulte active des courants K^+ dépendants des ions Ca^{2+} ($I_{K,Ca}$) responsables de la phase de repolarisation des bouffées (d-a). Cette hyperpolarisation permet la dé-inactivation de I_T et, peut-être, l'activation d'un courant cationique activé par l'hyperpolarisation (I_h). La membrane se dépolarise ensuite spontanément jusqu'au seuil d'activation de I_T sous l'effet d'une inactivation des $I_{K,Ca}$ due à des mécanismes de clairance des ions Ca^{2+} libres intracellulaires (a-b) et un nouveau cycle est initié. L'activité en bouffées des neurones du NST résulte donc d'un équilibre entre des influences dépolarisantes (I_T , I_L , I_{CAN}) et hyperpolarisante ($I_{K,Ca}$), équilibre est atteint dans une fourchette étroite de potentiel de membrane.

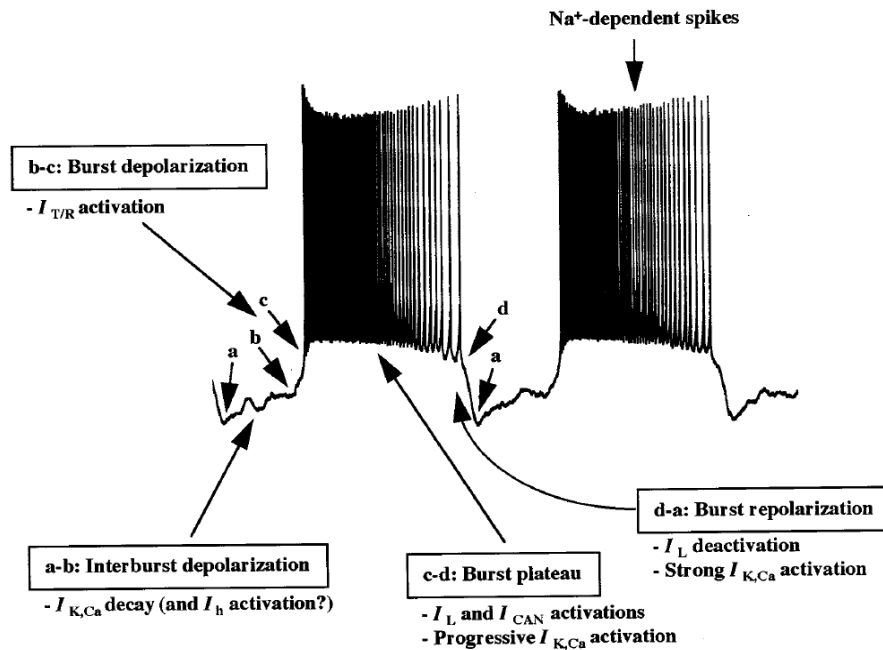


Figure 3. Hypothèse sur la cascade hypothétique des courants ioniques intervenant dans les différentes phases de l'activité en bouffées.

En ce qui concerne l'activité tonique, nos résultats ont montré qu'il s'agit d'une activité intrinsèque indépendante des entrées synaptiques. Contrairement à l'activité en bouffées, elle ne repose pas sur des courants Ca^{2+} ou Ca^{2+} -dépendants mais dépend essentiellement d'un courant Na^+ persistant (I_{Nap}). Dans certains neurones, I_h peut également participer à l'activité tonique en exerçant une influence dépolarisante qui amène le potentiel membranaire vers des valeurs proches du seuil d'activation de I_{Nap} , favorisant ainsi l'activité tonique.

II.1.3 La stimulation à haute fréquence du STN entraîne un blocage transitoire de conductances voltage-dépendantes essentielles à l'activité spontanée de ces neurones

Nous avons ensuite analysé les effets de la stimulation à haute fréquence du STN sur les propriétés intrinsèques de ces neurones que nous avons mises en évidence. Nous avons particulièrement prêté attention aux paramètres de stimulation appliqués afin de mimer au plus près la situation clinique. Cette étude a constitué à l'époque la première tentative pour expliquer les effets cellulaires de la stimulation à haute fréquence. En raison des artéfacts électriques générés par la stimulation, nous n'avons pas été en mesure d'étudier les phénomènes à l'œuvre pendant la stimulation mais nous avons montré qu'une stimulation appliquée au niveau du STN pendant 1 minute entraîne, juste après l'arrêt de la stimulation, un blocage transitoire de l'activité spontanée de ces neurones, qu'ils déchargent de façon tonique ou en bouffées (durée et intensité des stimuli : 100 μs , 5-8V) (fig. 4).

Cet effet suppressif est dépendant de la fréquence de la stimulation. Parmi les fréquences que nous avons testées, nous avons observé que l'activité n'était pratiquement pas modifiée à 100 Hz, fortement diminuée à 125 Hz et totalement supprimée à des fréquences \geq à 160 Hz. Une série d'expérience de pharmacologie et de voltage imposé nous a permis de déterminer que la stimulation à haute fréquence entraînait un blocage réversible de certaines conductances voltage-dépendantes impliquées dans la genèse de l'activité tonique et en bouffées (notamment les courants sodiques persistants et Ca^{2+} de type L et T).

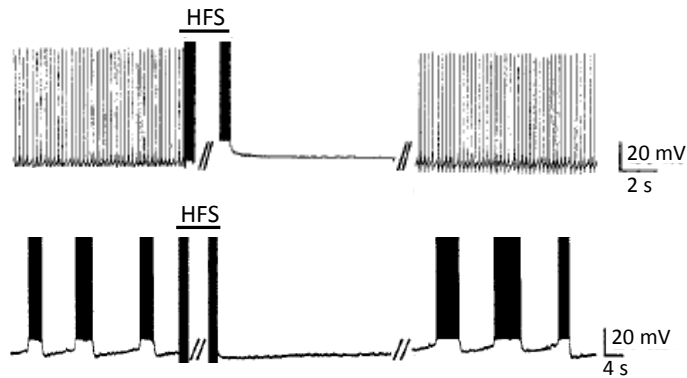


Figure 4. La stimulation à haute fréquence du STN bloque transitoirement l'activité tonique et en bouffées de ces neurones. HFS : high frequency stimulation (250 Hz en haut et 500 Hz en bas).

Les résultats obtenus au cours de ma thèse ont comblé un manque significatif quant aux données relatives aux propriétés intrinsèques des neurones du STN et au mécanisme d'action de la stimulation à haute fréquence, approche largement utilisée pour traiter un certain nombre de patients parkinsoniens. C'est en effet la première fois que la capacité de ces neurones à décharger selon deux modes est mise en évidence et qu'une analyse extensive des mécanismes ioniques qui sous-tendent leur patron de décharge est faite. En outre, au-delà de son intérêt fondamental, ce travail a mis en évidence les cibles pharmacologiques à viser qui permettraient de diminuer l'activité en bouffées des neurones du STN dans les états parkinsoniens et révélé un mécanisme possible de la stimulation à haute fréquence.

Articles

- **Beurrier C**, Congar P, Bioulac B and Hammond C (1999). Subthalamic nucleus neurons switch from single-spike activity to burst-firing mode. *Journal of Neuroscience*, 19(2): 599-609.
- **Beurrier C**, Bioulac B, Hammond C. The slowly inactivating sodium current (I_{NaP}) underlies single-spike activity in rat subthalamic neurons (2000). *Journal of Neurophysiology*, 83(4): 1951-1957.
- **Beurrier C**, Bioulac B, Audin J and Hammond C (2001). High-frequency stimulation produces a transient blockade of voltage-gated currents in subthalamic neurons. *Journal of Neurophysiology*, 85(4): 1351-6.

II.2 LA PLASTICITE A LONG TERME DANS LE NOYAU ACCUMBENS EST UN SUPPORT NEURONAL DE LA SENSIBILISATION A LA COCAÏNE

A la fin de ma thèse, j'ai décidé de partir aux Etats-Unis et j'ai choisi d'explorer le monde de la synapse que je n'avais pas abordé au cours de ma thèse en faisant mon stage post-doctoral chez Robert C. Malenka, expert dans le domaine de la transmission et de la plasticité synaptique. Ce choix m'a permis de rester dans le domaine des ganglions de la base en abordant le fonctionnement de ce réseau en condition d'hyperdopaminergie (addiction). Je me suis notamment intéressée au dysfonctionnement des synapses entre le cortex et le noyau accumbens (NAc) suite à un traitement chronique à la cocaïne. L'administration répétée de psychostimulants tels la cocaïne entraîne une sensibilisation comportementale qui peut se définir comme une augmentation progressive des effets d'une drogue lors de son usage répété, cette augmentation pouvant se maintenir après de longues périodes d'abstinence. Le modèle de sensibilisation comportementale à long terme est censé refléter l'envie incontrôlable ("craving") de prise de drogue et les nombreuses rechutes ("relapse") que l'on observe chez l'humain, même après de nombreuses années d'abstinence (Robinson and Berridge, 1993). L'identification des substrats neurobiologiques impliqués dans ces comportements a été un des buts principaux de la recherche fondamentale dans le domaine de la toxicomanie. En d'autres termes, quelles sont les modifications physiologiques entraînées par la prise chronique de drogue qui sont à l'origine de la sensibilisation ? Chez l'animal, l'hyperactivité locomotrice induite par les psychostimulants subit une sensibilisation importante et constitue un modèle expérimental couramment utilisé en laboratoire (Kalivas and Stewart, 1991). Ce phénomène se manifeste par une augmentation progressive de l'activité locomotrice suite à l'injection répétée de la même dose de drogue. Un aspect particulièrement intéressant est que cette sensibilisation peut persister même après une longue période d'abstinence. Chez les rongeurs, l'augmentation de l'activité locomotrice suite à une « injection challenge » de psychostimulants peut se manifester plusieurs mois après l'arrêt du traitement chronique. Dans le protocole que j'ai utilisé au cours de mon post-doctorat dans le laboratoire du Dr. Robert C. Malenka (fig. 5), l'activité locomotrice des souris est mesurée pendant 5 jours juste après une injection quotidienne de cocaïne (15 mg/kg). Après une interruption de 10 à 14 jours, les animaux reçoivent une dernière injection de cocaïne à la même dose (test). Ce protocole produit bien une sensibilisation des réponses locomotrices : l'activité locomotrice augmente progressivement suite à l'injection quotidienne de la même dose de cocaïne (jours 3 à 7) et cette augmentation persiste dans le temps puisque la réponse locomotrice est toujours augmentée après l'interruption du traitement (injection test).

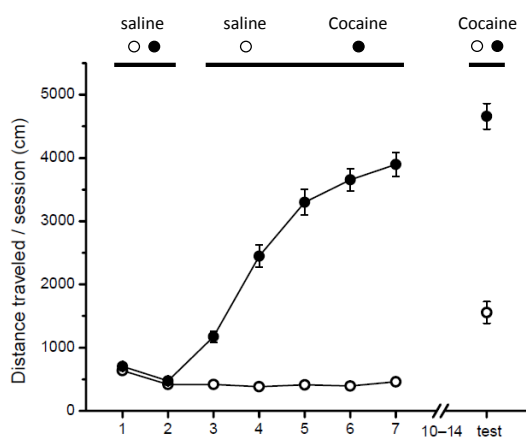


Figure 5. Sensibilisation comportementale induite par une administration répétée de cocaïne. L'activité locomotrice est mesurée pendant 15 min immédiatement après les injections de solution saline ou de cocaïne (15 mg/kg).

Les adaptations neuronales qui ont lieu après administration de cocaïne impliquent des structures appartenant au système mésolimbique, dont l'aire tegmentale ventrale, le cortex pré-frontal et le noyau accumbens (NAc) (Robinson and Berridge, 1993). A l'époque où j'ai rejoint le laboratoire de Robert C. Malenka, les données de la littérature suggéraient que les psychostimulants, au-delà de leurs effets directs sur la transmission dopaminergique, pouvaient également modifier la transmission synaptique glutamatergique dans le NAc ainsi que la modulation de cette transmission par la dopamine (Vanderschuren and Kalivas, 2000; Wolf, 1998). Pour tester ces hypothèses, nous avons enregistré les courants synaptiques glutamatergiques dans les MSNs du NAc sur des tranches de cerveau issues d'animaux préalablement traités à la cocaïne selon le protocole décrit ci-dessus (fig.5). Les tranches sont réalisées après la dernière injection de cocaïne ou saline (test). Trois questions ont guidé notre travail :

- Les propriétés basiques de la transmission glutamatergique des synapses cortex préfrontal/NAc sont-elles modifiées par un traitement chronique aux psychostimulants ?
- La plasticité de la transmission glutamatergique entre cortex préfrontal et NAc est-elle modifiée par un traitement chronique aux psychostimulants ?
- La modulation de la transmission glutamatergique par la dopamine est-elle modifiée par un traitement chronique aux psychostimulants ?

II.2.1 Un traitement chronique à la cocaïne diminue l'amplitude des courants synaptiques de type AMPA

La libération de glutamate ne semble pas être affectée par le traitement à la cocaïne puisque la "paired-pulse facilitation" (PPF) ainsi que la fréquence des courants post-synaptiques excitateurs miniatures (mEPSC) AMPA ne diffèrent pas dans le groupe « saline » et « cocaïne ». En revanche, un changement dans le nombre et/ou les propriétés des récepteurs glutamatergiques de la membrane postsynaptique peut avoir lieu. Pour vérifier cette hypothèse, nous avons calculé, pour chaque cellule, le rapport entre l'amplitude maximale des réponses AMPA et NMDA (AMPA/NMDA) afin d'évaluer la participation relative de ces deux courants dans la réponse synaptique globale. Nous enregistrons les EPSCs à +40 mV en absence puis en présence de D-APV (50 μ M), un bloquant des récepteurs NMDA. La réponse moyenne obtenue en présence de D-APV (EPSC AMPA) est ensuite soustraite à celle obtenue en son absence, permettant d'obtenir un EPSC NMDA moyen (fig. 6A). Nous avons observé une diminution du ratio chez les animaux « cocaïne » suggérant que le traitement à la cocaïne peut diminuer les courants AMPA et/ou augmenter les courants NMDA (fig. 6A).

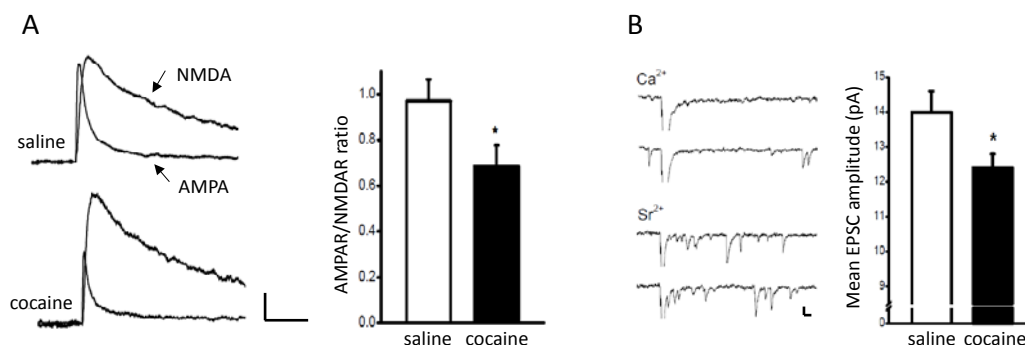


Figure 6. Diminution du ratio AMPA/NMDA (A) et de l'amplitude des mEPSCs enregistrés en présence de strontium (2.5 mM) des synapses corticales sur les neurones du NAc (B) après administration chronique de cocaïne. Echelles : A, 40 ms et 20 pA - B, 50 ms et 10 pA.

Pour déterminer la nature du changement des réponses NMDA et AMPA chez les animaux traités à la cocaïne, nous avons entrepris une série d'expériences dont les principaux résultats sont résumés ci-après. L'amplitude des mEPSCs AMPA et NMDA ne diffère pas chez les animaux « saline » et « cocaïne ». Cependant, si l'on considère que le traitement à la cocaïne ne modifie qu'un nombre limité de synapses, il est vraisemblable qu'il ne soit pas possible de détecter ces modifications avec la technique ci-dessus, les mEPSCs que nous enregistrons étant générés par l'ensemble des synapses glutamatergiques contactant le neurone postsynaptique. Grâce à l'utilisation du strontium (Sr^{2+}) qui a la propriété d'entrer dans les terminaisons stimulées à travers les canaux Ca^{2+} sensibles au voltage et de provoquer la libération asynchrone des vésicules (Goda and Stevens, 1994), nous avons pu spécifiquement étudier les mEPSCs issus de la stimulation des fibres pré- limbiques corticales qui projettent vers le NAc. Nous avons dans ce cas observé une diminution significative de l'amplitude moyenne des mEPSCs chez les animaux « cocaïne », suggérant que la diminution du rapport des courants AMPA/NMDA observée dans le groupe cocaïne est due à une diminution des réponses AMPA (fig. 6B). Nous n'avons en revanche pas mis en évidence de modification des réponses NMDA.

II.2.2 Un traitement chronique à la cocaïne entraîne une dépression à long terme de la transmission synaptique glutamatergique

Les données obtenues montrent que le traitement à la cocaïne entraîne une diminution des réponses AMPA due à une modification des récepteurs au niveau de la membrane postsynaptique. Cependant, les expériences ci-dessus ne nous permettaient pas de préciser les mécanismes à l'origine de cette diminution. Une des hypothèses serait que la cocaïne agit par un mécanisme similaire à celui de la dépression à long terme (LTD) de la transmission glutamatergique observée dans le NAc d'animaux contrôles (Thomas et al., 2000). Si tel est le cas, nous ne devrions plus être en mesure de déclencher une LTD des réponses glutamate de type AMPA dans le groupe cocaïne (phénomène d'occlusion). Nous avons en effet observé que l'amplitude de la LTD est significativement plus faible chez les souris « cocaïne » (fig. 7).

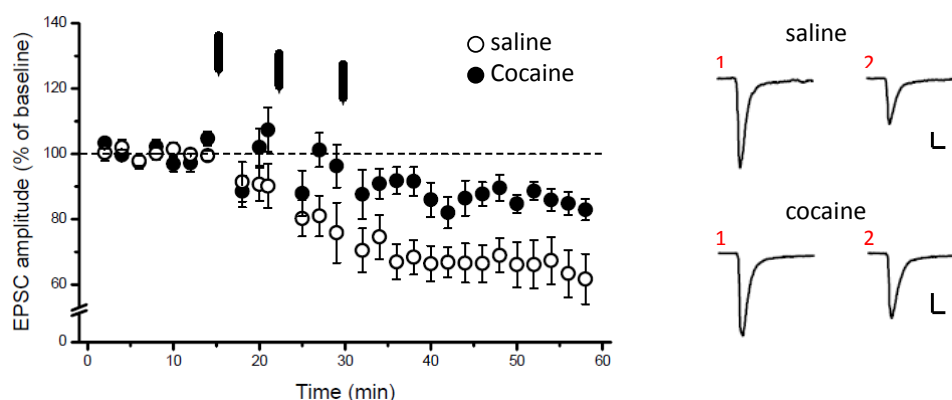


Figure 7. Le traitement chronique à la cocaïne diminue l'amplitude de la LTD dans le NAc. Le graphe montre la LTD moyenne obtenue chez les animaux saline et cocaïne. Le protocole d'induction de la LTD consiste en 1 train de stimulation synaptique à 5 Hz pendant 3 min répété 3 fois (flèches) couplé à une dépolarisation de la cellule à

-50 mV. Les traces montrent les EPSCs moyennés de deux cellules pendant la ligne de base (1) et 20 min après le dernier train de stimulation (2). Echelles : 20 ms et 50 pA.

II.2.3 La sensibilisation à la cocaïne augmente le contrôle inhibiteur de la dopamine sur la transmission synaptique glutamatergique

En situation contrôle, la dopamine inhibe de manière réversible la transmission glutamatergique dans le NAc en activant les récepteurs présynaptiques de type D1 (Harvey and Lacey, 1996; Nicola et al., 1996). Nous nous sommes demandé si cet effet inhibiteur était retrouvé chez les animaux « cocaïne » sachant que l'administration chronique de cocaïne entraîne une adaptation du système dopaminergique mésolimbique, dont une augmentation de la libération de dopamine dans le NAc. Pour répondre à cette question, nous avons testé l'effet de la dopamine sur les EPSCs AMPA enregistrés en configuration cellule entière sur des tranches de NAc provenant d'animaux « saline » et « cocaïne ». L'application de dopamine (20 μ M) pendant 10 min inhibe de façon significative les EPSCs dans le groupe cocaïne alors qu'elle n'a pratiquement aucun effet dans le groupe saline (fig. 8A). Dans le groupe cocaïne, l'inhibition entraînée par la dopamine (20 μ M) est fortement réduite par un antagoniste des récepteurs D1 (10 μ M SCH-23390) (fig. 8B). Le traitement à la cocaïne entraîne donc une augmentation de la modulation inhibitrice de la dopamine sur la transmission glutamatergique dans le NAc via l'activation de récepteurs D1. Le transporteur de la dopamine ne semble pas être impliqué dans cet effet puisque l'inhibition des EPSCs par la dopamine n'est pas modifiée en présence d'un inhibiteur spécifique du transporteur de la dopamine.

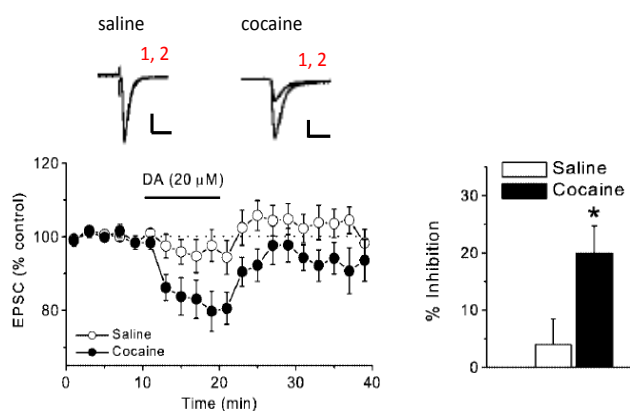


Figure 8. L'administration répétée de cocaïne augmente les effets inhibiteurs de la dopamine sur les courants AMPA. Le graphe à gauche illustre les effets de la dopamine (20 μ M) sur les souris contrôle ($n=9$ cellules, 7 souris) et cocaïne ($n=10$ cellules, $n=5$ souris). Les traces montrent les EPSCs moyennés de deux cellules à 10 (1) et 20 min (2). À droite, le graphe montre l'amplitude de l'inhibition des EPSCs AMPA après application de dopamine (20 μ M) ($*p<0.05$). Echelles : saline, 50 ms et 100 pA - cocaïne, 50 ms et 200 pA.

Si l'effet inhibiteur présynaptique de la dopamine sur la libération de glutamate a été largement décrit, certains auteurs ont aussi rapporté une potentialisation des courants NMDA via l'activation de récepteurs D1 postsynaptiques (Harvey and Lacey, 1997). Ce dernier point est cependant controversé puisque d'autres laboratoires, dont celui de Robert C. Malenka, n'ont jamais été en mesure de reproduire ce résultat (Nicola and Malenka, 1998). Le traitement à la cocaïne peut néanmoins révéler un effet de la dopamine qui n'est pas détectable dans des conditions contrôles. Il est difficile de tester une potentialisation des courants NMDA par la dopamine en raison de l'effet présynaptique inhibiteur de la dopamine sur la libération de glutamate comme nous l'avons montré ci-dessus. Un moyen de contourner ce problème est de tester l'effet de la dopamine simultanément sur les courants AMPA et NMDA. Si la dopamine potentialise les courants NMDA en plus de l'inhibition présynaptique de la libération de glutamate, les courants NMDA devraient être moins inhibés que les courants AMPA. Pour réaliser cette expérience, nous avons testé l'effet de la dopamine sur les EPSCs enregistrés à +40 mV.

L'application de dopamine (75 μ M) entraîne une inhibition comparable des EPSCs AMPA et NMDA dans le groupe saline. Le traitement à la cocaïne ne permet pas de révéler une potentialisation des courants NMDA puisque, dans ce groupe aussi, l'application de dopamine (75 μ M) entraîne une inhibition comparable des courants AMPA et NMDA. Pour s'assurer que la dialyse du milieu intracellulaire ne nous a pas empêchés de détecter un effet postsynaptique de la dopamine, nous avons répété la même expérience sur des souris contrôles en utilisant la technique du patch perforé. Cependant, une fois encore, l'amplitude de l'inhibition entraînée par la dopamine (100 μ M) est similaire pour les courants AMPA et NMDA (données non montrées).

L'ensemble du travail que j'ai réalisé en post-doctorat chez Robert C. Malenka a mis en évidence qu'un traitement chronique à la cocaïne modifie de façon durable la transmission glutamatergique au niveau des synapses cortico-accumbens. Une diminution des réponses de type AMPA chez les animaux « cocaïne » par un mécanisme s'apparentant à celui de la LTD semble être à l'origine de ce phénomène. Si la libération de glutamate ne semble pas être modifiée chez les animaux « cocaïne », sa modulation par la dopamine l'est. Nous avons en effet montré une inhibition accrue des EPSCs glutamate de type AMPA par la dopamine chez les animaux « cocaïne » mettant en jeu l'activation des récepteurs D1. L'ensemble de ces modifications pourrait donc entraîner une diminution considérable de l'efficacité de la transmission synaptique glutamatergique cortico-accumbens. Ces mécanismes pourraient contribuer à la diminution d'excitabilité des neurones de projection du NAc observée après traitement aux psychostimulants.

Articles

- Thomas MJ, **Beurrier C**, Bonci A and Malenka RC (2001). Long-term depression in the nucleus accumbens: a neural correlate of behavioral sensitization to cocaine. *Nature Neuroscience*, 4(12): 1217-23.
- **Beurrier C** and Malenka RC (2002). Enhanced inhibition of synaptic transmission by dopamine in the nucleus accumbens during behavioral sensitization to cocaine. *Journal of Neuroscience*, 22(14): 5817-5822.

II.3 L'ABLATION GENETIQUEMENT CIBLEE DES NEURONES STRIATO-NIGRAUX REVELE DES FONCTIONS TRES DIVERSES DE CES NEURONES

Après mon recrutement au CNRS en 2003 et un certain nombre de cellules enregistrées sur tranches, j'ai ressenti le besoin d'élargir mes compétences techniques. Mon arrivée dans l'équipe de Lydia Kerkerian en 2006 m'a donné cette possibilité : l'équipe de Lydia est en effet spécialisée dans la neuroanatomie des ganglions de la base et maîtrise parfaitement des techniques telles que hybridation *in situ*, immunohistochimie ... A la même époque, les premières souris transgéniques permettant d'identifier les deux sous-population de MSNs ont fait leur apparition (Gong et al., 2003). Un reporteur fluorescent est exprimé sous le contrôle du promoteur du récepteur dopaminergique D1 ou D2 et permet ainsi d'identifier en direct les MSNs enregistrés. Cet outil a constitué une mini-révolution dans le domaine des ganglions de la base et a permis, entre autre, d'établir le profil électrophysiologique des deux populations de MSNs. Peut-on relier des profils électrophysiologiques à des rôles fonctionnels particuliers ? Le modèle théorique des ganglions de la base attribue aux MSNs un rôle opposé dans le contrôle du mouvement : les MSNs D1 faciliteraient le mouvement (ou permettraient de sélectionner le programme moteur approprié) alors que les MSNs D2 l'inhiberaient (ou bloqueraient les programmes moteurs parasites). En raison d'un manque d'outil permettant de manipuler spécifiquement les deux populations de MSNs, cette dichotomie fonctionnelle est restée longtemps théorique. Ainsi, en 2006, j'ai décidé de créer une souris transgénique permettant l'ablation génétiquement ciblée des MSNs D1 appartenant à la voie directe afin de déterminer leur rôle dans différents paradigmes comportementaux. L'approche a consisté à faire exprimer le récepteur humain de la toxine diphtérique (DTR) spécifiquement dans les neurones de la voie directe, et à induire la mort de ces neurones par apoptose après administration intrastriatale de la DT. Cette technique présente l'avantage de contrôler spatialement et temporellement l'ablation de la population visée. Entre les premières PCR et la naissance de la première souris transgénique, plus d'un an s'est écoulé ... La caractérisation des souris au niveau cellulaire et comportementale a été réalisée par Delphine Révy, la première étudiante en thèse que j'ai encadrée.

II.3.1 Choix du modèle permettant l'ablation spécifique des MSNs D1 : création des souris transgéniques

Le ciblage a été réalisé en utilisant le promoteur du gène *slc35d3* (solute carrier family 35 member D3), gène spécifiquement exprimé dans les MSNs D1 par rapport aux MSNs D2 (Lobo et al., 2006). Ce modèle de transgénèse additive a été mis au point par le Dr. Hélène Marie (IPMC, CNRS UMR 6097, Sophia Antipolis) en collaboration avec Alban de Kerchove d'Exaerde (Université Libre de Bruxelles). Hélène Marie a cloné une chimère fusionnelle exprimant le DTR couplé à la GFP dans un chromosome bactérien artificiel (BAC) codant pour le gène *slc35d3*. Le BAC a ensuite été envoyé à l'Institut Pasteur à Paris afin d'être microinjecté dans des ovocytes de souris (Francina Langa, CIGM, Institut Pasteur, Paris). Nous avons ainsi obtenu 5 souris positives sur les 63 générées. L'obtention de ces 5 souris nous a permis de générer 5 lignées distinctes en les croisant avec des souris sauvages C57Bl/6. La descendance est donc un mélange de souris exprimant le transgène (DTR+) et de souris ne l'exprimant pas (DTR-, utilisées comme contrôles).

II.3.2 L'ablation des MSNs D1 a des répercussions sur l'organisation cellulaire du striatum

Cette partie a été réalisée en étroite collaboration avec le Dr. Pascal Salin dans le laboratoire et a été menée en plusieurs étapes (fig. 9):

- nous avons dans un premier temps utilisé une approche de traçage rétrograde basée sur l'utilisation de microbilles fluorescentes rouges injectées dans la SNr. Ces billes sont captées de manière rétrograde par les projections striatonigrales et vont marquer uniquement les corps cellulaires des MSNs D1. Nous observons que toutes les cellules marquées par celles-ci expriment aussi la GFP associée au DTR, confirmant l'expression spécifique du DTR dans les MSNs D1.
- nous avons ensuite vérifié si la GFP, associée au DTR, était spécifiquement exprimée dans le striatum des souris positives en réalisant une immunohistochimie avec un anticorps anti-GFP. Seules les souris positives (DTR+) expriment la GFP au niveau du striatum par rapport aux souris négatives de la même portée (DTR-). L'injection de DT dans le striatum par stéréotaxie entraîne une baisse significative de GFP dans l'hémisphère injecté par rapport à l'hémisphère non-injecté.
- dans un troisième temps, nous avons réalisé des hybridations *in situ* et des PCR quantitatives afin de quantifier le niveau d'ARNm de différents marqueurs exprimés spécifiquement dans l'une ou l'autre des deux populations de MSNs. L'injection de DT chez les souris DTR+ entraîne une baisse significative de l'expression génique de la SP et des récepteurs dopaminergiques de type D1, spécifiquement exprimés par les MSNs D1 alors qu'aucun des marqueurs spécifiquement exprimé par les MSNs D2 n'est affecté par l'injection de DT.

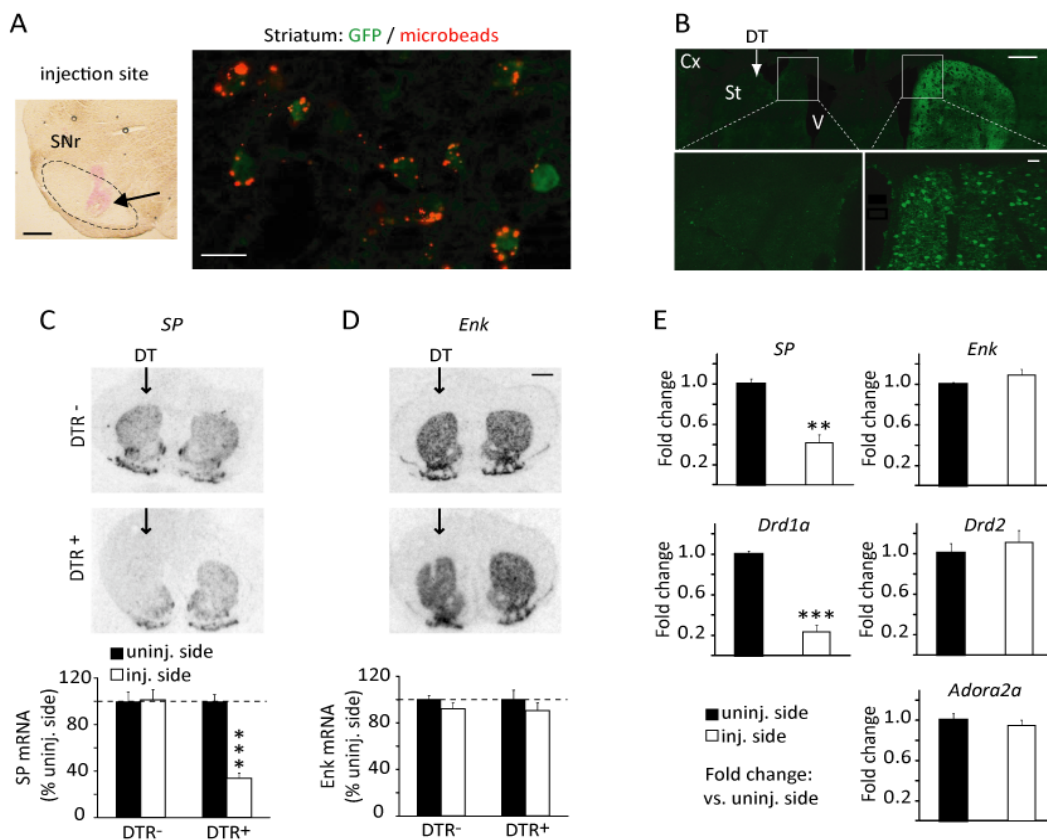


Figure 9. Expression sélective du DTR-GFP dans les MSNs D1 et impact de l'injection de DT. A : Site d'injection des microbilles dans la SNr (échelle : 200 µm) et détection par immunofluorescence de la GFP et des microbilles fluorescentes dans le striatum (échelle : 10 µm). B : Immunodétection de la GFP sur une coupe coronale de souris

*DTR+ 7 jours après injection unilatérale de DT. Cx: cortex, St: striatum, V: ventricule. Echelles : 500 μ m (haut) et 20 μ m (bas). C, D : Hybridations *in situ* radioactives (échelle : 1 mm) et quantification du niveau d'ARNm de la SP et des Enk dans le striatum après injection unilatérale de DT. Student's t test : *** $p < 0.001$ vs. uninjected side. E : RT-qPCR quantitative de gènes spécifiquement exprimés par les MSNs D1 (SP, *Drd1a*) et D2 (Enk, *Drd2*, *Adora2a*) après injection de DT. Student's t test : ** $p < 0.01$, *** $p < 0.001$ vs. uninjected side.*

L'ensemble de ces résultats montre que l'injection de la DT engendre une perte spécifique des MSNs D1 par rapport aux MSNs D2. Le striatum contient également différentes populations d'interneurones : 3 types d'interneurones GABAergiques qui expriment des protéines différentes et un type d'interneurones cholinergique qui exprime la choline acetyltransferase (ChAT). L'injection de DT n'affecte pas les interneurones GABAergiques. Nous avons en revanche observé de façon surprenante une baisse significative du nombre d'interneurones cholinergiques (CINs) suite à l'injection de DT. Des expériences d'immunohistochimie, d'hybridation *in situ* et de single-cell RT-PCR ont montré que les CINs n'expriment pas le DTR et que leur disparition est spécifiquement observée dans le striatum dorsal mais pas dans le noyau accumbens. Nous avons donc émis l'hypothèse que la perte des CINs est secondaire à l'ablation des MSNs D1 et que cette dépendance est territoire spécifique. Des expériences complémentaires seront nécessaires pour disséquer les mécanismes responsables de la disparition des CINs après ablation des MSNs D1.

II.3.3 L'ablation des MSNs D1 a des impacts comportementaux très divers

Afin de comprendre les conséquences fonctionnelles de l'absence de la voie striatonigrale, nous avons réalisé plusieurs tests comportementaux, certains ont été faits en collaboration avec le Dr. Marianne Amalric. Les tests mesurant l'activité locomotrice, l'anxiété et la sensibilisation à la cocaïne ont été réalisés chez des souris DTR+ et DTR- ayant reçu des injections bilatérales de DT dans le striatum dorsal. Pour le test d'induction des dyskinésies par la L-DOPA, les deux groupes de souris ont été injectées unilatéralement avec de la DT dans le striatum dorsal et après lésion unilatérale du système dopaminergique nigrostrié. Le niveau d'expression de la SP et de l'Enk a été vérifié à la fin des expériences comportementales.

[L'injection de DT altère la locomotion basale et la locomotion induite par la cocaïne](#)

Le striatum dorsal est impliqué dans la régulation de l'activité motrice ainsi que dans la réponse aux psychostimulants. Nous avons donc étudié l'activité locomotrice basale et suite à l'injection de cocaïne après ablation des MSNs D1. Nous avons observé d'une part une diminution de l'activité basale (fig. 10A, inset) et d'autre part une potentialisation de l'activité induite par la cocaïne (fig. 10).

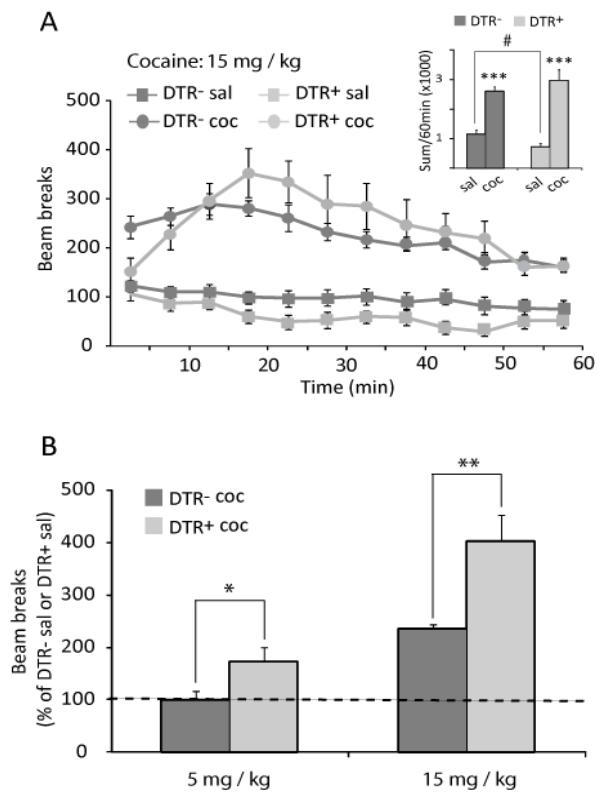


Figure 10. Réponse locomotrice basale et après injection de cocaïne de souris DTR- et DTR+. A : le graphe illustre le nombre d'interruption de faisceau infra-rouge par tranche de 5 min pendant une période de 60 min après injection de saline ou de cocaïne (15 mg/kg) chez des souris DTR- (n=14 saline et 10 cocaïne) et DTR+ (n=9 saline et 6 cocaïne). Inset : moyennes du nombre total d'interruption de faisceau infra-rouge pendant 60 min. Student's t test: *** $p < 0.001$ vs. DTR- sal or DTR+ sal, # $p < 0.05$ vs. DTR- sal. B : le graphe compare l'activité locomotrice à deux doses différentes de cocaïne (5 et 15 mg/kg). Les données sont exprimées pour chaque génotype en pourcentage des souris traitées au saline (groupe 5 mg/kg : souris DTR-, n=12 saline et 12 cocaïne and souris DTR+, n=5 saline et 5 cocaïne; groupe 15 mg/kg : souris DTR-, n=14 saline et 10 cocaïne et souris DTR+, n=9 saline et 6 cocaïne). Student's t test: * $p < 0.05$, ** $p < 0.01$ vs. DTR- coc.

L'hypoactivité des souris DTR+ après ablation des MSNs D1 dans le striatum dorsal est en accord avec le schéma classique des ganglions de la base qui propose que la voie directe ait un rôle facilitateur sur le mouvement et les travaux montrant que l'ablation ou l'activation par optogénétique des MSNs D1 induit une diminution ou une augmentation, respectivement, de l'activité locomotrice (Durieux et al., 2012; Kravitz et al., 2010). Notre étude est en revanche la première à montrer une réponse accrue à l'injection aiguë de cocaïne. Nous proposons que cette potentialisation soit due à la disparition des CINs plutôt qu'à l'ablation des MSNs striatonigraux. Des expériences permettant une destruction spécifique des CINs devraient permettre de confirmer ce résultat intéressant.

L'injection de DT diminue significativement les dyskinésies induites par la L-DOPA

Le traitement à la L-DOPA s'avère très efficace dans la MP mais, après une période plus ou moins longue selon les patients (10-15 ans), il induit l'apparition de mouvements anormaux involontaires appelés dyskinésies. Plusieurs études suggèrent qu'une des causes de l'apparition des dyskinésies induites par la L-DOPA serait l'hypersensibilité des récepteurs D1 exprimés sur les MSNs striatonigraux (Santini et al., 2009). Pour établir l'implication causale de cette population neuronale dans les dykinésies, nous avons testé les souris DTR+ et DTR- dans un protocole d'induction de dykinésies par un traitement chronique à la L-DOPA. L'injection de L-DOPA pendant 21 jours à des souris rendues préalablement parkinsoniennes par injection de 6-OHDA dans la SNc entraîne l'apparition de mouvements anormaux qui sont significativement réduits après ablation des MSNs D1 (fig. 11). Ces résultats démontrent que les MSNs D1 du striatum dorsal jouent un rôle causal dans l'expression des dyskinésies induites par la L-DOPA.

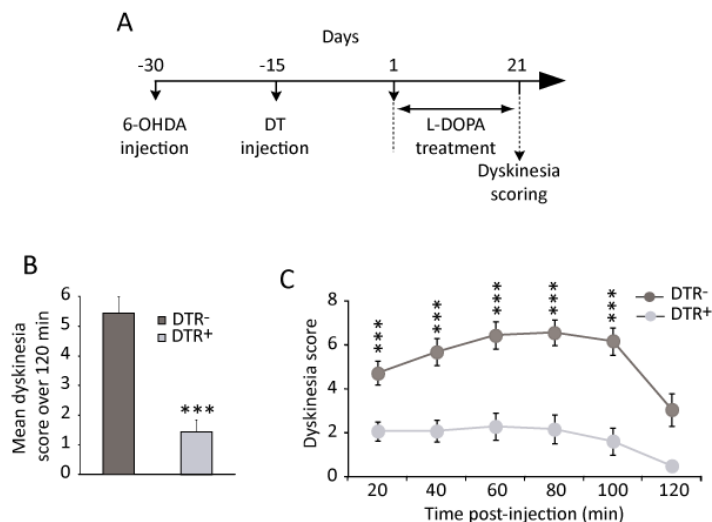


Figure 11. Les dykinésies induites par la L-DOPA sont réduites après ablation des MSNs D1. A : protocole expérimental. B : score moyen des dyskinésies évalué pendant 120 min après injection de L-DOPA au jour 21 (n=16 DTR- et n=12 DTR+). Student's t test : *** p < 0.001 vs. DTR- mice. C : évolution temporelle des dyskinésies mesurées toutes les 20 min sur une période de 120 min au jour 21 chez les souris DTR- (n=16) et DTR+ (n=12). Holm-Sidak post test: *** p < 0.001.

L'injection de DT diminue significativement l'anxiété

Un nombre croissant de données suggère que le striatum dorsal, en plus de son rôle dans les comportements moteurs, interviendrait aussi dans la régulation des comportements présentant une composante émotionnelle et motivationnelle (Balleine et al., 2007). Nous avons donc évalué l'état d'anxiété des souris dans le test du labyrinthe en croix surélevé constitué de deux bras ouverts et de deux bras fermés par des parois en plexiglas opaque. Le temps passé ainsi que le nombre d'entrée dans les bras ouverts (zones anxiogènes) sont significativement plus importants pour les souris DTR+ comparés aux souris DTR- démontrant une diminution significative de l'anxiété après ablation des MSNs D1 (fig. 12).

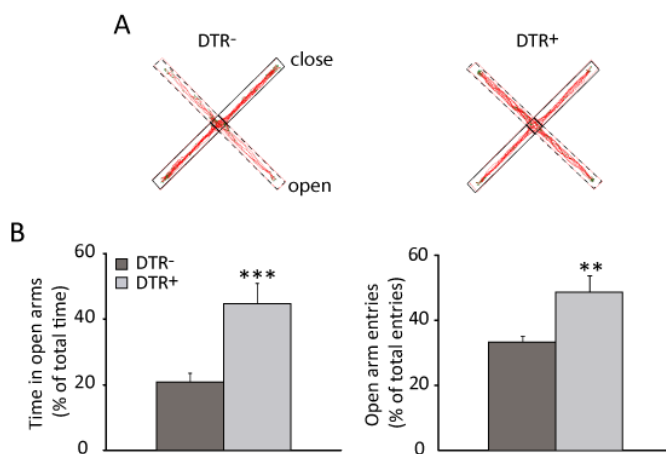


Figure 12. L'injection de DT diminue l'anxiété des souris DTR+. A : exemple de traces illustrant les trajets réalisés par les souris DTR+ ou DTR- pendant les 5 min de test. On peut noter que dans les 2 cas, les souris DTR+ se déplacent plus dans les bras ouverts que les souris DTR-. B : Quantification du temps passé et du nombre d'entrée dans les bras ouverts pour chaque groupe. Student's t test: ***p<0,001 vs. DTR-.

En résumé, le travail de thèse de Delphine a permis de montrer que l'ablation des MSNs D1 affecte peu les autres populations neuronales du striatum à l'exception des CINs. Un faisceau d'arguments démontre que la perte des CINs ne serait pas due à un effet direct de la DT sur ces interneurons mais serait secondaire à la perte des MSNs D1, mettant en évidence un lien étroit entre ces deux populations. D'un point de vue fonctionnel, nos résultats montrent l'implication des MSNs D1 dans la régulation de nombreux comportements, tant moteurs qu'émotionnels.

Article

• Révy D, Jaouen F, Salin P, Melon C, Chabbert D, Tafi E, Concetta L, Langa F, Amalric M, Kerkerian-Le Goff L, Marie H, **Beurrier C** (2014). Cellular and behavioral outcomes of dorsal striatonigral neuron ablation: new insights into striatal functions, *Neuropsychopharmacology*, 39(11): 2662-2672.

II.4 LES INTERNEURONES CHOLINERGIQUES DU STRIATUM SONT DES ACTEURS ESSENTIELS DANS LA PATHOPHYSIOLOGIE DE LA MALADIE DE PARKINSON

Le travail réalisé ci-dessus m'a fait prendre conscience de la nécessité d'allier les approches moléculaires/cellulaires à l'électrophysiologie pour appréhender le rôle d'une population neuronale. En outre, nous avons montré de façon tout à fait fortuite et inattendue une particularité des interneurones cholinergiques (CINs) dont la survie semblerait dépendre des MSNs D1. Au même moment dans le laboratoire, grâce à des expériences de traçage réalisées avec le virus de la rage, l'équipe venait de montrer que ces mêmes CINs subissaient un remaniement anatomique important en situation parkinsonienne. Après déplétion dopaminergique, le nombre de CINs innervant les MSNs D2 augmente alors que les CINs qui contactent les MSNs D1 diminuent (Salin et al., 2009). Ce résultat suggérait que les CINs pouvaient participer au déséquilibre des sorties striatales en situation parkinsonienne (hyperactivité de la voie indirecte et hypoactivité de la voie directe). La question qui s'est alors posée est la suivante : est-ce que ce remaniement anatomique a des impacts fonctionnels sur la circuiterie des ganglions de la base et plus particulièrement sur les deux populations de MSNs ? La seule expérience qui me semblait pertinente pour répondre à cette question était de comparer la réponse des MSNs D1 et D2 à la stimulation d'un nombre donné de CINs en situation contrôle puis en situation parkinsonienne. Les techniques conventionnelles d'activation (pharmacologique ou électrique) ne permettant pas de cibler spécifiquement une population cellulaire, l'optogénétique m'a semblé être l'outil idéal et j'ai décidé de développer cette technique dans le laboratoire. En outre, si on connaît depuis longtemps le rôle crucial de l'acétylcholine (ACh) dans un grand nombre de pathologies liées aux ganglions de la base et notamment dans la maladie de Parkinson, la démonstration expérimentale de son implication reste fragmentaire. Malgré leur faible nombre (1-3% de la population striatale), les CINs ont une arborisation dendritique très étendue qui les place dans une position idéale pour moduler l'activité des deux types de MSNs et donc la sortie du réseau des ganglions de la base (Bolam et al., 1986, 1984). L'efficacité des anti-cholinergiques sur les symptômes parkinsoniens est un argument supplémentaire renforçant l'idée que l'ACh peut profondément moduler les fonctions striatales. Pour établir l'implication causale des CINs dans la maladie de Parkinson et disséquer les mécanismes responsables de l'altération cholinergique-dépendante des fonctions striatales, nous avons étudié si et comment la manipulation optogénétique de ces neurones affecte la motricité et identifié les substrats neuronaux de l'action des CINs en situation normale et parkinsonienne. Ce projet a été financé par l'ANR et nous a permis de recruter un ingénieur, Florence Jaouen, qui a grandement participé à la mise en place de l'optogénétique dans le laboratoire. Nous avons combiné différentes approches : l'électrophysiologie *in vitro* (réalisée par moi-même) et *in vivo* (réalisée par Nicolas Maurice dans le laboratoire) et une approche comportementale qui a été faite en collaboration avec le laboratoire du Dr. Marianne Amalric.

II.4.1 Contrôle de l'activité des interneurones cholinergiques du striatum par optogénétique

Pour manipuler sélectivement les CINs nous avons exprimé la channelrhodopsine-2 fusionnée à la mCherry (ChR2-mCherry) ou l'halorhodopsine fusionnée à la TagRFP (eNpHR3.0-RFP) dans les neurones exprimant la ChAT en injectant un adénovirus associé (AAV) dont l'expression dépend de la cre-recombinase. L'injection de l'AAV contenant les gènes de la ChR2-mCherry ou de l'eNpHR3.0-RFP dans le striatum dorsal de souris transgéniques ChAT^{cre/cre} nous a permis d'obtenir une proportion importante de CINs exprimant soit la ChR2-mCherry soit l'eNpHR3.0-RFP. Au cours de l'étude, nous

avons pu nous procurer chez Jackson Laboratory des souris transgéniques qui expriment les opsines dans tous les neurones cholinergiques après croisement avec les souris transgéniques ChAT^{cre/cre} (souris Rosa^{eNpHR/+::ChAT^{cre/+}} et Rosa^{ChR2/+::ChAT^{cre/+}}). Nous avons donc mené une partie de la caractérisation comportementale sur le modèle AAV alors que la caractérisation électrophysiologique a été effectuée sur le modèle Rosa. Dans les deux cas, nous avons vérifié la fonctionnalité des opsines en enregistrant l'activité des CINs sur des tranches striatales ou *in vivo* sur des souris anesthésiées : l'activation de l'eNpHR par une lumière orange (589 nm) inhibe la décharge spontanée des CINs alors que l'activation de la ChR2 par une lumière bleue (473 nm) déclenche l'émission de potentiels d'action (fig. 13).

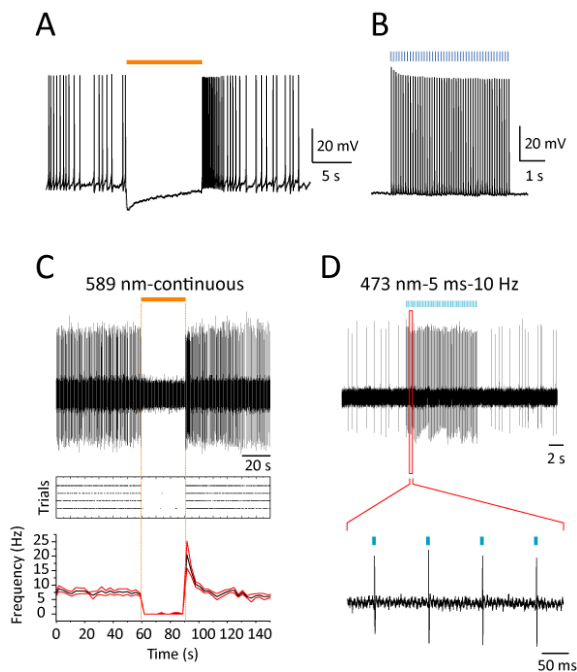


Figure 13. Expression fonctionnelle de l'eNpHR-RFP et de la ChR2-mCherry dans les CINs. Une lumière orange (589 nm) induit un inhibition des potentiels d'action dans les CINs exprimant la eNpHR-RFP que ce soit *in vitro* sur des tranches (A) ou *in vivo* sur des souris anesthésiées (C) alors que de brefs pulses de lumière bleue (473 nm, 5 ms) déclenchent des potentiels d'action dans les CINs exprimant la ChR2-mCherry enregistrés sur tranches (B) ou *in vivo* (D).

II.4.2 L'inhibition des interneurones cholinergiques du striatum réduit les déficits moteurs parkinsoniens

Nous avons dans un premier temps testé l'effet de la photoactivation et de la photoinhibition des CINs sur l'activité locomotrice basale de souris contrôles dans un open-field. Nous n'avons détecté aucun effet. Pour déterminer si la modulation des CINS pouvait en revanche affecter les symptômes parkinsoniens, nous avons d'abord utilisé un modèle pharmacologique aigu de l'akinésie parkinsonienne, la catalepsie induite par l'injection d'un antagoniste dopaminergique, l'halopéridol. L'inhibition des CINs réduit significativement l'état cataleptique des animaux alors que leur activation n'a aucun effet. Nous avons ensuite voulu voir si les effets bénéfiques de l'inhibition des CINs pouvaient être reproduits dans un modèle lésionnel de la maladie de Parkinson, le modèle 6-OHDA. Deux semaines après l'injection de 6-OHDA, les déficits moteurs des animaux ont été évalués dans le test du cylindre et dans le test du labyrinthe en croix. Dans le test du cylindre (fig. 14a, b), les souris lésées présentent une forte asymétrie dans l'utilisation de leurs pattes avant lors de l'exploration des parois du cylindre : l'utilisation de la patte controlatérale à la lésion est fortement réduite, reflétant une forte akinésie induite par la 6-OHDA (score d'asymétrie élevé). La photoinhibition des CINs réduit partiellement cette asymétrie alors que leur photoactivation n'a aucun effet. Nous avons aussi observé un effet bénéfique de la photoinhibition dans le test du labyrinthe (fig. 14c, d) : le biais dans l'exploration du bras ipsilatéral à la lésion est fortement réduit pendant l'inhibition des CINs alors que l'activation des CINs n'a encore une fois aucun effet.

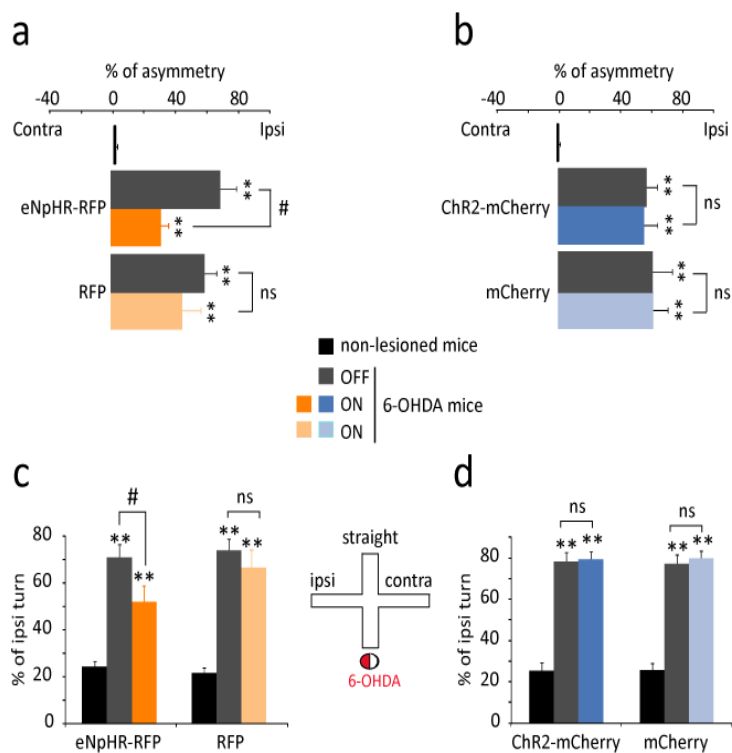


Figure 14. L'inhibition des interneurons cholinergiques réduit les symptômes moteurs parkinsoniens. A : les souris 6-OHDA présentent une forte asymétrie dans le test du cylindre (6-OHDA vs. non-lesioned: ** $p < 0.01$, Fisher PLSD test) qui est partiellement réduite par la photoinhibition des CINs (ON vs. OFF: # $p < 0.05$, Student's *t* test). B : la photoactivation des CINs n'a pas d'effet sur l'asymétrie des souris 6-OHDA. C : le biais ipsilatéral des souris 6-OHDA (6-OHDA vs. non-lesioned: ** $p < 0.01$, one-way ANOVA) est partiellement corrigé par l'inhibition des CINs (ON vs. OFF: # $p < 0.05$, paired Student's *t* test). D : le biais ipsilatéral n'est pas affecté par la photoactivation des CINs. Le cercle sous le labyrinthe représente une souris avec le côté en rouge injecté par la 6-OHDA.

II.4.3 L'inhibition des interneurons cholinergiques du striatum affecte la structure de sortie des ganglions de la base uniquement en situation parkinsonienne

Pour identifier les substrats cellulaires de ces effets anti-parkinsoniens, Nicolas Maurice dans l'équipe a enregistré *in vivo* l'activité de la principale structure de sortie des ganglions de la base, la SNr dans des souris transgéniques eNpHR anesthésiées. Nous avons étudié l'effet de l'inhibition des CINs sur l'activité électrique spontanée des neurones de la SNr ainsi que sur les réponses évoquées par la stimulation corticale. La photoinhibition des CINs normalise les changements de la décharge en bouffées induits par la lésion 6-OHDA sans modifier les paramètres non affectés par la lésion (fig. 15a). La stimulation corticale déclenche une réponse complexe au niveau des neurones de la SNr qui se compose de trois phases : une excitation précoce suivie d'une inhibition et d'une excitation tardive (fig. 15b, c). Nos travaux antérieurs (Maurice et al., 1999) ainsi que d'autres études (Ryan and Sanders, 1994) ont clairement montré que ces trois composantes résultaient de l'activation successive de la voie hyperdirecte cortico-subthalamique et des voies striatonigrées directe et indirecte. Sachant que l'akinésie parkinsonienne s'accompagne d'une hypoactivité de la voie directe et d'une hyperactivité de la voie indirecte, nous avons émis l'hypothèse que l'inhibition des CINs permettait de contrecarrer ce déséquilibre. Nous avons montré que la photoinhibition augmente en effet significativement la durée de l'inhibition sans affecter les autres composantes de la réponse (fig. 15d, e). Ce résultat suggère que l'inhibition des CINs exerce un effet anti-parkinsonien en renforçant la transmission de l'information corticale par la voie directe sans affecter la voie indirecte. De façon intéressante, l'inhibition des CINs sur des souris non-lésées n'affecte ni l'activité spontanée ni la réponse à la stimulation corticale des neurones de la SNr, suggérant que la modulation exercée par les CINs dans le striatum est fortement dépendante du niveau de dopamine.

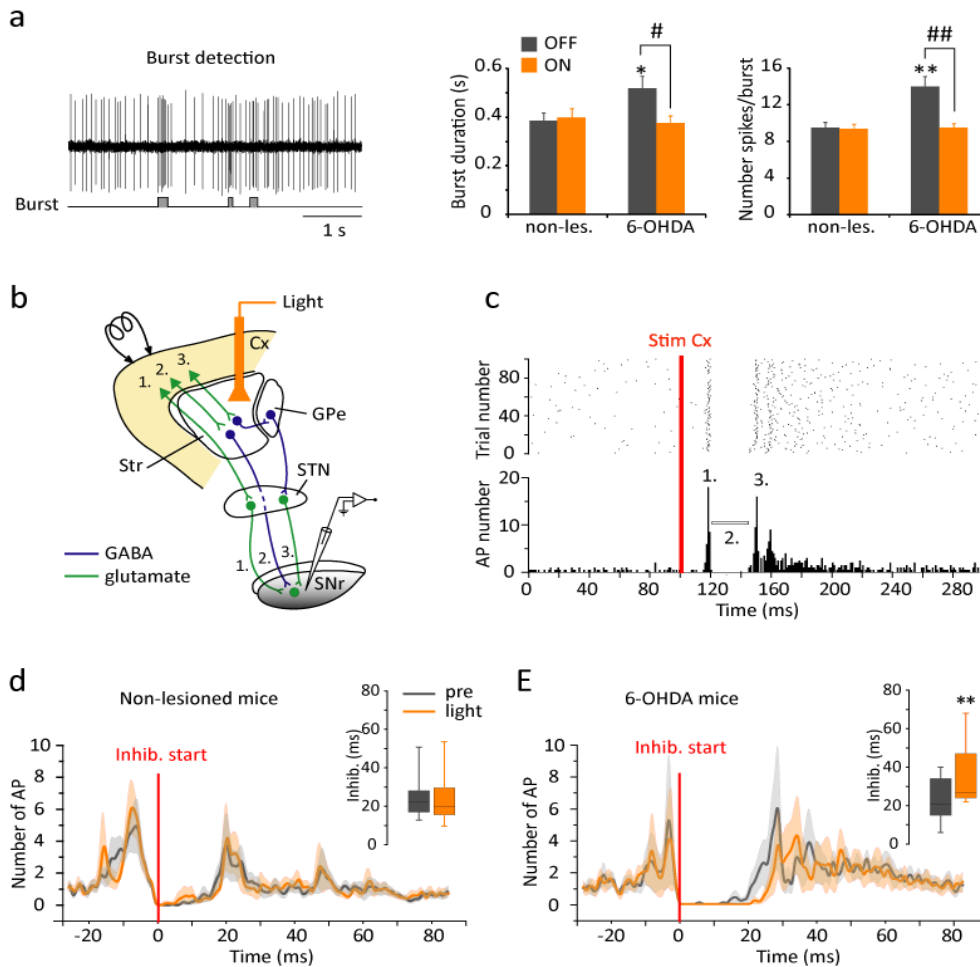


Figure 15. L'inhibition des interneurons cholinergiques normalise la décharge en bouffées des neurones de la SNr et renforce la voie directe striatonigrale chez les souris 6-OHDA. A : détection des bouffées avec l'analyse Poisson Surprise d'un neurone de la SNr enregistré chez une souris eNpHR 6-OHDA. L'augmentation de la durée et du nombre de potentiels d'action dans les bouffées induites par la 6-OHDA (6-OHDA vs. non-lesioned: * $p < 0.05$, ** $p < 0.01$, Student's t test) est supprimée par l'inhibition des CINs (6-OHDA ON vs. OFF: # $p < 0.05$, ## $p < 0.01$, Holm-Sidak test after significant one-way ANOVA). B : représentation schématique des voies projetant sur la SNr qui sont activées par la stimulation corticale. 1 : voie hyperdirecte, 2 : voie directe et 3 : voie indirecte. C : Raster et PSTH (peristimulus time histogram) de la réponse triphasique évoquée par la stimulation du cortex moteur chez une souris eNpHR lésée à la 6-OHDA. D, E : PSTHs moyens de la réponse des neurones de la SNr évoquée par la stimulation corticale chez des souris contrôles et lésées à la 6-OHDA. La photoinhibition des CINs induit une augmentation significative de la durée de la composante inhibitrice de la réponse triphasique uniquement chez les souris 6-OHDA (** $p < 0.01$, Holm-Sidak test after significant one-way repeated measure ANOVA).

II.4.4 L'inhibition des interneurons cholinergiques du striatum affecte de façon différentielle l'excitabilité des MSNs de la voie directe et indirecte

Quelles sont les cibles striatales modulées par les CINs qui pourraient renforcer l'activité de la voie directe ? Avant de répondre à cette question fondamentale, il nous a semblé important de déterminer les effets de la lésion 6-OHDA sur les CINs eux-mêmes. L'absence de dopamine peut en effet modifier l'homéostasie cholinergique dans le striatum mais il n'y a pas de consensus quant aux modifications engendrées par un tel changement. Nous avons donc enregistré l'activité des CINs en patch-clamp sur des tranches striatales et en extracellulaire *in vivo* chez des souris contrôles et 6-OHDA. Les CINs sont

caractérisés par une activité spontanée régulière et cette activité n'est pas modifiée par la lésion 6-OHDA en termes de fréquence et de patron de décharge, tant *in vitro* qu'*in vivo*. Nous avons en revanche observé une augmentation de l'excitabilité des CINs après lésion 6-OHDA qui se traduit par une diminution du courant de rhéobase et un shift vers la gauche de la courbe entrée-sortie. Ces résultats montrent donc que les CINs ne sont pas hyperactifs *per se* après lésion dopaminergique mais sont plus excitables.

Nous avons ensuite déterminé les effets de la photoinhibition des CINs sur les MSNs à l'origine des voies directe et indirecte. Afin d'identifier le type de MSNs enregistré, nous avons utilisé des souris exprimant à la fois la protéine fluorescente tdTomato sous le contrôle du promoteur du récepteur dopaminergique D1 exprimé par les MSNs de la voie directe et l'eNpHR dans les CINs. En accord avec la littérature, nous avons retrouvé la dichotomie de l'excitabilité des MSNs en situation contrôle : les MSNs de la voie directe (D1 MSNs) sont moins excitables que ceux de la voie indirecte (D2 MSNs) (fig. 16a) (Gertler et al., 2008; Kreitzer and Malenka, 2007). La lésion dopaminergique réduit cette différence puisque l'excitabilité des MSNs de la voie directe est spécifiquement augmentée chez les souris 6-OHDA (fig. 16a). Lorsque les CINs sont photoinhibés, les deux populations de MSNs émettent moins de potentiels d'action mais cet effet inhibiteur est moins marqué sur les MSNs de la voie indirecte que sur ceux de la voie directe chez les souris 6-OHDA alors qu'il est équivalent en situation contrôle (fig. 16b). Ainsi, l'inhibition des CINs permettrait de restaurer la dichotomie d'excitabilité entre les deux populations de MSNs ce qui pourrait expliquer en partie l'effet antiparkinsonien de la photoinhibition. Ce résultat est en revanche plus difficile à réconcilier avec le renforcement de l'inhibition évoquée par la stimulation corticale dans les neurones de la SNr lié à l'activation des MSNs de la voie directe en condition 6-OHDA (fig. 15d, e). Une hypothèse possible est que l'inhibition des CINs affecte *in vivo* l'intégration dendritique des entrées corticales par les MSNs, paramètre que nous n'avons pas mesuré dans nos expériences *in vitro*.

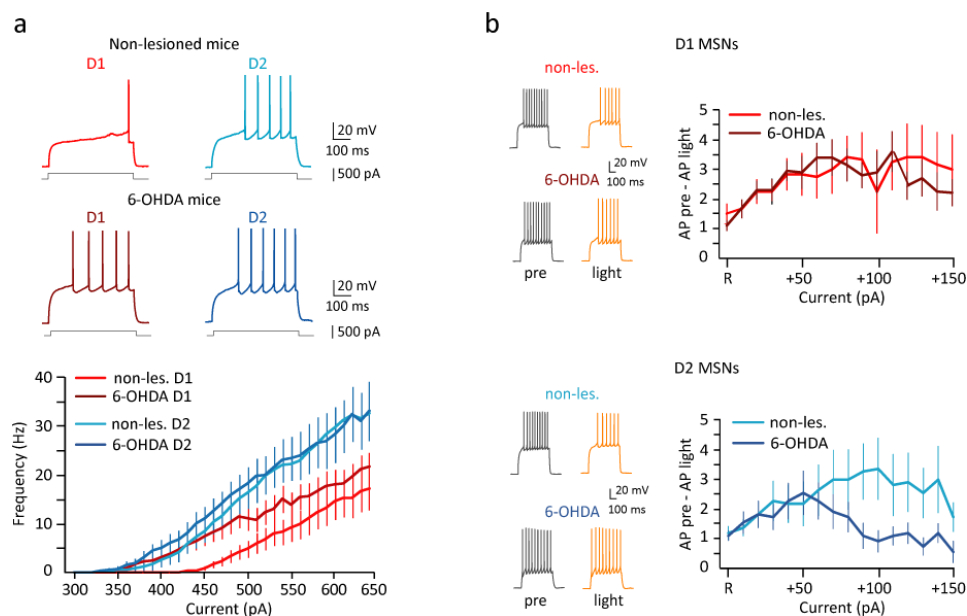


Figure 16. Impact de la lésion 6-OHDA et de l'inhibition des CINs sur l'excitabilité des MSNs. A : enregistrements en courant-imposé montrant la réponse des MSNs des voies directe (D1) et indirecte (D2) à des pulses de courant dépolarisant chez une souris contrôle (+400 pA) et 6-OHDA (+450 pA). Le graphe montre la fréquence des potentiels d'action en fonction du courant injecté dans les deux populations de MSNs en condition contrôle et 6-OHDA. B : les enregistrements électrophysiologiques montrent la réponse de MSNs D1 et D2 à des pulses de

courant avant (pre, gris) et pendant (light, orange) l'application de la lumière chez des souris contrôles et 6-OHDA. Les graphes illustrent la différence dans le nombre de potentiels d'action évoqués avant et pendant l'application de la lumière. R représente l'intensité minimale de courant déclenchant un potentiel d'action en condition pre. A partir de R, l'intensité du courant augmente de 10 pA. A partir de R+80 pA, les MSNs D2 sont moins inhibés que les MSNs D1 pendant l'application de la lumière chez les souris 6-OHDA comme le montre l'interaction significative entre la lésion et l'intensité de courant pour les MSNs D2 [F(15,300)=2.39, p<0.05].

Pour conclure, nous avons montré dans cette étude que :

- l'inhibition des CINs dans le striatum dorsal permet de réduire les symptômes moteurs parkinsoniens, attestant leur implication causale dans la maladie de Parkinson.
- l'inhibition des CINs chez les souris parkinsoniennes module de façon différentielle l'excitabilité des MSNs des voies directe et indirecte, normalise la décharge pathologique en bouffées des neurones de la SNr et augmente le contrôle inhibiteur de la voie directe sur ces mêmes neurones.
- en revanche, l'inhibition des CINs chez les souris contrôles n'a pas d'effet sur l'activité locomotrice, réduit l'excitabilité des deux populations de MSNs de façon similaire et n'affecte ni l'activité spontanée ni les réponses corticales des neurones de la SNr. Le rôle des CINs dans les fonctions motrices est donc fortement dépendant du niveau de dopamine.

Article

- Maurice N, Liberge M, Jaouen F, Ztaou S, Hanini M, Camon J, Deisseroth K, Amalric M, Kerkerian-Le Goff L, **Beurrier C** (2015). Striatal Cholinergic Interneurons Control Motor Behavior and Basal Ganglia Function in Experimental Parkinsonism, *Cell Rep.*, 13(4):657-666.

III. PROJET DE RECHERCHE

Mon projet de recherche dans les années à venir s'inscrit dans la continuité de mon questionnement sur le rôle des CINs dans le réseau des ganglions de la base. Après avoir mis en place l'optogénétique dans le laboratoire et montré, grâce à cet outil, le rôle fondamental des CINs dans le contrôle moteur en situation pathologique (II.4), je voudrais maintenant aborder la fonction des CINs dans la planification de l'action et les apprentissages. Pour cela, il me semble important de décortiquer les interactions entre trois acteurs essentiels au fonctionnement du réseau des ganglions de la base qui sont : les CINs du striatum, les projections thalamostriatales et les synapses corticostriées. L'implication respective de chaque partenaire dans les fonctions et les pathologies associées au réseau des ganglions de la base a été largement étudiée mais la façon dont ils interagissent reste à démontrer. Les changements à long terme de la transmission synaptique corticostriée sont les bases cellulaires des apprentissages sensorimoteurs et un dysfonctionnement de cette plasticité corticostriée jouerait un rôle fondamental dans l'expression des symptômes parkinsoniens. L'ACh, provenant des CINs, agit sur de nombreuses cibles striatales et module de façon complexe la plasticité corticostriée. *In vivo*, les CINs correspondent aux neurones toniquement actifs du striatum qui présentent une pause dans leur activité lors de la présentation d'un stimulus saillant pendant les apprentissages par renforcement. Au fur et à mesure de l'apprentissage, cette réponse conditionnée semble se synchroniser dans un ensemble de CINs. Le complexe centromédian parafasciculaire du thalamus jouerait un rôle clef à la fois dans la genèse de la pause et de sa synchronisation. Ces trois protagonistes présentent des altérations majeures dans la maladie de Parkinson qui pourraient être à l'origine de certains symptômes. Afin d'expliquer les interactions complexes de ce trio, une hypothèse souvent évoquée propose que les CINs, en intégrant les informations thalamiques, fournit au striatum des informations sensorielles saillantes et peuvent ainsi modifier la transmission corticostriée et donc faciliter l'apprentissage. Cette hypothèse reste cependant à démontrer. Le projet que je souhaite développer utilisera des techniques de pointe combinant l'optogénétique et l'électrophysiologie que nous avons mises en place dans le laboratoire lors de l'obtention de notre dernier contrat ANR. Ces outils se sont révélés tout à fait pertinents pour mettre en lumière le rôle des CINs dans le contrôle du comportement moteur en situation pathologique. Cependant, une différence fondamentale est la façon dont l'optogénétique sera utilisée dans ce projet : les activations/inhibitions de longue durée que nous avons appliquées précédemment seront remplacées par des paramètres de photoactivation plus physiologiques nous permettant de mimer des patrons d'activité observés *in vivo* dans les CINs. Le Dr. Nicolas Maurice, chercheur au sein de l'équipe avec qui je collabore (cf. notre dernière publication : Maurice et al., 2016) apportera sa compétence en électrophysiologie *in vivo*. Un partenaire extérieur, le Dr. Nicolas Mallet (Institut des maladies neurodégénératives, UMR5293 CNRS/Université de Bordeaux) participera également au projet et nous permettra d'apporter un autre niveau d'analyse, l'électrophysiologie sur l'animal éveillé en comportement. L'association de ces différentes compétences me semble essentielle pour répondre aux questions suivantes :

- **Quelle est la signification de la pause des CINs pour la plasticité corticostriée ?** Cette partie sera réalisée *in vitro* sur des tranches de cerveau dans le laboratoire sous ma direction.
- **Est-ce que les afférences thalamostriatales affectent la plasticité corticostriée ? Cet effet passe-t-il par les CINs ?** Cette partie sera réalisée *in vivo* sur des souris anesthésiées et sera menée dans le laboratoire sous la responsabilité du Dr. Nicolas Maurice.

• **La pause des CINs affecte-t-elle les apprentissages associatifs ?** Ces expériences seront réalisées par le Dr. Nicolas Mallet à l'université de Bordeaux et ne seront pas détaillées dans ce rapport.

Ce projet a été pré-sélectionné par l'ANR en 2015 et 2016 mais n'a pas été retenu en phase finale. J'envisage de le resoumettre cette année. Le projet est détaillé, en anglais, dans les pages suivantes. J'encadre en ce moment Gwenaëlle Laverne qui a fait son Master 2 avec moi et qui a débuté sa thèse en 2016. Gwenaëlle travaille à plein temps sur ce projet et se charge de tous les enregistrements électrophysiologiques sur tranches de cerveaux et participe également à la gestion des souris transgéniques. Au-delà de ce questionnement sur le rôle des CINs dans les apprentissages et la plasticité corticostriée à long terme, qui constitue le cœur de mon travail, je collabore avec différentes personnes de façon ponctuelle sur des questions diverses en leur apportant ma compétence d'électrophysiologiste. Je ne détaillerai pas ces différents projets dans le manuscrit.

III.1 OBJECTIVES AND HYPOTHESES

Our driving hypothesis is that the cholinergic interneurons, by integrating thalamostriatal information, provide the striatum with behaviorally significant events that, in turn, enable long-term changes of corticostriatal transmission. Therefore, the thalamic gating of corticostriatal synaptic plasticity *via* CINs would be critical for sensor-motor transformation, striatal-dependent learning and could also be involved in mediating some of the behavioral abnormalities present in Parkinson's disease (PD).

Despite the fact that cholinergic interneurons (CINs) are well positioned to play an important role in the function of striatal circuit, especially in reward-dependent learning, several key questions remain unaddressed. Tonically active neurons (TANs) in the striatum, which are likely to be CINs, have been shown to have very interesting *in vivo* temporal dynamics, including a brief pause in their tonic firing which is often preceded and/or followed by bursts of activity around the time of salient or reward-predicting events. This complex response is synchronized among CINs that are widely scattered throughout the striatum. For several reasons, including a lack of appropriate tools, most of the studies do not replicate this very peculiar endogenous dynamics, hampering a full understanding of CIN functions in basal ganglia (BG)-related behaviors. The main strength of our proposal is to use **innovative cutting-edge techniques, such as optogenetics, transgenic mice and electrophysiological recordings (*in vitro/in vivo*), to test whether a physiologically-relevant pattern in CINs causally impacts long-term plasticity.** While optogenetics has been used so far to induce prolonged inhibition or activation of CINs, we propose here to go a step ahead by using this powerful technique to mimic or prevent the typical physiological response of CINs. We will address the following specific questions: first, what are the cellular actions mediated by CINs at the striatal level that could impact changes in BG-related behaviors? We will particularly focus on long-term corticostriatal plasticity, thought to be the cellular substrate of learning in the BG network. As the two main types of striatal output neurons form distinct functional subcircuits, we will identify them by using transgenic mice to determine whether CINs differentially affect plasticity in these two populations. Second, does CIN synchronization play a crucial role through a modulation of striatal plasticity? If it is increasingly clear that the precise timing and synchronous activity of CINs are critical to their function, how it happens in real life is still enigmatic. Here, we will decipher how the thalamic centromedian/parafascicular complex (CM/Pf), which processes stimuli with attentional value and massively target CINs, contributes to their temporal

dynamics and affects corticostriatal plasticity *via* CINs. Finally, considering that CINs, thalamostriatal inputs and corticostriatal plasticity exhibit profound dysfunctions after dopamine depletion, some experiments will be extended to the classical 6-OHDA rodent model of PD. These additional experiments will help understanding how this trio is affected by dopamine depletion and its causal contribution to the pathophysiology of the disease. To build a comprehensive system-level view of these interactions, our project is focused toward two main objectives:

- 1: determine the impact of the pause response of CINs on long-term plasticity in direct and indirect MSNs. We strongly believe that the effect of CINs on corticostriatal plasticity cannot be apprehended without considering the temporal dynamic of their typical pause response, which is closely associated with reward-associative learning. We have developed an optogenetic approach enabling us to mimic closely the physiological pause response in CINs, in striatal slices. We will therefore be able, by combining optogenetics with patch-clamp recordings, to analyze for the first time how a physiologically-relevant pattern induced in CINs impacts long-term corticostriatal plasticity in normal and parkinsonian conditions. As the differential expression of GPCRs in direct and indirect MSNs may reflect important differences in the way neuromodulators control synaptic plasticity, this question will be investigated in identified MSNs.

- 2: decipher whether CM/Pf inputs modulate corticostriatal long-term transmission through CINs.

Here, our hypothesis is that thalamostriatal inputs modulate corticostriatal long-term plasticity *via* CIN synchronization. We will investigate this issue *in vivo* in anesthetized mice by combining intracellular recordings of MSNs and optogenetic manipulations of CINs to block their recruitment by thalamic inputs. This preparation has two main advantages: it preserves the integrity of the thalamostriatal system and the “*in vivo*-like” activity of striatal output neurons that exhibit fluctuations in their membrane voltage known as up and down states. These experiments will thus provide crucial cues on the impact of the thalamically-driven pause in CINs on corticostriatal synaptic plasticity *in vivo*.

To address these issues, our project will be split-up in several tasks undertaken in parallel but all converging towards the same goal: underpinning the hypothesis that the thalamically-driven pause response in TANs is crucial for reward-related learning through a modulation of corticostriatal plasticity.

III.2 SCIENTIFIC BACKGROUND

III.2.1 The cellular basis of learning in the basal ganglia network: corticostriatal long-term plasticity

A primary function of the BG is the selection of appropriate actions that lead to positive outcome (Balleine et al., 2007). At the cellular level, such associative learning is thought to occur through long-term changes in synaptic strength at corticostriatal synapses. Disruption of this property is a common feature of many neurological disorders, both motor (Parkinson’s disease, Huntington disease...) and psychiatric (obsessive-compulsive disorder, autism spectrum disorder...). The long-term modulation of synaptic transmission efficacy is expressed as long-term potentiation (LTP) and depression (LTD). The vast majority of striatal cells are GABAergic projecting neurons, known as medium spiny neurons (MSNs), and exhibit both forms of plasticity. They receive massive glutamatergic inputs from the cortex

and the thalamus and project to downstream BG nuclei. MSNs can be categorized into two different subpopulations, based on their differential expression of G-protein-coupled receptors (GPCRs) and axonal projections (Gerfen et al., 1990; Smith et al., 1998). Striatonigral MSNs express D1 dopamine and muscarinic M4 acetylcholine receptors and project directly to the BG output nuclei, represented mainly in rodents by the substantia nigra pars reticulata (SNr), and are called direct MSNs. In contrast, striatopallidal MSNs, also called indirect MSNs, express D2 dopamine and A2A adenosine receptors and project indirectly to BG output nuclei *via* the external globus pallidus and the subthalamic nucleus. These pathways are thought to work in an antagonistic way during action selection although recent findings suggest cooperative interactions depending on the behavioral context (Cui et al., 2013). Data published until now suggest that the mechanisms involved in corticostriatal long-term plasticity are roughly similar in both the direct and indirect MSNs (Kreitzer and Malenka, 2008; Lovinger, 2010). However, a fundamental difference lies in the way neuromodulators gate plasticity in the two types of MSNs (Lerner and Kreitzer, 2011; Lovinger, 2010). Whereas it is now clearly established that the type and level of activation of dopamine receptors (D1 vs. D2) present on MSNs play a critical role in the control of corticostriatal plasticity (Centonze et al., 2001; Lovinger, 2010; Shen et al., 2008), much less is known about acetylcholine (ACh), especially on its differential effect on the two populations of MSNs. Both ionotropic nicotinic and metabotropic muscarinic receptors are expressed in the striatum, at presynaptic and postsynaptic levels. Pharmacological manipulations of cholinergic receptors have been shown to modulate corticostriatal plasticity *in vitro* (Bonsi et al., 2008; Calabresi et al., 1998, 1999) but these experiments are far from recapitulating the complex actions of CINs on striatal circuit. For instance, it is known that CINs co-release glutamate with ACh and that glutamate can also modulate striatal behavioral and cellular functions (Gras et al., 2008; Guzman et al., 2011; Higley et al., 2011). Determining the resulting effect of all these actions, which could sometimes oppose each other, is highly challenging. Although investigating the respective role of ACh and glutamate is beyond the scope of this project, we think that direct manipulation of CIN activity as proposed here will give a more accurate view of CIN functions. Most importantly, these interneurons exhibit an intriguing pattern of activity in response to salient events *in vivo* and it is very likely that the effects of CINs on corticostriatal plasticity depend on the temporal dynamic of their firing at a given moment in a specific context. **Hence, our understanding of CIN regulation of striatal function cannot be reached without considering the very particular features of their activity.**

III.2.2 Reward-related learning and striatal cholinergic interneurons

Learning is a complex process where one needs to use previous experience to guide behavior towards actions that have led to positive outcome in the past and away from actions that have led to negative outcome. In our daily life, this type of learning requires forming relationships between an action or a context and its potential outcome value, whether positive or negative. Such cognitive operation can be studied in rodents and primates that are trained to select an action (e.g. pressing a lever) in response to a stimulus (e.g. an auditory cue) that has been associated with a certain outcome value (e.g. often a reward). While it remains very challenging to record the electrical activity of neurons during the initial learning phase of such instrumental task, it is commonly accepted that the optimization of action outcome relies on an online associative learning process that is likely to share similar cellular basis as the ones described by *in vitro* synaptic plasticity experiments. In the BG, corticostriatal synapses need to be informed about which action will lead to the best outcomes. In

other words they need to select the most rewarding actions. Dopamine has long been considered as the principal modulatory component, providing “hedonistic” flavor to particular actions and participating in action selection. Indeed, a wealth of data has shown that dopamine released by substantia nigra pars compacta (SNc) neurons is playing a fundamental role in reward signaling by indicating a “reward prediction error” that signals the discrepancy between the prediction of a reward and its actual occurrence (Schultz, 2007). This teaching signal is essential to learn the value of stimuli in the environment. However, CINs also show very peculiar patterns of firing activity during reward-related learning. Despite their small numbers (1-3% of striatal cells) and scattered distribution throughout the striatum, CINs have dense terminal fields primarily directed to the two populations of MSNs that overlap those of dopaminergic projections (Bolam et al., 1984). Such a particular architecture positions them as potent modulators of striatal output. Unlike most striatal neurons recorded *in vitro*, CINs exhibit a regular spiking activity in the absence of synaptic input, demonstrating that their activity is autonomously generated (Bennett and Wilson, 1999). Extracellular recordings in the striatum also reveal the presence of tonically active neurons (TANs) *in vivo*, both in rodents and monkeys (Apicella et al., 1991; Wilson et al., 1990). The distribution of TANs is similar to that of choline acetyltransferase positive neurons, suggesting that TANs and CINs are one and the same (Aosaki et al., 1995). However, we will use the term TANs when referring to *in vivo* recordings. In the seminal study of Aosaki et al., (Aosaki et al., 1994a) the authors repeatedly paired neutral stimuli with reward presentation, and observed that the monkeys learned to respond to those stimuli that predict the reward. During acquisition of conditioning, TANs develop a transient suppression (pause) of their tonic firing, which is frequently flanked by brief excitations (bursts) in response to salient stimuli. The pause tends to be time-locked in TANs recorded at distant sites in the striatum (Aosaki et al., 1995). This observation strongly suggests that, besides SNc dopaminergic neurons, the coordinated response of TANs has also a fundamental role in reward signaling. However, the precise operational mode carried out by TANs remains difficult to apprehend. One possible reason to explain the lack of consensus is that most past studies have focused on describing the correlatives changes in the electrical activity of presumed-CINs during behavior. Key features of the relationship between dopaminergic and cholinergic inputs provide clues to their possible functional implications. For instance, the responses of CINs and SNc neurons are time-locked and inversely polarized: while dopaminergic neurons respond to reward-predicting events by a phasic increase in firing rate, CINs exhibit a coincident pause in their tonic activity (Morris et al., 2004). Moreover, the magnitude of dopaminergic responses is modulated according to reward probability whereas the pause in CINs seems more stereotyped (Morris et al., 2004; Tobler et al., 2005). Despite the apparent importance of CINs in learning, their precise role remains difficult to apprehend and a number of unsolved questions remain. First, the function of the dual representation of reward-related information by CINs and dopaminergic neurons is still enigmatic. Does the response of these two neuronal systems offer different meaning beyond the information conveyed by a single neuron type? A main current hypothesis suggests that CINs cooperate with the dopaminergic system, but carry a different meaning that has been proposed to teach the BG ‘when’ to form new learning as opposed to ‘what’ to learn (Bradfield et al., 2013; Morris et al., 2004). The pause in CIN firing and the resulting drop in ACh would create a permissive temporal window (a “sensitive” window) allowing long-term modulation of efficacy at corticostriatal synapses to facilitate learning (Deffains and Bergman, 2015). A second puzzling issue is the functional meaning of the brief increase in firing that could precede and/or follow the pause. If the pause is reliably observed after presentation of a reward-related stimulus, these bursts seem more labile and whether they engage some processes critical for learning is still unknown. This aspect needs specific investigation since it may account for a

fine temporal tuning of corticostriatal synapses. The early and/or late ACh release occurring during the bursts may modulate MSN responses, having a potential effect on the polarity of synaptic changes. Finally, another issue concerns the mechanisms responsible for the pause generation and its synchronization in CINs. While this matter is still debated, there is however unquestionable evidence showing that both dopamine from SNc neurons and the glutamatergic input from the thalamic CM/Pf complex are important for its generation (Aosaki et al., 1994b; Matsumoto et al., 2001; Raz et al., 1996). CM/Pf neurons, which respond to behaviorally significant sensory events, project to the entire striatal complex and massively target CINs in addition to MSNs (Matsumoto et al., 2001). This broad thalamic projection pattern might then be able to synchronize the scattered population of CINs but how it precisely impacts the striatal circuitry at the cellular level is still elusive. One hypothesis that will be addressed in this proposal is that thalamostriatal inputs modulate corticostriatal long-term plasticity *via* synchronizing the pause in CIN firing. The demonstration that activation of thalamic axons induces a burst-pause response in CINs, supports this hypothesis (Ding et al., 2010; Doig et al., 2014; Threlfell et al., 2012). Nevertheless, the causal relationship of such response and behavior still needs to be demonstrated and, more importantly, **the impact of the thalamically-driven synchronization in CINs on corticostriatal plasticity is still unknown.**

Considering the intimate link between ACh and dopamine, one could wonder what happens in pathological conditions in which the dopaminergic system is compromised such as in PD. Besides the well characterized impairment of corticostriatal long-term plasticity occurring after dopamine depletion (Centonze et al., 2001), there is also compelling evidence implicating CINs and their thalamic inputs from CM/Pf in PD pathophysiology. In a recent study from our lab, we demonstrated that optogenetic inhibition of CINs reduces parkinsonian motor deficits by, among other things, increasing the functional weight of the direct striatonigral pathway (Maurice et al., 2015). Although we employed a prolonged optogenetic inhibition in this study that did not replicate the *in vivo* dynamics of CINs, we nonetheless provided an experimental support to the longstanding hypothesis that poses PD as a striatal cholinergic disorder. We were also among the firsts to show that CM/Pf lesioning or high-frequency stimulation reversed some molecular changes induced by dopamine lesion and alleviated parkinsonian symptoms (Bacci et al., 2004; Jouve et al., 2010; Kerkerian-Le Goff et al., 2009). The positive outcome of CM/Pf inhibition on parkinsonian motor deficits was recently confirmed with a chemogenetic approach (Parker et al., 2016). Hence, both CINs and their major input coming from the CM/Pf appear as main players in the maladaptive changes following dopamine depletion, highlighting the need for a better understanding of their interactions.

To conclude, the development of the temporally coordinated pause observed in CINs seems critical for their function in reward-related learning and is likely to carry a different meaning than the burst response of dopaminergic neurons. The thalamostriatal inputs coming from the CM/Pf are well positioned to synchronize the pause response among CINs. However, the meaning of such neural signal and its overall impact on striatal network, particularly on corticostriatal plasticity and reward-related learning, is far from being understood. All these processes are altered following dopamine depletion and might be determinant in parkinsonian symptom expression. Deciphering how these different players interact with each other at the network and behavioral levels is then a key question to understand striatal function in health and disease.

III.3 MEANS FOR ACHIEVING THE OBJECTIVES

III.3.1 Generation and impact of the pause responses on corticostriatal long-term plasticity in direct and indirect MSNs

In this task, we will address the following points: can the typical pause response exhibited by CINs *in vivo* be mimicked *in vitro*? Does it affect corticostriatal long-term plasticity? Does the pause response differentially impact direct and indirect MSNs? All the experiments proposed in this section will be performed by patch-clamp recordings in striatal slices combined to optogenetics under the supervision of C. Beurrier.

Strategy to mimic the pause response of CINs in vitro

In vivo, the response of CINs to salient stimuli consisted in a transient reduction in firing rate that could sometimes be preceded and/or followed by an increase activity. The initial and late excitations flanking the pause are usually designed as burst and rebound, respectively. While the pause is robustly observed across different experimental paradigms, the functions of the burst and rebound are still enigmatic (Doig et al., 2014). To shed light on this complex multiphasic response, we will trigger the pause response in two different ways.

(1) Burst-pause sequence. In many circumstances, the pause response seems to be a direct result of excitatory inputs (e.g. CM/Pf inputs) (Schulz and Reynolds, 2013). This ability is explained, in part, by the intrinsic properties of CINs allowing them to generate membrane hyperpolarization following excitation (Bennett et al., 2000). We will then first use transgenic mice expressing Channelrhodopsin-2 (ChR2), a nonspecific cation channel that drives action potential firing under blue-light illumination, in cholinergic neurons to drive the pause in CINs (for clarity's sake, these mice will be subsequently referred to as ChR2 mice). Our preliminary data show that in such mice, blue light illumination (473 nm) evoked not only a burst of spikes but also a subsequent pause in CIN firing (burst-pause sequence, fig.17). To our knowledge, this is the first demonstration that a physiologically-relevant burst-pause response is induced *in vitro* in CINs with optogenetics. To check to what extent our optogenetically-induced response mimics the *in vivo* response, we will first determine the light parameters allowing to best replicate the pause-duration observed *in vivo*. A second crucial feature to mimic closely the *in vivo* situation is the synchronization of the response among a large population of CINs. Contrary to firing manipulation induced by intracellular current injection in individual CIN, optogenetic stimulation synchronizes CIN activity in striatal slices as described in a recent paper (Threlfell et al., 2012) and as shown in our recordings (fig.17). Another factor that might play a role in the generation of the *in vivo* response is dopamine. In striatal slices, the group of S. Cragg nicely showed that light-evoked firing in CINs is able to drive dopamine release from dopaminergic terminals *via* nACh receptor activation (Threlfell et al., 2012). To investigate whether our optogenetically-induced response does so, we will test the effects of nAChR or D2 receptor antagonists on the light-evoked pause. Finally to ensure that our optogenetically burst-pause sequence is relevant to the thalamically-driven response (as shown in our preliminary *in vivo* recordings, fig.19), we will test whether a similar pause response is elicited in CINs by activation of thalamostriatal ChR2-expressing axons. If this point is confirmed, we will use direct manipulation of CINs to avoid confounding effect of thalamic activation on MSNs in the following experiments.

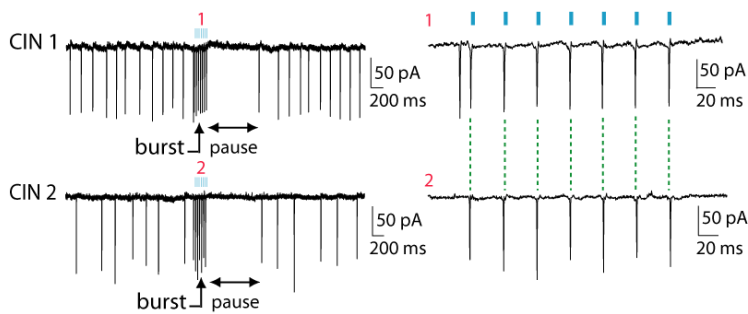


Figure 17: Optogenetic stimulation of Chr2-expressing CINs generates a burst-pause response. Sample traces of cell-attached recordings from 2 different CINs in response to pulses (5-ms pulse width, 30 Hz) of blue light illumination. As shown in the expanded traces on the right, synchronization of action potentials is achieved with pulses of light.

(2) Pause-rebound sequence. *In vivo*, some studies reported that in response to reward-predicting stimuli a substantial proportion of CINs exhibits a pause followed by a rebound without a preceding burst (Doig et al., 2014). Oswald et al., (Oswald et al., 2009) demonstrated that two types of inputs can trigger the pause: either a burst of spikes or a subthreshold excitatory synaptic input. This result might explain the occurrence of a pause without a preceding burst *in vivo*. However, a main functional difference between a burst-pause sequence and a pause-rebound sequence is the level of ACh released around the pause. In another word, is the ACh released during the initial burst or during the rebound engages some processes critical for the effect of the pause? To answer this question, we will also drive a pause in CINs without a preceding burst by using transgenic mice expressing halorhodopsin (eNpHR), a chloride pump that inhibits action potential firing under orange-light illumination. Our data show that in such mice, short illumination (500 ms) triggers an inhibition of firing rate followed by an increase in activity that closely looks like the pause-rebound sequence described *in vivo*.

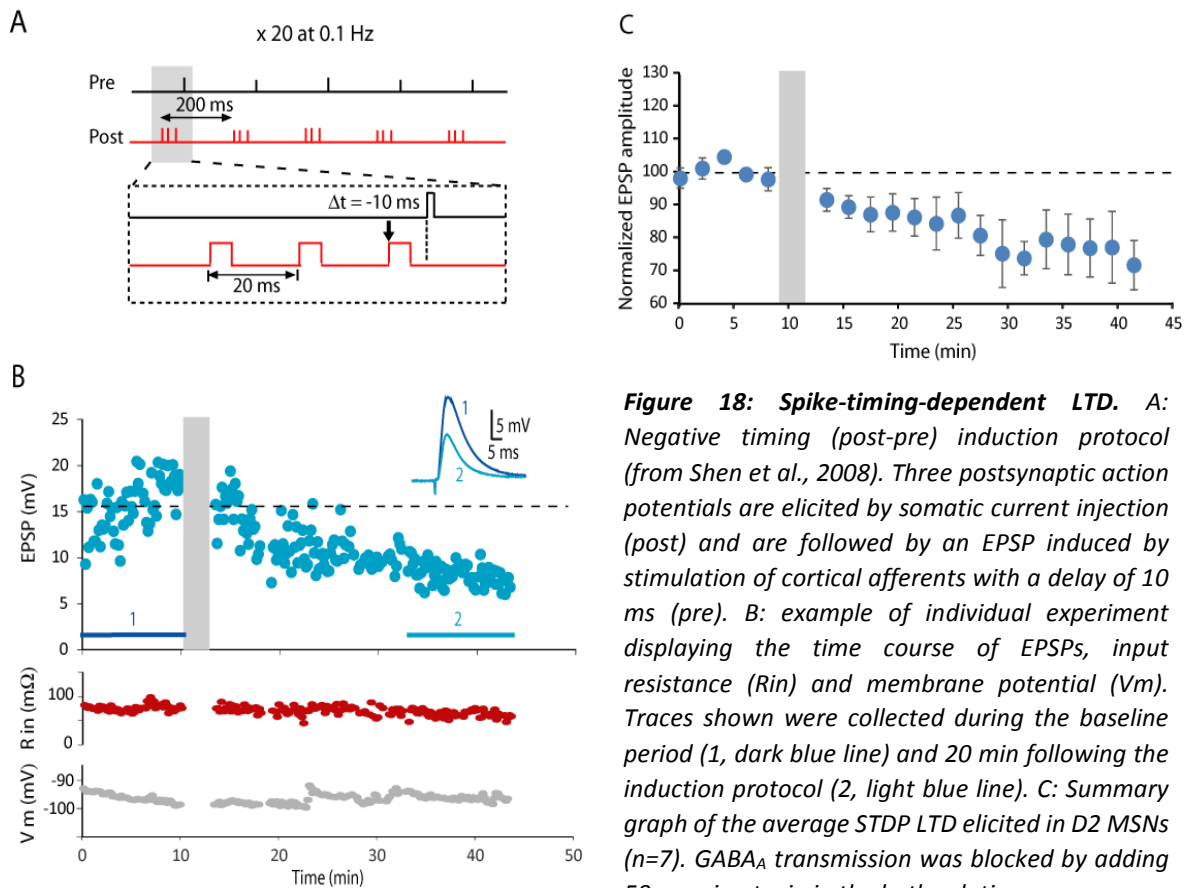
We will then compare the effects of the two types of optogenetically-driven pause (burst-pause or pause-rebound) on corticostriatal synaptic transmission (see below). These experiments will bring valuable information not only on the function of the pause itself but also on the burst and rebound flanking the pause.

A recent study indicates that the striatum also receives extrinsic cholinergic innervation from the brainstem (Dautan et al., 2014). To determine the potential contribution of this extrinsic input, some experiments will be done after injecting a Cre-dependent adeno-associated virus carrying Chr2 (pAAV-Ef1a-DIO-hChr2(H134R)-mCherry) in the striatum or brainstem of ChAT^{cre/cre} mice. We already used this viral strategy to target cholinergic neurons in our previous paper (Maurice et al., 2015).

All these experiments, and the following ones, are based on the assumption that optogenetic manipulation of CINs modulates ACh release. We think that checking this point is crucial for interpreting our data and we propose to implement in our lab fast-scan cyclic voltammetry using carbon fiber microelectrodes recently optimize by Asri et al., (Asri et al., 2016) to measure ACh concentration in striatal slice.

[Induction of long-term plasticity at corticostriatal synapses and modulation by the light-evoked response induced in CINs in normal and parkinsonian mice](#)

In this task, we seek to induce long-term plasticity at corticostriatal synapses in identified MSNs. As conventional high-frequency stimulation protocols might trigger the release of a mixture of neuromodulators that is poorly controlled, we will use more physiologically relevant setting such as spike-timing-dependent plasticity (STDP) protocols based on the near-coincidence between presynaptic input and postsynaptic spiking within a millisecond time scale. As LTD is more reliably induced and is the most characterized form of plasticity at corticostriatal synapses, we first focus on this form of plasticity. As STDP rules might differ in D1 and D2 MSNs (Paille et al., 2013; Shen et al., 2008), we will test our protocol in transgenic mice expressing the fluorescent reporter tdTomato in D1 receptor-containing neurons to identify MSN subtypes. Our preliminary data obtained in D2 MSNs show that we are able to induce STDP LTD according to the protocol described in Shen et al., (2008) (fig.18). We are currently testing this protocol in D1 MSNs.



We will then test whether the light-induced pause (burst-pause or pause-rebound) in CINs modulates LTD STDP in direct and indirect MSNs. ACh can affect plasticity in several ways by changing its polarity, the shape of the STDP window and/or the number of trials required to achieve plasticity. In a first step, optogenetic stimulation of CINs, as defined above, will be applied during the STDP protocol. In a second step, to be even closer to physiological conditions, we will also mimic the patterns recorded during the

instrumental associative learning in behaving animals. The exact timing and frequency of optogenetic stimulation necessary to modulate STDP will be determined experimentally.

Among the major changes that occur following dopamine depletion in PD, there is a loss of the pause response in TANs and an impairment of corticostriatal synaptic plasticity. To investigate whether these two pathological changes are causally linked, we will study the impact of the optogenetically-induced response in CINs on long-term plasticity in parkinsonian mice. These experiments will be conducted in a mouse model of PD based on the extensive unilateral lesion of dopamine neurons by intranigral injection of 6-OHDA. This mice PD model is routinely used in our lab and results in a near-total loss of nigral dopaminergic neurons in the injected side and their terminals in the ipsilateral striatum. Recordings will be made 2-3 weeks after 6-OHDA injections and the extent of the lesion will be systematically assessed by anti-tyrosine hydroxylase immunodetection. We will compare the effect of the optogenetically-induced pause in CINs on STDP in direct and indirect MSNs between naive and DA-depleted mice.

With these experiments, we expect to show that endogenous manipulation of ACh by our optogenetically-induced responses modulates corticostriatal STDP. These results might unravel novel findings highly instrumental to understand the role of CINs in reward-related learning. All the techniques used in this task are available in the lab except fast scan cyclic voltammetry. The technician associated to this project (C. Melon) has a strong experience in electrochemical neurotransmitter measurements and will be in charge of implementing this technique in the lab. All the transgenic lines necessary to perform this task (and the following one) are present in the lab (Maurice et al., 2015). The VGluT2 cre mice to drive ChR2 expression in thalamic neurons will be purchased at Jackson lab (stock #: 016963).

III.3.2 Impact of CINs and thalamostriatal system on corticostriatal long-term plasticity *in vivo* in anaesthetized mice

In this task, we will perform intracellular recordings of MSNs in anesthetized mice as shown in our preliminary results (fig. 19) to test whether STDP rules described *in vitro* operate *in vivo*. The *in vivo* situation provides an additional level of complexity mainly due to the fact that MSNs are the target of continuous barrages of ongoing presynaptic activity that leads to fluctuations in the membrane voltage of MSNs known as “up and down states”. A strong synchronization of corticostriatal neurons is required for a transition from the down (hyperpolarized) to the up (depolarized) state that could trigger action potentials. These naturally occurring spikes backpropagate throughout the neuron, potentially interacting with the vast number of dendritically located channels. We will specifically address the three following points: (i) how spikes and MSN up/down transitions affect corticostriatal plasticity? (ii) does CM/Pf stimulation affect plasticity at corticostriatal synapses and (iii) are CINs mediating the thalamic influence? The *in vivo* recordings combined to optogenetics will be performed in anaesthetized mice under the supervision of Nicolas Maurice.

Impact of the spontaneous synaptic activity in vivo on corticostriatal plasticity

Here, we will determine the experimental conditions that reliably induce, *in vivo* in anesthetized mice, plasticity at corticostriatal synapses in MSNs. *In vivo* intracellular recordings, that are essential for investigating the corticostriatal plasticity, require the use of anesthesia which imposes particular activity patterns on MSNs. Barbiturate anesthesia will be preferred to study corticostriatal plasticity since: (i) it induces, in MSNs, up and down states that are not as exacerbated as under

ketamine/xylazine and (ii) MSNs fire spikes at low frequency as observed in the awake situation. ECoG recorded from the dura above the cerebral cortex will be combined with intracellular recordings from the MSNs located within the corresponding projection field. Corticostriatal plasticity will be induced by post-pre pairing protocols, the presynaptic element being activated by electrical cortical stimulation. This stimulation will be driven either by naturally occurring spikes or by transitions from down to up states in the postsynaptic element, using a window discriminator. Pre-post pairing protocols will use direct current injection into MSNs through the recording electrode.

Impact of thalamostriatal system on corticostriatal plasticity

STDP depends not only on spike timing but also on multifactors such as neuromodulators, postsynaptic voltage (see above) or synaptic cooperativity, which refers to the need for multiple coactive synaptic inputs to generate sufficient depolarization or spiking to drive plasticity. The purpose of this part is to study whether the CM/Pf input directly or indirectly impacts corticostriatal plasticity *in vivo*. CM/Pf will be electrically stimulated while using STDP protocols to pair postsynaptic spikes or down to up transitions in MSNs with presynaptic cortical inputs as defined above. We will precisely determine the impact of the timing, the strength (number of spikes) and the frequency of CM/Pf stimulation relative to the activation of the presynaptic element.

Contribution of CINs to the thalamostriatal modulation of corticostriatal plasticity

CINs are a preferential target of CM/Pf which represents their main excitatory input. Here, we will determine whether and how the microcircuits involving CINs contribute to the gating of corticostriatal plasticity by the thalamostriatal system. To answer this question, the impact of CM/Pf stimulation on corticostriatal plasticity will be investigated while rendering ineffective the recruitment of CINs by the thalamic input. This will be done by optogenetic inhibition of CINs with halorhodopsin (eNpHR mice). In CINs, CM/Pf electrical stimulation induces a burst followed by a pause (fig.19B). Our preliminary data show that a brief (15 ms) optogenetic inhibition of CINs, 5 ms after CM/Pf stimulation, totally shunts the recruitment of CINs by CM/Pf, abolishing not only the burst but also the pause (fig.19B). We will also examine whether the sole burst-pause response evoked in CINs by their direct optogenetic activation (as described *in vitro*) mimics the effect of thalamic stimulation on corticostriatal synaptic plasticity.

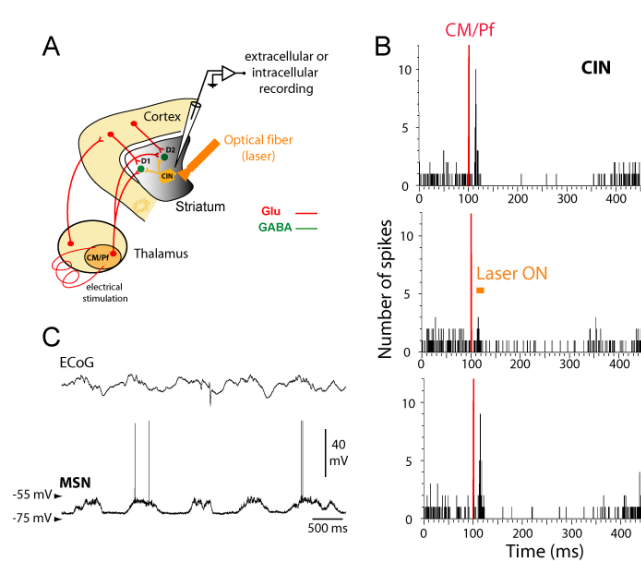


Figure 19: Responses of CINs to electrical stimulation of CM/Pf and intracellular recording of MSN in vivo. **A.** Schematic representation of the experimental set-up. **B.** Peristimulus time histograms of one eNpHR-expressing CIN responding to CM/Pf electrical stimulation before (left), during (middle) and after application of a 15-ms pulse width of yellow light. Glu: glutamate. **C.** Intracellular activity of a single MSN under ketamine-xylazine anesthesia simultaneously recorded with the corresponding ECoG. The membrane potential fluctuations consisted of depolarizing plateaus (-55 mV, up states) interrupted by hyperpolarizing periods (-72 mV, down states).

This part of the work will provide crucial information on two fundamental issues: (i) Does STDP have a functional relevance in corticostriatal synapses *in vivo*? Indeed, although striatal STDP has been shown *in vitro*, whether this process happens *in vivo* is still unknown and (ii) Does the thalamostriatal system impact the strength of corticostriatal synaptic connections *via* CINs? No STDP studies on MSNs have been conducted *in vivo* so far but literature relative to other synapses (Pawlak et al., 2013) demonstrate the feasibility of such approach. All the protocols and transgenic mice used in this task are available in the lab.

IV. REFERENCES

- Albin, R.L., Young, A.B., and Penney, J.B. (1989). The functional anatomy of basal ganglia disorders. *Trends Neurosci.* *12*, 366–375.
- Aosaki, T., Tsubokawa, H., Ishida, A., Watanabe, K., Graybiel, A.M., and Kimura, M. (1994a). Responses of tonically active neurons in the primate's striatum undergo systematic changes during behavioral sensorimotor conditioning. *J. Neurosci.* *14*, 3969–3984.
- Aosaki, T., Graybiel, A.M., and Kimura, M. (1994b). Effect of the nigrostriatal dopamine system on acquired neural responses in the striatum of behaving monkeys. *Science* *265*, 412–415.
- Aosaki, T., Kimura, M., and Graybiel, A.M. (1995). Temporal and spatial characteristics of tonically active neurons of the primate's striatum. *J. Neurophysiol.* *73*, 1234–1252.
- Apicella, P., Scarnati, E., and Schultz, W. (1991). Tonicly discharging neurons of monkey striatum respond to preparatory and rewarding stimuli. *Brain Res.* *84*, 672–675.
- Asri, R., O'Neill, B., Patel, J.C., Siletti, K.A., and Rice, M.E. (2016). Detection of evoked acetylcholine release in mouse brain slices. *Analyst* *141*, 6416–6421.
- Bacci, J.-J., Kachidian, P., Kerkerian-Le Goff, L., and Salin, P. (2004). Intralaminar Thalamic Nuclei Lesions: Widespread Impact on Dopamine Denervation-Mediated Cellular Defects in the Rat Basal Ganglia. *J. Neuropathol. Exp. Neurol.* *63*, 20–31.
- Balleine, B.W., Delgado, M.R., and Hikosaka, O. (2007). The role of the dorsal striatum in reward and decision-making. *J. Neurosci.* *27*, 8161–8165.
- Benazzouz, A., Breit, S., Koudsie, A., Pollak, P., Krack, P., and Benabid, A.-L. (2002). Intraoperative microrecordings of the subthalamic nucleus in Parkinson's disease. *Mov. Disord.* *17 Suppl 3*, S145-9.
- Bennett, B.D., and Wilson, C.J. (1999). Spontaneous Activity of Neostriatal Cholinergic Interneurons In Vitro. *J. Neurosci.* *19*, 5586–5596.
- Bennett, B.D., Callaway, J.C., and Wilson, C.J. (2000). Intrinsic membrane properties underlying spontaneous tonic firing in neostriatal cholinergic interneurons. *J. Neurosci.* *20*, 8493–8503.
- Bergman, H., Wichmann, T., Karmon, B., and DeLong, M.R. (1994). The primate subthalamic nucleus. II. Neuronal activity in the MPTP model of parkinsonism. *J. Neurophysiol.* *72*, 507–520.
- Bolam, J.P., Ingham, C.A., Izzo, P.N., Levey, A.I., Rye, D.B., Smith, A.D., and Wainer, B.H. (1986). Substance P-containing terminals in synaptic contact with cholinergic neurons in the neostriatum and basal forebrain: a double immunocytochemical study in the rat. *Brain Res.* *397*, 279–289.
- Bolam, J.P.P., Wainer, B.H.H., and Smith, A.D.D. (1984). Characterization of cholinergic neurons in the rat neostriatum. A combination of choline acetyltransferase immunocytochemistry, Golgi-impregnation and electron microscopy. *Neuroscience* *12*, 711–718.
- Bonsi, P., Martella, G., Cuomo, D., Platania, P., Sciamanna, G., Bernardi, G., Wess, J., and Pisani, A.

(2008). Loss of Muscarinic Autoreceptor Function Impairs Long-Term Depression But Not Long-Term Potentiation in the Striatum. *J. Neurosci.* *28*, 6258–6263.

Bradfield, L.A., Bertran-Gonzalez, J., Chieng, B., and Balleine, B.W. (2013). The thalamostriatal pathway and cholinergic control of goal-directed action: interlacing new with existing learning in the striatum. *Neuron* *79*, 153–166.

Calabresi, P., Centonze, D., Gubellini, P., Pisani, A., and Bernardi, G. (1998). Blockade of M2-like muscarinic receptors enhances long-term potentiation at corticostriatal synapses. *Eur. J. Neurosci.* *10*, 3020–3023.

Calabresi, P., Centonze, D., Gubellini, P., and Bernardi, G. (1999). Activation of M1-like muscarinic receptors is required for the induction of corticostriatal LTP. *Neuropharmacology* *38*, 323–326.

Calabresi, P., Picconi, B., Tozzi, A., Ghiglieri, V., and Di Filippo, M. (2014). Direct and indirect pathways of basal ganglia: a critical reappraisal. *Nat. Neurosci.* *17*, 1022–1030.

Centonze, D., Picconi, B., Gubellini, P., Bernardi, G., and Calabresi, P. (2001). Dopaminergic control of synaptic plasticity in the dorsal striatum. *Eur. J. Neurosci.* *13*, 1071–1077.

Cui, G., Jun, S.B., Jin, X., Pham, M.D., Vogel, S.S., Lovinger, D.M., and Costa, R.M. (2013). Concurrent activation of striatal direct and indirect pathways during action initiation. *Nature* *494*, 238–242.

Dautan, D., Huerta-Ocampo, I., Witten, I.B., Deisseroth, K., Bolam, J.P., Gerdjikov, T., and Mena-Segovia, J. (2014). A major external source of cholinergic innervation of the striatum and nucleus accumbens originates in the brainstem. *J Neurosci* *34*, 4509–4518.

Deffains, M., and Bergman, H. (2015). Striatal cholinergic interneurons and cortico-striatal synaptic plasticity in health and disease. *Mov. Disord.* *30*, 1014–1025.

DeLong, M.R. (1990). Primate models of movement disorders of basal ganglia origin. *Trends Neurosci.* *13*, 281–285.

Ding, J.B., Guzman, J.N., Peterson, J.D., Goldberg, J. a., and Surmeier, D.J. (2010). Thalamic gating of corticostriatal signaling by cholinergic interneurons. *Neuron* *67*, 294–307.

Doig, N.M., Magill, P.J., Apicella, P., Bolam, J.P., and Sharott, A. (2014). Cortical and thalamic excitation mediate the multiphasic responses of striatal cholinergic interneurons to motivationally salient stimuli. *J. Neurosci.* *34*, 3101–3117.

Durieux, P.F., Schiffmann, S.N., and de Kerchove, d’Exaerde A. (2012). Differential regulation of motor control and response to dopaminergic drugs by D1R and D2R neurons in distinct dorsal striatum subregions. *EMBO J.* *31*, 640–653.

Gerfen, C.R., Engber, T.M., Mahan, L.C., Susel, Z., Chase, T.N., Monsma Jr., F.J., Sibley, D.R., Monsma, F.J., and Sibley, D.R. (1990). D1 and D2 dopamine receptor-regulated gene expression of striatonigral and striatopallidal neurons. *Science* *250*, 1429–1432.

Gertler, T.S., Chan, C.S., and Surmeier, D.J. (2008). Dichotomous anatomical properties of adult striatal

medium spiny neurons. *J. Neurosci.* *28*, 10814–10824.

Goda, Y., and Stevens, C.F. (1994). Two components of transmitter release at a central synapse. *Proc. Natl. Acad. Sci. U. S. A.* *91*, 12942–12946.

Gong, S., Zheng, C., Doughty, M.L., Losos, K., Didkovsky, N., Schambra, U.B., Nowak, N.J., Joyner, A., Leblanc, G., Hatten, M.E., et al. (2003). A gene expression atlas of the central nervous system based on bacterial artificial chromosomes. *Nature* *425*, 917–925.

Gras, C., Amilhon, B., Lepicard, E.M., Poirel, O., Vinatier, J., Herbin, M., Dumas, S., Tzavara, E.T., Wade, M.R., Nomikos, G.G., et al. (2008). The vesicular glutamate transporter VGLUT3 synergizes striatal acetylcholine tone. *Nat. Neurosci.* *11*, 292–300.

Guzman, M.S., De Jaeger, X., Raulic, S., Souza, I.A., Li, A.X., Schmid, S., Menon, R.S., Gainetdinov, R.R., Caron, M.G., Bartha, R., et al. (2011). Elimination of the vesicular acetylcholine transporter in the striatum reveals regulation of behaviour by cholinergic-glutamatergic co-transmission. *PLoS Biol.* *9*, e1001194.

Harvey, J., and Lacey, M.G. (1996). Endogenous and exogenous dopamine depress EPSCs in rat nucleus accumbens in vitro via D1 receptors activation. *J. Physiol.* *492 (Pt 1)*, 143–154.

Harvey, J., and Lacey, M.G. (1997). A postsynaptic interaction between dopamine D1 and NMDA receptors promotes presynaptic inhibition in the rat nucleus accumbens via adenosine release. *J. Neurosci.* *17*, 5271–5280.

Hassani, O.K., Mouroux, M., and Féger, J. (1996). Increased subthalamic neuronal activity after nigral dopaminergic lesion independent of disinhibition via the globus pallidus. *Neuroscience* *72*, 105–115.

Higley, M.J., Gittis, A.H., Oldenburg, I.A., Balthasar, N., Seal, R.P., Edwards, R.H., Lowell, B.B., Kreitzer, A.C., and Sabatini, B.L. (2011). Cholinergic interneurons mediate fast VGLUT3-dependent glutamatergic transmission in the striatum. *PLoS One* *6*, e19155.

Hollerman, J.R., and Grace, A.A. (1992). Subthalamic nucleus cell firing in the 6-OHDA-treated rat: basal activity and response to haloperidol. *Brain Res.* *590*, 291–299.

Jouve, L., Salin, P., Melon, C., and Kerkerian-Le Goff, L. (2010). Deep brain stimulation of the center median-parafascicular complex of the thalamus has efficient anti-parkinsonian action associated with widespread cellular responses in the basal ganglia network in a rat model of Parkinson's disease. *J. Neurosci.* *30*, 9919–9928.

Kalivas, P.W., and Stewart, J. (1991). Dopamine transmission in the initiation and expression of drug- and stress-induced sensitization of motor activity. *Brain Res. Brain Res. Rev.* *16*, 223–244.

Kerkerian-Le Goff, L., Bacci, J.-J., Jouve, L., Melon, C., and Salin, P. (2009). Impact of surgery targeting the caudal intralaminar thalamic nuclei on the pathophysiological functioning of basal ganglia in a rat model of Parkinson's disease. *Brain Res. Bull.* *78*, 80–84.

Kravitz, A. V., Freeze, B.S., Parker, P.R., Kay, K., Thwin, M.T., Deisseroth, K., and Kreitzer, A.C. (2010).

Regulation of parkinsonian motor behaviours by optogenetic control of basal ganglia circuitry. *Nature* 466, 622–626.

Kreiss, D.S., Mastropietro, C.W., Rawji, S.S., and Walters, J.R. (1997). The response of subthalamic nucleus neurons to dopamine receptor stimulation in a rodent model of Parkinson's disease. *J. Neurosci.* 17, 6807–6819.

Kreitzer, A.C., and Malenka, R.C. (2007). Endocannabinoid-mediated rescue of striatal LTD and motor deficits in Parkinson's disease models. *Nature* 445, 643–647.

Kreitzer, A.C., and Malenka, R.C. (2008). Striatal Plasticity and Basal Ganglia Circuit Function. *Neuron* 60, 543–554.

Lerner, T.N., and Kreitzer, A.C. (2011). Neuromodulatory control of striatal plasticity and behavior. *Curr. Opin. Neurobiol.* 21, 322–327.

Lobo, M.K., Karsten, S.L., Gray, M., Geschwind, D.H., and Yang, X.W. (2006). FACS-array profiling of striatal projection neuron subtypes in juvenile and adult mouse brains. *Nat. Neurosci.* 9, 443–452.

Lovinger, D.M. (2010). Neurotransmitter roles in synaptic modulation, plasticity and learning in the dorsal striatum. *Neuropharmacology* 58, 951–961.

Matsumoto, N., Minamimoto, T., Graybiel, a M., and Kimura, M. (2001). Neurons in the thalamic CM-Pf complex supply striatal neurons with information about behaviorally significant sensory events. *J. Neurophysiol.* 85, 960–976.

Maurice, N., Deniau, J.M., Glowinski, J., and Thierry, A.M. (1999). Relationships between the prefrontal cortex and the basal ganglia in the rat: physiology of the cortico-nigral circuits. *J. Neurosci.* 19, 4674–4681.

Maurice, N., Liberge, M., Jaouen, F., Ztaou, S., Hanini, M., Camon, J., Deisseroth, K., Amalric, M., Kerkerian-Le Goff, L., and Beurrier, C. (2015). Striatal Cholinergic Interneurons Control Motor Behavior and Basal Ganglia Function in Experimental Parkinsonism. *Cell Rep.* 13, 657–666.

Morris, G., Arkadir, D., Nevet, A., Vaadia, E., and Bergman, H. (2004). Coincident but distinct messages of midbrain dopamine and striatal tonically active neurons. *Neuron* 43, 133–143.

Nicola, S.M., and Malenka, R.C. (1998). Modulation of synaptic transmission by dopamine and norepinephrine in ventral but not dorsal striatum. *J. Neurophysiol.* 79, 1768–1776.

Nicola, S.M., Kombian, S.B., and Malenka, R.C. (1996). Psychostimulants depress excitatory synaptic transmission in the nucleus accumbens via presynaptic D1-like dopamine receptors. *J. Neurosci.* 16, 1591–1604.

Oswald, M.J., Oorschot, D.E., Schulz, J.M., Lipski, J., and Reynolds, J.N.J. (2009). IH current generates the afterhyperpolarisation following activation of subthreshold cortical synaptic inputs to striatal cholinergic interneurons. *J. Physiol.* 587, 5879–5897.

Paille, V., Fino, E., Du, K., Morera-Herreras, T., Perez, S., Kotaleski, J.H., and Venance, L. (2013).

GABAergic Circuits Control Spike-Timing-Dependent Plasticity. *J. Neurosci.* *33*, 9353–9363.

Parent, A., and Hazrati, L.N. (1995). Functional anatomy of the basal ganglia. II. The place of subthalamic nucleus and external pallidum in basal ganglia circuitry. *Brain Res. Brain Res. Rev.* *20*, 128–154.

Parker, P.R.L., Lalive, A.L., and Kreitzer, A.C. (2016). Pathway-Specific Remodeling of Thalamostriatal Synapses in Parkinsonian Mice. *Neuron* *89*, 734–740.

Pawlak, V., Greenberg, D.S., Sprekeler, H., Gerstner, W., and Kerr, J.N.D. (2013). Changing the responses of cortical neurons from sub- to suprathreshold using single spikes in vivo. *Elife* *2*, e00012.

Raz, A., Feingold, A., Zelanskaya, V., Vaadia, E., and Bergman, H. (1996). Neuronal synchronization of tonically active neurons in the striatum of normal and parkinsonian primates. *J. Neurophysiol.* *76*, 2083–2088.

Robinson, T.E., and Berridge, K.C. (1993). The neural basis of drug craving: an incentive-sensitization theory of addiction. *Brain Res. Brain Res. Rev.* *18*, 247–291.

Robledo, P., and Féger, J. (1990). Excitatory influence of rat subthalamic nucleus to substantia nigra pars reticulata and the pallidal complex: electrophysiological data. *Brain Res.* *518*, 47–54.

Rodriguez-Oroz, M.C., Rodriguez, M., Guridi, J., Mewes, K., Chockkman, V., Vitek, J., DeLong, M.R., and Obeso, J.A. (2001). The subthalamic nucleus in Parkinson's disease: somatotopic organization and physiological characteristics. *Brain* *124*, 1777–1790.

Ryan, L.J., and Sanders, D.J. (1994). Subthalamic nucleus and globus pallidus lesions alter activity in nigrothalamic neurons in rats. *Brain Res.* *34*, 19–26.

Ryan, L.J., Sanders, D.J., and Clark, K.B. (1992). Auto- and cross-correlation analysis of subthalamic nucleus neuronal activity in neostriatal- and globus pallidal-lesioned rats. *Brain Res.* *583*, 253–261.

Salin, P., Lopez, I.P., Kachidian, P., Barroso-Chinea, P., Rico, A.J., Gomez-Bautista, V., Coulon, P., Kerkerian-Le, G.L., and Lanciego, J.L. (2009). Changes to interneuron-driven striatal microcircuits in a rat model of Parkinson's disease. *Neurobiol.Dis.* *34*, 545–552.

Santini, E., Alcacer, C., Cacciatore, S., Heiman, M., Herve, D., Greengard, P., Girault, J.A., Valjent, E., and Fisone, G. (2009). L-DOPA activates ERK signaling and phosphorylates histone H3 in the striatonigral medium spiny neurons of hemiparkinsonian mice. *J.Neurochem.* *108*, 621–633.

Schultz, W. (2007). Multiple dopamine functions at different time courses. *Annu. Rev. Neurosci.* *30*, 259–288.

Schulz, J.M., and Reynolds, J.N.J. (2013). Pause and rebound: sensory control of cholinergic signaling in the striatum. *Trends Neurosci.* *36*, 41–50.

Shen, W., Flajolet, M., Greengard, P., and Surmeier, D.J. (2008). Dichotomous dopaminergic control of striatal synaptic plasticity. *Science* *321*, 848–851.

Smith, Y., Bevan, M.D., Shink, E., and Bolam, J.P. (1998). Microcircuitry of the direct and indirect

pathways of the basal ganglia. *Neuroscience* 86, 353–387.

Thomas, M.J., Malenka, R.C., and Bonci, A. (2000). Modulation of long-term depression by dopamine in the mesolimbic system. *J. Neurosci.* 20, 5581–5586.

Threlfell, S., Lalic, T., Platt, N.J., Jennings, K.A., Deisseroth, K., and Cragg, S.J. (2012). Striatal dopamine release is triggered by synchronized activity in cholinergic interneurons. *Neuron* 75, 58–64.

Tobler, P.N., Fiorillo, C.D., and Schultz, W. (2005). Adaptive Coding of Reward Value by Dopamine Neurons. *Science* (80-.). 307, 1642–1645.

Vanderschuren, L.J., and Kalivas, P.W. (2000). Alterations in dopaminergic and glutamatergic transmission in the induction and expression of behavioral sensitization: a critical review of preclinical studies. *Psychopharmacology (Berl)*. 151, 99–120.

Wilson, C.J., Chang, H.T., and Kitai, S.T. (1990). Firing patterns and synaptic potentials of identified giant aspiny interneurons in the rat neostriatum. *J. Neurosci.* 10, 508–519.

Wolf, M.E. (1998). The role of excitatory amino acids in behavioral sensitization to psychomotor stimulants. *Prog. Neurobiol.* 54, 679–720.

V. ARTICLES

Subthalamic Nucleus Neurons Switch from Single-Spike Activity to Burst-Firing Mode

Corinne Beurrier,¹ Patrice Congar,² Bernard Bioulac,¹ and Constance Hammond³

¹Université de Bordeaux II, Centre National de la Recherche Scientifique Unité Mixte de Recherche 5543, 33076 Bordeaux cédex, France, ²Université René Descartes, Institut National de la Santé et de la Recherche Médicale U 29, 75674 Paris cédex 14, France, and ³Centre Paul Broca, Institut National de la Santé et de la Recherche Médicale U 159, 75014 Paris, France

The modification of the discharge pattern of subthalamic nucleus (STN) neurons from single-spike activity to mixed burst-firing mode is one of the characteristics of parkinsonism in rat and primates. However, the mechanism of this process is not yet understood. Intrinsic firing patterns of STN neurons were examined in rat brain slices with intracellular and patch-clamp techniques. Almost half of the STN neurons that spontaneously discharged in the single-spike mode had the intrinsic property of switching to pure or mixed burst-firing mode when the membrane was hyperpolarized from -41.3 ± 1.0 mV (range, -35 to -50 mV; $n = 15$) to -51.0 ± 1.0 mV (range, -42 to -60 mV; $n = 20$). This switch was greatly facilitated by activation of metabotropic glutamate receptors with 1S,3R-ACPD. Recurrent membrane oscillations underlying burst-firing mode were endogenous and Ca^{2+} -dependent because they were largely reduced by nifedipine ($3 \mu\text{M}$), Ni^{2+} ($40 \mu\text{M}$), and BAPTA-AM

(10 – $50 \mu\text{M}$) at any potential tested, whereas TTX ($1 \mu\text{M}$) had no effect. In contrast, simultaneous application of TEA (1 mM) and apamin ($0.2 \mu\text{M}$) prolonged burst duration. Moreover, in response to intracellular stimulation at hyperpolarized potentials, a plateau potential with a voltage and ionic basis similar to those of spontaneous bursts was recorded in 82% of the tested STN neurons, all of which displayed a low-threshold Ni^{2+} -sensitive spike. We propose that recurrent membrane oscillations during bursts result from the sequential activation of T/R- and L-type Ca^{2+} currents, a Ca^{2+} -activated inward current, and Ca^{2+} -activated K^+ currents.

Key words: tonic and bursting activities of STN neurons in slices; burst ionic mechanisms; low-threshold spike; Ca^{2+} -dependent plateau potential; intracellular and patch-clamp recordings; Parkinson's disease

The subthalamic nucleus (STN) is composed of glutamatergic neurons that control the circuitry of the basal ganglia by modulating the activity of the two principal output structures of the network: the internal pallidal segment and the substantia nigra pars reticulata (for review, see Albin et al., 1989; DeLong, 1990; Parent and Hazrati, 1995; Mink, 1996; Féger et al., 1997). The importance of this control is exemplified by the various consequences of STN lesion in both control animals and animal models of Parkinson's disease.

Electrolytic lesions of the STN in normal monkeys produce a hyperkinetic syndrome (Whittier and Mettler, 1949). This has also been reproduced by toxic lesions restricted to the STN, sparing the fibers of passage (Hammond et al., 1979; Hamada and DeLong, 1992), transient pharmacological blockade of STN activity (Crossman et al., 1984), and high-frequency STN stimulation (Beurrier et al., 1997). All these observations reflect the importance of the control exerted by the STN in control animals and provide an explanation for the violent, involuntary move-

ments of the contralateral limbs (termed "hemiballism") that occur in STN-lesioned humans (Martin, 1927; Bathia and Marsden, 1994). Manipulating STN neurons in animal models of Parkinson's disease leads to a very different consequence. In monkeys treated with the neurotoxic 1-methyl-4-phenyl-1,2,3,6-tetrahydropyridine (MPTP), STN lesion (Bergman et al., 1990; Aziz et al., 1991; Guridi et al., 1996), pharmacological blockade of the subthalamopallidal pathway (Graham et al., 1990; Brotchie et al., 1991), or high-frequency stimulation of the STN (Benazzouz et al., 1993), produce a reduction in motor impairments. These results suggest that STN constitutes a good therapeutic target for the treatment of Parkinson's disease. For this reason, high-frequency stimulation of the STN is being performed in several patients suffering from severe parkinsonism and gives very consistent results (Limousin et al., 1995).

To understand how the activity of STN neurons can regulate the operational mode of basal ganglia, it is essential to determine in detail the electrical properties of STN neurons and the underlying ionic mechanisms in physiological conditions *in vitro*. Previous studies have described the responses of STN neurons to intracellular current pulses (Nakanishi et al., 1987; Overton and Greenfield, 1995; Overton et al., 1995; Plenz et al., 1997). However, their ionic basis, as well as those of spontaneous firing patterns, have not been fully characterized. We now report, with the use of intracellular and patch-clamp techniques in rat brain slices, that a substantial proportion of STN neurons can shift from a regular single-spike mode to a burst-firing mode. We have analyzed the intrinsic membrane properties underlying this prop-

Received Oct. 13, 1998; accepted Oct. 29, 1998.

This work was supported by grants from Centre National de la Recherche Scientifique, Fondation pour la Recherche Médicale, Conseil Régional d'Aquitaine, and Université de Bordeaux II. C.B. has a scholarship from Ministère de l'Enseignement Supérieur et de la Recherche (French Ministry of Research and Higher Education) and from the Lilly Institute. We thank S. Olliet and A. Taupignon for their comments on this manuscript, J. Audin, R. Bonhomme, J. M. Calvinhac, and G. Gaurier for technical assistance. Outstanding thanks to J. M. Israel.

Correspondence should be addressed to Corinne Beurrier, Université de Bordeaux II, Centre National de la Recherche Scientifique Unité Mixte de Recherche 5543, 146 rue Léo Saignat, 33 076 Bordeaux cédex, France.

Copyright © 1999 Society for Neuroscience 0270-6474/99/190599-11\$05.00/0

erty and propose that this electrical behavior provides a cellular substrate for the functional role of the STN in controlling movements under normal and altered conditions.

MATERIALS AND METHODS

Slice preparation. Experiments were performed on STN neurons in slices obtained from 20- to 28-d-old male Wistar rats. Rats were anesthetized with ether and decapitated. The brain was quickly removed, and a block of tissue containing the STN was isolated on ice in a 0–5°C oxygenated solution containing (in mM): 1.15 NaH_2PO_4 , 2 KCl, 26 NaHCO_3 , 7 MgCl_2 , 0.5 CaCl_2 , 11 glucose, and 250 saccharose, equilibrated with 95% O_2 and 5% CO_2 , pH 7.4. This cold solution, with a low NaCl and CaCl_2 content, improved tissue viability. In the same medium, 300- to 400- μm -thick coronal slices were prepared using a Vibratome (Campden Instruments LTD, Loughborough, UK) and were then incubated at room temperature in a Krebs' solution containing (in mM): 124 NaCl, 3.6 KCl, 1.25 HEPES, 26 NaHCO_3 , 1.3 MgCl_2 , 2.4 CaCl_2 , and 10 glucose, equilibrated with 95% O_2 and 5% CO_2 , pH 7.4. After a 2 hr recovery period, STN slices were transferred one at a time to an interface-type recording chamber, maintained at $30 \pm 2^\circ\text{C}$ and continuously superfused (1–1.5 ml/minute) with the oxygenated Krebs' solution.

Electrophysiological recordings. Slices were visualized using a dissecting microscope, and the recording electrode was precisely positioned in the STN. Electrophysiological recordings of STN neurons were performed in current-clamp mode using the intracellular or patch-clamp technique. Signals were recorded using an Axoclamp 2A (Axon Instruments, Foster City, CA) in bridge or continuous single-electrode voltage-clamp mode for intracellular and patch-clamp experiments, respectively.

For intracellular recordings, microelectrodes were pulled from filamented borosilicate glass (BF-100–50–10; Sutter Instruments, Novato,

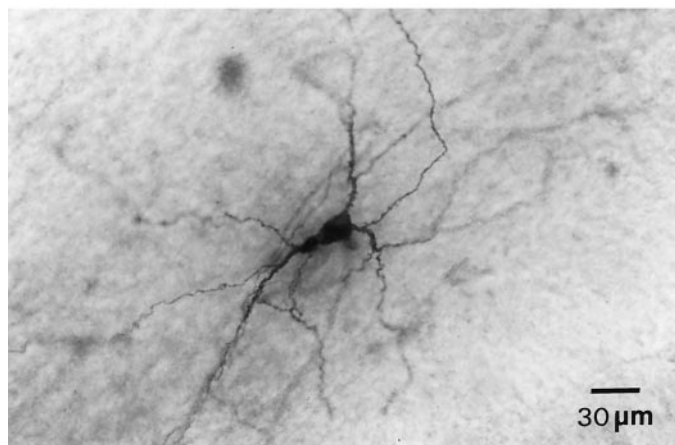
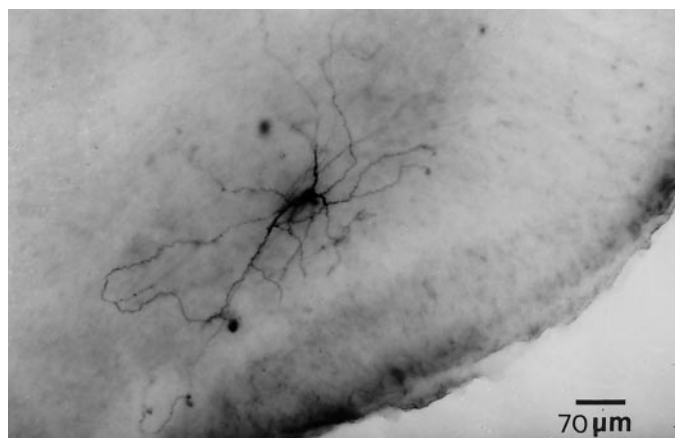


Figure 1. Microphotographs of a biocytin-filled STN neuron at two magnifications. The labeled neuron is located within the boundaries of the STN (*top*) and presents a dense dendritic arborization (*top*) and numerous spines on dendrites (*bottom*).

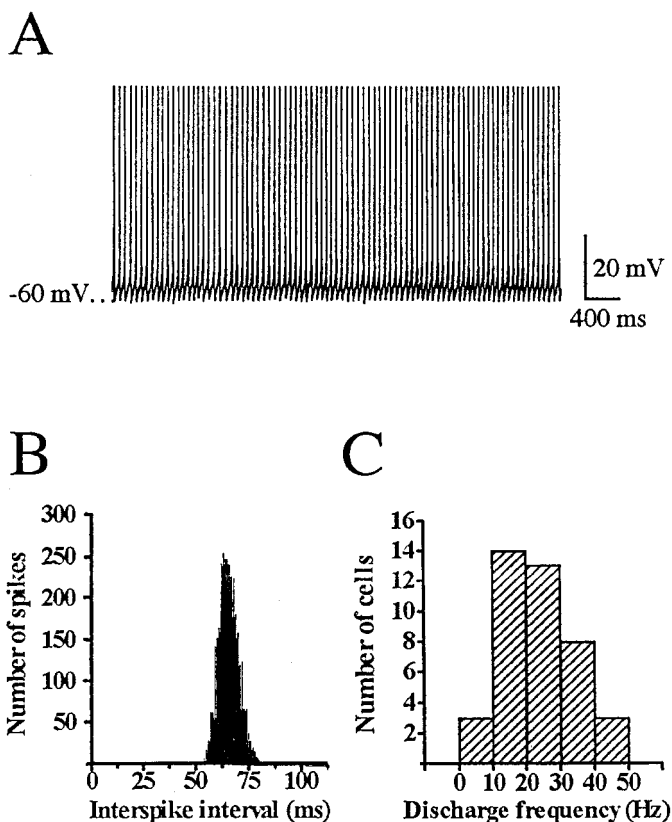


Figure 2. Single-spike mode. *A*, Tonic and regular activity (single-spike mode) of an STN neuron, recorded with intracellular techniques at resting membrane potential and (*B*) corresponding interspike interval histogram (mean interval, 66.1 ± 15.6 msec; bin width, 12.5 msec). *C*, Discharge frequency histogram of single-spike mode recorded in 41 STN neurons (mean frequency, 22.3 ± 1.5 Hz; bin width, 10 Hz). Spikes in *A* are truncated.

CA) on a horizontal Flaming–Brown micropipette puller (P-87; Sutter Instruments). They had a resistance of 150–200 M Ω when filled with 2 M potassium acetate. For patch-clamp experiments, recordings were made using the blind patch-clamp technique in the cell-attached or whole-cell configuration. Patch electrodes were pulled from filamented borosilicate thin-wall glass capillaries (GC150F-15; Clark Electromedical Instruments, Pangbourne, UK) with a vertical puller (LM-3P-A; List Instruments, Darmstadt-Eberstad, Germany) and had a resistance of 10–12 M Ω when filled with (in mM): 120 Kgluconate, 10 KCl, 10 NaCl, 10 EGTA, 10 HEPES, 1 CaCl_2 , 2 MgATP, and 0.5 GTP, pH 7.25.

Drugs. All drugs were purchased from Sigma (St. Louis, MO), except 1*S*,3*R*-1-aminocyclopentane-1,3-dicarboxylate (1*S*,3*R*-ACPD) purchased from Tocris Cookson (Bristol, UK) and tetrodotoxin (TTX) and apamin purchased from Latoxan (Rosans, France). Biocytin and 1,2-bis(2-aminophenoxy)-ethane-*N,N,N',N'*-tetraacetic acid (BAPTA) were diluted in the pipette solutions. All other drugs were diluted in the oxygenated Krebs' solution and applied through this superfusion medium. Nifedipine and BAPTA-AM were dissolved in dimethylsulfoxide (final concentration, 0.03–0.5%). For experiments with cobalt (Co^{2+}), calcium (Ca^{2+})-free (Ca^{2+} was substituted for equimolar concentration of Co^{2+}) or low Ca^{2+} solutions (0.4 mM with 2 mM Co^{2+}) were used.

Histology. In some experiments, recordings were performed with pipette solution containing biocytin (0.5–1%) to allow the subsequent identification and morphological analysis of the recorded neurons. The avidin–biotinylated horseradish peroxidase (ABC complex) reaction was used to visualize the biocytin-filled neurons. After recording, slices were fixed for 1–2 d in a solution containing 4% paraformaldehyde and 0.15% picric acid in phosphate buffer (0.1 M, pH 7.4) at 4°C. After several rinsings in Tris-buffered saline (TBS; 0.05 M, pH 7.4), the sections were treated with a mixture of methanol and H_2O_2 for 30 min, rinsed again in TBS, and processed for 2 or 3 d with the standard ABC complex

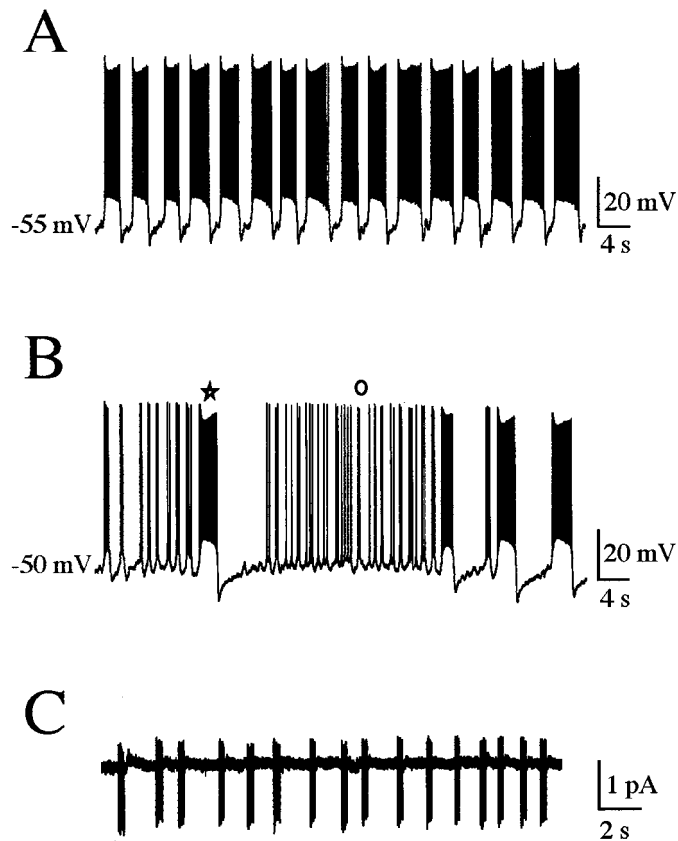


Figure 3. Burst-firing mode. Two types of burst mode recorded with patch-clamp techniques in two different STN neurons: pure burst mode (*A*) and mixed burst mode (*B*), consisting of long bursts (*) separated by sequences of short bursts (○). *C*, Spontaneous bursts recorded in the cell-attached configuration in voltage-clamp mode.

(Vectastain ABC kit, Vector laboratories, Burlingame, CA) at 4°C. After several washes in TBS, sections were treated with diaminobenzidine as a chromogen and H₂O₂ for 5–10 min (DAB substrate peroxidase kit; Vector Laboratories). The sections were then rinsed several times in TBS, dehydrated and rehydrated in graded ethanol, stained with cresyl violet, dehydrated again in graded ethanol, cleared in xylene, and mounted in Eukitt (053–47505; Labonord, Villeneuve d'Ascq, France).

Data analysis. Current and voltage outputs were displayed simultaneously on a storage oscilloscope and a four-channel chart recorder (Gould Instruments, Longjumeau, France), digitized (DR-890; NeuroData Instruments, New York, NY), and stored on a videotape for subsequent off-line analysis with pClamp6 software (Axon Instruments). Values are expressed as mean ± SEM. Statistical significance was assessed using the Student's *t* test (unpaired data). Parameters of the single-spike and bursting modes were quantified from intracellular and patch-clamp recordings, respectively.

RESULTS

Morphology and passive membrane properties of STN neurons

Results were obtained from 141 STN neurons. The soma of biocytin-filled recorded neurons (*n* = 5) were all located within the boundaries of the STN identified with the cresyl violet staining technique (Fig. 1*A*). Soma had diameters of 10–25 μm and gave rise to four or five dendritic trunks (Fig. 1*B*). Axons gave rise to numerous collaterals. Only neurons with an input membrane resistance >100 MΩ, firing action potentials with an amplitude of at least 50 mV, and an afterhyperpolarizing potential (AHP) at a threshold of –50 mV, were included in the present study. The resting potential of spontaneously firing neurons was

difficult to establish because of the absence of a stable membrane potential. The input resistance of STN neurons was 200.2 ± 6.8 MΩ (*n* = 88) and not significantly different when measured with both the patch-clamp and intracellular techniques (*p* = 0.36; *n* = 88).

Firing patterns of STN neurons: single-spike and burst-firing modes

All tested STN neurons (*n* = 83) displayed a tonic discharge of single spikes (Fig. 2, single-spike mode) that totally disappeared in the presence of TTX (1 μM, *n* = 33 of 33, data not shown). Among STN neurons, 46% (*n* = 38 of 83) were also able to fire in bursts (burst-firing mode, Fig. 3). These STN neurons switched from one mode to the other depending on membrane potential (Fig. 4). Single-spike mode was recorded at membrane potentials between –35 and –50 mV (–41.3 ± 1.0 mV; *n* = 15), whereas burst firing was present in the membrane potential range of –42 to –60 mV (–51.0 ± 1.0 mV; *n* = 20) (Fig. 4). These values represent the threshold potential of spikes in the single-spike mode (Table 1, parameter 3) and that of bursts in the burst-firing mode (Table 2, parameter 1). At membrane potentials more hyperpolarized than –60 to –70 mV, most STN neurons were silent (Fig. 4). At membrane potentials more depolarized than –30 mV, spike amplitude decreased, and spike frequency increased, leading rapidly to a blockade of STN tonic activity. Activation of group I and II metabotropic glutamate receptors (I-II mGluRs) by 1*S*,3*R*-ACPD (25 μM) (Nakanishi, 1994; Pin and

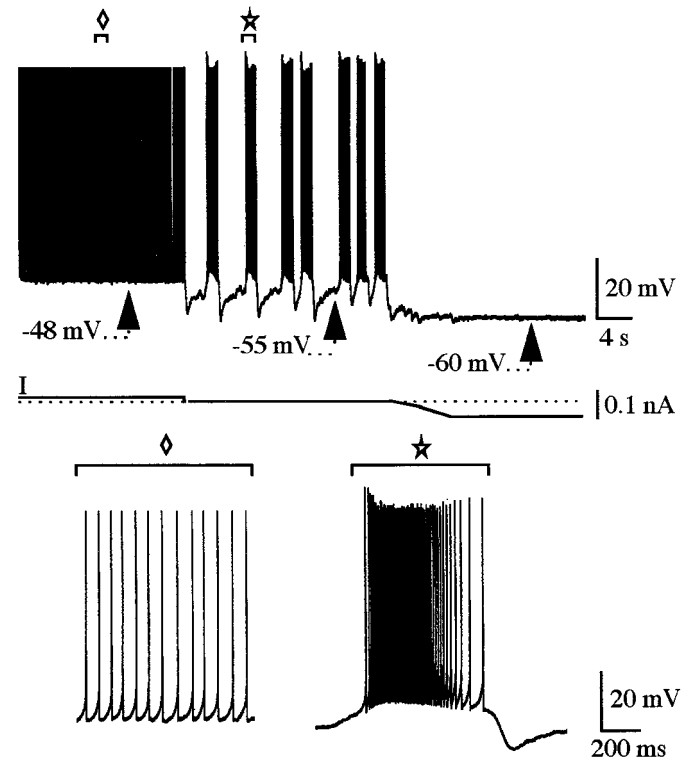
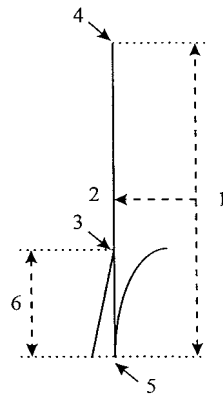


Figure 4. Switch of firing mode according to membrane potential. Pure burst mode (*) was triggered at resting membrane potential (*I* = 0, dotted line, middle) in a whole-cell-recorded neuron that displayed the single-spike mode (◇) at a more depolarized membrane potential (*I* = +0.2 nA, left). At a more hyperpolarized potential (*I* = –0.6 nA, right), the cell became silent. The two bottom traces are taken from the above records and displayed at an expanded time scale. Spikes of the single-spike mode in the left part are truncated.

Table 1. Quantitative parameters of the single-spike mode

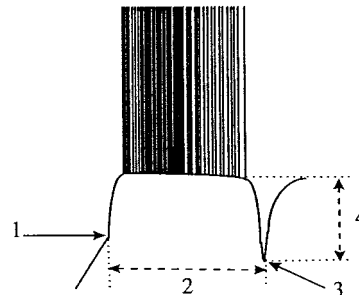
	Mean \pm SEM	Range	Number of cells
Discharge frequency (Hz)	22.3 \pm 1.5	5/43	<i>n</i> = 41
1. Spike amplitude (mV)	74.7 \pm 1.1	57/85	<i>n</i> = 34
2. Half duration of spikes (msec)	0.65 \pm 0.03	0.3/1.2	<i>n</i> = 41
3. Spike threshold (mV)	-41.4 \pm 0.7	-34/-54	<i>n</i> = 41
4. V Overshoot (mV)	15.4 \pm 0.9	6/24	<i>n</i> = 34
5. V AHP (mV)	-60.3 \pm 0.8	-50/-76	<i>n</i> = 41
6. AHP amplitude (mV)	13.8 \pm 0.5	7.5/20.0	<i>n</i> = 41



The different parameters were obtained from intracellularly recorded STN neurons. The numbers on the diagram of a single spike indicate how the different parameters were measured.

Table 2. Quantitative parameters of the burst-firing mode

	A. Long bursts (pure mode)	B. Long bursts (mixed mode)	A vs B
1. Threshold (mV)	-50.4 \pm 1.0 (-40/-60, <i>n</i> = 20)	-49.1 \pm 1.2 (-45/-60, <i>n</i> = 12)	<i>p</i> = 0.41
2. Duration (sec)	1.9 \pm 0.1 (0.8/3.0, <i>n</i> = 22)	2.1 \pm 0.2 (1.0/3.6, <i>n</i> = 14)	<i>p</i> = 0.44
3. V AHP (mV)	-61.8 \pm 0.8 (-58.0/-72.0, <i>n</i> = 20)	-60.8 \pm 0.9 (-58.0/-70.0, <i>n</i> = 12)	<i>p</i> = 0.43
4. AHP Amplitude (mV)	17.7 \pm 0.7 (10.3/25.0, <i>n</i> = 22)	18.9 \pm 0.6 (15.0/22.5, <i>n</i> = 14)	<i>p</i> = 0.23



The different parameters were obtained from patch-clamp-recorded STN neurons. Parameters in column A refer to long bursts of the pure burst mode, whereas parameters in column B refer to long bursts from the mixed burst mode. Values are expressed as mean \pm SEM; the range (minimum and maximum values) and the number of cells are indicated in parentheses. The numbers on the diagram of a long burst indicate how the different parameters were measured.

Duvoisin, 1995) induced burst firing in some STN neurons that bursted poorly in control (*n* = 16 of 20, data not shown).

Quantitative characteristics of the two firing modes are summarized in Tables 1 and 2. The single-spike mode was characterized by an extreme regularity and a rather high frequency (22.3 \pm 1.5 Hz; *n* = 41; Fig. 2). Burst-firing mode could be divided into "pure burst mode" consisting of long-lasting bursts of even dura-

tion (Fig. 3A) and "mixed burst mode" alternating bursts of long and short duration (Fig. 3B). Discharge frequency of long bursts in the pure burst mode was highly variable (15.0 \pm 1.4 bursts/min; range, 7-29 bursts/min; *n* = 21). Long bursts (lasting >800 msec) gave rise to numerous spikes with a "crescendo-decrescendo" frequency sequence: the first spike was followed by a rapid increase in spike frequency that reached a maximum before the end

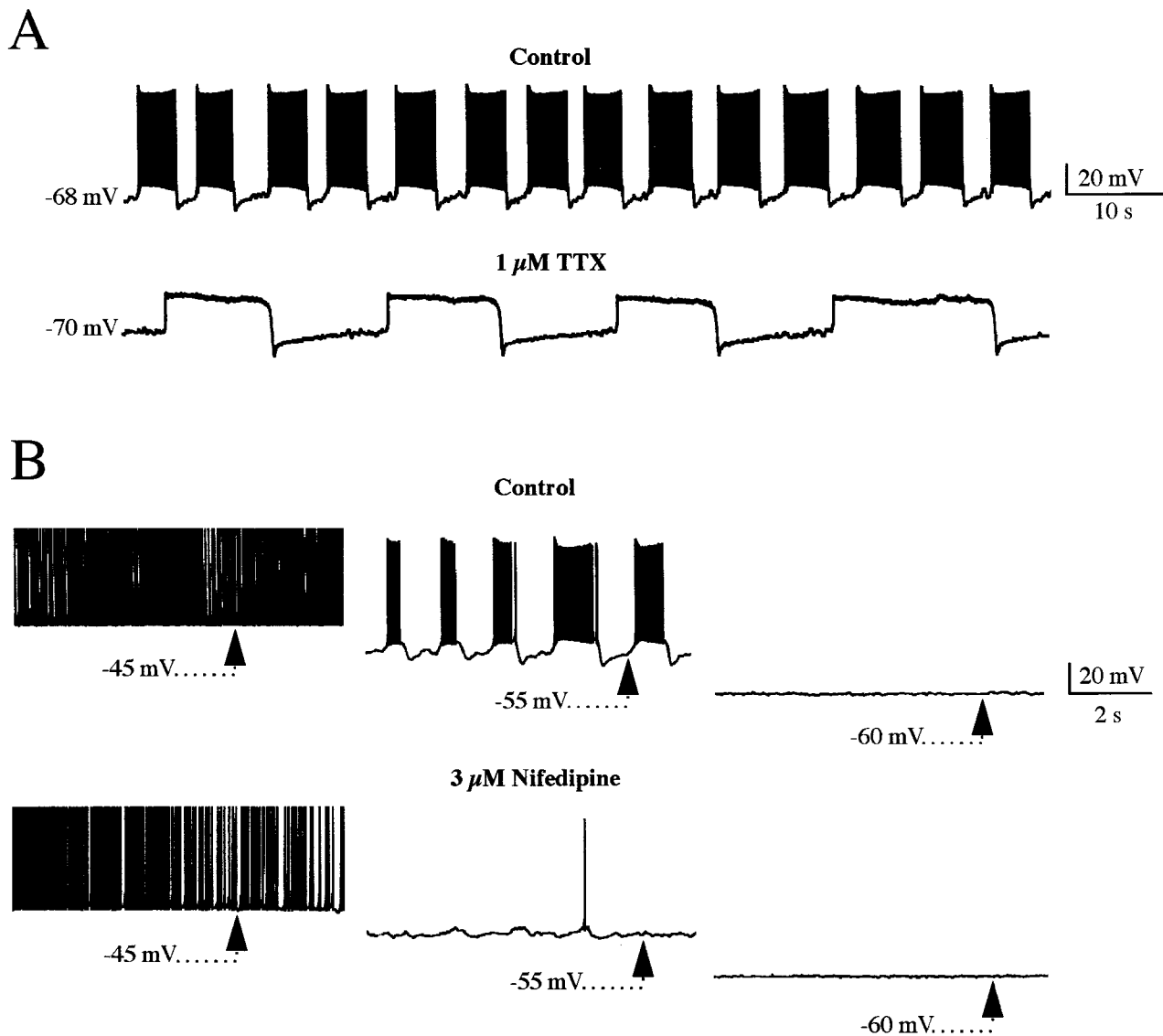


Figure 5. Ionic basis of the burst-firing mode I. *A*, TTX (1 μ M) totally suppressed action potentials evoked during bursts while sparing the rhythmic oscillations of the membrane potential that underlie bursts. Note the increase in the duration of membrane oscillations in the presence of TTX (from 5.0 ± 0.0 sec to 16.4 ± 3.1 sec). *B*, The duration of bursts was irreversibly decreased by an application of nifedipine (3 μ M, bottom trace) at all tested potentials, whereas the single-spike mode was unaffected. Traces in *A* and *B* were obtained from two different STN neurons recorded with patch-clamp techniques in whole-cell configuration. Spikes from the single-spike mode in *B* are truncated. Calibration is the same for traces of each section.

of the burst. Frequency then decreased as membrane potential slowly repolarized during bursts (Fig. 4, right bottom trace). Table 2 recapitulates the quantitative characteristics of the burst-firing mode. On the basis of the three parameters studied, there was no statistical difference between long bursts taken from “pure burst” or from “mixed burst” firing modes (Table 2).

Burst-firing mode was recorded using both patch-clamp and intracellular techniques. Noteworthy, spontaneous bursts were also observed in the cell-attached configuration in patch-clamp experiments (Fig. 3C). However, the relative percentage of bursting neurons varied according to the recording technique, because burst firing was more often observed in patch-clamp recordings (48%) than in intracellular recordings (36%). The input resistance of bursting cells was not significantly different from that of cells that did not burst (195.2 ± 9.4 M Ω and 225.2 ± 15.0 M Ω , respectively; $p = 0.1$; $n = 48$; whole-cell recordings).

Ionic basis of burst-firing mode

Pharmacological studies were performed in the whole-cell configuration. TTX (1 μ M) suppressed action potentials, but spared rhythmic membrane oscillations underlying bursts whose duration was increased by $358 \pm 76\%$ as compared with control ($n = 5$; Fig. 5A). Knowing that Ca^{2+} -dependent mechanisms are often involved in burst generation, we tested several drugs known to interfere with Ca^{2+} entry or intracellular free Ca^{2+} ions. They all had an inhibitory effect on burst firing. Bath application of nifedipine (3 μ M), an L-type Ca^{2+} channel blocker, largely reduced the duration of bursts and even suppressed burst firing ($n = 9$) at any potential tested ($n = 4$; Fig. 5B). This effect did not reverse throughout the experiment (1–2 hr). Nickel (Ni^{2+}) at a concentration that preferentially blocks T/R-type Ca^{2+} channels (40 μ M, data not shown) (Fox et al., 1987) had a similar, but

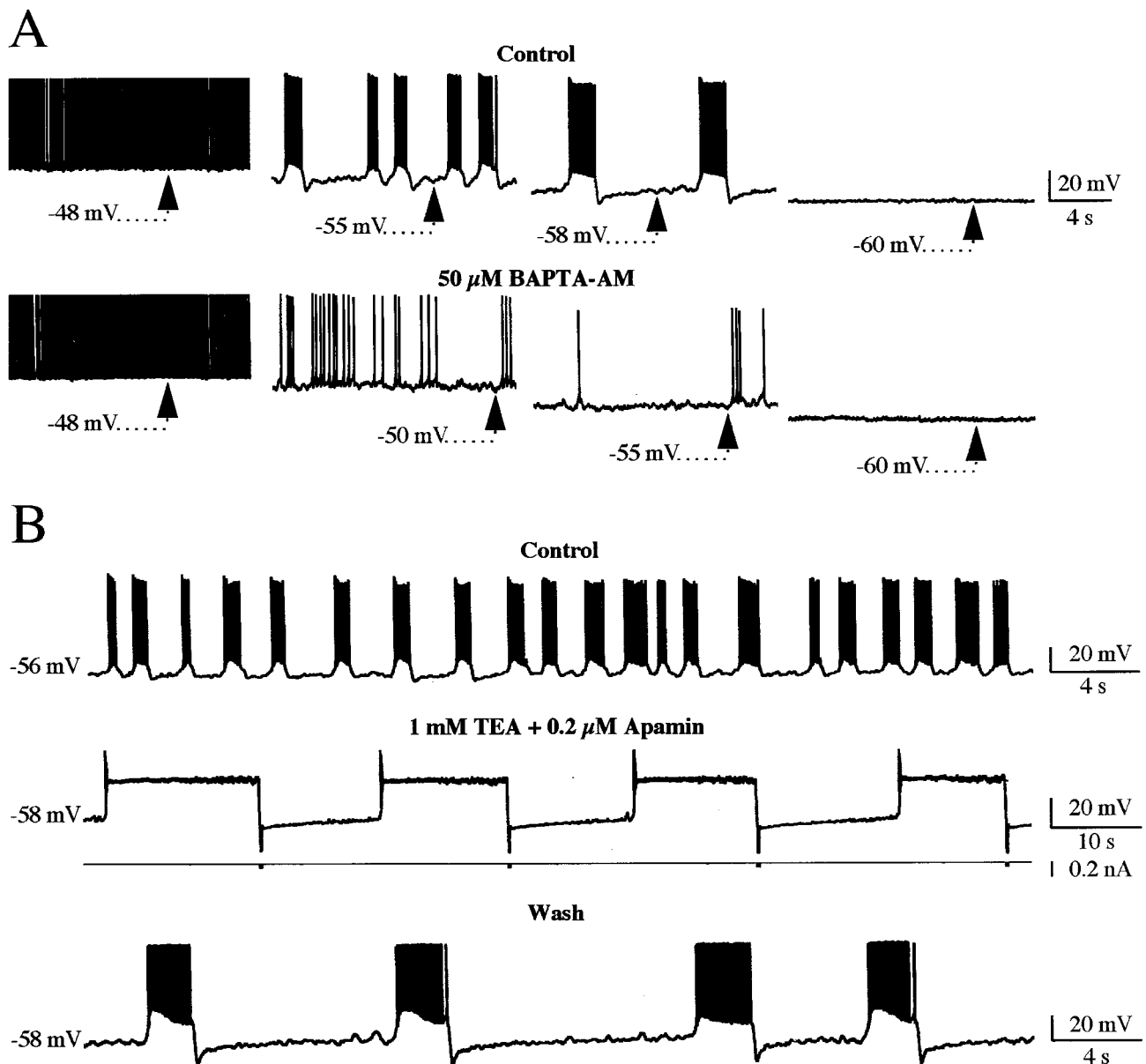


Figure 6. Ionic basis of the burst-firing mode II. *A*, Bath application of BAPTA-AM ($50 \mu\text{M}$) decreased burst duration at any potential tested, although it spared the single-spike activity (*left column*). *B*, Simultaneous application of TEA (1 mM) and apamin ($0.2 \mu\text{M}$) prevented burst repolarization and locked membrane potential at -30 mV . Repolarizations were obtained by injecting brief hyperpolarizing current pulses (-80 pA , 100 msec). After each repolarizing command, the membrane spontaneously depolarized again (*middle trace*). As drugs washed out, bursts reappeared, but with a longer duration ($2.9 \pm 0.1 \text{ sec}$ vs $1.7 \pm 0.2 \text{ sec}$, *bottom trace*). Traces in *A* and *B* were obtained from two different STN neurons with patch-clamp recordings in whole-cell configuration. Spikes from the single-spike mode in *A* (on the *left*) are truncated.

reversible effect: it decreased the duration of bursts ($n = 8$) at any potential tested ($n = 3$). Finally, bath application of the permeable form of the Ca^{2+} chelator BAPTA (BAPTA-AM, $10\text{--}50 \mu\text{M}$) largely reduced the duration of bursts and even suppressed burst firing after a delay of $\sim 40 \text{ min}$ ($n = 7$) at any potential tested ($n = 4$; Fig. 6*A*).

To analyze whether Ca^{2+} -activated K^+ currents play a role in burst repolarization, tetraethylammonium (TEA; 1 mM) was applied at a concentration that blocks the big conductance Ca^{2+} -dependent K^+ current, but not the delayed rectifier one. The TEA was applied in combination with apamin ($0.2 \mu\text{M}$), the selective blocker of the small conductance Ca^{2+} -dependent K^+ current (for review, see Sah, 1996). TEA and apamin totally

prevented burst repolarization and suppressed spikes, except a few early ones (Fig. 6*B*; $n = 4$). The sustained depolarization of the membrane, resulting from the blockade of Ca^{2+} -activated K^+ currents suppressed spikes, probably by inactivating Na^+ -channels as already described in cortical neurons (Prince and Connors, 1986). Short hyperpolarizing current pulses (100 msec , -80 pA) were needed to cut off bursts (Fig. 6*B*, *middle traces*). As the drugs washed out, bursts spontaneously repolarized, although after a longer duration than in control, and spikes reappeared (Fig. 6*B*, *bottom trace*).

To better understand the Ca^{2+} and Ca^{2+} -activated currents present in STN neurons, their responses to current pulses were then analyzed.

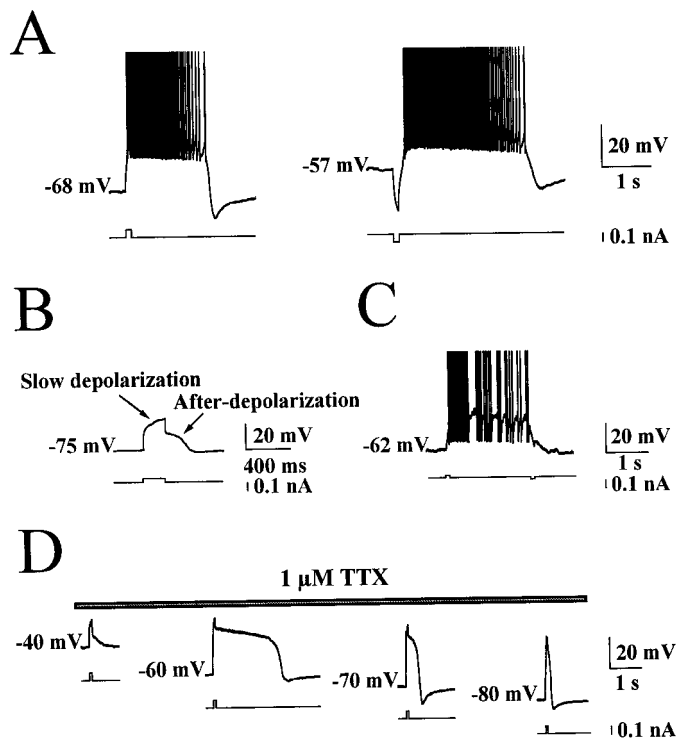


Figure 7. Plateau potentials. *A*, A short depolarizing (100 pA, 100 msec, left trace) or hyperpolarizing (−100 pA, 100 msec, right trace) current pulse triggered both a plateau potential (1.8 and 2.6 msec duration, respectively) that considerably outlasted the duration of the stimulus and was followed by a prominent AHP (28 and 17 mV amplitude, respectively). *B*, TTX (1 μ M) revealed the presence of two different phases in the plateau potential: a slow depolarization triggered by the depolarizing current pulse (50 pA, 200 msec) and an afterdepolarization (267 msec) triggered at the break of the current pulse. *C*, Long duration plateau potential terminated by a short hyperpolarizing current pulse (−20 pA, 100 msec). *D*, Amplitude and duration of the plateau potential according to membrane potential. In the presence of TTX (1 μ M), the same depolarizing current pulse (100 pA, 100 msec) evoked a plateau potential in the membrane potential range of −60 to −70 mV. At more depolarized (−40 mV, extreme left) or hyperpolarized (−80 mV, extreme right) potentials, the amplitude and duration of the plateau potential was considerably reduced. Traces in *A*, *C*, and *D* were obtained with patch-clamp recordings (whole-cell configuration), and traces in *B* were obtained with intracellular recordings. All spikes are truncated.

Ionic basis of responses to intracellular current pulses

Injection of depolarizing or hyperpolarizing current pulses in STN neurons triggered two kinds of responses: a long depolarization that outlasted the current pulse (Figs. 7, 8, plateau potentials) and/or a short depolarizing rebound [low-threshold spike (LTS); Fig. 9].

The plateau potential

Plateau potentials, as burst-firing mode, were more often observed in whole-cell patch-clamp recordings than in intracellular recordings (93 vs 62%, respectively). In response to depolarizing or hyperpolarizing current pulses (100 pA, 100 msec), 86 STN neurons of the 106 tested (82%) generated long-lasting plateau potentials (mean duration, 1043.7 ± 69.8 msec; range, 300–2500 msec; $n = 52$) that gave rise to numerous action potentials (Fig. 7*A*). Plateau potential duration was measured from the beginning of the current pulse to the peak of the AHP. During plateau, spike frequency increased until the end of the depolarizing current pulse and then gradually decreased during the rest of the

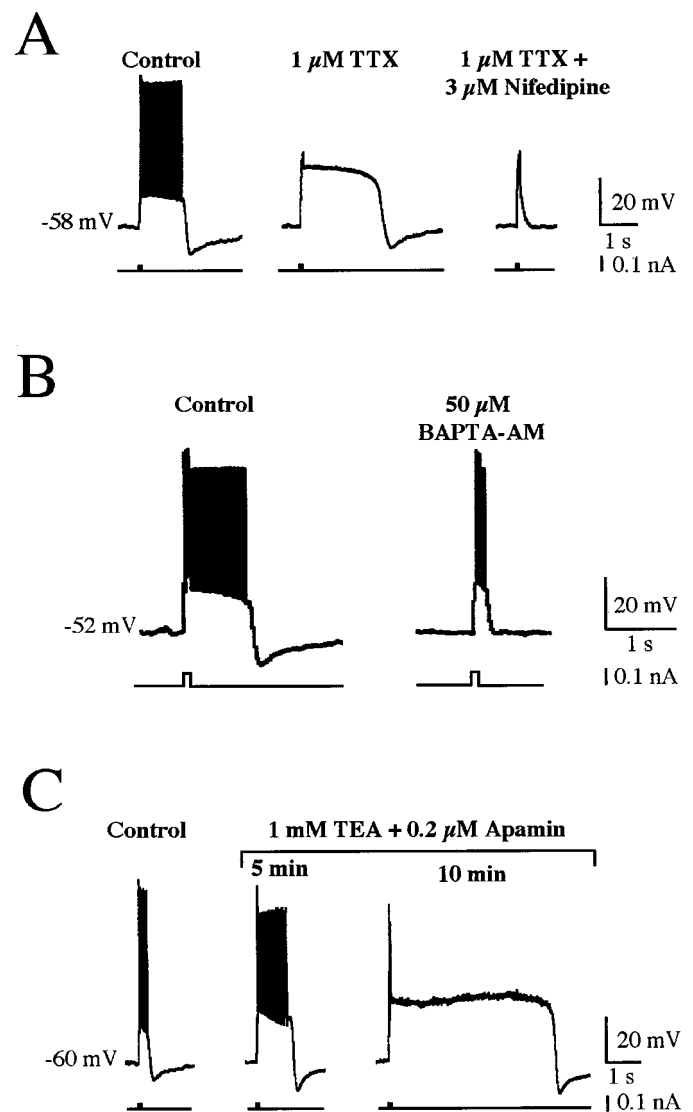


Figure 8. Ionic basis of the plateau response. *A*, TTX (1 μ M) suppressed action potentials but not the plateau potential (middle trace) evoked by a 100 pA, 100 msec current pulse (left trace). In the presence of TTX, bath application of nifedipine (3 μ M) suppressed the plateau potential (right trace). *B*, The duration of the plateau potential was also decreased by bath application of BAPTA-AM (50 μ M). Note that the cell fired some action potentials during the current pulse (100 pA, 100 msec). *C*, In contrast, the plateau potential was significantly increased by simultaneous application of TEA (1 mM) and apamin (0.2 μ M) from 0.5 sec (left trace) to 5.5 sec (right trace). All traces were obtained with patch-clamp recordings (whole-cell configuration).

plateau phase, thus showing some adaptation (Fig. 7*A*). Two different phases were easily identified in the presence of TTX (1 μ M): a ramp-like, slow-rising depolarization that corresponded to the duration of the depolarizing current pulse, and an afterdepolarization that outlasted the current pulse (Fig. 7*B*). Plateau potentials spontaneously ended with an AHP of 20.6 ± 0.8 mV amplitude (range, 10–35 mV; $n = 52$) and could also be terminated by a short hyperpolarizing current pulse (Fig. 7*C*). AHP amplitude was measured in the same way as in burst-firing mode (Table 2). Plateau potentials were triggered within a narrow range of membrane potentials, between −50 and −75 mV ($n = 43$; Fig. 7*D*), thus showing that they resulted from the activation of voltage-dependent conductances.

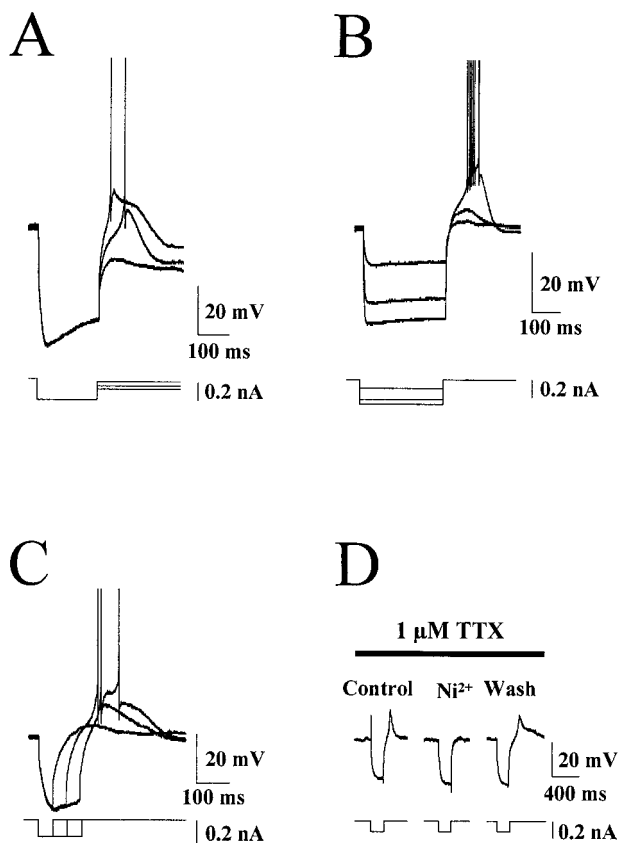


Figure 9. Voltage dependency and pharmacological properties of LTS. *A*, The three superimposed voltage traces show that LTS was recorded at the break of a hyperpolarizing current pulse (-300 pA, 200 msec) applied at a membrane potential of -63 mV. Its amplitude and rise time depended on the value of membrane potential at the end of the negative current pulse: at -78 mV, LTS was not evoked (*bottom trace*), whereas at a slightly more depolarized potential (approximately -72 mV, *middle trace*) it was present and gave rise to a spike. With increased depolarization, LTS amplitude increased, and spike delay decreased (*top trace*). *B*, Three superimposed responses to hyperpolarizing current pulses of increasing amplitude (-100 , -250 , and -350 pA) and fixed duration (300 msec) from $V_m = -53$ mV. LTS was only evoked when the membrane was held for 300 msec at a potential more hyperpolarized than -78 mV for 300 msec. *C*, Three superimposed voltage traces in response to hyperpolarizing current pulses of fixed amplitude (-150 pA) and increasing duration (40, 80, and 120 msec). LTS was evoked in a neuron maintained at -64 mV when the membrane was held at -85 mV for at least 80 msec during the application of a hyperpolarizing current pulse. *D*, In the presence of TTX ($1 \mu\text{M}$), LTS evoked in response to a hyperpolarizing current pulse (-130 pA, 200 msec) from $V_m = -70$ mV was not affected (Control and Wash), whereas it was reversibly suppressed by the concomitant application of Ni^{2+} ($40 \mu\text{M}$). Traces in *A*, *C*, and *D* were obtained with intracellular recordings, and traces in *B* were obtained with patch-clamp recordings (whole-cell configuration). All spikes are truncated.

Ionic currents underlying plateau potentials were analyzed in whole-cell recordings with the use of channel blockers. TTX ($1 \mu\text{M}$) suppressed Na^+ -dependent spikes ($n = 19$ of 19) (Fig. 8*A*, *middle trace*) but did not affect the plateau response. A low Ca^{2+} (0.4 mM) extracellular solution containing Co^{2+} (2 mM) completely suppressed plateau potentials ($n = 5$, data not shown). To determine the type of voltage-gated Ca^{2+} currents involved, Ca^{2+} channel blockers were tested. Nifedipine ($3 \mu\text{M}$) suppressed plateau potentials ($n = 8$; Fig. 8*A*), whereas Ni^{2+} ($40 \mu\text{M}$) had no effect ($n = 5$; data not shown). Chelation of intracellular Ca^{2+}

with either BAPTA-AM (10 – $50 \mu\text{M}$; $n = 4$; Fig. 8*B*) or BAPTA in the pipette solution (20 mM; $n = 2$; data not shown) suppressed or decreased the plateau potential duration after ~ 30 and 20 min, respectively. These results suggest that both Ca^{2+} entry through L-type Ca^{2+} channels and intracellular free Ca^{2+} ions are involved in the generation of plateau potentials. Simultaneous application of TEA (1 mM) and apamin ($0.2 \mu\text{M}$) increased the duration of plateau potentials by $610 \pm 297\%$ ($n = 7$; Fig. 8*C*). In some cells ($n = 2$), spikes were suppressed probably as a result of the sustained membrane depolarization and the consequent Na^+ -channels inactivation. Similarly, $1\text{S},3\text{R-ACPD}$ ($25 \mu\text{M}$) increased plateau potential duration by $252 \pm 37\%$ ($n = 10$; data not shown).

The low-threshold spike

A small, transient depolarization triggering a few spikes was observed at the break of a short hyperpolarizing current pulse in 71% of the STN neurons tested ($n = 66$ of 93; Fig. 9). In the remaining 29% ($n = 27$), the small depolarizing rebound was masked by a plateau potential response. This postinhibitory rebound, previously described in STN neurons (Nakanishi et al., 1987; Overton et al., 1995) and in other preparations (for review, see Huguenard, 1996), has been called an LTS, because of its negative threshold compared with that of Na^+ -dependent spikes. As illustrated in Figure 9*A*, LTS amplitude increased with membrane depolarization at the end of the pulse. It is worthwhile noting the depolarizing sag of the membrane potential, a typical sign of the presence of the hyperpolarization-activated cation current (I_h) previously described in STN neurons (Nakanishi et al., 1987; Overton et al., 1995). Currents underlying LTS inactivated with depolarization as LTS was triggered, but only after maintaining the membrane at potentials more hyperpolarized than -84 mV for 300–400 msec ($n = 9$; Fig. 9*B*). LTS inactivation was also time-dependent, as illustrated in Figure 9*C*, in which membrane potential had to be maintained at -85 mV for at least 80 msec to trigger an LTS. LTS was unaffected by TTX ($1 \mu\text{M}$; $n = 6$; Fig. 9*D*) but completely disappeared in a Ca^{2+} -free Co^{2+} -containing (2.4 mM) external solution ($n = 3$; data not shown), or in the presence of a low concentration of Ni^{2+} ($40 \mu\text{M}$; $n = 5$; Fig. 9*D*). All these results suggest that a rapid voltage-inactivating, Ni^{2+} -sensitive current such as the low-threshold T/R-type Ca^{2+} current underlies LTS.

DISCUSSION

The main result of our study is that approximately half of the STN neurons in the slices have the intrinsic property of switching from single-spike activity to burst-firing mode. To the best of our knowledge, this type of functional property is unknown in neurons of the various basal ganglia nuclei. It may emphasize the role of STN neurons in normal and parkinsonian states.

The cascade of currents underlying burst-firing mode

In tonic and bursting modes, STN neurons fire Na^+ -dependent action potentials. In burst-firing mode, neurons display cycles of membrane oscillations (Fig. 10*b-a*) separated by slow membrane depolarizations (Fig. 10*a-b*). We have shown that the three phases of bursts: depolarization (*b-c*), slowly declining plateau (*c-d*), and repolarization to the AHP (*d-a*), are dependent on Ca^{2+} entry through voltage-sensitive Ca^{2+} channels. We propose that the depolarization phase (*b-c*) results from a low-threshold T/R-type Ca^{2+} current ($I_{\text{T/R}}$) that depolarizes the membrane to the threshold potential of the nifedipine-sensitive L-type Ca^{2+} current (I_L) and then inactivates. The slowly inac-

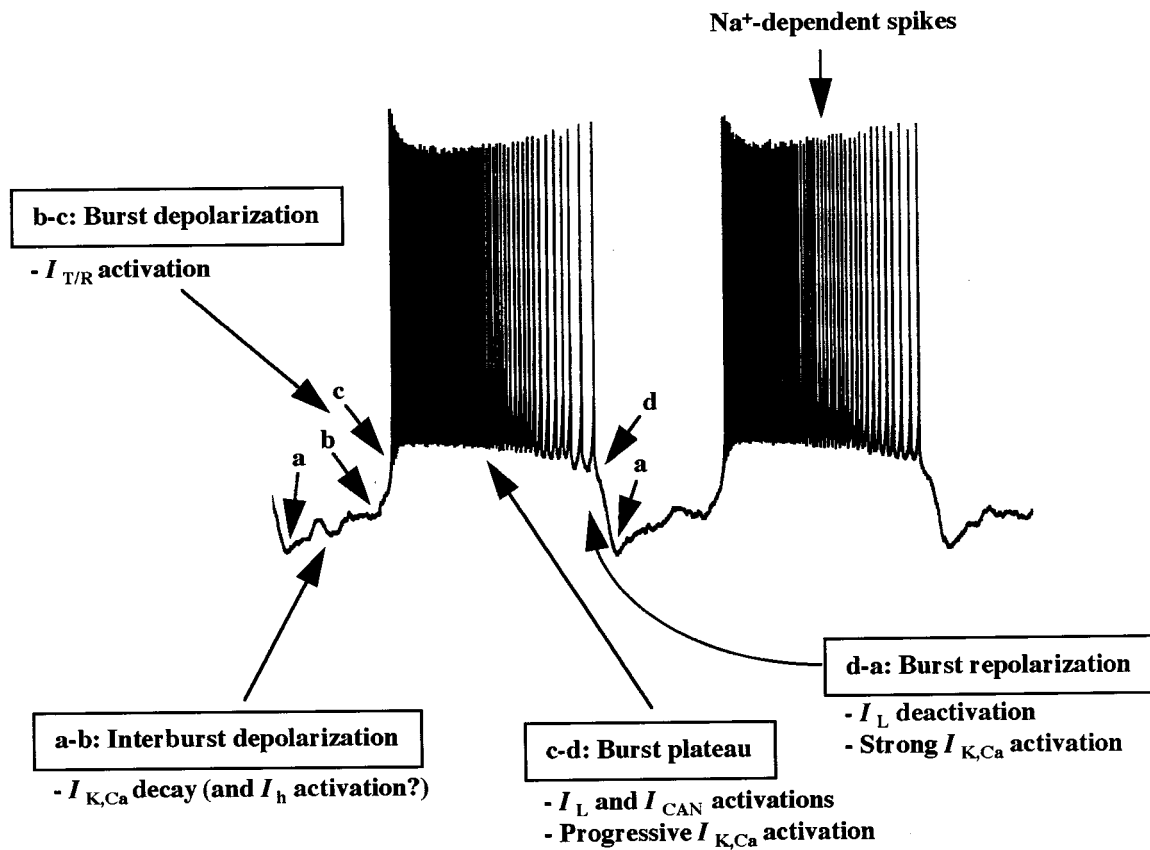


Figure 10. The hypothetical cascade of currents underlying the different phases of burst-firing mode. See Discussion for explanation.

tivating I_L depolarizes the membrane to the plateau phase of bursts during which spikes are evoked ($c-d$). Spikes amplify Ca^{2+} entry by activating more I_L and, possibly, other types of high-threshold Ca^{2+} currents (Song et al., 1997). The resulting increase in intracellular Ca^{2+} concentration activates the TEA- and apamin-sensitive Ca^{2+} -activated K^+ currents ($I_{K,Ca}$). The balance between depolarizing (I_L) and hyperpolarizing ($I_{K,Ca}$) currents, slightly in favor of the latter, explains the gradual decline of the plateau (decrecendo phase). When membrane potential has declined to a certain level, it suddenly repolarizes ($d-a$) because of rapid I_L deactivation (Reuveni et al., 1993) and stronger $I_{K,Ca}$ activation. This leads to the peak of AHP, during which $I_{T/R}$ deactivates. The membrane then spontaneously depolarizes ($a-b$) as $I_{K,Ca}$ decays because of Ca^{2+} clearance mechanisms. Depolarization to the threshold potential of $I_{T/R}$ initiates a new cycle. Because BAPTA suppressed burst firing, instead of blocking burst repolarization by preventing $I_{K,Ca}$ activation, this suggests the participation of a Ca^{2+} -dependent inward current, such as the nonspecific cationic current (I_{CAN}) in the plateau phase of bursts ($c-d$). The progressive activation of this inward current (together with high voltage-activated Ca^{2+} currents) may underlie spike acceleration (crescendo phase) during burst and plateau potential as previously described for bursts of rat thalamic reticular neurons (Huguenard and Prince, 1992). Finally, I_h (Nakanishi et al., 1987; Overton et al., 1995; present study) recorded in some STN neurons (Fig. 9A) may also participate in the slow depolarization between consecutive bursts.

Burst-firing mode was observed in whole-cell recordings as well as in recording configurations in which the intracellular medium was left intact, such as cell-attached or intracellular recordings.

These results showed that burst firing is a physiological firing mode of STN cells. This mode was, however, more easily obtained when K^+ currents were decreased because of the presence of gluconate in the pipette solution (Velumian et al., 1997), or when I-II mGluRs were activated with 1S,3R-ACPD (Nakanishi, 1994; Pin and Duvoisin, 1995). The activation of I_L (Chavis et al., 1995; Russo et al., 1997; Svirsakis and Hounsgaard, 1998) or I_{CAN} (Crépel et al., 1994; Guérineau et al., 1995; Congar et al., 1997), and/or the inhibition of K^+ currents (Chapack et al., 1990; Guérineau et al., 1994; Schrader and Tasker, 1997) by the stimulation of mGluRs may account for the triggering of burst firing by 1S,3R-ACPD. Indeed, the presence of mGluRs (subtypes 2, 3, and 1a) has been reported in the STN neuropile (Martin et al., 1992; Testa et al., 1998) as well as that of mGluR2 mRNA in STN neurons (Testa et al., 1994).

The presence of a plateau potential response is a characteristic of bursting STN neurons

We have shown in the present study that the ionic conductances underlying bursts and plateau potentials are the same: (1) bursts and plateau potentials shared the same pharmacological sensitivity; (2) the same promoting effect of intracellular gluconate and 1S,3R-ACPD was observed in the occurrence of bursts and plateau potentials, and (3) only cells exhibiting a plateau potential were able to generate bursts, either spontaneously or in response to 1S,3R-ACPD, and the reverse also holds true: STN neurons in which plateau potentials could not be triggered were not able to burst. However, this was not the only prerequisite for bursting, because 76% of cells responding with a plateau potential never bursted. The only difference is the lack of effect of a low concen-

tration of extracellular Ni^{2+} on plateau potentials. This can be explained by the fact that the depolarizing current pulse applied to trigger the plateau potential replaced the Ni^{2+} -sensitive T/R-type Ca^{2+} current that normally supported the slow depolarization between bursts. The other type of triggered response, LTS, was present in all recorded STN neurons. Therefore, we propose to distinguish between two populations of STN neurons *in vitro*, those that are able to burst and generate LTS and plateau potentials and those that are not able to burst and only respond with an LTS. We propose that the difference between these two populations is the presence of the inward currents that underlie the plateau phase of bursts or the plateau potentials i.e., mainly I_L and I_{CAN} .

Single-spike modes with frequencies comparable to the ones reported in the present study (Nakanishi et al., 1987; Overton et al., 1995) have already been described in STN neurons in acute slices. To our knowledge, burst-firing mode had only once been recorded *in vitro*, (in organotypic cultures of STN neurons with intracellular recording techniques), but their ionic mechanisms were not analyzed (Plenz et al., 1997). In contrast, evoked responses similar to the ones reported here have been previously described. The “slow depolarizing potentials” mentioned by Nakanishi et al. (1987) are similar to the plateau potentials we described, which were triggered when the membrane potential was in the -50 to -60 mV range. Likewise, the “slow action potentials” (Nakanishi et al., 1987), “strong rebound bursts” (Plenz et al., 1997), and the “LTS” (Overton et al., 1995) correspond to the LTS described in the present study. Because these different studies did not include precise pharmacological characterization, this similarity is based only on the voltage dependence of the responses. *In vivo*, both tonic and bursting activities have been recorded in rat and monkey STN (Hollerman and Grace, 1992; Fujimoto and Kita, 1993; Bergman et al., 1994; Overton and Greenfield, 1995; Kreiss et al., 1997). However, the switch from one mode to the other, and the ionic mechanisms of the bursting mode, have not been observed or analyzed in either of the preparations.

Functional implications

In a normal *in vivo* situation, the great majority of rat and monkey STN neurons present a tonic activity with a frequency varying from 5 to 65 Hz, and few neurons discharge in bursts (Matsumara et al., 1992; Wichmann et al., 1994; Overton and Greenfield, 1995). In relation with conditioned arm (Georgopoulos et al., 1983; Miller and DeLong, 1987; Wichmann et al., 1994) or saccadic eye (Matsumara et al., 1992) movements, a burst of high-frequency spikes lasting ~ 200 – 300 msec is usually recorded after the onset of the movement. Because we showed in the present study that bursts or plateau potentials are triggered by membrane hyperpolarization, the movement-correlated burst of action potentials may result from the activation of inhibitory afferents to the STN.

The increase in the percentage of bursts in the discharge of STN neurons is noteworthy after a lesion of the substantia nigra pars compacta in rats and monkeys *in vivo* (Hollerman and Grace, 1992; Bergman et al., 1994; Hassani et al., 1996) and in parkinsonian patients (Benazzouz et al., 1996; Rodriguez et al., 1997). The origin of this modification in STN activity in a pathological situation is still under debate (for review, see Chesselet and Delfs 1996; Levy et al., 1997), although a disinhibition mechanism and increased activity of glutamatergic STN afferents seem to be crucial, according to DeLong's (1990) model. We have in fact

shown that the activation of metabotropic glutamate receptors that may occur because of increased activity of glutamatergic STN afferents, strongly favored the bursting mode, as also observed in the hippocampus (Bianchi and Wong, 1995). Bursting STN neurons may drive target neurons in the internal segment of the pallidum and in substantia nigra pars reticulata, where an oscillatory activity or an increase in cytochrome oxidase activity, a marker of metabolic activity, have been recorded in animal parkinson models (Miller and DeLong, 1987; Filion et al., 1988; Bergman et al., 1994; Nini et al., 1995; Vila et al., 1997; Bergman et al., 1998) and in parkinsonian patients (Hutchison et al., 1997; Vila et al., 1997). This suggests that the strong regulation exerted on STN neurons in control animals is disorganized in animal models of parkinsonism. This may indeed account for the switch from a tonic to a bursting mode.

REFERENCES

- Albin RL, Young AB, Penney JB (1989) The functional anatomy of the basal ganglia disorders. *Trends Neurosci* 12:366–375.
- Aziz TZ, Peggs D, Sambrook MA, Crossman AR (1991) Lesion of the subthalamic nucleus for the alleviation of 1-methyl-4-phenyl-1,2,3-6-tetrahydropyridine (MPTP)-induced parkinsonism in the primate. *Mov Disord* 6:288–292.
- Bathia KP, Marsden CD (1994) The behavioral and motor consequences of focal lesions of the basal ganglia in man. *Brain* 117:859–876.
- Benazzouz A, Gross Ch, Féger J, Boraud Th, Bioulac B (1993) Reversal of rigidity and improvement in motor performance by subthalamic high-frequency stimulation in MPTP-treated monkeys. *Eur J Neurosci* 5:382–389.
- Benazzouz A, Piallat B, Pollak P, Limousin P, Gao DM, Krack P, Benabid AL (1996) Single unit recordings of subthalamic nucleus and pars reticulata of substantia nigra in akineto-rigid parkinsonian patients. *Soc Neurosci Abstr* 22:91.18.
- Bergman H, Wichmann T, DeLong MR (1990) Reversal of experimental parkinsonism by lesions of the subthalamic nucleus. *Science* 249:1346–1348.
- Bergman H, Wichmann T, Karmon B, DeLong MR (1994) The primate subthalamic nucleus II. Neuronal activity in the MPTP model of Parkinsonism. *J Neurophysiol* 72:507–520.
- Bergman H, Feingold A, Nini A, Raz A, Slovin H, Abeles M, Vaadia E (1998) Physiological aspects of information processing in the basal ganglia of normal and parkinsonian primates. *Trends Neurosci* 21:32–38.
- Beurrier C, Bezard E, Bioulac B, Gross C (1997) Subthalamic stimulation elicits hemiballismus in normal monkey. *NeuroReport* 8:1625–1629.
- Bianchi R, Wong RKS (1995) Excitatory synaptic potentials dependent on metabotropic glutamate receptor activation in guinea-pig hippocampal pyramidal cells. *J Physiol (Lond)* 487:663–676.
- Brotchie JM, Mitchell IJ, Sambrook MA, Crossman AR (1991) Alleviation of parkinsonism by antagonism of excitatory amino acid transmission in the medial segment of the globus pallidus in rat and primate. *Mov Disord* 6:133–138.
- Chapak S, Gähwiler BH, Do KQ, Knöpfel T (1990) Potassium conductances in hippocampal neurons blocked by excitatory amino-acid transmitters. *Nature* 347:765–767.
- Chavis P, Nooney JM, Bockaert J, Fagni L, Feltz A, Bossu JL (1995) Facilitatory coupling between a glutamate metabotropic receptor and dihydropyridine-sensitive calcium channels in cultured cerebellar granule cells. *J Neurosci* 15:135–143.
- Chesselet MF, Delfs JM (1996) Basal ganglia and movement disorders: an update. *Trends Neurosci* 19:417–422.
- Congar P, Leinekugel X, Ben-Ari Y, Crépel V (1997) A long-lasting calcium-activated nonselective cationic current is generated by synaptic stimulation or exogenous activation of group I metabotropic glutamate receptors in CA1 pyramidal neurons. *J Neurosci* 17:5366–5379.
- Crépel V, Anikstejn L, Ben-Ari Y, Hammond C (1994) Glutamate metabotropic receptors increase a Ca^{2+} -activated nonspecific cationic current in CA1 hippocampal neurons. *J Neurophysiol* 72:1561–1569.
- Crossman AR, Sambrook MA, Jackson A (1984) Experimental hemichorea/hemiballismus in the monkey. Studies of the intracerebral site of action in a drug induced dyskinesia. *Brain* 107:579–596.

- DeLong MR (1990) Primate models of movement disorders of basal ganglia origin. *Trends Neurosci* 13:281–285.
- Féger J, Hassani OK, Mouroux M (1997) The subthalamic nucleus and its connections. New electrophysiological and pharmacological data. *Adv Neurol* 74:31–43.
- Filion M, Tremblay L, Bédard PJ (1988) Abnormal influences of passive limb movement on the activity of globus pallidus neurons in parkinsonian monkeys. *Brain Res* 444:165–176.
- Fox AP, Nowycky MC, Tsien RW (1987) Kinetic and pharmacological properties distinguishing three types of calcium currents in chick sensory neurones. *J Physiol (Lond)* 394:149–172.
- Fujimoto K, Kita H (1993) Response characteristics of subthalamic neurons to the stimulation of the sensorimotor cortex in the rat. *Brain Res* 609:185–192.
- Georgopoulos AP, DeLong MR, Crutcher MD (1983) Relations between parameters of step-tracking movements and single cell discharge in the globus pallidus and subthalamic nucleus of the behaving monkey. *J Neurosci* 3:1586–1598.
- Graham WC, Robertson RG, Sambrook MA, Crossman AR (1990) Injection of excitatory amino acid antagonists into the pallidal segment of the MPTP-treated primate reverses motor symptoms of parkinsonism. *Life Sci* 47:91–97.
- Guérineau NC, Gähwiler BH, Gerber U (1994) Reduction of resting K^+ current by metabotropic glutamate and muscarinic receptors in rat CA3 cells: mediation by G-proteins. *J Physiol (Lond)* 474:27–33.
- Guérineau NC, Bossu JL, Gähwiler BH, Gerber U (1995) Activation of a nonselective cationic conductance by metabotropic glutamatergic and muscarinic agonists in CA3 pyramidal neurons of the rat hippocampus. *J Neurosci* 15:4395–4407.
- Guridi J, Herrero MT, Luquin MR, Guillén J, Ruberg M, Laguna J, Vila M, Javoy-Agud F, Agud Y, Hirsch E, Obeso A (1996) Subthalamotomy in parkinsonian monkeys. Behavioural and biochemical analysis. *Brain* 119:1717–1727.
- Hamada I, DeLong MR (1992) Excitotoxic acid lesions of the primate subthalamic nucleus result in transient dyskinesias of the contralateral limbs. *J Neurophysiol* 68:1850–1858.
- Hammond C, Féger J, Bioulac B, Souteyrand JP (1979) Experimental hemiballism in the monkey produced by unilateral kainic acid lesion in corpus Luysii. *Brain Res* 171:577–580.
- Hassani OK, Mouroux M, Féger J (1996) Increased subthalamic neuronal activity after nigral dopaminergic lesion independent of disinhibition via the globus pallidus. *Neuroscience* 72:105–115.
- Hollerman JR, Grace AA (1992) Subthalamic nucleus cell firing in the 6-OHDA-treated rat: basal activity and response to haloperidol. *Brain Res* 590:291–299.
- Huguenard JR, Prince DA (1992) A novel T-type current underlies prolonged Ca^{2+} -dependent burst firing in GABAergic neurons of rat thalamic reticular nucleus. *J Neurosci* 12:3804–3817.
- Huguenard JR (1996) Low-threshold calcium currents in central nervous system neurons. *Annu Rev Physiol* 58:329–348.
- Hutchinson WD, Lozano AM, Tasker RR, Lang AE, Dostrovsky JO (1997) Identification and characterization of neurons with tremor-frequency activity in human globus pallidus. *Exp Brain Res* 113:557–563.
- Kreiss DS, Mastropietro CW, Rawji SS, Walters JR (1997) The response of subthalamic nucleus neurons to dopamine receptor stimulation in a rodent model of Parkinson's disease. *J Neurosci* 17:6807–6819.
- Levy R, Hazrati LN, Herrero MT, Vila M, Hassani OK, Mouroux M, Ruberg M, Asensi H, Agud Y, Féger J, Obeso JA, Parent A, Hirsch EC (1997) Re-evaluation of the functional anatomy of the basal ganglia in normal and parkinsonian states. *Neuroscience* 76:335–343.
- Limousin P, Pollak P, Benazzouz A, Hoffmann D, Le Bas JF, Broussolle E, Perret JE, Benabid AL (1995) Effect on parkinsonian signs and symptoms of bilateral subthalamic nucleus stimulation. *Lancet* 345:91–95.
- Martin JP (1927) Hemichorea resulting from a local lesion of the brain (the syndrome of the body of Luys). *Brain* 50:637–651.
- Martin LJ, Blackstone CD, Haganir RL, Price DL (1992) Cellular localization of a metabotropic glutamate receptor in rat brain. *Neuron* 9:259–270.
- Matsumura M, Kojima J, Gardiner TW, Hikosaka O (1992) Visual and oculomotor functions of monkey subthalamic nucleus. *J Neurophysiol* 67:1615–1632.
- Miller WC, DeLong MR (1987) Altered tonic activity of neurons in the globus pallidus and subthalamic nucleus in the primate MPTP model parkinsonian. In: *The basal ganglia II* (Carpenter MB, Jayaraman A, eds), pp 415–427. New York: Plenum.
- Mink JW (1996) The basal ganglia: focused selection and inhibition of competing motor programs. *Prog Neurobiol* 50:381–425.
- Nakanishi H, Kita H, Kitai ST (1987) Electrical membrane properties of rat subthalamic neurons in an *in vitro* slice preparation. *Brain Res* 437:35–44.
- Nakanishi S (1994) Metabotropic glutamate receptors: synaptic transmission, modulation, and plasticity. *Neuron* 13:1031–1037.
- Nini A, Feingold A, Sloviter H, Bergman H (1995) Neurons in the globus pallidus do not show correlated activity in the normal monkey, but phase-locked oscillations appear in the MPTP model of parkinsonism. *J Neurophysiol* 74:1800–1805.
- Overton PG, Greenfield SA (1995) Determinants of neuronal firing pattern in the guinea-pig subthalamic nucleus: an *in vivo* and *in vitro* comparison. *J Neural Transm* 10:41–54.
- Overton PG, O'Callaghan JFX, Greenfield SA (1995) Possible intermixing of neurons from the subthalamic and substantia nigra pars compacta in the guinea-pig. *Exp Brain Res* 107:151–165.
- Parent A, Hazrati LN (1995) Functional anatomy of the basal ganglia II. The place of subthalamic nucleus and external pallidum in basal ganglia circuitry. *Brain Res Rev* 20:128–154.
- Pin JP, Duvoisin R (1995) The metabotropic glutamate receptors: structure and functions. *Neuropharmacology* 34:1–26.
- Plenz D, Herrera-Marschitz M, Kitai ST (1997) The oscillatory feedback circuitry between subthalamic nucleus and globus pallidus as a putative generator for resting tremor. *Soc Neurosci Abstr* 23:181.2.
- Prince DA, Connors BW (1986) Mechanisms of interictal epileptogenesis. In: *Advances in neurology* (Delgado-Escueta AV, Ward Jr AA, Woodbury DM, Porter RJ, eds), pp 275–299. New York: Raven.
- Reuveni I, Friedman A, Amitai Y, Gutnick MJ (1993) Stepwise repolarization from Ca^{2+} plateaus in neocortical pyramidal cells: evidence for nonhomogeneous distribution of HVA Ca^{2+} channels in dendrites. *J Neurosci* 13:4609–4621.
- Rodriguez MC, Gorospe A, Mozo A, Guridi J, Ramos E, Linazasoro G, Obeso JA (1997) Characteristics of neuronal activity in the subthalamic nucleus (STN) and substantia nigra pars reticulata (SNr) in Parkinson's disease (PD). *Soc Neurosci Abstr* 23:183.6.
- Russo RE, Nagy F, Hounsgaard J (1997) Modulation of plateau properties in dorsal horn neurones in a slice preparation of the turtle spinal cord. *J Physiol (Lond)* 499:459–474.
- Sah P (1996) Ca^{2+} -activated K^+ currents in neurones: types, physiological roles and modulation. *Trends Neurosci* 19:150–154.
- Schrader LA, Tasker JG (1997) Modulation of multiple potassium currents by metabotropic glutamate receptors in neurons of the hypothalamic supraoptic nucleus. *J Neurophysiol* 78:3428–3437.
- Song WJ, Otsuka T, Baba Y, Murakami F (1997) Characterization of Ca^{2+} currents in acutely isolated rat subthalamic nucleus neurons. *Soc Neurosci Abstr* 23:83.1.
- Svirskis G, Hounsgaard J (1998) Transmitter regulation of plateau properties in turtle motoneurons. *J Neurophysiol* 79:45–50.
- Testa CM, Standaert DG, Young AB, Penney Jr JB (1994) Metabotropic glutamate receptor mRNA expression in the basal ganglia of the rat. *J Neurosci* 14:3005–3018.
- Testa CM, Friberg IK, Weiss SA, Standaert DG (1998) Immunohistochemical localization of metabotropic glutamate receptors mGluR1a and mGluR2/3 in the rat basal ganglia. *J Comp Neurol* 390:5–19.
- Velumian AA, Zhang L, Pennafather P, Carlen PL (1997) Reversible inhibition of I_K , I_{AHP} , I_h and I_{Ca} currents by internally applied gluconate in rat hippocampal pyramidal neurones. *Pflügers Arch* 433:343–350.
- Vila M, Levy R, Herrero M-T, Ruberg M, Faucheux B, Obeso JA, Agud Y, Hirsch E (1997) Consequences of nigrostriatal denervation on the functioning of the basal ganglia in human and nonhuman primates: an *in situ* hybridization study of cytochrome oxidase subunit I mRNA. *J Neurosci* 17:765–773.
- Whittier JR, Mettler FA (1949) Studies of the subthalamus of the rhesus monkey. II. Hyperkinesia and other physiologic effects of subthalamic lesions, with special reference to the subthalamic nucleus of Luys. *J Comp Neurol* 90:319–372.
- Wichmann T, Bergman H, DeLong MR (1994) The primate subthalamic nucleus I. Functional properties in intact animals. *J Neurophysiol* 72:494–506.

Slowly Inactivating Sodium Current (I_{NaP}) Underlies Single-Spike Activity in Rat Subthalamic Neurons

CORINNE BEURRIER,¹ BERNARD BIOULAC,¹ AND CONSTANCE HAMMOND²

¹Laboratoire de neurophysiologie, Centre National de la Recherche Scientifique, 33076 Bordeaux Cedex; and ²Institut National de la Santé et de la Recherche Médicale U29, Institut de Neurobiologie de la Méditerranée, 13273 Marseille Cedex 09, France

Beurrier, Corinne, Bernard Bioulac, and Constance Hammond.

Slowly inactivating sodium current (I_{NaP}) underlies single-spike activity in rat subthalamic neurons. *J. Neurophysiol.* 83: 1951–1957, 2000. One-half of the subthalamic nucleus (STN) neurons switch from single-spike activity to burst-firing mode according to membrane potential. In an earlier study, the ionic mechanisms of the bursting mode were studied but the ionic currents underlying single-spike activity were not determined. The single-spike mode of activity of STN neurons recorded from acute slices in the current clamp mode is TTX-sensitive but is not abolished by antagonists of ionotropic glutamatergic and GABAergic receptors, blockers of calcium currents (2 mM cobalt or 40 μ M nickel), or intracellular Ca^{2+} ions chelators. Tonic activity is characterized by a pacemaker depolarization that spontaneously brings the membrane from the peak of the after-spike hyperpolarization (AHP) to firing threshold (from -57.1 ± 0.5 mV to -42.2 ± 0.3 mV). Voltage-clamp recordings suggest that the Ni^{2+} -sensitive, T-type Ca^{2+} current does not play a significant role in single-spike activity because it is totally inactivated at potentials more depolarized than -60 mV. In contrast, the TTX-sensitive, I_{NaP} that activated at -54.4 ± 0.6 mV fulfills the conditions for underlying pacemaker depolarization because it is activated below spike threshold and is not fully inactivated in the pacemaker range. In some cases, the depolarization required to reach the threshold for I_{NaP} activation is mediated by hyperpolarization-activated cation current (I_h). This was directly confirmed by the cesium-induced shift from single-spike to burst-firing mode which was observed in some STN neurons. Therefore, a fraction of I_h which is tonically activated at rest, exerts a depolarizing influence and enables membrane potential to reach the threshold for I_{NaP} activation, thus favoring the single-spike mode. The combined action of I_{NaP} and I_h is responsible for the dual mode of discharge of STN neurons.

INTRODUCTION

The subthalamic nucleus (STN) is a basal ganglia nucleus that plays an important role in normal (Matsumara et al. 1992; Wichmann et al. 1994) and pathological (Bergman et al. 1994) motor behavior. By way of its glutamatergic projections (Smith and Parent 1988), STN imposes its rhythm to the two principal output structures of the basal ganglia, the internal pallidal segment and the substantia nigra pars reticulata (Féger et al. 1997; Parent and Hazrati 1995). In a normal in vivo situation, the great majority of rat and monkey STN neurons present a tonic activity with a frequency varying from 5 to 65 Hz and few neurons discharge in bursts (Matsumara et al. 1992; Over-

ton and Greenfield 1995; Wichmann et al. 1994). After the onset of a conditioned movement, a period of high-frequency spikes is usually recorded (Georgopoulos et al. 1983; Matsumara et al. 1992; Miller and DeLong 1987; Wichmann et al. 1994). In a pathological situation, after a lesion of nigral dopaminergic neurons, there was an observed increase in the percentage of bursts in the discharge of STN neurons in rats and monkeys in vivo (Bergman et al. 1994; Hassani et al. 1996; Hollerman and Grace 1992) as well as in Parkinsonian patients (Benazzouz et al. 1996). We previously showed that approximately one-half of the STN neurons recorded in slices in vitro have intrinsic membrane properties that allow them to switch from a tonic to a burst-firing mode in response to membrane hyperpolarization (Beurrier et al. 1999).

This raises the question as to which conductances are altered by afferent synaptic inputs to switch the activity of STN neurons from single-spike to burst-firing mode (or the reverse). It is desirable to first identify the set of ionic currents that are of demonstrable importance in regulating the different firing modes. We previously analyzed the cascade of currents underlying burst firing mode (Beurrier et al. 1999). The aim of this study was to build up a picture of the ionic mechanisms of the tonic firing mode with the use of whole cell recordings of STN neurons in slices, in current, or voltage-clamp mode. We analyzed the ionic currents underlying the spontaneous depolarization that during the interspike interval bring the membrane potential from the peak of the after-spike hyperpolarization (AHP) to the threshold potential of Na^+ spike initiation. We now report that pacemaker depolarization mainly results from the activation of a subthreshold, slowly inactivating, TTX-sensitive Na^+ current (I_{NaP}). We also show that in approximately one-half of the neurons tested, the hyperpolarization-activated cation current (I_h) blockade hyperpolarizes the membrane sufficiently to switch STN activity to burst-firing mode, thus suggesting that the fraction of I_h opened at rest allows STN neurons to maintain a single-spike mode of activity.

METHODS

Slice preparation

Experiments were performed on STN neurons in slices obtained from 20- to 28-day-old male Wistar rats. Rats were anesthetized with ether and decapitated. The brain was removed quickly and a block of tissue containing the STN was isolated on ice in a 0–5°C oxygenated solution containing (in mM) 1.15 NaH_2PO_4 , 2 KCl, 26 $NaHCO_3$, 7 $MgCl_2$, 0.5 $CaCl_2$, 11 glucose, and 250 saccharose, equilibrated with 95% O_2 -5% CO_2 (pH 7.4). This cold solution, with a low NaCl and $CaCl_2$ content, improved tissue viability. In the same medium, 300- to

The costs of publication of this article were defrayed in part by the payment of page charges. The article must therefore be hereby marked "advertisement" in accordance with 18 U.S.C. Section 1734 solely to indicate this fact.

400- μm thick coronal slices were prepared using a vibratome (Campden Instruments, Loughborough, UK) and were incubated at room temperature in a Krebs solution containing (in mM) 124 NaCl, 3.6 KCl, 1.25 HEPES, 26 NaHCO_3 , 1.3 MgCl_2 , 2.4 CaCl_2 , and 10 glucose, equilibrated with 95% O_2 -5% CO_2 (pH 7.4). After a 2-h recovery period, STN slices were transferred one at a time to an interface-type recording chamber, maintained at $30 \pm 2^\circ\text{C}$, and continuously superfused ($1\text{--}1.5 \text{ ml} \cdot \text{min}^{-1}$) with the oxygenated Krebs solution.

Electrophysiological recordings

Slices were viewed using a dissecting microscope and the recording electrode was precisely positioned in the STN. Electrophysiological recordings of STN neurons were performed in current or in voltage-clamp mode using the blind patch-clamp technique in the whole cell configuration. Patch electrodes were pulled from filamented borosilicate thin-wall glass capillaries (GC150F-15, Clark Electromedical Instruments, Pangbourne, UK) with a vertical puller (PP-830, Narishige, Japan) and had a resistance of 10 to 12 $\text{M}\Omega$ when filled with solution 1 (see *Intracellular solutions*).

Intracellular solutions

For current-clamp recordings a K-gluconate-based solution (*solution 1*) was used. It contained (in mM) 120 K-gluconate, 10 KCl, 10 NaCl, 10 EGTA, 10 HEPES, 1 CaCl_2 , 2 MgATP , and 0.5 NaGTP (pH 7.25). To study low-threshold voltage-activated T-type Ca^{2+} current (I_{CaT}), the 120 mM K-gluconate in *solution 1* was substituted for an equimolar concentration of CsCl and KCl was omitted as was ATP and GTP to reduce the L-type Ca^{2+} current which is known to be sensitive to run-down (*solution 2*). In some experiments the Ca^{2+} chelator 1,2-bis(2-aminophenoxy)-ethane- N,N,N',N' -tetraacetic acid, tetrapotassium salt (BAPTA, 10 mM) was added to *solution 1* which contained 80 mM K-gluconate instead of 120 mM to obtain an osmolarity $\sim 270 \text{ mOsm} \cdot \text{l}^{-1}$. In this solution, the Ca^{2+} ion concentration was decreased from 1 to 0.1 mM (*solution 3*). To record Na^+ currents, the 120 mM K-gluconate in *solution 1* was substituted for an equimolar concentration of CsCl and KCl was omitted (*solution 4*).

Extracellular solutions

For voltage-clamp experiments, the Krebs solution contained 1 μM TTX, 3 μM nifedipine, and 1 mM Cs^+ for the I_{CaT} study (*solution A*). For the I_{NaP} study, 2 mM Co^{2+} and 1 mM Cs^+ were added and the Ca^{2+} ions concentration was decreased from 2.4 to 0.5 mM (*solution B*). For the I_{h} study, 1 μM TTX was added (*solution C*).

Drugs

All drugs were purchased from Sigma (St. Louis, MO), except 6-cyano-7-nitroquinoline-2,3-dione (CNQX), D-(–)-2-amino-5-phosphopentanoic acid (D-APV), and bicuculline which were purchased from Tocris (Bristol, UK). BAPTA was diluted in the pipette solution. All other drugs were diluted in the oxygenated Krebs and applied through this superfusion medium. Nifedipine and CNQX were dissolved in dimethylsulfoxide (final concentration, 0.03–0.3%).

Data analysis

Membrane potential was recorded using an Axoclamp 2A or Axopatch 1D amplifier (Axon Instruments, Foster City, CA), displayed simultaneously on a storage oscilloscope and a four-channel chart recorder (Gould Instruments, Longjumeau, France), digitized (DR-890, NeuroData Instruments, NY), and stored on a videotape for subsequent offline analysis. In voltage-clamp experiments, membrane currents were amplified by an Axopatch 1D or an Axoclamp 2A, fed

into an A/D converter (Digidata 1200, Axon Instruments), and stored and analyzed on a PC using pCLAMP software (version 6.0.1, Axon Instruments). Because different recording solutions were used throughout the study, corrections for the liquid junction potential were performed. The correction was -6 mV for the K-gluconate-based pipette solution as estimated with a 3 M KCl ground electrode (Neher 1992).

RESULTS

Data presented here are based on patch-clamp recordings of 155 STN neurons. Neuronal activity was recorded in current-clamp mode ($n = 57$) and subthreshold currents were recorded in voltage-clamp mode (whole cell configuration, $n = 106$).

Characteristics of single-spike activity and pacemaker depolarization

All STN neurons displayed a single-spike mode of Na^+ action potentials (Fig. 1A) that was totally abolished in the

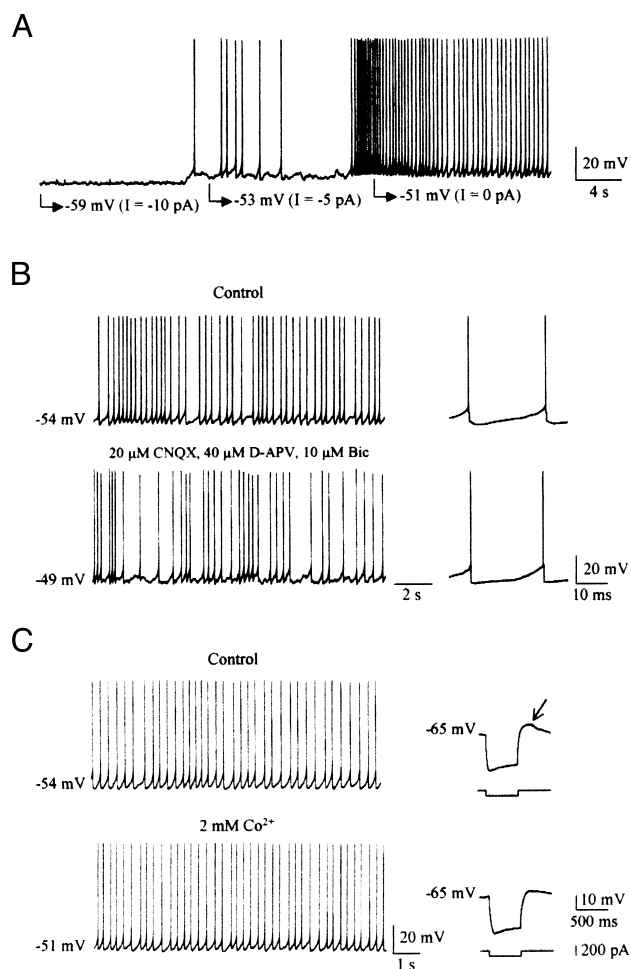


FIG. 1. Single-spike activity of subthalamic nucleus (STN) neurons. A: dependence on membrane potential. Tonic activity present at resting membrane potential ($I = 0 \text{ pA}$), decreased in frequency at a more hyperpolarized potential ($I = -5 \text{ pA}$), and stopped ($I = -10 \text{ pA}$). B and C: dependence on synaptic activity. A bath application of blockers of AMPA/kainate (CNQX), NMDA (D-APV), and GABA_A (bicuculline) receptors and of voltage-activated Ca^{2+} currents (Co^{2+}) did not block single-spike activity. Inset in B shows 2 traces of pacemaker depolarization in control (top) and treated (bottom) conditions. Insets in C show the low-threshold Ca^{2+} spike at the break of a hyperpolarizing pulse in control (arrow, top) and during Co^{2+} application (bottom). External Krebs, intrapipette *solution 1*.

presence of 1 μM TTX. Action potentials had a mean threshold of -42.2 ± 0.3 mV (range: -45 to -40 mV, $n = 24$) and were followed by an AHP that peaked at -57.1 ± 0.5 mV (range: -54 to -62 mV, $n = 25$). Between consecutive spikes, the membrane spontaneously depolarized by ~ 15 mV from the peak of the AHP to the threshold potential of the following spike (Fig. 1B, control *inset*). By analogy with the pacemaker activity of cardiac cells, we called this phase “pacemaker depolarization” (DiFrancesco 1993). The mean frequency was 7.6 ± 0.8 Hz (range: 5.0–17.1 Hz, $n = 16$) in the absence of current injection. When cells were hyperpolarized by negative current injection, approximately one-half of the recorded STN neurons shifted to burst-firing mode (Beurrier et al. 1999) with an AHP peaking at -61.8 ± 0.8 mV (range: -58 to -72 mV, $n = 20$) whereas the remaining one-half displayed single-spike mode but at lower frequencies (Fig. 1A). At more hyperpolarized potentials both types of STN neurons were silent (Fig. 1A).

Single-spike mode was not blocked by a concomitant application of CNQX, D-APV, and bicuculline, the respective antagonists of AMPA/kainate, NMDA, and GABA_A ionotropic receptors (Fig. 1B, $n = 6$), neither was it suppressed by cobalt (Fig. 1C, Co^{2+} 2 mM, $n = 32$). These findings showed that the TTX-sensitive, voltage-dependent single-spike activity is independent of afferent synaptic activity (and particularly activation of glutamatergic and GABAergic ionotropic receptors). This raised the possibility that single-spike activity results from intrinsic voltage-dependent properties of the membrane (i.e., from currents underlying the pacemaker depolarization of the interspike interval that spontaneously brings the membrane potential from the peak of the AHP to the threshold potential for Na^+ -spike initiation). During this phase, the net current is inward because a decreasing outward current cannot by itself depolarize the membrane to Na^+ -spike threshold (Irisawa et al. 1993). Moreover, inward currents are more efficient in depolarizing the membrane whereas outward currents are decreasing and membrane resistance is thus increased. More precisely, increase of resistance depends on the density and deactivation characteristics (kinetics and voltage dependence) of outward currents open at the peak of the AHP. The subthreshold inward currents we analyzed were I_{CaT} , Ca^{2+} -activated inward (cationic) currents (I_{CAN}), I_{NaP} , and I_{h} . To identify which of these currents was involved, we studied the effects of their pharmacological blockade in current-clamp mode and analyzed their voltage dependence in voltage-clamp mode. Does the membrane reach a level of depolarization sufficient for this current to be activated during the interspike interval? Does this current inactivate during repetitive firing?

I_{CaT}

Nickel chloride at a concentration (Ni^{2+} , 40 μM) that preferentially blocks T-type Ca^{2+} currents (Huguenard 1996) (Fig. 2B) did not affect single-spike activity (Fig. 2A, $n = 28$) but strongly reduced the rebound potential called low-threshold Ca^{2+} spike (Nakanishi et al. 1987) seen at the break of a hyperpolarizing current pulse (Fig. 2A, *insets*). This is consistent with above observations that single-spike activity was still present under 2 mM Co^{2+} (Fig. 1C). Voltage-clamp experiments were performed in the presence of L-type Ca^{2+} current blockers (see METHODS solutions A and 2). Currents were

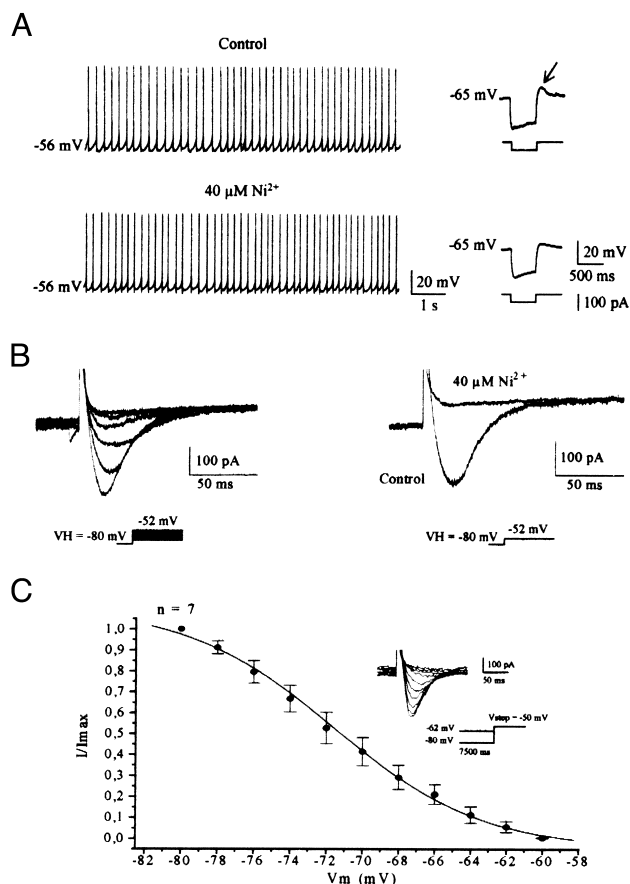


FIG. 2. Single-spike activity is not mediated by low-threshold T-type Ca^{2+} current (I_{CaT}). A: a bath application of Ni^{2+} (40 μM) did not affect tonic activity recorded in current clamp mode though it strongly reduced the amplitude of rebound potential evoked at break of a 500-ms hyperpolarizing pulse to -88 mV (*insets*). B: inward Ca^{2+} currents recorded in response to 200-ms depolarizing steps from -62 to -52 mV (2 mV increment, $V_{\text{H}} = -80$ mV, *left*) were strongly depressed by Ni^{2+} (*right*, step to -52 mV). Inactivation was fitted with a double exponential ($\tau_1 = 13.0$ and $\tau_2 = 165.7$ ms). C: steady state inactivation curve obtained from current traces shown in *inset*: 7,500-ms conditioning prepulses from -80 to -62 mV (2 mV increment) were followed by a fixed 200-ms step to -50 mV. Currents were normalized (I/I_{max}) to maximal current (I_{max}) recorded at -80 mV. Data were fitted with a smooth curve derived from the Boltzmann equation ($V_{1/2}$ of inactivation = -71.6 mV and slope factor $k = 4.1$, $n = 7$). A: external Krebs and intrapipette solution 1. B and C: external solution A and intrapipette solution 2.

evoked by step depolarizations to varying test potentials from a holding potential of -80 mV. A low voltage-activated inward current that had the characteristics of I_{CaT} was recorded; it activated at -59.3 ± 0.7 mV (range: -62 to -55 mV, $n = 10$), presented a rather slow kinetic of inactivation (Fig. 2B, *left*), and was totally abolished in the presence of 40 μM Ni^{2+} (Fig. 2B, *right*). After a 7.5-s conditioning step at -59.9 ± 2.3 mV (range: -66 to -45 mV, $n = 8$), it was fully inactivated (Fig. 2C). Because I_{CaT} is totally inactivated at potentials crossed by the membrane during repetitive discharge, it is unlikely that it participates significantly to the slow pacemaker depolarization.

Calcium-activated inward currents

BAPTA (10 mM), a Ca^{2+} chelator, was introduced into the pipette solution (solution 3) to test the participation of Ca^{2+} -

activated currents such as I_{CAN} , a current that is inward in the potential range of the pacemaker depolarization (Crépel et al. 1994). In agreement with our previous results (Beurrier et al. 1999), BAPTA did not affect single-spike mode (Fig. 3, $n = 5$) although it effectively blocked Ca^{2+} -activated inward current as shown by the strong reduction of the plateau potential duration evoked by a depolarizing current pulse (Fig. 3, *insets*). This suggested that Ca^{2+} -activated currents are not absolutely necessary to sustain single-spike activity. However, they may be activated by a single spike and contribute to the pacemaker depolarization.

I_{NaP}

I_{NaP} is a TTX-sensitive Na^+ current that activates below spike threshold and slowly inactivates (Crill 1996). The role of I_{NaP} on the pattern of discharge in current-clamp recordings is difficult to study because the pharmacological substances that block it (e.g., TTX or QX 314, a derivative of lidocaine) are also blockers of the Na^+ spike. The role of I_{NaP} in the pacemaker depolarization was deduced from the analysis of its voltage dependence. Two protocols were used, either a depolarizing ramp (Fig. 4A, speed $5 \text{ mV} \cdot \text{s}^{-1}$) or long depolarizing steps (1,500 ms) of increasing amplitude (Fig. 4B). K^+ currents were reduced by replacing K^+ ions by Cs^+ in the pipette solution (*solution 4*) and by adding $1 \text{ mM } Cs^+$ in the bath medium. Ca^{2+} currents were suppressed by adding $2 \text{ mM } Co^{2+}$ in the bath medium and by decreasing the external concentration of Ca^{2+} ions (*solution B*). In response to the voltage ramp, an inward current that had the characteristics of a persistent Na^+ current (I_{NaP}) was recorded; it activated at $-54.4 \pm 0.6 \text{ mV}$ (range: -57.2 to -50.3 mV), peaked at $-32.9 \pm 0.8 \text{ mV}$ (range: -37.4 to -26.8 mV), had a maximal amplitude of $-211.1 \pm 8.5 \text{ pA}$ (range: -266.1 to -164.2 pA), and was totally abolished in the presence of $1 \mu\text{M}$ TTX (Fig. 4A, $n = 13$). Because I_{NaP} peaked fast during the ramp protocol, probably because it came out of voltage control and because I_{NaP} can partially

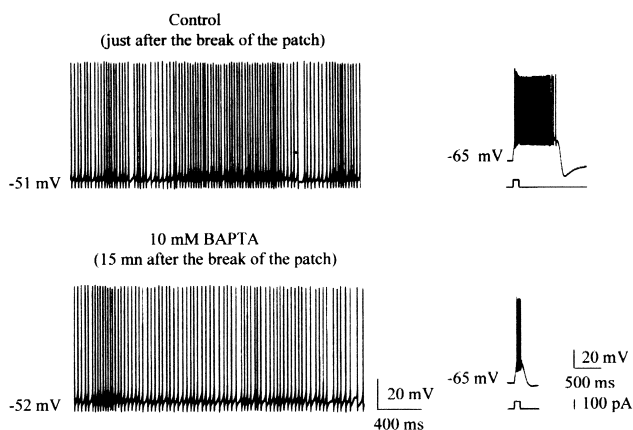


FIG. 3. Single-spike activity does not depend on Ca^{2+} -activated currents. BAPTA (10 mM), the Ca^{2+} chelator, was present in the pipette solution. Single-spike activity was recorded in current-clamp mode (whole cell configuration) just after breaking through the patch of membrane (control) when BAPTA had not yet diffused into the cell as shown by the presence of plateau potential in response to a depolarizing current pulse (*inset*). Fifteen minutes later (*bottom*), plateau potential was strongly reduced (*inset*) but tonic activity was still present. External Krebs and intrapipette *solution 3*.

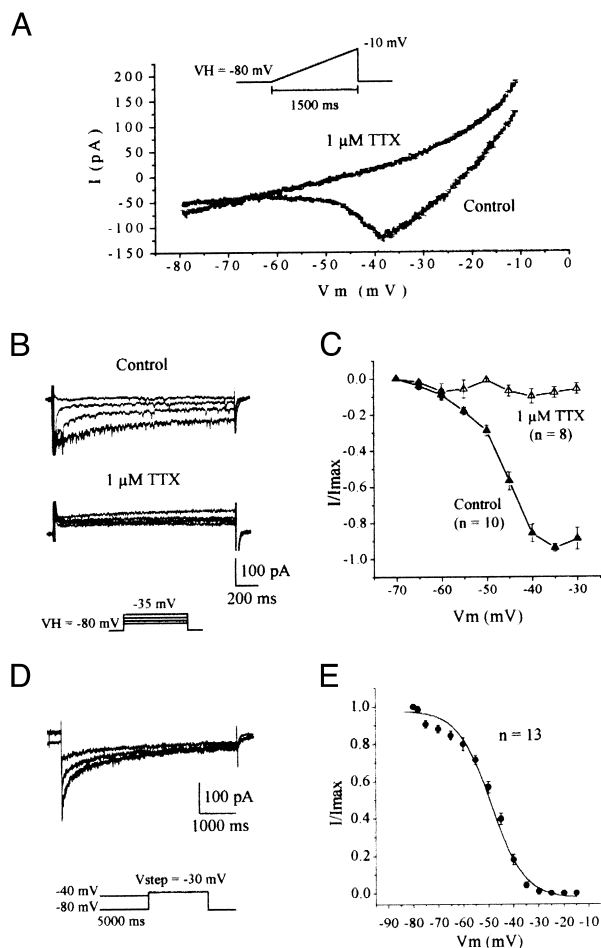


FIG. 4. Persistent TTX-sensitive Na^+ current (I_{NaP}). A: current response to a voltage ramp applied at $5 \text{ mV} \cdot \text{s}^{-1}$ in absence (control) and presence (TTX) of $1 \mu\text{M}$ TTX. Outward current is present in both situations as a result of the absence of blockers of delayed rectifier K^+ current in extracellular medium. B: currents evoked by 1,500-ms step commands from -70 to -30 mV (from bottom to top, steps to -60 , -55 , -50 , and -35 mV) in control conditions (control) and in presence of TTX. C: I - V relationship obtained with a protocol similar to that in B. Leak and outward currents were subtracted. Current amplitudes were normalized (I/I_{max}) to maximal current (I_{max}) recorded. D: current responses to a 5-s step to -30 mV preceded by a 5-s conditioning pulse from -80 to -40 mV (from bottom to top conditioning pulses at -75 , -50 , and -40 mV). E: steady-state inactivation curve of I_{NaP} obtained with a protocol similar to that in D. Current amplitudes were measured 300 ms after onset of depolarization and were normalized (I/I_{max}) to maximal current (I_{max}) recorded (leak was subtracted). Data were fitted with a smooth curve derived from the Boltzmann equation ($V_{1/2}$ of inactivation = -48.8 mV and slope factor $k = 6.5 \text{ mV}$, $n = 7$). External *solution B* and intrapipette *solution 4*. Fast Na^+ current was truncated in B and D.

inactivate during the time course of the ramp command, the voltage step protocol was also tested. From a holding potential of -80 mV , a slowly inactivating Na^+ current was observed (Fig. 4B). It activated from $-56.9 \pm 1.3 \text{ mV}$ (range: -60 to -50 mV , $n = 10$) and was totally abolished in the presence of $1 \mu\text{M}$ TTX (Fig. 4, B and C). I_{NaP} inactivated slowly ($\sim 20\%$) during a 5-s voltage step at -42 mV ($V_H = -60 \text{ mV}$, $n = 5$, data not shown). Voltage-dependent steady-state inactivation was studied with the protocol shown in Fig. 4D. After 5 s at approximately -50 mV ($n = 13$), I_{NaP} was one-half inactivated and after 5 s at -30 mV was fully inactivated (Fig. 4, D and E). To approach the situation during regular spiking, another protocol

was tested. A situation where the membrane was rather depolarized was chosen; from a holding potential of -50 mV (to mimic the AHP), a 1-ms step to $+20$ mV was applied (to mimic a spike) and was followed by a 5-s step to -35 mV (to evoke I_{NaP} and measure channel availability). The two steps were separated by an interval of variable duration (15–60 ms) at -50 mV (to mimic the interspike interval) (Fig. 5, *left*). It was noteworthy that I_{NaP} was not inactivated by the first depolarizing pulse but also that it had a larger amplitude at shorter intervals. Further increases in interval duration gave a stable 30% reduction of I_{NaP} (Fig. 5, *right*). In conclusion, I_{NaP} activates in a potential range crossed by the membrane during the interspike interval and is not totally inactivated after a spike.

I_h

The cesium-sensitive cation current I_h is turned on by membrane hyperpolarization and is inward (depolarizing) at potentials more hyperpolarized than its reversal potential (approximately -30 mV) (Pape 1996). In $\sim 50\%$ of the neurons tested ($n = 5$ of 11), adding cesium chloride (Cs^+ , 1–3 mM) to external Krebs solution hyperpolarized the membrane by approximately -12 mV and switched their activity from tonic-firing to burst-firing mode (Fig. 6A). When positive current was injected, tonic activity reappeared though I_h was still blocked (Fig. 6A, *bottom right and inset*). In the remaining one-half of the cells, Cs^+ did not affect membrane potential or tonic activity ($n = 6$).

Characteristics of I_h were studied in current-clamp and voltage-clamp modes (*solutions C and I*). In response to long hyperpolarizing currents pulses (500 ms), a time-dependent, Cs^+ -sensitive anomalous rectification, seen as a slowly developing depolarizing sag, was observed (Fig. 6A, *insets*). This sag corresponded in voltage-clamp recordings to a slowly developing inward current that activated at -56.5 ± 0.8 mV (range: -60 to -55 mV, $n = 10$) in response to hyperpolarizing steps from a holding potential of -45 mV and increased in amplitude with membrane hyperpolarization (Fig. 6, *B and C*). This current was strongly depressed in the presence of 1 to 3 mM external Cs^+ (Fig. 6, *B and C*). From the above results we conclude that I_h is not essential for a tonic mode of discharge. However, in some cells it contributes toward maintaining

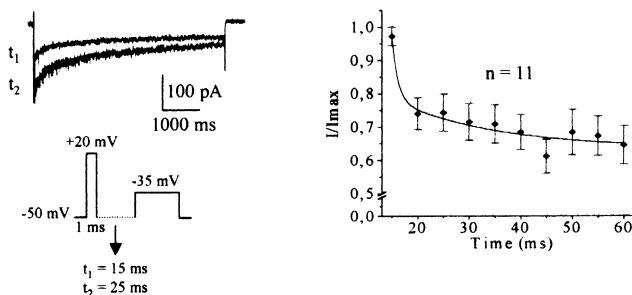


FIG. 5. I_{NaP} inactivation after a spike. Intensity of I_{NaP} in response to a 5-s depolarizing step to -35 mV was studied at different times (15–60 ms) after a short (1 ms) depolarizing step to $+20$ mV ($V_H = -50$ mV). I_{NaP} current traces (*left*) and I_{NaP} amplitude normalized (I/I_{max}) to maximal current (I_{max}) recorded after interval $t = 15$ ms vs. interval duration (*right*). Data were fitted with a monoexponential curve. External solution B and intrapipette solution 4.

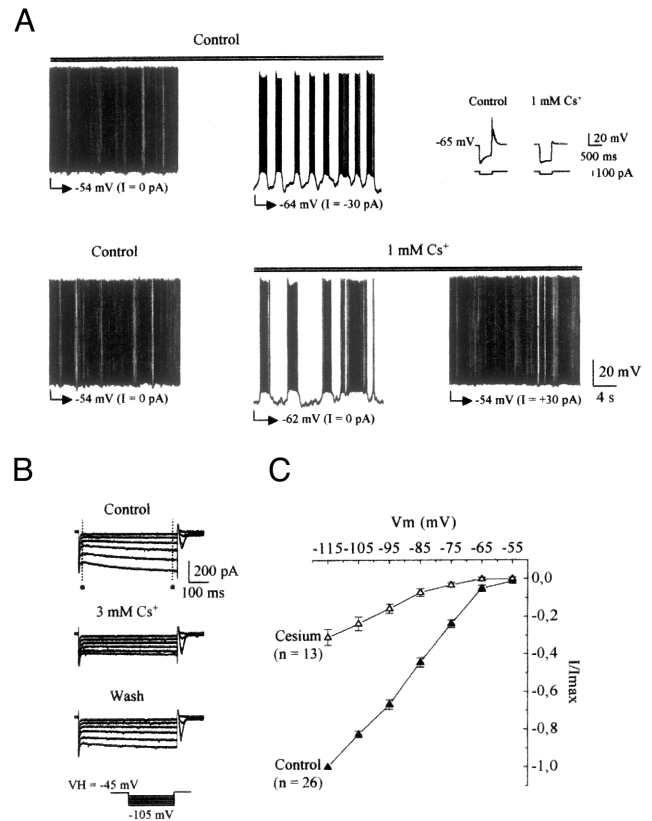


FIG. 6. Role of Cs^+ -sensitive I_h current on membrane potential and firing mode. *A*: in control conditions, a STN neuron displayed single-spike activity at resting membrane potential ($I = 0$ pA) and burst firing mode at more hyperpolarized potentials (*top, control*). In the same neuron, bath application of Cs^+ at resting potential hyperpolarized the membrane by 8 mV and shifted STN activity to burst firing mode (in the absence of any current injection). Continuous injection of positive current shifted back membrane potential to control value and to single-spike activity though Cs^+ was still present (*bottom*). Concomitantly, in the presence of Cs^+ the depolarizing sag recorded in response to a negative current pulse was strongly decreased as well as the depolarizing rebound seen at the break of the hyperpolarizing pulse; spike was truncated (*inset, left*). *B*: from a holding potential (V_H) of -45 mV, a family of currents was evoked in response to 1,500-ms hyperpolarizing steps from -55 to -105 mV (10 mV increment, *left column*) in control conditions (*top*), after bath application of Cs^+ (*middle*), and after recovery from Cs^+ (*bottom*). *C*: I - V relationship in absence (control) and presence of cesium (1–3 mM). Values of I are obtained by subtracting value of current at the beginning of trace (\bullet) from that at end of trace (\blacksquare). Currents were normalized (I/I_{max}) to the maximal current (I_{max}) recorded at -115 mV. *A*: external Krebs and intrapipette solution 1. *B*: external solution C and intrapipette solution 1.

membrane potential at a more depolarized value where tonic mode is present.

DISCUSSION

These results show that single-spike activity of STN neurons is independent of afferent synaptic activity and of Ca^{2+} or Ca^{2+} -activated currents. It mainly results from the persistent Na^+ current, I_{NaP} . Moreover, in some neurons a sustained fraction of I_h exerts a depolarizing influence, enables the membrane potential to reach the threshold for I_{NaP} activation and thus favors the single-spike mode of discharge. The role of I_{NaP} in STN neurons has been deduced from its voltage-dependent characteristics whereas that of I_h was also deduced from the effect of its blockade by external Cs^+ .

I_{NaP} underlies the pacemaker depolarization in the single-spike mode

We propose that the pacemaker depolarization that precedes each action potential is mainly mediated by the slowly inactivating Na^+ current, I_{NaP} . Single-spike mode is voltage-dependent and both action potentials and pacemaker depolarizations were abolished by TTX, a specific blocker of voltage-sensitive Na^+ currents whereas they were insensitive to blockers of Ca^{2+} currents. These observations can be linked to voltage-clamp experiments where a TTX-sensitive inward current recorded in all STN neurons tested, activated at voltages clearly below spike threshold and normally traversed by spontaneously firing cells. This current represented I_{NaP} because there was no residual current in the presence of TTX and a contribution of Ca^{2+} currents is most unlikely in the presence of cobalt and very low concentrations of Ca^{2+} in the extracellular medium. Interestingly, nonbursting STN neurons were silent at voltages more hyperpolarized than the I_{NaP} threshold of activation. However, insights into the functional relevance of I_{NaP} for single-spike activity need also to consider its inactivation properties. I_{NaP} could still be evoked a few milliseconds after a short depolarization that mimicked a spike.

Comparison with other preparations where I_{NaP} plays also a role in spontaneous tonic firing showed that the voltage range of I_{NaP} activation threshold in our experiments is ~ 5 – 10 mV more positive than that found in other central neurons such as neocortical layer V pyramidal neurons (Stafstrom et al. 1985), medial entorhinal neurons (Alonso and Llinas 1989), suprachiasmatic neurons (Pennartz et al. 1997), Purkinje cells (Llinas and Sugimori 1980), and hippocampal neurons (French et al. 1990; MacVicar 1985).

I_{CaT} recorded in this study does not play a significant role in single-spike mode because it is inactivated at potentials where STN neurons fire tonically. Kinetic of inactivation of I_{CaT} recorded in this study is close to that described for a T current mediated by the recently cloned $\alpha 11$ subunit (Lee et al. 1999), which transcript is highly expressed in the STN (Talley et al. 1999).

Role of a sustained I_h component

We suggest that a sustained component of the Cs^+ -sensitive I_h , open at resting membrane potential, contributes toward maintaining single-spike firing in some STN neurons. This is important because the value of membrane potential critically determines the pattern of firing of STN neurons (Beurrier et al. 1999). Cs^+ produced a hyperpolarization that was large enough to move the cell into the burst mode of action potential generation. This was only observed for cells that displayed a plateau potential in control conditions. We have certainly underestimated I_h amplitude and the effects of its blockade with the use of gluconate ions in the pipette solution. Gluconate ions give more physiological recordings but are known to inhibit I_h (Velumian et al. 1997). Moreover, it could also be argued that external Cs^+ also affects delayed and inward rectifier K^+ currents. However, because these currents are outward, their blockade will result in membrane depolarization instead of hyperpolarization. We can hypothesize that a sustained component of I_h as a result of its depolarizing influence moves the membrane potential from a range of Ca^{2+} -mediated burst

activity into a region where it activates I_{NaP} and allows a single-spike mode of discharge. Such a contribution of I_h to resting parameters has already been described in thalamic relay neurons, cells that also display two intrinsic modes of discharge depending on membrane potential (McCormick and Pape 1990; Pape 1996). For the fraction of I_h that is activated on hyperpolarization and deactivated with depolarization, most of its depolarizing effect would be efficient at hyperpolarized potentials when STN neurons are discharging in the bursting mode. One remarkable feature of I_h channels is the presence of a cyclic nucleotide binding region that allows I_h to be modulated by second messengers. Cyclic AMP or cyclic GMP increase I_h channels activities by shifting their activation curve to more depolarized values (Ludwig et al. 1999; Santoro et al. 1998). The modulation of the voltage dependence of I_h through the production of cAMP would thus have important consequences on the firing pattern of STN neurons.

We propose that STN activity shifts from burst-firing mode to single-spike activity in response to a depolarization which induces inactivation of the calcium conductances such as I_{CaT} (which cannot generate any more slow membrane oscillations) and activation of the subthreshold depolarizing currents I_h and I_{NaP} . Conversely, tonic-firing mode would cease once the membrane is more hyperpolarized than the I_{NaP} threshold of activation. Therefore the increase in the percentage of bursts recorded in the STN after the experimental lesion of nigral dopaminergic neurons (Bergman et al. 1994; Hassani et al. 1996; Hollerman and Grace 1992) or in the absence of dopaminergic neurons (Plenz and Kitai 1999) would result from a synaptically driven hyperpolarizing shift of the background resting potential of STN neurons.

Present address of C. Beurrier: Stanford University, School of Medicine, Dept. of Psychiatry and Behavioral Sciences, 1201 Welch Rd., Palo Alto, CA 94304-5485.

Address for reprint requests: C. Hammond, INSERM U29, INMED, Route de Luminy, BP13, 13273 Marseille Cedex 09, France.

Received 20 September 1999; accepted in final form 29 November 1999.

NOTE ADDED IN PROOF

Since this paper was submitted for publication, a report by Bevan et al. was published (*J. Neurosci.* 19: 7617–7628, 1999) showing also that I_{NaP} plays a role in the tonic mode of discharge of STN neurons. However, the contribution of I_h has not been studied by the authors.

REFERENCES

- ALONSO, A. AND LLINAS, R. R. Subthreshold Na^+ -dependent theta like rhythmicity in stellate cells of entorhinal cortex layer II. *Nature* 342: 175–177, 1989.
- BENAZZOZ, A., BORAUD, T., FÉGER, J., BURBAUD, P., BIOULAC, B., AND GROSS, C. Alleviation of experimental hemiparkinsonism by high-frequency stimulation of the subthalamic nucleus in primates: a comparison with L-Dopa treatment. *Mov. Disord.* 11: 627–632, 1996.
- BERGMAN, H., WICHMANN, T., KARMON, B., AND DELONG, M. R. The primate subthalamic nucleus. II. Neuronal activity in the MPTP model of parkinsonism. *J. Neurophysiol.* 72: 507–520, 1994.
- BEURRIER, C., CONGAR, P., BIOULAC, B., AND HAMMOND, C. Subthalamic nucleus neurons switch from single-spike activity to burst-firing mode. *J. Neurosci.* 19: 599–609, 1999.
- CRÉPEL, V., ANIKSZTEIN, L., BEN ARI, Y., AND HAMMOND, C. Glutamate metabotropic receptors increase a Ca^{2+} -activated non specific cationic current in CA1 hippocampal neurons. *J. Neurophysiol.* 72: 1561–1569, 1994.
- CRILL, W. E. Persistent sodium current in mammalian central neurons. *Annu. Rev. Physiol.* 58: 349–362, 1996.
- DIFRANCESCO, D. Pacemaker mechanisms in cardiac tissue. *Annu. Rev. Physiol.* 55: 455–472, 1993.

- FÉGER, J., HASSANI, O. K., AND MOUROUX, M. The subthalamic nucleus and its connections. New electrophysiological and pharmacological data. *Adv. Neurol.* 74: 31–43, 1997.
- FRENCH, C. R., SAH, P., BUCKETT, K. J., AND GAGE, P. W. A voltage-dependent persistent sodium current in mammalian hippocampal neurons. *J. Gen. Physiol.* 95: 1139–1157, 1990.
- GEORGOPOULOS, A. P., DELONG, M. R., AND CRUTCHER, M. D. Relations between parameters of step-tracking movements and single cell discharge in the globus pallidus and subthalamic nucleus of the behaving monkey. *J. Neurosci.* 3: 1586–1598, 1983.
- HASSANI, O. K., MOUROUX, M., AND FÉGER, J. Increased subthalamic neuronal activity after nigral dopaminergic lesion independent of disinhibition via the globus pallidus. *Neuroscience* 72: 105–115, 1996.
- HOLLERMAN, J. R. AND GRACE, A. A. Subthalamic nucleus cell firing in the 6-OHDA-treated rat: basal activity and response to haloperidol. *Brain Res.* 590: 291–299, 1992.
- HUGUENARD, J. R. Low-threshold calcium currents in central nervous system neurons. *Annu. Rev. Physiol.* 58: 329–348, 1996.
- IRISAWA, H., BROWN, H. F., AND GILES, W. Cardiac pacemaking in the sinoatrial node. *Physiol. Rev.* 73: 197–227, 1993.
- LEE, J. H., DAUD, A. N., CRIBBS, L. L., LACERDA, A. E., PEREVERZEV, A., KLÖCKNER, U., SCHNEIDER, T., AND PEREZ-REYES, E. Cloning and expression of a novel member of the low voltage-activated T-type calcium channel family. *J. Neurosci.* 19: 1912–1921, 1999.
- LLINAS, R. AND SUGIMORI, M. Electrophysiological properties of in vitro Purkinje cell somata in mammalian cerebellar slices. *J. Physiol. (Lond.)* 305: 171–195, 1980.
- LUDWIG, A., ZONG, X., STIEBER, J., HULLIN, R., HOFMANN, F., AND BIEL, M. Two pacemaker channels with profoundly different activation kinetics. *EMBO J.* 18: 2323–2329, 1999.
- MACVICAR, B. A. Depolarizing potentials are Na^+ -dependent in CA1 pyramidal neurons. *Brain Res.* 333: 378–381, 1985.
- MATSUMARA, M., KOJIMA, J., GARDINER, T. W., AND HIKOSADA, O. Visual and oculomotor functions of monkey subthalamic nucleus. *J. Neurophysiol.* 67: 1615–1632, 1992.
- MCCORMICK, D. A. AND PAPE, H. C. Properties of hyperpolarization-activated cation current and its role in rhythmic oscillation in thalamic relay neurones. *J. Physiol. (Lond.)* 431: 291–318, 1990.
- MILLER, W. C. AND DELONG, M. R. Altered tonic activity of neurons in the globus pallidus and subthalamic nucleus in the primate MPTP model parkinsonian. In: *The Basal Ganglia II. Structure and function: current concepts*, edited by M. B. Carpenter and A. Jayaraman. New York: Plenum, 1987.
- NAKANISHI, H., KITA, H., AND KITAI, S. T. Electrical membrane properties of rat subthalamic neurons in an in vitro slice preparation. *Brain Res.* 437: 35–44, 1987.
- NEHER, E. Correction for liquid junction potentials in patch clamp experiments. *Meth. Enzymol.* 207: 123–131, 1992.
- OVERTON, P. G. AND GREENFIELD, S. A. Determinants of neuronal firing pattern in the guinea-pig subthalamic nucleus: an in vivo and in vitro comparison. *J. Neural Transm.* 10: 41–54, 1995.
- PAPE, H. Queer current and pacemaker: the hyperpolarization-activated cation current in neurons. *Annu. Rev. Physiol.* 58: 299–327, 1996.
- PARENT, A. AND HAZRATI, L. N. Functional anatomy of the basal ganglia. II. The place of subthalamic nucleus and external pallidum in basal ganglia circuitry. *Brain Res. Rev.* 20: 128–154, 1995.
- PENNARTZ, C.M.A., BIERLAAGH, M. A., AND GEURTSSEN, A.M.S. Cellular mechanisms underlying spontaneous firing in rat suprachiasmatic nucleus: involvement of a slowly inactivating component of sodium current. *J. Neurophysiol.* 78: 1811–1825, 1997.
- PLENZ, D. AND KITAI, S. T. A basal ganglia pacemaker formed by the subthalamic nucleus and external globus pallidus. *Nature* 400: 677–682, 1999.
- SANTORO, B., LIU, D. T., YAO, H., BARTSCH, D., KANDEL, E. R., SIEGELBAUM, S. A., AND TIBBS, G. R. Identification of a gene encoding a hyperpolarization-activated pacemaker channel of brain. *Cell* 93: 717–729, 1998.
- SMITH, Y. AND PARENT, A. Neurons of the subthalamic nucleus in primates display glutamate but not GABA immunoreactivity. *Brain Res.* 453: 353–356, 1988.
- STAFSTROM, C. E., SCHWINDT, P. C., CHUBB, M. C., AND CRILL, W. E. Properties of persistent sodium conductance and calcium conductance of layer V neurons from cat sensorimotor cortex. *J. Neurophysiol.* 53: 153–170, 1985.
- TALLEY, E. M., CRIBBS, L. L., LEE, J. H., DAUD, A., PEREZ-REYES, E., AND BAYLISS, D. A. Differential distribution of three members of a gene family encoding low voltage-activated (T-type) calcium channels. *J. Neurosci.* 19: 1895–1911, 1999.
- VELUMIAN, A. A., ZHANG, L., PENNEFATHER, P., AND CARLEN, P. Reversible inhibition of I_K , I_{AHP} , I_h and I_{Ca} currents by internally applied gluconate in rat hippocampal pyramidal neurones. *Pflügers Arch.* 433: 343–350, 1997.
- WICHMANN, T., BERGMAN, H., AND DELONG, M. R. The primate subthalamic nucleus. III. Changes in motor behavior and neuronal activity in the internal pallidum induced by subthalamic inactivation in the MPTP model of parkinsonism. *J. Neurophysiol.* 72: 521–530, 1994.

High-Frequency Stimulation Produces a Transient Blockade of Voltage-Gated Currents in Subthalamic Neurons

CORINNE BEURRIER,¹ BERNARD BIOULAC,¹ JACQUES AUDIN,¹ AND CONSTANCE HAMMOND²

¹Laboratoire de Neurophysiologie, Centre National de la Recherche Scientifique, Unite Mixte de Recherche 5543, Université Bordeaux II, 33076 Bordeaux Cedex; and ²Institut National de la Santé et de la Recherche Médicale U29, 13273 Marseille Cedex 09, France

Received 8 June 2000; accepted in final form 22 December 2000

Beurrier, Corinne, Bernard Bioulac, Jacques Audin, and Constance Hammond. High-frequency stimulation produces a transient blockade of voltage-gated currents in subthalamic neurons. *J Neurophysiol* 85: 1351–1356, 2001. The effect of high-frequency stimulation (HFS) of the subthalamic nucleus (STN) was analyzed with patch-clamp techniques (whole cell configuration, current- and voltage-clamp modes) in rat STN slices in vitro. A brief tetanus, consisting of 100- μ s bipolar stimuli at a frequency of 100–250 Hz during 1 min, produced a full blockade of ongoing STN activity whether it was in the tonic or bursting mode. This HFS-induced silence lasted around 6 min after the end of stimulation, was frequency dependent, could be repeated without alteration, and was not synaptically induced as it was still observed in the presence of blockers of ionotropic GABA and glutamate receptors or in the presence of cobalt at a concentration (2 mM) that blocks voltage-gated Ca^{2+} channels and synaptic transmission. During HFS-induced silence, the following alterations were observed: the persistent Na^+ current (I_{NaP}) was totally blocked (by 99%), the Ca^{2+} -mediated responses were strongly reduced including the posthyperpolarization rebound (–62% in amplitude) and the plateau potential (–76% in duration), suggesting that T- and L-type Ca^{2+} currents are transiently depressed by HFS, whereas the Cs^+ -sensitive, hyperpolarization-activated cationic current (I_{h}) was little affected. Thus a high-frequency tetanus produces a blockade of the spontaneous activities of STN neurons as a result of a strong depression of intrinsic voltage-gated currents underlying single-spike and bursting modes of discharge. These effects of HFS, which are completely independent of synaptic transmission, provide a mechanism for interrupting ongoing activities of STN neurons.

INTRODUCTION

The observation that deep brain stimulation applied at a high-frequency (HFS) in the subthalamic nucleus (STN) and its surgical destruction, both greatly ameliorate motor signs of Parkinson's disease in patients, led to the hypothesis that HFS blocks, partly or completely, the activity of STN neurons. In keeping with this, HFS in the STN has been shown to significantly decrease the frequency of extracellularly recorded STN neurons in rats in vivo (Benazzouz et al. 1997). As STN neurons are glutamatergic excitatory output neurons (Hammond et al. 1978; Robledo and Féger 1990; Smith and Parent 1988), the immediate consequence of their reduction of activity could be the decrease of activity in target nuclei [substantia nigra pars reticulata (SNr) and entopeduncular nucleus/globus

pallidus internal part (EP/GPi)] as observed in 1-methyl-4-phenyl-1,2,3,6-tetrahydropyridine (MPTP)-treated monkeys and naive rats (Benazzouz et al. 1995; Burbaud et al. 1994; Hayase et al. 1996). It has also been suggested that the consequence of clinical HFS will be to somehow counteract the abnormal bursting pattern recorded in the STN in animal models of Parkinson disease (Bergman et al. 1994; Hassani et al. 1996; Hollerman and Grace 1992; Vila et al. 2000).

To understand the contribution of HFS in pathological conditions, it is clearly essential to determine whether a HFS of the STN could modify or block the intrinsic activities of STN neurons and to analyze the underlying mechanisms. This is best achieved in vitro, as slice preparations enable to better isolate the various effects of a tetanus on neuronal properties. In the present study, using patch-clamp recordings of rat STN neurons in slices, we report that HFS of the STN suppresses the spontaneous activity of both single-spike and bursting STN neurons. The effects of HFS are synaptic-independent and are mediated by a blockade of the voltage-gated currents and particularly the persistent Na^+ (I_{NaP}) current and the L- and T-type Ca^{2+} currents (I_{CaL} and I_{CaT}) that are known to generate the intrinsic spontaneous discharge modes of STN neurons (Beurrier et al. 1999, 2000; Bevan and Wilson 1999).

METHODS

Slice preparation

Experiments were performed on STN neurons in slices obtained from 20- to 28-day-old male Wistar rats. Rats were anesthetized with ether and decapitated. The brain was quickly removed, and a block of tissue containing the STN was isolated on ice in a 0–5°C oxygenated solution containing (in mM) 1.15 NaH_2PO_4 , 2 KCl, 26 NaHCO_3 , 7 MgCl_2 , 0.5 CaCl_2 , 11 glucose, and 250 saccharose, equilibrated with 95% O_2 -5% CO_2 (pH 7.4). This cold solution, with a low NaCl and CaCl_2 content, improved tissue viability. In the same medium, 300- to 400- μ m-thick coronal slices were prepared using a vibratome (Campden Instruments, Loughborough, UK) and were then incubated at room temperature in a Krebs solution containing (in mM) 124 NaCl, 3.6 KCl, 1.25 *N*-[2-hydroxyethyl]piperazine-*N'*-[2-ethanesulfonic acid] (HEPES), 26 NaHCO_3 , 1.3 MgCl_2 , 2.4 CaCl_2 , and 10 glucose, equilibrated with 95% O_2 -5% CO_2 (pH 7.4). After a 2-h recovery period, STN slices were transferred individually to an interface-type

Address for reprint requests: C. Hammond, INSERM U29, Route de Luminy, 13273 Marseille Cedex 09, France (E-mail: hammond@inmed.univ-mrs.fr).

The costs of publication of this article were defrayed in part by the payment of page charges. The article must therefore be hereby marked "advertisement" in accordance with 18 U.S.C. Section 1734 solely to indicate this fact.

recording chamber, maintained at $30 \pm 2^\circ\text{C}$ (mean \pm SD) and continuously superfused (1–1.5 ml/min) with the oxygenated Krebs solution.

STN stimulation

The stimulating electrode was positioned in the middle of the STN identified as an ovoid structure just lying at the border of the basal part of the cerebral peduncle. Two types of stimulating electrodes were tested: The bipolar concentric electrode measuring 0.5 mm in diameter (NEX-100, Rhodes Medical Instruments) used by Burbaud (Burbaud et al. 1994) and Benazzouz (Benazzouz et al. 1995) for the *in vivo* stimulation of the rat STN and a much thinner electrode (0.01 mm in diameter) that we designed to avoid any mechanical lesion of the STN.

Electrophysiological recordings

Slices were visualized using a dissecting microscope and the recording electrode was precisely positioned in the STN. Electrophysiological recordings of STN neurons were performed in the current- or voltage-clamp mode using the blind patch-clamp technique in the whole cell configuration. Patch electrodes were pulled from filamented borosilicate thin-wall glass capillaries (GC150F-15, Clark Electromedical Instruments, Pangbourne, UK) with a vertical puller (PP-830, Narishige, Japan) and had a resistance of 10–12 M Ω when filled with the following (in mM): 120 Kgluconate, 10 KCl, 10 NaCl, 10 ethylene glycol-bis(b-aminoethyl ether)-*N,N,N',N'*-tetraacetic acid (EGTA), 10 HEPES, 1 CaCl₂, 2 MgATP, and 0.5 NaGTP, pH 7.25.

Reagents

Drugs were applied by bath. Reagents were procured from Sigma (St. Louis, MO), except 6-cyano-7-nitroquinoxaline-2,3-dione (CNQX), *D*-(-)-2-amino-5-phosphopentanoic acid (*D*-APV), and bicuculline, which were purchased from Tocris (Bristol, UK).

Data analysis

Membrane potential was recorded using Axoclamp 2A or Axopatch 1D amplifier (Axon Instruments, Foster City, CA), displayed simultaneously on a storage oscilloscope and a four-channel chart recorder (Gould Instruments, Longjumeau, France), digitized (DR-890, NeuroData Instruments, New York), and stored on a videotape for subsequent off-line analysis. During voltage-clamp recordings, membrane currents were fed into an A/D converter (Digidata 1200, Axon Instruments), stored, and analyzed on a PC using pCLAMP software (version 6.0.3, Axon Instruments). Corrections for the liquid junction potential were performed according to Neher (1992): -6 mV for the K-gluconate-based pipette solution as estimated with a 3 M KCl ground electrode.

RESULTS

HFS-induced arrest of single-spike or bursting activity

STN activity was recorded in current-clamp mode (whole cell configuration) for at least 1 min before the HFS was applied. Using a bipolar concentric stimulating electrode similar to that used in rat *in vivo* (see METHODS), a brief (1 min) HFS consisting of 100 μs stimuli of 5–8 V amplitude, produced a blockade of ongoing activity whether it was in single-spike (Fig. 1) or bursting (Fig. 2) mode. This effect was frequency dependent (Figs. 1A and 2) with an optimal frequency of 166 up to 250 Hz that produced a full blockade of the activity ($n = 17$). The latency of the HFS-induced silence could not be determined in detail as during the 1-min stimu-

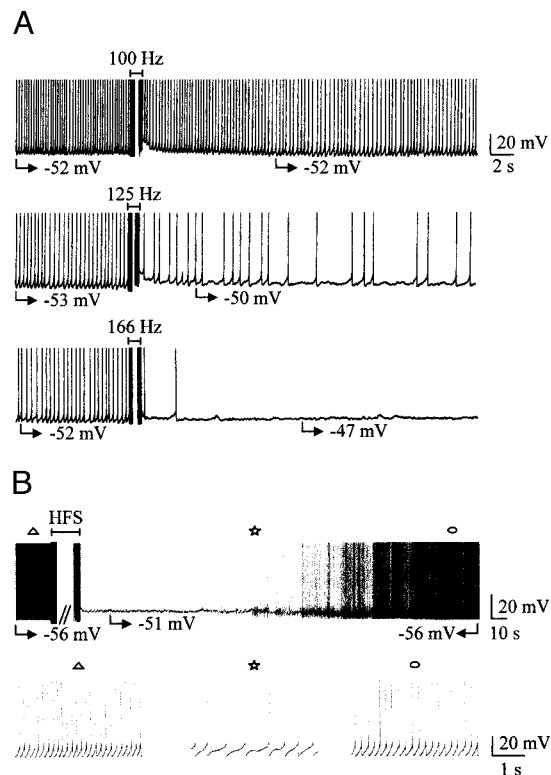


FIG. 1. Effect of high-frequency stimulation (HFS) on the spontaneous single-spike activity of 2 subthalamic nucleus (STN) neurons. *A*: frequency dependence of HFS. Applied at 100 Hz, HFS had nearly no posteffect whereas at 125 Hz it decreased the frequency of tonic activity and at 166 Hz stopped single-spike activity for 5 min. *B*: continuous chart recording (*top*) at slow time resolution of the activity of another STN neuron. HFS (250 Hz) stopped single-spike activity at a potential of -51 mV for 1 min 12 s. Symbols indicate the parts of the top recording that are shown at an expanded time scale in *bottom* traces.

lation period, artifacts prevented analysis of the activity. Nevertheless as shown in Figs. 1B and 2, above a certain frequency, the onset of the blockade was immediately obvious by the end of the train. Interestingly, HFS blocked both single spike (Fig. 1) and burst firing (Fig. 2) modes, suggesting that its mechanisms do not involve a current(s) that is expressed only in one type of discharge.

The suppression of STN spontaneous activity was observed for 5.8 ± 0.7 min (range: 1.1–18.0, $n = 31$) after HFS. At the end of the silence period, spontaneous activity slowly recovered in the same mode as before stimulation (Figs. 1B to 6). During cell silence, membrane potential remained stable at -52.2 ± 0.8 mV (range: -40 to -68 , $n = 45$) for tonic cells and at -56.2 ± 1.4 mV (range: -48 to -61 mV, $n = 8$) for bursting cells. These membrane potentials were significantly more depolarized than the potentials at which cells were silent in control conditions: before HFS, cells tested in the tonic mode were silent at -60.2 ± 0.6 mV (range: -49 to -68 mV, $n = 45$, $P < 0.001$, paired *t*-test) and cells tested in the bursting mode were silent at -63.5 ± 1.3 mV (range: -56 to -68 mV, $n = 8$, $P = 0.015$, paired *t*-test). This suggested that HFS did not stop STN cell activity simply by transiently hyperpolarizing the membrane.

Spikes could still be evoked during the silence period in all tested neurons ($n = 60$). However, in half of the cells, spike threshold was significantly higher during the silence period

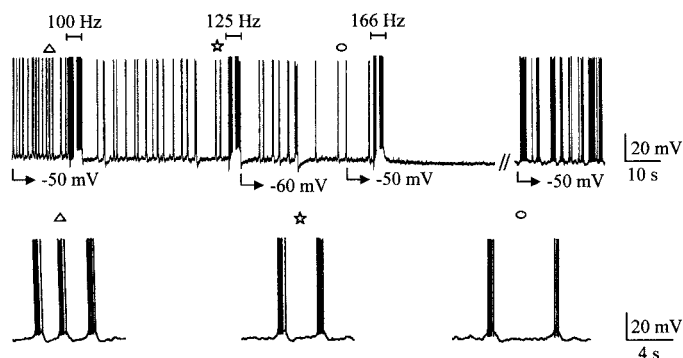


FIG. 2. Frequency-dependent effect of HFS on spontaneous bursting activity of a STN neuron. Chart recording at slow time base of a bursting STN neuron (burst firing was evoked by continuous injection of -150 pA). At 100 and 125 Hz, HFS decreased burst frequency (*bottom traces*) whereas at 166 Hz it totally suppressed bursting activity for 1 min and 49 s. Activity then recovered in burst firing mode. Symbols indicate the parts of the *top recording* that are shown at an expanded time scale in *bottom traces*.

(-39.3 ± 1.6 mV, $n = 30$) compared with the control (-47.5 ± 0.6 mV, $n = 30$, $P < 0.001$; Fig. 3). So was also input membrane resistance, which was significantly increased during HFS-induced silence, when tested at $V_m = -65$ mV by applying hyperpolarizing current pulses of -100 – 200 pA amplitude (247.2 ± 21.1 vs. 226.1 ± 16.3 M Ω , $P = 0.035$, $n = 20$). A second tetanus, applied after the cell recovered from the first one, reversibly silenced the cell again ($n = 15$). This could be repeated as long as patch recording could last. Therefore HFS does depress neuronal activity in slices, and this effect is short lasting and can be repeated. In subsequent experiments, we used a thinner electrode designed to avoid any mechanical lesion of the STN. We chose to use the same parameters of train duration (1 min) and of bipolar stimuli intensity (5–8 V) and duration (100 μ s) but to vary their frequency in the train (range 100–500 Hz) to obtain a clear-cut suppression of activity during which a long-lasting analysis of currents or specific responses could be performed.

HFS-induced suppression of activity is independent of synaptic activity

An important issue was to determine whether effects of the train were mediated by synaptic transmission. Bath applica-

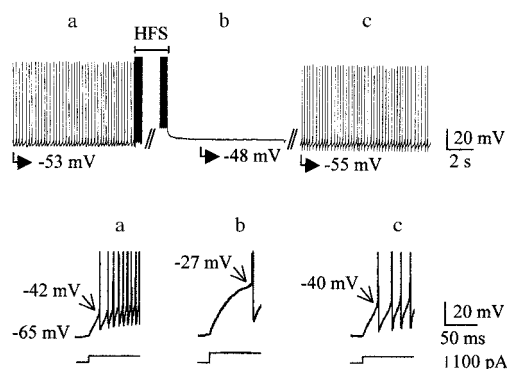


FIG. 3. Increase of threshold potential for Na^+ -dependent spikes during HFS-induced silence. Chart recording at low time base of a tonic STN neuron (*top*). HFS (250 Hz) stopped single-spike activity at a potential of -48 mV for 1 min 25 s. *Bottom*: Na^+ -dependent spikes evoked by a depolarizing pulse of 100 ms, before HFS (*a*, 80 pA), during HFS-induced silence (*b*, 100 pA), and after recovery of activity (*c*, 80 pA).

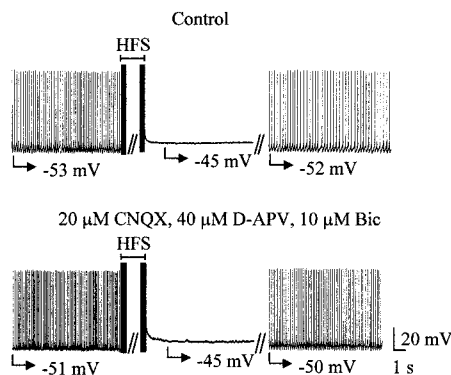


FIG. 4. HFS-induced silence is independent of ionotropic synaptic transmission. HFS (500 Hz) reversibly stopped single-spike activity of a STN neuron for 8 min at -45 mV (control). A 2nd HFS (500 Hz) was applied in the continuous presence of D-APV, CNQX, and bicuculline (Bic). Single-spike activity was stopped at -45 mV for 9 min.

tions of ionotropic glutamate and GABA_A receptor antagonists, CNQX (20 μ M), D-APV (40 μ M), and bicuculline (10 μ M) failed to prevent the effects of HFS ($n = 6$, Fig. 4). Furthermore HFS still suppressed single-spike activity when synaptic transmission was blocked by 2 mM Co^{2+} ($n = 16$, Fig. 5A, *top*). Since the silencing effect of HFS did not require Ca^{2+} -dependent transmitter release, we tested whether it was possible to mimic this effect with intracellular stimulation of the recorded cell. When comparing the two types of HFS (extracellular and intracellular) in the same tonically active STN neurons ($n = 8$), it appeared that both HFS resulted in a silence of the cell. However, intracellular HFS had a different effect on membrane potential: there was a strong hyperpolarization of the membrane at the break of the intracellular pulses (to -63.2 ± 3.1 mV) that declined in about 20 s to -48.1 ± 4.1 mV, a potential at which tonic activity recovered ($n = 8$, data not shown). Such an after hyperpolarization and slow membrane repolarization were never observed after extracellular HFS where membrane potential remained stable during cell silence (Figs. 1–6).

HFS-induced decrease of voltage-gated currents

We hypothesized that HFS induced a modification of voltage-sensitive currents essential for the expression of tonic and burst-firing modes (Beurrier et al. 2000; Bevan and Wilson 1999). In the tonic mode, the silencing effect of HFS did not require Ca^{2+} influx since it was still observed in the presence of 2 mM Co^{2+} nor increase of intracellular Ca^{2+} concentration since it was present in BAPTA-loaded cells ($n = 4$, data not shown). We therefore tested the effect of HFS on spontaneous tonic activity and I_{NaP} recorded from the same STN neurons by shifting from current- to voltage-clamp mode before, during, and after HFS-induced silence. In voltage-clamp mode, in response to a voltage ramp and in the continuous presence of Co^{2+} , a TTX-sensitive inward current that had the characteristics of a persistent Na^+ current was recorded. It was strongly reduced during HFS-induced silence (Fig. 5). *I-V* relationships before and during HFS-induced silence showed that peak amplitude of I_{NaP} was reduced by 99% during cell silence as compared with the control (from -122.2 ± 13.1 to -1.1 ± 1.1 pA, $n = 9$; Fig. 5, B and C). This effect reversed to 78% of control (to -92.5 ± 9.9 pA, $n = 8$) once cell activity recov-

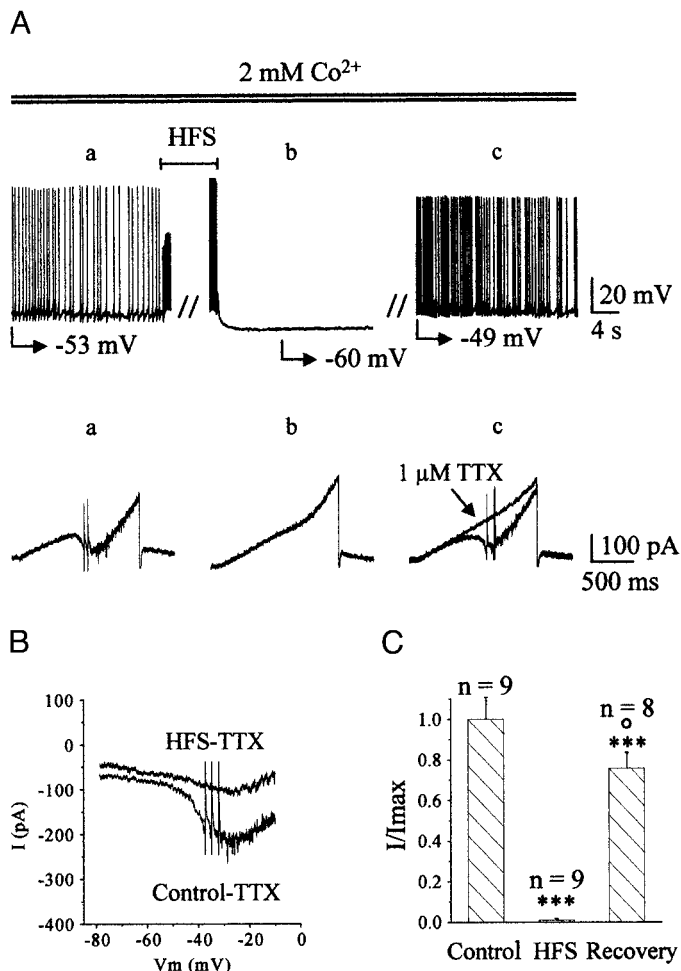


FIG. 5. Effect of HFS on the persistent Na^+ current in the absence of synaptic transmission. *A*: HFS (500 Hz) applied in the continuous presence of Co^{2+} (2 mM) stopped the activity of a tonically firing STN neuron (for 18 min at -60 mV; *top*). In response to a 5-mV/s depolarizing ramp from -80 to -10 mV, a slow inward current was recorded before HFS (*a*), 110 s after HFS (*b*, during HFS-induced silence), and 36 min after HFS (*c*, after recovery of activity). TTX ($1 \mu M$) applied at the end of the experiment totally abolished the slow inward current as well as the fast ones (*c*, *bottom*). *B*: I - V relationships of the persistent Na^+ current obtained from the same cell in *A*. The curve HFS-TTX represents the subtraction of traces Ab - Ac . The curve control-TTX represents the subtraction of traces Aa - Ac . *C*: histogram of I_{NaP} peak amplitude before (control), during (HFS), and after (recovery) HFS-induced silence. *, comparison with preceding column; \circ , comparison with control. * $P < 0.05$; ** $P < 0.001$; *** $P < 0.0001$.

ered. When applied at the end of the experiment, TTX ($1 \mu M$) totally blocked this current, confirming that it was I_{NaP} (Fig. 5A).

Spontaneous bursting mode and I_{Ca} were then analyzed. However, since the recording of Ca^{2+} currents requires the presence of K^+ channel blockers, a procedure incompatible with the recording of burst firing in current-clamp mode, the amplitude of Ca^{2+} currents was therefore evaluated from the evoked potentials they underlie: the rebound depolarization, also called low-threshold Ca^{2+} spike (LTS), that results from the activation of a T-type Ca^{2+} current and the plateau potential that results from the combined action of the nifedipine-sensitive L-type Ca^{2+} current and a Ca^{2+} -activated inward current (Beurrier et al. 1999). Following HFS, during minutes of silence, plateau duration was reduced by 62% (from

1119.4 ± 150.6 to 425.6 ± 111.4 ms, $n = 32$) sometimes with a total suppression of the after spike depolarization (Fig. 6, *A*, *top* and *middle*, and *B*, *left*). Concomitantly, the amplitude of the rebound potential was reduced by 75.9% (from 8.8 ± 0.4 to 2.1 ± 0.5 mV, $n = 23$; Fig. 6, *A*, *top* and *bottom*, and *B*, *right*). Once cell activity recovered, the effects on plateau potential duration and on the amplitude of rebound potential reversed to 66% of control (to 739.4 ± 217.9 ms, $n = 18$) and to 39% of control (to 3.4 ± 0.8 mV, $n = 14$), respectively.

In contrast, the Cs^+ -sensitive, hyperpolarization-activated cation current (I_h) was not affected by HFS at potentials normally traversed by the membrane during tonic firing. It was

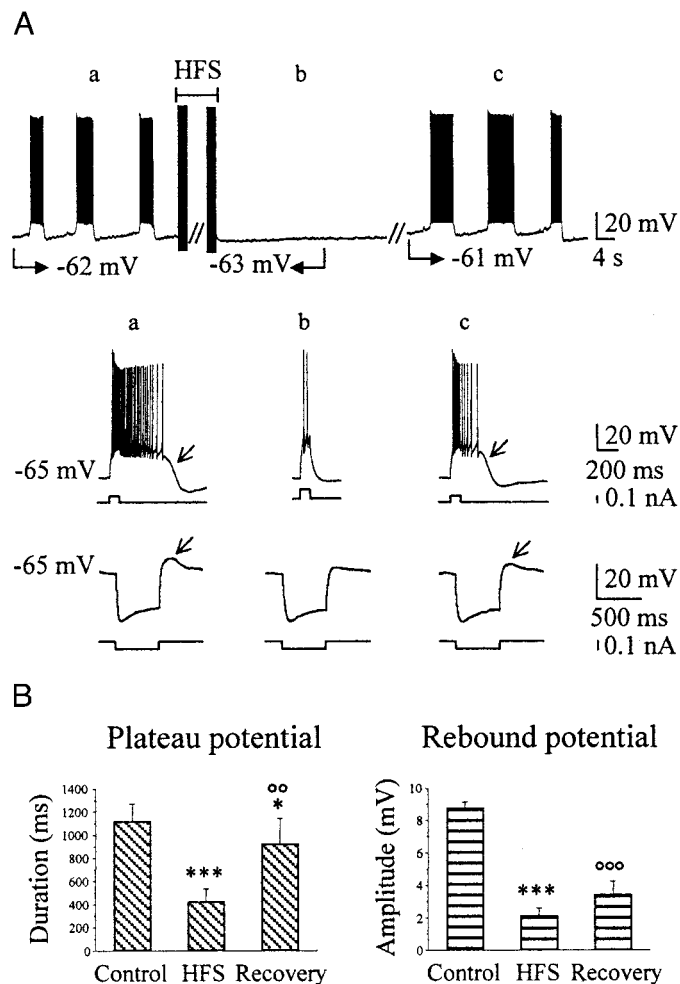


FIG. 6. Effect of HFS on Ca^{2+} -mediated responses. *A*, *top*: HFS (500 Hz) stopped the activity of a burst-firing STN neuron (at -63 mV). *Middle*: plateau potential triggered by a depolarizing current pulse at $V_m = -65$ mV ($+80$ pA, 100 ms), lasted 760 ms before HFS (*a*), lasted 150 ms during cell silence (*b*, 70 s after HFS), and lasted 520 ms during recovery of bursting activity (*c*, 17 min after HFS). \downarrow indicates the after spike depolarization (ADP) present in *a* and *c* and absent in *b*. *Bottom*: rebound potential (\downarrow) recorded at the break of a hyperpolarizing pulse (-80 pA, 500 ms) had an amplitude of 10 mV before HFS (*a*), of 2.5 mV during silence (*b*, 8 min 30 s after HFS), and of 5 mV after recovery of bursting activity (*c*, 34 min after HFS). In the same traces, note the absence of modification of the depolarizing sag that developed during the current pulse. All recordings were obtained from the same STN neuron. *B*, *left*: histogram of plateau potential duration before (control), during (HFS), and after (recovery) HFS-induced silence. *Right*: histogram of rebound potential amplitude before, during, and after HFS-induced silence. *, comparison with preceding column; \circ , comparison with control. * $P < 0.05$; ** or $\circ\circ$: $P < 0.001$; *** or $\circ\circ\circ$: $P < 0.0001$.

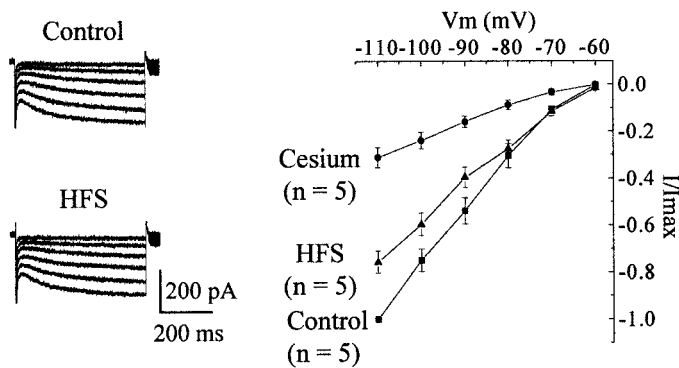


FIG. 7. Effect of HFS on the hyperpolarization-activated cation current I_h . *Left*: from a holding potential of -50 mV, a family of currents was evoked in response to 1,500-ms hyperpolarizing steps from -60 to -110 mV (10-mV increment) before HFS (control) and during HFS-induced silence (HFS). *Right*: I - V relationship of I_h before (control), during HFS-induced silence (HFS), and in the presence of 1–3 mM cesium in the bath ($V_H = -50$ mV). Values of I were obtained by subtracting the value of the current at the beginning of the hyperpolarizing pulse from that at the end of the pulse. Currents were normalized (I/I_{max}) to the maximal current (I_{max}) recorded at -110 mV.

reduced between -80 and -110 mV (by 26.5% at -90 mV, $n = 5$, Fig. 7). Consistent with these findings on I_h , the amplitude of the depolarizing sag observed during a hyperpolarizing current pulse was not significantly affected (it was reduced by 4.8%, from 5.21 ± 0.82 to 4.99 ± 0.80 mV, $P = 0.69$, $n = 12$; Fig. 6A, *bottom*).

DISCUSSION

Our results show that HFS blocks the spontaneous activity of tonic and bursting STN neurons with a mechanism that does not require Ca^{2+} -dependent transmitter release. The silencing effect of HFS has a short latency, is brief, reversible, can be repeated several times with little change, and is frequency dependent. It is mediated by a dramatic reduction of Na^+ and Ca^{2+} voltage-gated currents leading to an interruption of the spontaneous activities of the neurons. In fact, in single-spike activity, a TTX-sensitive, persistent Na^+ current (I_{NaP}), underlies the slow pacemaker depolarization that spontaneously depolarizes the membrane from the peak of the after spike hyperpolarization to the threshold potential for spike initiation (Beurrier et al. 2000; Bevan and Wilson 1999). In contrast, in burst-firing mode, the interplay between a T-type Ca^{2+} current (I_{CaT}), an L-type Ca^{2+} current (I_{CaL}), and a Ca^{2+} -activated inward current, all insensitive to TTX, underlie recurrent membrane oscillations (Beurrier et al. 1999). The blockade of these subliminal currents can also explain the increase of membrane resistance observed during HFS-induced silence.

The silencing effect of HFS does not result from the activation of a local network and is not mediated by the stimulation of afferents to the STN, since it was still observed in the presence of blockers of glutamatergic and GABAergic ionotropic synaptic transmission and in the presence of cobalt at a concentration that totally blocked synaptic transmission in the STN. It was in fact reproduced by direct stimulation of the recorded STN cell as previously tested by Borde et al. (2000) in hippocampal CA1 pyramidal neurons. In this preparation, a low-frequency intracellular stimulation induced a depression of activity that developed rapidly, was reversible, persisted up to

3 min and was still observed when synaptic transmission was strongly reduced by the P-type Ca^{2+} channel blocker ω -agatoxin IVA or enhanced by 4-aminopyridine. The insensitivity of depression to synaptic blockade indicates little if any involvement of synaptic mechanisms and implies that postsynaptic mechanisms are key factors as observed in the present study with extracellular HFS. However, mechanisms underlying intracellular stimulation may be different from those underlying extracellular HFS. The silencing effect of intracellular stimulation is Ca^{2+} -dependent since it requires Ca^{2+} influx and intracellular Ca^{2+} increase in the stimulated cell (Borde et al. 2000), whereas that of extracellular HFS is Ca^{2+} -independent (the present study).

As the pattern of discharge of STN neurons may play an important role in the physio-pathology of parkinsonism (Bergman et al. 1994; Hollerman and Grace 1992), it is tempting to correlate the present effects of *in vitro* HFS on the spontaneous STN activity, to the beneficial effects of high-frequency deep brain stimulation in the STN of MPTP-treated monkeys (Benazzou et al. 1992; Hayase et al. 1996) or parkinsonian patients (Benabid et al. 1994; Limousin et al. 1998). However, such a direct correlation needs further experiments. First, clinical HFS is performed *in vivo* where it could affect the whole basal ganglia network, at least at the onset of stimulation. Second, clinical HFS is efficient at lower frequencies (125–185 Hz) than sometimes *in vitro* HFS does. This could be explained by the differences in the characteristics of the stimulating electrode. Finally, beneficial clinical effects are observed during the continuous application of the stimulation and only for a short while after the stimulation, whereas in the present study, only events that followed the stimulation have been studied. Nevertheless, the present results give some insights in the way intrinsic activity of STN neurons can be depressed.

Present address of C. Beurrier: Dept. of Psychiatry and Behavioral Sciences, School of Medicine, Stanford University, 1201 Welch Rd., Palo Alto, CA 94304-5485.

REFERENCES

- BENABID AL, POLLAK P, GROSS C, HOFFMANN D, BENAZZOUZ A, GAO DM, LAURENT A, GENTIL M, AND PERRET J. Acute and long-term effects of subthalamic nucleus stimulation in Parkinson's disease. *Stereotac Funct Neurosurg* 62: 76–84, 1994.
- BENAZZOUZ A, GAO DM, PIALLAT B, BRESSAND K, AND BENABID AL. Inhibitory response of substantia nigra reticulata neurons to high frequency stimulation of the subthalamic nucleus is independent of globus pallidus activation. *Abstr Soc Neurosci* 83: 3, 1997.
- BENAZZOUZ A, GROSS C, FÉGER J, BORAUD T, AND BIOULAC B. Reversal of rigidity and improvement in motor performance by subthalamic high frequency stimulation in MPTP-treated monkeys. *Eur J Neurosci* 5: 382–389, 1992.
- BENAZZOUZ A, PIALLAT B, POLLAK P, AND BENABID AL. Responses of substantia nigra pars reticulata and globus pallidus complex to high frequency stimulation of the subthalamic nucleus in rats: electrophysiological data. *Neurosci Lett* 189: 77–80, 1995.
- BERGMAN H, WICHMANN T, KARMON B, AND DELONG MR. The primate subthalamic nucleus. II. Neuronal activity in the MPTP model of parkinsonism. *J Neurophysiol* 72: 507–520, 1994.
- BEURRIER C, BIOULAC B, AND HAMMOND C. Slowly inactivating sodium current (I_{NaP}) underlies single-spike activity in rat subthalamic neurons. *J Neurophysiol* 83: 1951–1957, 2000.
- BEURRIER C, CONGAR P, BIOULAC B, AND HAMMOND C. Subthalamic nucleus neurons switch from single-spike activity to burst-firing mode. *J Neurosci* 19: 599–609, 1999.

- BEVAN MD AND WILSON CJ. Mechanisms underlying spontaneous oscillation and rhythmic firing in rat subthalamic neurons. *J Neurosci* 19: 7617–7628, 1999.
- BORDE M, CAZALETS JR, AND BUNO W. Activity-dependent response depression in rat hippocampal CA1 pyramidal neurons in vitro. *J Neurophysiol* 74: 1714–1729, 2000.
- BURBAUD P, GROSS C, AND BIOULAC B. Effect of subthalamic high frequency stimulation in substantia nigra pars reticulata and globus pallidus neurons in normal rats. *J Physiol (Paris)* 88: 359–361, 1994.
- HAMMOND C, DENIAU JM, RIZK A, AND FEGER J. Electrophysiological demonstration of an excitatory subthalamonigral pathway in the rat. *Brain Res* 151: 235–244, 1978.
- HASSANI OK, MOURoux M, AND FEGER J. Increased subthalamic neuronal activity after nigral dopaminergic lesion independent of disinhibition via the globus pallidus. *Neuroscience* 72: 105–115, 1996.
- HAYASE N, FILIION M, RICHARD H, AND BORAUD T. Electrical stimulation of the subthalamic nucleus in fully parkinsonian (MPTP) monkeys. In: *The Basal Ganglia V*, edited by Ohye C. New York: Plenum, 1996, p. 241–248.
- HOLLERMAN JR AND GRACE AA. Subthalamic nucleus cell firing in the 6-OHDA-treated rat: basal activity and response to haloperidol. *Brain Res* 590: 291–299, 1992.
- LIMOUSIN P, KRACK P, POLLAK P, BENAZZOuz A, ARDOUIN C, HOFFMANN D, AND BENABID AL. Electrical stimulation of the subthalamic nucleus in advanced Parkinson's disease. *N Engl J Med* 339: 1105–1111, 1998.
- NEHER E. Correction for liquid junction potentials in patch clamp experiments. *Methods Enzymol* 207: 123–131, 1992.
- ROBLEDO P AND FEGER J. Excitatory influence of rat subthalamic nucleus to substantia nigra and the pallidal complex: electrophysiological data. *Brain Res* 518: 47–54, 1990.
- SMITH Y AND PARENT A. Neurons of the subthalamic nucleus in primates display glutamate but not GABA immunoreactivity. *Brain Res* 453: 353–356, 1988.
- VILA M, PERIER C, FEGER J, YELNIK J, FAUCHEUX B, RUBERG M, RAISMAN-VOZARI R, AGID Y, AND HIRSCH EC. Evolution of changes in neuronal activity in the subthalamic nucleus of rats with unilateral lesion of the substantia nigra assessed with metabolic and electrophysiological measurements. *Eur J Neurosci* 12: 337–344, 2000.

Long-term depression in the nucleus accumbens: a neural correlate of behavioral sensitization to cocaine

Mark J. Thomas¹, Corinne Beurrier¹, Antonello Bonci² and Robert C. Malenka¹

¹ Nancy Pritzker Laboratory, Department of Psychiatry and Behavioral Sciences, Stanford University School of Medicine, Palo Alto, California 94304, USA

² Ernest Gallo Clinic and Research Center, Department of Neurology, University of California, San Francisco, California 94110, USA

Correspondence should be addressed to R.M. (malenka@stanford.edu)

Published online: 5 November 2001, DOI: 10.1038/nn757

A compelling model of experience-dependent plasticity is the long-lasting sensitization to the locomotor stimulatory effects of drugs of abuse. Adaptations in the nucleus accumbens (NAc), a component of the mesolimbic dopamine system, are thought to contribute to this behavioral change. Here we examine excitatory synaptic transmission in NAc slices prepared from animals displaying sensitization 10–14 days after repeated *in vivo* cocaine exposure. The ratio of AMPA (α -amino-3-hydroxy-5-methyl-4-isoxazole propionic acid) receptor- to NMDA (*N*-methyl-D-aspartate) receptor-mediated excitatory postsynaptic currents (EPSCs) was decreased at synapses made by prefrontal cortical afferents onto medium spiny neurons in the shell of the NAc. The amplitude of miniature EPSCs at these synapses also was decreased, as was the magnitude of long-term depression. These data suggest that chronic *in vivo* administration of cocaine elicits a long-lasting depression of excitatory synaptic transmission in the NAc, a change that may contribute to behavioral sensitization and addiction.

Drug addiction is a pathological behavior characterized by compulsive drug seeking and drug ingestion despite severe adverse consequences. Animal models of addiction mimic several of the core features of addiction in humans and therefore can be used to study the neural mechanisms underlying this pathological form of experience-dependent behavioral plasticity. Because of advances in molecular neurobiology, much is known about how drugs of abuse interact with and modify their molecular targets. Furthermore, the molecular adaptations that occur in specific brain regions in response to acute and chronic administration of drugs of abuse are being determined at a rapid pace¹. There is a relative paucity of information, however, about the changes in synapses and circuits that occur as a consequence of these drug-induced molecular changes; this information is critical for a thorough understanding of the neural mechanisms of addiction.

A key feature of addiction is the intensification of drug craving that occurs in human addicts with repeated drug exposure. A prominent model for this behavioral change is the long-lasting increase in locomotor response to drugs of abuse following repeated exposures. This increased response, termed behavioral sensitization, is thought to reflect adaptations in neural circuits that determine the incentive value of external stimuli rendering the circuits hypersensitive or sensitized². Many of the neural adaptations that have been identified following psychostimulant administration take place in the mesolimbic dopamine system, major components of which are the ventral tegmental area (VTA) and the nucleus accumbens (NAc). Modifications in the VTA are involved in the induction of behavioral sensitization, and modifications in the NAc are involved in its long-term maintenance^{3,4}. For example, repeated injection of psychostimulants into the VTA

induces behavioral sensitization, whereas in sensitized animals, the injection of psychostimulants into the NAc is sufficient to elicit sensitized responses (for review, see refs. 3, 4).

Much of the initial work on the adaptations that mediate behavioral sensitization appropriately focused on pre- and postsynaptic changes in dopaminergic transmission. Recently, however, evidence has accumulated that excitatory inputs to the VTA and NAc are critical. Consistent with the VTA's involvement in triggering sensitization, repeated electrical stimulation of excitatory cortical afferents to the VTA induces sensitization that, when elicited by systemic drug exposure, is blocked by local injection of glutamate receptor antagonists into the VTA⁵. Indeed, *in vivo* administration of cocaine elicits a robust enhancement of excitatory synaptic transmission in this structure⁶. On the other hand, the expression of behavioral sensitization is blocked by inhibiting excitatory synaptic transmission in the NAc⁷ or by lesions of the excitatory cortical afferents to this structure⁸ (but see ref. 9).

What changes occur in the NAc that account for its importance in behavioral sensitization? The major cell type in the NAc (>95% of total) is the medium spiny neuron that receives glutamatergic inputs from a variety of cortical and subcortical limbic areas, including the hippocampus, prefrontal cortex and amygdala. Because these neurons have high resting membrane potentials and are generally quiescent, they depend on these excitatory inputs to generate output to their main targets, the VTA and ventral pallidum. It is therefore reasonable to hypothesize that changes in the efficacy of these inputs would have a significant effect on the functioning of mesolimbic dopamine circuitry and would thereby alter the behavioral

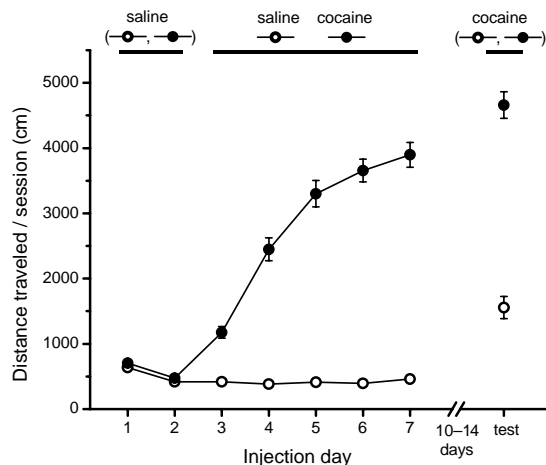


Fig. 1. Behavioral sensitization induced by repeated cocaine administration. Mean (\pm s.e.m.) locomotor activity in response to saline and cocaine injections. Locomotor activity was monitored for 15 min immediately following each injection.

response to a drug of abuse. To test this hypothesis, we examined excitatory synaptic transmission in slices of NAc prepared from mice in which behavioral sensitization was induced by repeated *in vivo* administration of cocaine. This *in vivo* treatment caused a long-lasting depression of synaptic strength at synapses made by prefrontal cortical afferents onto medium spiny neurons in the shell of the NAc.

RESULTS

Long-lasting locomotor sensitization to cocaine

To induce behavioral sensitization, we paired repeated cocaine injections with exposure of the animals to a distinct test environment. After two days of saline injections to habituate the animals to the activity box, the immediate locomotor response to a fixed dose of cocaine (15 mg/kg) increased dramatically across days of testing (Fig. 1; distance traveled, day 3, saline, 418 ± 22 cm, $n = 51$; cocaine, 1176 ± 90 cm, $n = 47$; day 7, saline, 462 ± 36 cm, $n = 51$; cocaine, 3896 ± 191 cm, $n = 47$; $p < 0.001$). To test whether this procedure produced long-lasting sensitization, we administered a challenge dose of cocaine to both saline- and cocaine-treated groups 10 to 14 days following the last dose of the initial treatment regimen. Mice pretreated with cocaine showed a much greater locomotor response to cocaine than did saline-pretreated animals (cocaine, 4660 ± 204 cm, $n = 47$; saline, 1556 ± 170 cm, $n = 51$; $p < 0.001$). These results indicate that the initial five-day exposure to cocaine caused behavioral sensitization that lasted for at least two weeks.

Fig. 2. Repeated cocaine administration induces a decrease in the AMPAR/NMDAR ratio of synaptic currents in the shell but not in the core of NAc. (a) Sample EPSCs from saline and cocaine-treated animals. Scale bars, 40 ms and 20 pA. (b, d) Cumulative probability plots of AMPAR/NMDAR ratio in shell (b) and core (d) neurons from saline ($n = 9$ shell; $n = 8$ core) and cocaine-treated ($n = 12$ shell; $n = 7$ core) mice. (c, e) Mean AMPAR/NMDAR ratio in shell (c) and core (e) neurons from saline and cocaine-treated mice. * $p < 0.05$.

Synaptic transmission in cocaine-treated mice

To determine whether changes in the efficacy of AMPA receptor (AMPA)-mediated synaptic transmission had occurred as a result of the chronic cocaine treatment, we first measured field EPSPs from the NAc¹⁰ in slices prepared from the animals one day after the final cocaine challenge. The NAc is commonly divided into two components, the shell and the core, which are distinguished both anatomically and functionally¹¹. Therefore, data were divided according to the location of the recording. Despite using a range of stimulus intensities, we could not detect any difference in the size of the field EPSPs in either the shell or core between cocaine- and saline-treated groups (data not shown).

Differences in the placement of stimulating and recording electrodes and the density of afferent fibers may be considerable sources of experimental variability when attempting to measure differences in synaptic strength between slices. To reduce the slice-to-slice variability that might have obscured any cocaine-induced changes in synaptic efficacy, we repeated our analysis using a more sensitive assay that compared the relative contributions of AMPARs and NMDA receptors (NMDARs) to EPSCs. This procedure involved evoking EPSCs while holding cells at +40 mV in the absence and then in the presence of the NMDAR antagonist D-APV (50 μ M)⁶ (see Methods). Using this assay, we observed a decrease in the AMPAR/NMDAR ratio in cells in the NAc shell from cocaine-treated compared to saline-treated mice (Fig. 2a–c; cocaine, 0.68 ± 0.09 , $n = 12$; saline 0.97 ± 0.09 , $n = 9$; $p < 0.05$)

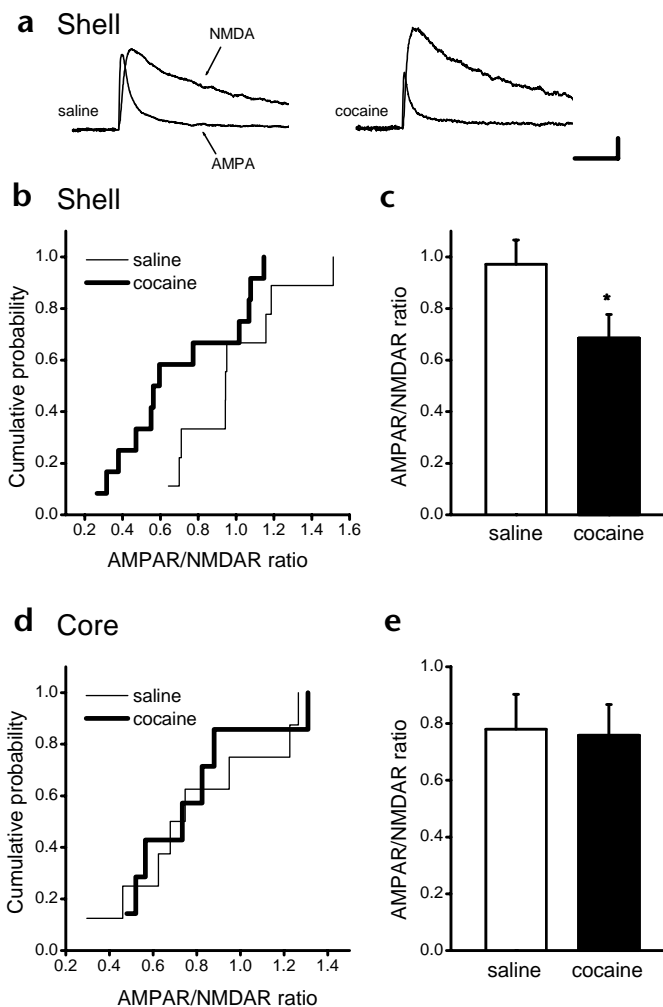
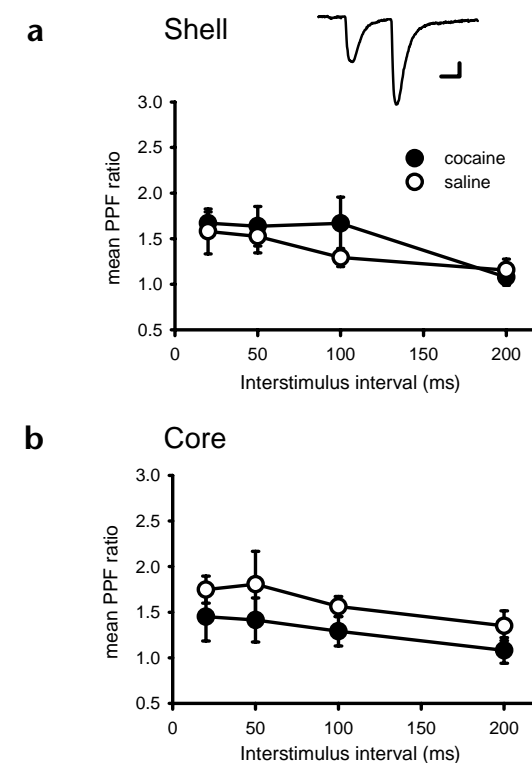


Fig. 3. Repeated cocaine had no significant effect on paired-pulse facilitation in either shell or core. (**a, b**) Mean paired-pulse facilitation (PPF) values in shell (**a**; saline, $n = 7$; cocaine, $n = 9$) and in core (**b**; saline, $n = 9$; cocaine, $n = 8$) are shown for different interstimulus intervals. A sample trace from a shell neuron in the cocaine group is shown (50 ms ISI; calibration bars are 20 ms, 20 pA). Values did not differ significantly between groups at any interval tested ($p > 0.05$; ANOVA).

but not in cells in the core (Fig. 2d and e; cocaine, 0.76 ± 0.11 , $n = 7$; saline 0.78 ± 0.12 , $n = 8$; $p > 0.05$).

Because a single dose of cocaine can elicit behavioral sensitization and an increase in the AMPAR/NMDAR ratio in the VTA⁶, we wondered if the single injection of cocaine received by the saline-treated mice may have affected the AMPAR/NMDAR ratio and thereby influenced our results. Therefore, in another set of experiments, mice were given either one cocaine or one saline injection and AMPAR/NMDAR ratios for shell neurons were determined the next day. There was no significant difference between the mean AMPAR/NMDAR ratios of these groups (data not shown) indicating that, unlike the VTA, a single cocaine exposure does not affect this measurement in the NAc shell.

A decrease in the AMPAR/NMDAR ratio likely reflects a decrease in AMPAR function and/or number, an increase in NMDAR function and/or number, or a combination of these. Such a change, however, does not rule out that changes in transmitter release mechanisms may be induced by *in vivo* cocaine exposure as well. To assess whether changes in the probability of transmitter release (P_r) occurred in the cocaine-treated animals, we compared the magnitude of the facilitation that occurs in response to paired-pulse stimulation, a measure that routinely



changes with changes in P_r ¹². The paired-pulse ratio did not differ between cocaine- and saline-treated mice when tested at a variety of intervals in either shell or core neurons following the cocaine treatment regimen (Fig. 3), suggesting that significant changes in P_r did not occur in cocaine-treated mice.

Changes in mEPSC amplitude in cocaine-treated mice

To address whether AMPAR function and/or number was modified in the NAc shell of cocaine-treated mice, we examined miniature AMPAR-mediated EPSCs (mEPSCs). We found no difference between cocaine and saline-treated mice in either the frequency or the amplitude of mEPSCs in shell neurons (Fig. 4). This suggested that the decrease in the AMPAR/NMDAR ratio might be due to an increase in the function and/or number of NMDARs. Testing this possibility is difficult because the relatively high frequency of mEPSCs in this preparation (~7 Hz), the increased 'noise' generated by opening of NMDARs by ambient glutamate¹³ and the slow rise-time of NMDAR events make it problematic to reliably detect NMDAR-mediated mEPSCs. To circumvent these problems, we bathed slices in Mg^{2+} -free solution to record mEPSCs containing both AMPAR and NMDAR components using the fast rise-time of the AMPAR component to reliably detect the mEPSCs. We then applied D-APV and collected AMPAR mEPSCs from the same cell. Subtracting average mEPSCs in the presence of D-APV from those collected in its absence yielded an average NMDAR mEPSC for each cell (Fig. 5a and b). This mea-

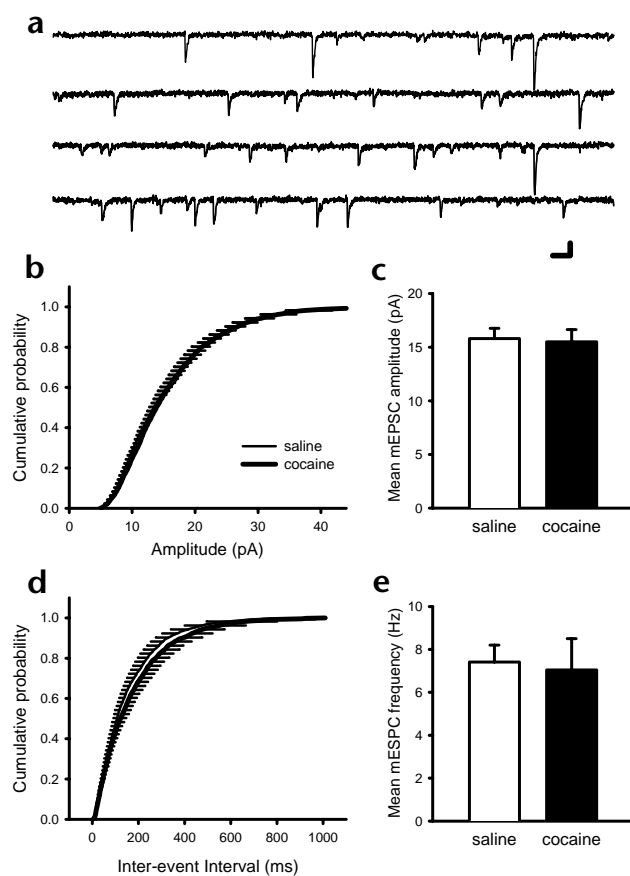


Fig. 4. Repeated cocaine administration had no effect on the amplitude or frequency of shell AMPAR mEPSCs. (**a**) Sample traces of mEPSCs in a shell neuron in a cocaine-treated mouse. Scale bars, 80 ms and 10 pA. (**b, d**) Cumulative amplitude (**b**) and inter-event interval (**d**) distributions of shell mEPSCs obtained in cocaine and saline-treated mice ($n = 400$ events per cell, 8 cells in each group). (**c, e**) Means of mEPSCs amplitude (**c**) and frequency (**e**) $p > 0.05$.

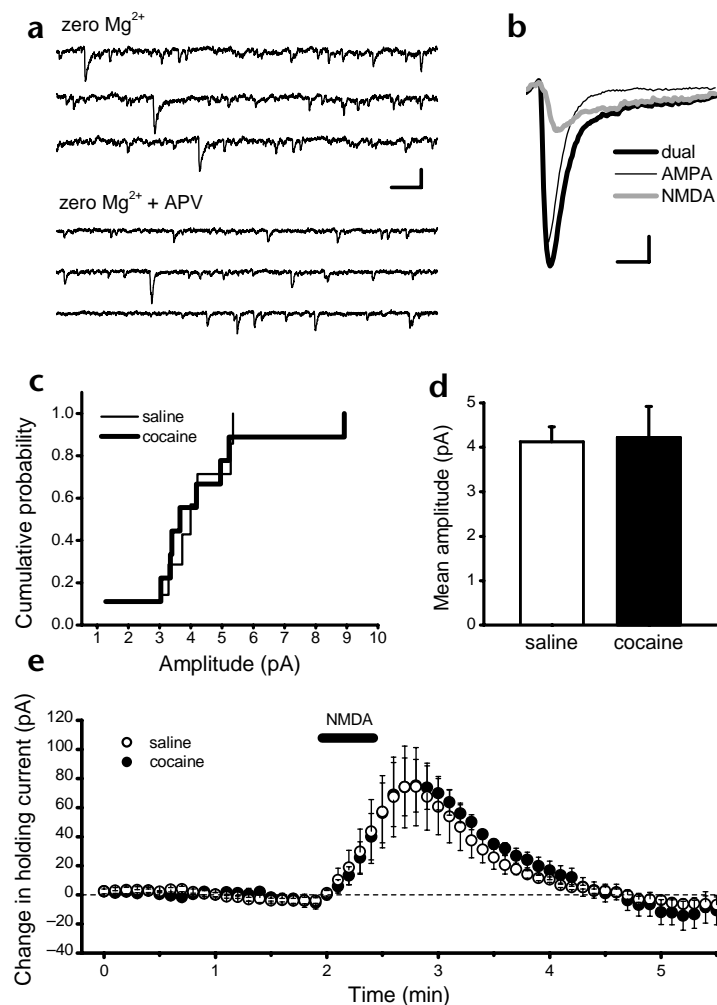


Fig. 5. Repeated cocaine administration did not affect NMDAR mEPSC amplitude or response to NMDA in shell neurons. (a) Samples of mEPSCs recorded at -65 mV in zero Mg^{2+} solution in the absence (top) and presence (bottom) of D-APV ($50 \mu M$) in a cocaine-treated mouse. Scale bars, 100 ms and 20 pA. (b) Sample averaged traces of mEPSCs obtained in each condition plus the subtracted trace that yielded an average NMDAR mEPSC. Scale bars, 10 ms and 2 pA. (c) Cumulative probability plot for NMDAR mEPSC amplitude ($n = 9$ cocaine; $n = 7$ saline). (d) Means of NMDAR mEPSCs amplitude ($p > 0.05$). (e) Bath application of NMDA ($10 \mu M$) for 30 s elicited similar change in holding current in neurons held at $+40$ mV (cocaine, $n = 5$; saline, $n = 4$; $p > 0.05$).

surement did not differ significantly in shell neurons from cocaine- and saline-treated mice (Fig. 5c and d), suggesting that NMDAR function and/or number is not altered at synapses that contain both AMPARs and NMDARs.

Another plausible explanation for the decrease in the AMPAR/NMDAR ratio in cocaine-treated mice is that cocaine causes an increase in the proportion of synapses that contain only NMDARs, so-called silent synapses¹⁴. Such synapses would not have been sampled in our experiments examining dual-component mEPSCs, but may have been recruited when we evoked EPSCs at $+40$ mV. An initial finding that led to the proposal of silent synapses is that the coefficient of variation (CV) of EPSCs was higher for the AMPAR component of EPSCs relative to the NMDAR component¹⁵. When we examined CV ratios in shell neurons from cocaine and saline-treated mice, we found that in 13 of 19 cells examined, the AMPAR/NMDAR CV ratio was greater than 1, suggesting that some synapses on a proportion of medium spiny neurons may contain only NMDARs. However, there was no significant difference between the groups in this ratio (cocaine, 1.39 ± 0.16 , $n = 11$; saline, 1.15 ± 0.09 , $n = 8$; $p > 0.05$). As a final test to determine whether the function or number of NMDARs increased in cocaine-treated mice, we bath-applied NMDA ($10 \mu M$, 30 s) and recorded the change in holding current (Fig. 5e). Again, there was no significant difference between cocaine and saline-treated groups (cocaine, 82 ± 16 pA, $n = 5$; saline, 76 ± 17 pA, $n = 4$; $p > 0.05$).

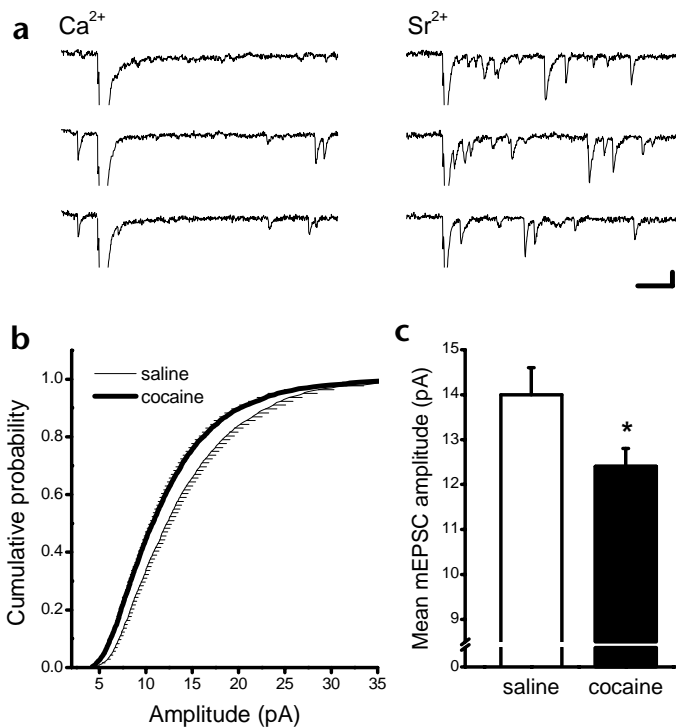
A limitation of our analysis of mEPSCs is that medium spiny neurons receive excitatory projections from several sources and there was no way of knowing from which synapses the mEPSCs were generated. If the changes in the AMPAR/NMDAR ratio of the evoked EPSC occurred primarily at the stimulated synapses, presumably those made by cortical afferents, we may have missed detecting a change in mEPSCs. To circumvent this problem, we replaced the Ca^{2+} in our bathing solution with Sr^{2+} and applied short bursts of afferent stimulation that causes the asynchronous release of vesicles from the set of synapses that were activated (Fig. 6a)¹⁶. Using this technique, it was possible to preferentially sample mEPSCs from the same subset of synapses that were activated to yield the evoked EPSC¹⁷. Although no significant difference in the frequency of asynchronous quantal events between shell neurons from cocaine and saline groups was observed (cocaine, 25 ± 3 Hz, $n = 11$; saline, 23 ± 2 Hz, $n = 12$; $p > 0.05$), the mean amplitude distribution of quantal events in the cocaine group was significantly shifted to the left compared to the saline group (Fig. 6b; $n = 11, 12$; Kolmogorov–Smirnov test; $p < 0.05$) and their mean amplitude was also decreased (Fig. 6c)

(cocaine, 12.4 ± 0.4 pA; saline 14.0 ± 0.6 pA, $p < 0.05$). These results indicate that AMPAR-mediated quantal events generated by the synapses activated by cortical afferents are significantly smaller in the cocaine-treated group, suggesting that the decrease in AMPAR/NMDAR ratio is due, at least in part, to a reduction in AMPAR function and/or number specifically at these synapses.

Changes in LTD in cocaine-treated mice

Given that the synapses made by cortical afferents onto medium spiny neurons can express NMDAR-dependent LTD¹⁸, a form of synaptic plasticity that is associated with a reduction in AMPAR function and number^{17,19,20}, we predicted that the expression of LTD would be reduced in cocaine-treated mice. We first tested whether the triggering of LTD at NAc synapses was significantly impaired in cocaine-treated mice by delivering an LTD-inducing train of stimuli (5 Hz, 3 min) while monitoring field EPSPs. This induced a modest amount of LTD that did not differ between the two groups (cocaine, $79 \pm 6\%$ of baseline, $n = 6$; saline, $85 \pm 5\%$ of baseline, $n = 6$; data not shown). To determine whether the magnitude of LTD was reduced, as would be expected if the decrease in synaptic strength in cocaine-treated mice was due to mechanisms shared with LTD, we made whole-cell recordings from shell neurons and used a strong LTD induction protocol that generated a near-saturating amount of LTD (3 bouts of 5 Hz, 3 min stimulation paired with depolarization to -50 mV). This elicited robust LTD in saline-treated animals (Fig. 7;

Fig. 6. Repeated cocaine treatment decreased the amplitude of AMPAR quantal EPSCs in cortical synapses onto NAc shell neurons. **(a)** Sample traces of evoked EPSCs in the presence of Ca^{2+} or Sr^{2+} . Scale bars, 50 ms and 10 pA. **(b)** Cumulative amplitude distributions of AMPAR quantal EPSCs in Sr^{2+} solution for saline and cocaine-treated mice ($n = 300$ events per cell; saline, $n = 11$; cocaine, $n = 12$). Distributions are significantly different ($p < 0.05$; Kolmogorov–Smirnov test). **(c)** Mean amplitude of quantal EPSCs in Sr^{2+} solution for saline and cocaine-treated mice. Cocaine treatment induced a significant decrease in Sr^{2+} -induced AMPAR mEPSC amplitude ($p < 0.05$; t-test).



$66 \pm 7\%$ of baseline, $n = 7$), but much smaller LTD in the cocaine group (Fig. 7; $84 \pm 4\%$ of baseline, $n = 8$, $p < 0.05$).

DISCUSSION

Psychostimulant-induced behavioral sensitization is thought to model some of the core features of addiction^{2–4}, as well as the development of drug-elicited psychosis²¹. It is of interest not only because it serves as a model for the pathological changes that occur as a consequence of repeated exposure to drugs of abuse but also because it is a robust form of experience-dependent behavioral plasticity. Indeed, sensitized animals can remain hypersensitive to the locomotor and rewarding actions of drugs for periods of months to years^{2–4}. Over the last few years, evidence has accumulated that modifications in excitatory neural circuitry in the VTA and NAc may be particularly important in this form of experience-dependent plasticity. However, excitatory synaptic transmission following repeated drug exposure has not been examined directly. In this study, we measured excitatory synaptic responses in slices of the NAc prepared from animals in which behavioral

sensitization was induced by repeated *in vivo* treatment with cocaine. We found that cocaine treatment decreased synaptic strength at excitatory synapses made by cortical afferents onto medium spiny neurons and that this occurred in the shell region of the NAc but not in the core. Changes in NMDAR-mediated synaptic responses and in the probability of transmitter release were not detected. Consistent with the idea that the cocaine-induced decrease in synaptic strength shares expression mechanisms with LTD, we found that the magnitude of LTD was significantly reduced in the cocaine-treated mice.

Our observations are consistent with several previous findings. First, the single-unit responses of NAc neurons to glutamate are decreased for at least 14 days following a cocaine or amphetamine sensitization regimen²². Although a decrease in AMPAR function and/or number, as our results suggest, could explain this result, changes in voltage-dependent conductances following chronic cocaine exposure²³ may also contribute. Second, a decrease in the levels of the AMPAR subunits, GluR1 and GluR2 is observed in the NAc 14 days following amphetamine-induced sensitization^{24,25} (but see ref. 26). Third, the inward current generated by AMPA/kainate application to acutely dissociated striatal neurons is decreased in cells from animals that have received chronic cocaine²⁷. Fourth, viral-mediated overexpression of GluR2 in the NAc, a manipulation that would be expected to decrease AMPAR function, increases behavioral sensitivity to cocaine as measured by place conditioning²⁸. The functional importance of

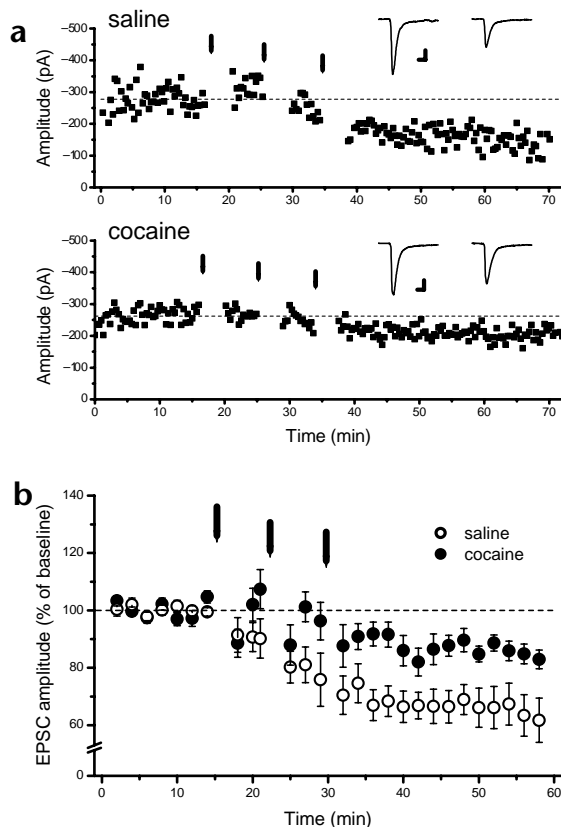


Fig. 7. Repeated cocaine treatment decreased the magnitude of LTD in shell neurons. **(a)** Examples of individual experiments in saline (top) and cocaine-treated mice (bottom) displaying the time course of EPSCs before and after 3 bouts of 5 Hz, 3 min synaptic stimulation paired with depolarization of the cell to -50 mV. Traces shown were collected during the baseline period and 20 min following the last bout. Scale bars, 20 ms and 50 pA. **(b)** Summary graph of the average LTD elicited in saline ($n = 7$) and cocaine-treated ($n = 8$) mice. LTD was significantly decreased in cocaine-treated animals compared with saline animals ($p < 0.05$).



a decrease in the strength of excitatory inputs to the NAc is supported by the findings that virtually all drugs of abuse decrease the firing of NAc neurons²⁹ and that such decreases have been associated with enhanced locomotor activity³⁰. Furthermore, animals will self-administer glutamate receptor antagonists directly into the NAc shell³¹, suggesting that decreases in excitatory drive are reinforcing. It has been proposed that cocaine-induced behavioral sensitization involves an enhancement, not a depression, of excitatory synaptic transmission in the NAc⁴. This conclusion, however, is based primarily on microdialysis measurements of extracellular glutamate concentration, an assay that is not a direct measure of synaptic strength.

The NAc is commonly divided into two regions: the core, which is considered a functional extension of the dorsal striatum, and the shell, which is thought to be a transitional region between the striatum and the extended amygdala³². There is evidence that the shell is particularly important for mediating the effects of drugs of abuse as well as behavioral sensitization. Certain drugs of abuse are preferentially self-administered in the shell compared to core^{31,33,34}. Similarly, drug-induced increases in extracellular dopamine levels may preferentially occur in the shell^{35,36}. It has also been reported that injections of D1 receptor antagonists into the shell reduce the reinforcing effects of cocaine³⁷. In the context of drug-induced locomotor activity, three weeks after repeated cocaine exposure, injection of amphetamine into the shell, but not the core, elicits sensitized locomotor responses³⁸. Conversely, lesions of the shell markedly impair the locomotor effects of amphetamine as well as its rewarding properties³⁹. There is also evidence, however, that excitatory synaptic transmission in the core is important for the expression of behavioral sensitization^{3,4} and thus, our results should not be taken to indicate that modifications in this structure are not also important.

All of our findings are consistent with the hypothesis that chronic *in vivo* cocaine administration induces a form of LTD that shares expression mechanisms with the NMDAR-dependent LTD previously described at these synapses¹⁸. We were unable to detect any change in NMDAR properties but we would caution that our assays might have been relatively insensitive, especially if such changes are restricted to synapses formed by a subset of NAc afferents. The relationship between our findings and the increase in spine density and proportion of branched spines that occurs following psychostimulant-induced sensitization^{40,41} is unclear. Although an increase in spines would suggest that the total afferent input to medium spiny neurons was increased, nothing is known about the detailed properties of these new spines. Indeed, if they contained small numbers of AMPARs or were functionally silent, they could contribute to our observed decrease in the AMPAR/NMDAR ratio.

We have demonstrated that an LTD-like process in the NAc may contribute to the reorganization of neural circuitry that underlies behavioral sensitization to cocaine, and thus may be an important factor in the development of addiction. Also, the decrease in the ability of synaptic activity to elicit LTD in the NAc shell may contribute to the drug-induced behavioral changes. Together with the recent demonstration of a cocaine-induced LTP in the VTA⁶, these results suggest that like other forms of experience-dependent behavioral plasticity^{42–46}, drug-induced changes in behavior may be due, at least in part, to modifications of synaptic efficacy in critical neural circuits. The sort of approaches taken here should further our understanding of how the molecular adaptations caused by drugs of abuse lead to the changes in the behavior of neural circuitry that ultimately must underlie addiction. Furthermore, because of shared molecular and circuit mechanisms, drug-induced behavioral changes such

as psychostimulant-induced behavioral sensitization offer relatively simple models for understanding the neural mechanisms underlying many forms of experience-dependent plasticity, including learning and memory^{1–4,47}.

METHODS

Treatment regimen and locomotor activity. Male C57/Bl6 mice (24–26 days old) were given intraperitoneal injections of either saline (0.9% NaCl) or saline with cocaine (15 mg/kg). Immediately following each injection, horizontal locomotor activity was monitored in open-field chambers (Med Associates, St. Albans, Vermont) for 15 min. After two days of saline injections, mice were divided into groups that received five daily injections of either cocaine or saline. Following 10–14 days without injections, both groups received cocaine injections and locomotor activity was assessed. Brain slices were prepared on the following day. All procedures were approved by the Institutional Animal Care and Use Committee.

Electrophysiology. Sagittal slices of the NAc (200–250 μm) were prepared with a vibratome (Leica, Nussloch, Germany) as described¹⁰. Slices (four per animal) were placed in a holding chamber and allowed to recover for at least 1 h before being placed in the recording chamber and superfused with bicarbonate-buffered solution (ACSF) saturated with 95% O₂/5% CO₂ and containing 119 mM NaCl, 2.5 mM KCl, 1.0 mM NaH₂PO₄, 1.3 mM MgCl₂, 2.5 mM CaCl₂, 26.2 mM NaHCO₃ and 11 mM glucose (at 28–30°C). Picrotoxin (100 μM) was added to block GABA_A receptor-mediated IPSCs. Cells were visualized using infrared-differential interference contrast video microscopy. Whole-cell voltage-clamp recordings were made using an Axopatch1D amplifier (Axon Instruments, Foster City, California). Electrodes (3–8 M Ω) contained 117 mM cesium gluconate, 2.8 mM NaCl, 20 mM HEPES, 0.4 mM EGTA, 5 TEA-Cl, 2.5 MgATP, and 0.25 MgGTP, pH 7.2–7.4 (285–295 mOsm) for whole-cell experiments and ACSF for field recordings. Series resistance (10–40 M Ω) and input resistance were monitored on-line with a 4-mV depolarizing step (50 ms) given with every afferent stimulus. Medium spiny neurons were identified by their morphology and high resting membrane potential (–75 to –85 mV).

We examined core neurons in slices in which rostral and caudal limbs of the anterior commissure as well as caudate/putamen were present. Shell neurons were examined in medial NAc slices that did not contain dorsal striatal tissue. Stainless steel bipolar microelectrodes were placed at the prefrontal cortex–NAc border to stimulate afferents preferentially from the prefrontal cortex. Afferents were stimulated at 0.1 Hz except where noted. Neurons were voltage-clamped at –80 mV except where noted. Data were filtered at 1–2 kHz, digitized at 2–5 kHz and collected on-line using custom software (Igor Pro; Wavemetrics, Lake Oswego, Oregon). EPSC amplitudes were calculated by taking the mean of a 1–2 ms (AMPA EPSCs) or 3–4 ms (NMDAR EPSCs) window around the peak and comparing this with the mean of an 8-ms window immediately before the stimulation artifact. AMPAR/NMDAR ratios were computed by taking the average of EPSCs at +40 mV (25–30 EPSCs) in the absence and presence of D-APV (50 μM). The average response in the presence of D-APV (AMPA-only) was subtracted from that seen in its absence and an average NMDAR EPSC was calculated. The peak of the AMPAR EPSC was divided by the peak of the NMDAR EPSC to yield an AMPAR/NMDAR ratio. To compute AMPAR and NMDAR CVs, short latency (AMPA; 2–4 ms following stimulus) and long latency (NMDAR; 45–50 ms following stimulus) amplitude measurements (25–30 per cell) were made at +40 mV and amplitude variances were divided by amplitude means after subtracting the variance of the recording noise. Miniature EPSCs (300–600 per cell) were collected in the presence of either tetrodotoxin (TTX, 1.5 μM) or lidocaine hydrochloride (0.6–0.8 mM). Dual-component mEPSCs were collected in the additional presence of 20 μM glycine, in the absence of added Mg²⁺ and at a holding potential of –65 mV. In strontium experiments, AMPAR-mediated quantal events were collected during a 400-ms period beginning 50 ms following each stimulus of a 2-Hz, 10-pulse train delivered once every 30 s in bath solution containing D-APV (50 μM), 2.6 mM MgCl₂, 2.5 mM Sr²⁺ and no Ca²⁺. Quantal events were analyzed using Mini-analysis software (Synaptosoft, Decatur, Georgia) with detection para-

meters set at greater than 4 pA amplitude and less than 3 ms rise time and verified by eye. For each cell, a random stretch of 300 mEPSCs was taken for constructing cumulative probability plots and calculating mean mEPSC amplitudes. LTD was induced by delivering a single train (5 Hz, 3 min; field experiments) or multiple trains (3 × 5 Hz, 3 min, 5 min inter-train interval) paired with depolarization to -50 mV.

In over 90% of experiments, data acquisition and analysis were performed blindly without knowledge of the treatment history of the slices. On over 75% of recording days, a similar amount of data was collected from both cocaine and saline groups. Results are presented as mean ± s.e.m. Statistical significance was assessed using two-tailed Student's *t*-tests, ANOVA for paired-pulse experiments, or Kolmogorov-Smirnov tests for comparing the cumulative probability histograms. Traces in figures have had stimulus artifacts removed and are averages of 10–12 consecutive responses.

ACKNOWLEDGEMENTS

This work was supported by grants from NIDA (R.M., M.T.) and the State of California for medical research on alcohol and substance abuse through the University of California, San Francisco (A.B.). We thank T. Robinson, S. Nicola and G. Hjelmstad for comments on the paper and D. Saal for help with some experiments.

RECEIVED 6 AUGUST; ACCEPTED 16 OCTOBER 2001

- Nestler, E. J. Molecular basis of long-term plasticity underlying addiction. *Nat. Rev. Neurosci.* 2, 119–128 (2001).
- Robinson, T. E. & Berridge, K. C. The neural basis of drug craving: an incentive-sensitization theory of addiction. *Brain Res. Brain Res. Rev.* 18, 247–291 (1993).
- Wolf, M. E. The role of excitatory amino acids in behavioral sensitization to psychomotor stimulants. *Prog. Neurobiol.* 54, 679–720 (1998).
- Vanderschuren, L. J. & Kalivas, P. W. Alterations in dopaminergic and glutamatergic transmission in the induction and expression of behavioral sensitization: a critical review of preclinical studies. *Psychopharmacology (Berl.)* 151, 99–120 (2000).
- Schenk, S. & Snow, S. Sensitization to cocaine's motor activating properties produced by electrical kindling of the medial prefrontal cortex but not of the hippocampus. *Brain Res.* 659, 17–22 (1994).
- Ungless, M. A., Whisler, J. L., Malenka, R. C. & Bonci, A. Single cocaine exposure *in vivo* induces long-term potentiation in dopamine neurons. *Nature* 411, 583–587 (2001).
- Pierce, R. C., Bell, K., Duffy, P. & Kalivas, P. W. Repeated cocaine augments excitatory amino acid transmission in the nucleus accumbens only in rats having developed behavioral sensitization. *J. Neurosci.* 16, 1550–1560 (1996).
- Pierce, R. C., Reeder, D. C., Hicks, J., Morgan, Z. R. & Kalivas, P. W. Ibotenic acid lesions of the dorsal prefrontal cortex disrupt the expression of behavioral sensitization to cocaine. *Neuroscience* 82, 1103–1114 (1998).
- Li, Y. & Wolf, M. E. Ibotenic acid lesions of prefrontal cortex do not prevent expression of behavioral sensitization to amphetamine. *Behav. Brain Res.* 84, 285–289 (1997).
- Nicola, S. M., Kambian, S. B. & Malenka, R. C. Psychostimulants depress excitatory synaptic transmission in the nucleus accumbens via presynaptic D1-like dopamine receptors. *J. Neurosci.* 16, 1591–1604 (1996).
- Zahm, D. S. Functional-anatomical implications of the nucleus accumbens core and shell subterritories. *Ann. NY Acad. Sci.* 877, 113–128 (1999).
- Zucker, R. S. Short-term synaptic plasticity. *Annu. Rev. Neurosci.* 12, 13–31 (1989).
- Sah, P., Hestrin, S. & Nicoll, R. A. Tonic activation of NMDA receptors by ambient glutamate enhances excitability of neurons. *Science* 246, 815–818 (1989).
- Malenka, R. C. & Nicoll, R. A. Silent synapses speak up. *Neuron* 19, 473–476 (1997).
- Kullmann, D. M. Amplitude fluctuations of dual-component EPSCs in hippocampal pyramidal cells: implications for long-term potentiation. *Neuron* 12, 1111–1120 (1994).
- Godar, Y. & Stevens, C. F. Two components of transmitter release at a central synapse. *Proc. Natl. Acad. Sci. USA* 91, 12942–12946 (1994).
- Oliet, S. H., Malenka, R. C. & Nicoll, R. A. Bidirectional control of quantal size by synaptic activity in the hippocampus. *Science* 271, 1294–1297 (1996).
- Thomas, M. J., Malenka, R. C. & Bonci, A. Modulation of long-term depression by dopamine in the mesolimbic system. *J. Neurosci.* 20, 5581–5586 (2000).
- Carroll, R. C., Beattie, E. C., von Zastrow, M. & Malenka, R. C. Role of AMPA receptor endocytosis in synaptic plasticity. *Nat. Rev. Neurosci.* 2, 315–324 (2001).
- Lee, H. K., Barbarosie, M., Kameyama, K., Bear, M. F. & Huganir, R. L. Regulation of distinct AMPA receptor phosphorylation sites during bidirectional synaptic plasticity. *Nature* 405, 955–959 (2000).
- Segal, D. S. & Schuckit, M. A. in *Stimulants: Neurochemical, Behavioral and Clinical Perspectives* (ed. Creese, I.) 131–167 (Raven, New York, 1983).
- White, F. J., Hu, X. T., Zhang, X. F. & Wolf, M. E. Repeated administration of cocaine or amphetamine alters neuronal responses to glutamate in the mesoaccumbens dopamine system. *J. Pharmacol. Exp. Ther.* 273, 445–454 (1995).
- Zhang, X. F., Hu, X. T. & White, F. J. Whole-cell plasticity in cocaine withdrawal: reduced sodium currents in nucleus accumbens neurons. *J. Neurosci.* 18, 488–498 (1998).
- Lu, W., Chen, H., Xue, C. J. & Wolf, M. E. Repeated amphetamine administration alters the expression of mRNA for AMPA receptor subunits in rat nucleus accumbens and prefrontal cortex. *Synapse* 26, 269–280 (1997).
- Lu, W. & Wolf, M. E. Repeated amphetamine administration alters AMPA receptor subunit expression in rat nucleus accumbens and medial prefrontal cortex. *Synapse* 32, 119–131 (1999).
- Churchill, L., Swanson, C. J., Urbina, M. & Kalivas, P. W. Repeated cocaine alters glutamate receptor subunit levels in the nucleus accumbens and ventral tegmental area of rats that develop behavioral sensitization. *J. Neurochem.* 72, 2397–2403 (1999).
- Bibb, J. A. *et al.* Effects of chronic exposure to cocaine are regulated by the neuronal protein Cdk5. *Nature* 410, 376–380 (2001).
- Kelz, M. B. *et al.* Expression of the transcription factor deltaFosB in the brain controls sensitivity to cocaine. *Nature* 401, 272–276 (1999).
- Wise, R. A. Drug-activation of brain reward pathways. *Drug Alcohol. Depend.* 51, 13–22 (1998).
- Pennartz, C. M., Groenewegen, H. J. & Lopes da Silva, F. H. The nucleus accumbens as a complex of functionally distinct neuronal ensembles: an integration of behavioural, electrophysiological and anatomical data. *Prog. Neurobiol.* 42, 719–761 (1994).
- Carlezon, W. A. Jr. & Wise, R. A. Rewarding actions of phencyclidine and related drugs in nucleus accumbens shell and frontal cortex. *J. Neurosci.* 16, 3112–3122 (1996).
- McGinty, J. F., ed. *Advancing from the Ventral Striatum to the Extended Amygdala: Implications for Neuropsychiatry and Drug Abuse* Vol. 877 (New York Academy of Sciences, New York, New York, 1999).
- Carlezon, W. A. Jr., Devine, D. P. & Wise, R. A. Habit-forming actions of nomifensine in nucleus accumbens. *Psychopharmacology (Berl.)* 122, 194–197 (1995).
- McKinzie, D. L., Rodd-Henricks, Z. A., Dagon, C. T., Murphy, J. M. & McBride, W. J. Cocaine is self-administered into the shell region of the nucleus accumbens in Wistar rats. *Ann. NY Acad. Sci.* 877, 788–791 (1999).
- Pontieri, F. E. *et al.* Psychostimulant drugs increase glucose utilization in the shell of the rat nucleus accumbens. *Neuroreport* 5, 2561–2564 (1994).
- Pontieri, F. E., Tanda, G. & Di Chiara, G. Intravenous cocaine, morphine, and amphetamine preferentially increase extracellular dopamine in the "shell" as compared with the "core" of the rat nucleus accumbens. *Proc. Natl. Acad. Sci. USA* 92, 12304–12308 (1995).
- Caine, S. B., Heinrichs, S. C., Coffin, V. L. & Koob, G. F. Effects of the dopamine D-1 antagonist SCH 23390 microinjected into the accumbens, amygdala or striatum on cocaine self-administration in the rat. *Brain Res.* 692, 47–56 (1995).
- Pierce, R. C. & Kalivas, P. W. Amphetamine produces sensitized increases in locomotion and extracellular dopamine preferentially in the nucleus accumbens shell of rats administered repeated cocaine. *J. Pharmacol. Exp. Ther.* 275, 1019–1029 (1995).
- Parkinson, J. A., Olmstead, M. C., Burns, L. H., Robbins, T. W. & Everitt, B. J. Dissociation in effects of lesions of the nucleus accumbens core and shell on appetitive pavlovian approach behavior and the potentiation of conditioned reinforcement and locomotor activity by D-amphetamine. *J. Neurosci.* 19, 2401–2411 (1999).
- Robinson, T. E. & Kolb, B. Persistent structural modifications in nucleus accumbens and prefrontal cortex neurons produced by previous experience with amphetamine. *J. Neurosci.* 17, 8491–8497 (1997).
- Robinson, T. E. & Kolb, B. Alterations in the morphology of dendrites and dendritic spines in the nucleus accumbens and prefrontal cortex following repeated treatment with amphetamine or cocaine. *Eur. J. Neurosci.* 11, 1598–1604 (1999).
- Rogan, M. T., Staubli, U. V. & LeDoux, J. E. Fear conditioning induces associative long-term potentiation in the amygdala. *Nature* 390, 604–607 (1997).
- McKernan, M. G. & Shinnick-Gallagher, P. Fear conditioning induces a lasting potentiation of synaptic currents *in vitro*. *Nature* 390, 607–611 (1997).
- Moser, E. I., Krobber, K. A., Moser, M. B. & Morris, R. G. Impaired spatial learning after saturation of long-term potentiation. *Science* 281, 2038–2042 (1998).
- Andersen, P., Moser, E., Moser, M. B. & Trommald, M. Cellular correlates to spatial learning in the rat hippocampus. *J. Physiol. (Paris)* 90, 349 (1996).
- Rioult-Pedotti, M. S., Friedman, D. & Donoghue, J. P. Learning-induced LTP in neocortex. *Science* 290, 533–536 (2000).
- Hyman, S. E. & Malenka, R. C. Addiction and the brain: the neurobiology of compulsion and its persistence. *Nat. Rev. Neurosci.* 2, 695–703 (2001).

Brief Communication

Enhanced Inhibition of Synaptic Transmission by Dopamine in the Nucleus Accumbens during Behavioral Sensitization to Cocaine

Corinne Beurrier and Robert C. Malenka

Nancy Pritzker Laboratory, Department of Psychiatry and Behavioral Sciences, Stanford University School of Medicine, Palo Alto, California 94304

Neural adaptations in the nucleus accumbens (NAc), a key component of the mesolimbic dopamine (DA) system, are thought to mediate several of the long-term behavioral sequelae of chronic *in vivo* exposure to drugs of abuse. Here, we examine whether the modulation of excitatory synaptic transmission by DA in the NAc shell is modified after chronic cocaine exposure that induced behavioral sensitization. The DA-induced inhibition of AMPA receptor-mediated synaptic responses was enhanced in cocaine-treated mice, an effect that was caused by activation of D1-like receptors. DA did not

enhance NMDA receptor-mediated synaptic responses in saline- and cocaine-treated mice or in the dorsal striatum of control mice. We hypothesize that the enhanced inhibitory effects of DA on synaptic transmission in the NAc are one of a number of adaptations that contribute to a decrease in excitatory drive to NAc after exposure to drugs of abuse.

Key words: addiction; cocaine; dopamine; nucleus accumbens; striatum; synaptic transmission; glutamate; AMPA receptors; NMDA receptors

The reinforcing effects of drugs of abuse are thought to be mediated in part by the release of dopamine (DA) in the mesolimbic dopaminergic pathway, which projects from A10 dopaminergic cell bodies within the ventral tegmental area to the nucleus accumbens (NAc) (Wise, 1998). Thus, critical questions for understanding the neural mechanisms responsible for mediating the behavioral effects of drugs of abuse include (1) what are the effects of DA on synaptic transmission in the NAc and (2) how are these effects modified by chronic *in vivo* exposure to drugs of abuse? GABAergic medium spiny neurons are the major cell type in the NAc and receive glutamatergic inputs from cortical and subcortical limbic areas, including the hippocampus, prefrontal cortex, and amygdala (Groenewegen et al., 1999; Nicola et al., 2000). Because these cells display very negative resting potentials (Higashi et al., 1989; Uchimura and North, 1991), they are highly dependent on these excitatory inputs to generate their outputs. DA, as well as psychostimulants such as amphetamine, depresses synaptic transmission at these excitatory synapses via activation of a D1-like receptor, although the exact mechanism by which this occurs is contentious (Higashi et al., 1989; Pennartz et al., 1992; Harvey and Lacey, 1996, 1997; Nicola et al., 1996; Nicola and Malenka, 1997). Here, we examine how the modulation of excitatory synaptic transmission in the NAc by DA is modified after chronic *in vivo* cocaine administration sufficient to elicit behavioral sensitization, a prominent animal model for certain core features of addiction (Robinson and Berridge, 1993; Wolf, 1998; Vanderschuren and Kalivas, 2000).

MATERIALS AND METHODS

Treatment regimen and locomotor activity. Male C57BL/6 mice (22 d) were given intraperitoneal injections of either saline (0.9% NaCl) or saline with cocaine (15 mg/kg). Immediately after each injection, horizontal locomotor activity was monitored in open-field chambers (Med Associates Inc., St. Albans, VT) for 15 min. After an initial 2 d of receiving only saline injections, mice were randomly divided into groups that received five daily injections of either cocaine or saline. After 10–14 d without injections, both groups received cocaine injections, and locomotor activity was assessed. Brain slices were prepared from these animals on the following day. Some of these animals (10 of 31 saline animals; 10 of 43 cocaine animals) were included in our previous study on behavioral sensitization (Thomas et al., 2001).

Electrophysiology. Sagittal slices of the NAc (200–250 μm) were prepared as described previously (Thomas et al., 2001). After a 1 hr recovery period, slices were placed in a submersion-type recording chamber and perfused (1.5–2 ml/min) at room temperature with a bicarbonate-buffered solution (artificial CSF) saturated with 95% O₂/5% CO₂ and containing (in mM): 119 NaCl, 2.5 KCl, 1 NaH₂PO₄, 1.3 MgCl₂, 2.5 CaCl₂, 26.2 NaHCO₃, 11 glucose, and 0.1 picrotoxin.

Cells were visualized with an upright microscope (Zeiss, Thornwood, NY), and whole-cell voltage-clamp recordings were made using an Axopatch 1D amplifier (Axon Instruments, Foster City, CA). Electrodes (5–8 M Ω) contained (in mM): 117 cesium gluconate, 2.8 NaCl, 20 HEPES, 0.4 EGTA, 5 TEA-Cl, 2.5 MgATP, and 0.25 MgGTP, pH 7.2–7.4 (285–295 mOsm). Field potential recordings were made using pipettes filled with 1 M NaCl. For perforated-patch experiments, amphotericin B (30 mg/ml) dissolved in DMSO was added to internal solution (0.02–0.03% final concentration) containing (in mM): 110 cesium gluconate, 2.8 NaCl, 20 HEPES, 0.4 EGTA, 5 TEA-Cl, and 20 CsCl. Experiments were begun only after series resistance had stabilized. Medium spiny neurons were identified by their morphology and high resting membrane potential (–75 to –85 mV) as monitored at break-in.

Stainless steel bipolar microelectrodes were placed at the prefrontal cortex–NAc border to stimulate afferents, preferentially from the prefrontal cortex at a baseline frequency of 0.1 Hz. Neurons were voltage clamped at a membrane potential of –80 mV. Series and input resistances were determined with each afferent stimulus and were monitored for stability throughout each experiment. Data were filtered at 2 kHz, digitized at 5 kHz, and collected on-line using custom software (Igor Pro; Wavemetrics, Lake Oswego, OR). Evoked response amplitudes were calculated by taking the mean of a 1 msec window around the peak and

Received March 29, 2002; revised May 1, 2002; accepted May 7, 2002.

This work was supported by grants from Fondation pour la Recherche Médicale (C.B.) and the National Institute on Drug Abuse (R.C.M.). We thank A. Bonci, D. Saal, and M. Thomas for helpful comments.

Correspondence should be addressed to Robert C. Malenka, Department of Psychiatry and Behavioral Sciences, 1201 Welch Road, Room P105, Stanford Medical Center, Palo Alto, CA 94304. E-mail: malenka@stanford.edu.

Copyright © 2002 Society for Neuroscience 0270-6474/02/225817-06\$15.00/0

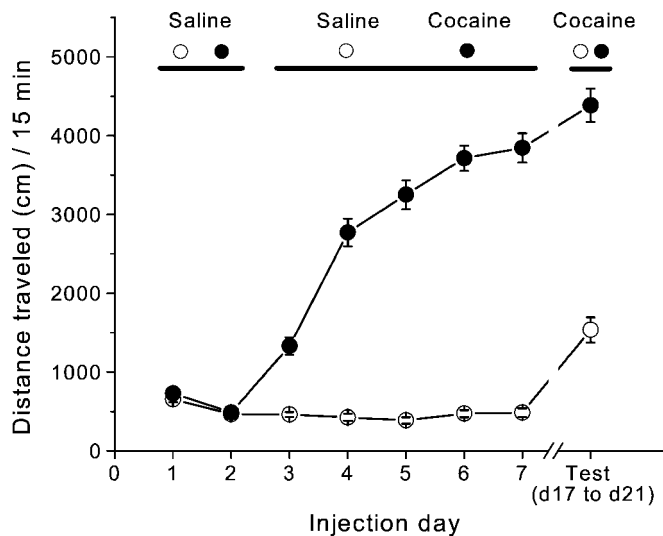


Figure 1. Repeated cocaine administration induces behavioral sensitization. Mean \pm SEM acute locomotor activity in response to saline and cocaine injections is shown. Locomotor activity was monitored for 15 min immediately after each injection.

comparing this with the mean of an 8 msec window immediately before the stimulation artifact. To simultaneously monitor AMPA receptor (AMPA) and NMDA receptor (NMDAR) EPSCs, cells were rapidly depolarized to +40 mV and held for 1–3 min before beginning afferent stimulation to allow voltage-dependent conductances to inactivate completely. AMPAR EPSCs were measured on the rising phase of the EPSCs at a time point that was minimally affected (<10%) by application of D-APV, on average 6.1 msec ($n = 32$) after the stimulation artifact (see Fig. 4A). The NMDAR EPSC was measured 250 msec after the stimulation artifact, a time at which there was no AMPAR-mediated component. AMPAR/NMDAR ratios were calculated by averaging 10–20 consecutive responses immediately before or at the end of DA application and making measurements as described above. The data in Figure 2 were collected and analyzed in a blind manner. Results are presented as mean \pm SEM. Statistical significance was assessed using two-tailed Student's *t* tests. Traces in figures have had stimulus artifacts removed and are the average of 10–20 consecutive responses.

Drugs. All drugs were purchased from Sigma-RBI (St. Louis, MO) except cocaine hydrochloride (Stanford Health Services Pharmacy, Palo Alto, CA) and D-APV (Toocris Cookson, Ballwin, MO). Stock solutions of dopamine hydrochloride, *R*(+)-7-chloro-8-hydroxy-3-methyl-1-phenyl-2,3,4,5-tetrahydro-1H-3-benzazepine hydrochloride [R(+)-(+)-SCH-23390], 1-[2-bis[4-fluorophenyl]methoxyethyl]-4-(3-phenylpropyl)piperazine dihydrochloride (GBR-12909), and cocaine hydrochloride were made in water and applied through the superfusion medium. Sodium metabisulfite (final concentration, 50 μ M) was added to the dopamine solution. Cocaine for *in vivo* injections was dissolved in NaCl (0.9%).

RESULTS

Long-lasting locomotor sensitization to cocaine in mice

To induce behavioral sensitization, we paired repeated cocaine injections with exposure of the animals to a distinct test environment. After 2 d of saline injections to habituate the animals to the activity box, the locomotor response to a fixed dose of cocaine (15 mg/kg) increased dramatically across days of testing (Fig. 1) (day 3 distance traveled: saline, 463.5 ± 31.1 cm, $n = 31$; cocaine, 1329.5 ± 111.1 cm, $n = 43$; day 7 distance traveled: saline, 484.6 ± 54.8 cm, $n = 31$; cocaine, 3843.9 ± 185.5 cm, $n = 43$; $p < 0.0001$). To test whether this procedure produced long-lasting locomotor sensitization, we administered a challenge dose of cocaine to both saline- and cocaine-treated groups 10–14 d after the last dose of the initial treatment regimen. Mice pretreated with cocaine

showed a much greater locomotor response to cocaine than did saline-pretreated animals (Fig. 1) (cocaine, 4384.9 ± 212.8 cm, $n = 43$; saline, 1535.3 ± 159.1 cm, $n = 31$; $p < 0.0001$). These results indicate that the initial 5 d exposure to cocaine caused behavioral sensitization that lasted for ≥ 2 weeks.

Increased inhibition of excitatory synaptic transmission by dopamine in sensitized mice

The NAc is commonly divided into two components, the shell and the core, which can be distinguished both anatomically and functionally (Zahm, 1999). Previous work found modification of excitatory synaptic transmission after chronic cocaine treatment in the shell but not in the core of the NAc (Thomas et al., 2001). Therefore, all recordings were made in the NAc shell. In initial experiments, we used whole-cell recordings to monitor AMPAR-mediated EPSCs (AMPA EPSCs) and applied a concentration of DA (75 μ M) that reliably elicits a depression of synaptic transmission in the NAc (Nicola et al., 1996). We found that there was no difference between slices from saline- and cocaine-treated mice at the end of the 10 min DA application (Fig. 2A,D) (cocaine, $-26.9 \pm 4\%$ change from initial baseline, $n = 12$; saline, $-25.8 \pm 3.7\%$, $n = 12$; $p > 0.05$). However, the effect of DA washed out much more slowly in the cocaine group (Fig. 2A) (between 5 and 11 min after washout: cocaine, $-13.7 \pm 4.8\%$, $n = 12$; saline, $1.7 \pm 4\%$, $n = 12$; $p < 0.05$). Because slices are exposed to concentrations of DA < 75 μ M during the washout, this difference in washout rate may reflect the fact that lower concentrations of DA had a greater effect in cocaine-treated mice. To test this possibility, we applied a lower concentration of DA (20 μ M) that had a minimal effect on slices from saline-treated mice (Fig. 2B–D) ($-3.9 \pm 4.5\%$, $n = 9$). In contrast, this same concentration of DA caused a significant depression of synaptic transmission in slices from cocaine-treated animals (Fig. 2B–D) ($-19.9 \pm 4.9\%$, $n = 10$, $p < 0.05$). These results indicate that the chronic *in vivo* cocaine treatment enhanced the inhibitory actions of DA on excitatory synaptic transmission in the NAc shell.

Synaptic actions of DA in cocaine-treated mice are caused by D1-like receptors

DA receptors are commonly subdivided into two classes: (1) D1-like receptors (D1 and D5) and (2) D2-like receptors (D2, D3, and D4) (Sibley and Monsma, 1992; Civelli et al., 1993; Jarvie and Caron, 1993). The inhibition of excitatory synaptic transmission by DA in the NAc appears to be mediated primarily by a D1-like receptor (Higashi et al., 1989; Pennartz et al., 1992; Nicola et al., 1996). To address whether D1-like receptors also mediate the synaptic actions of DA after *in vivo* cocaine treatment, we made extracellular field potential recordings (fEPSPs) and tested the ability of the specific D1 receptor antagonist SCH-23390 (10 μ M) to antagonize the inhibitory actions of DA (20 μ M). As observed using whole-cell recordings, the inhibition of fEPSPs by DA was greater in slices from the cocaine treatment group (Fig. 3A) (cocaine, $-17.8 \pm 2.1\%$, $n = 28$; saline, $-5.4 \pm 2.2\%$, $n = 11$; $p < 0.01$). This depressant action of DA in the cocaine group was significantly reduced by SCH-23390 (Fig. 3B) (first DA application, $-25.5 \pm 4.9\%$; second application in the presence of SCH-23390, $-8.5 \pm 3.5\%$; $n = 6$; $p < 0.05$), indicating that as is the case in untreated animals (Higashi et al., 1989; Pennartz et al., 1992; Nicola et al., 1996), this action of DA is mediated in large part by D1-like receptors that presynaptically depress glutamate release (Nicola et al., 1996, 2000; Nicola and Malenka, 1997).

The enhanced inhibition of excitatory transmission by DA in

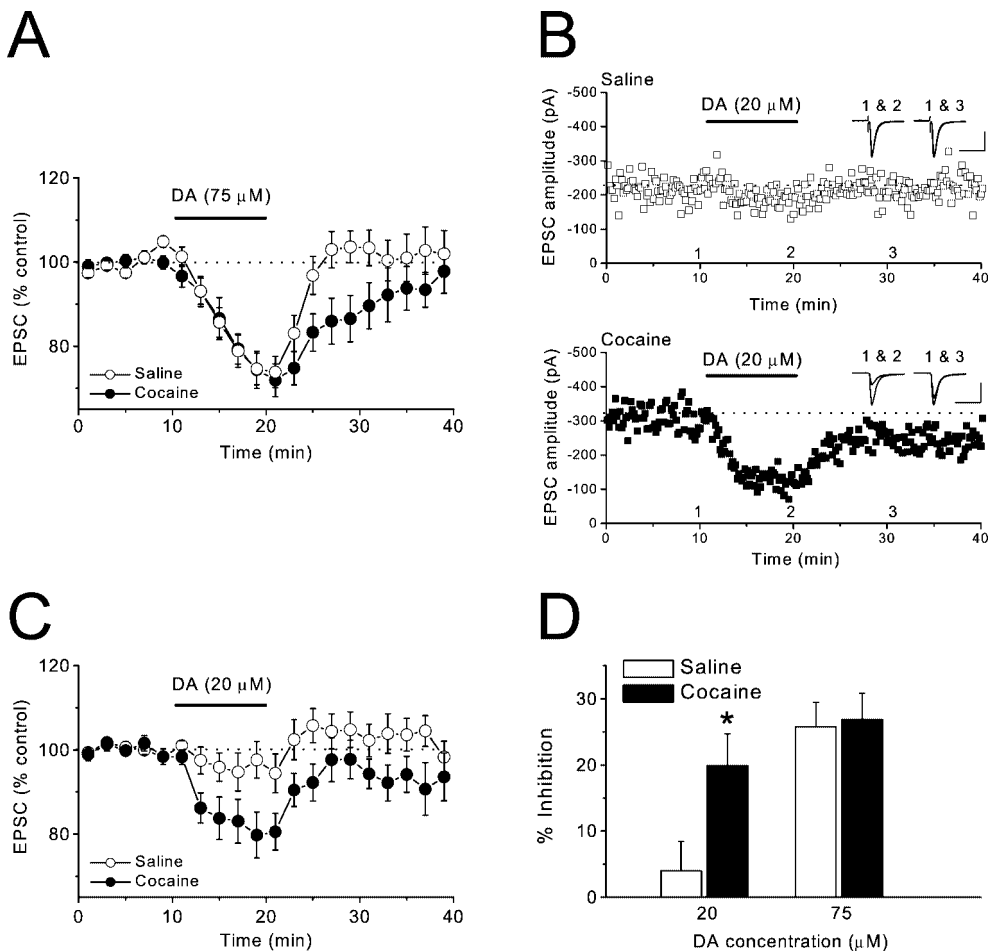


Figure 2. Chronic cocaine treatment enhances inhibitory actions of DA on AMPAR EPSCs. *A*, Summary graph of the effects of DA (75 μ M) in saline ($n = 12$ cells, 8 mice, 8 mice) and cocaine-treated ($n = 12$ cells, 9 mice) mice. *B*, Sample experiments from saline (*top*) and cocaine-treated (*bottom*) mice displaying the effect of 20 μ M DA. Sample traces were collected at the times indicated on the graph. Calibration: *top*, 50 msec, 100 pA; *bottom*, 50 msec, 200 pA. *C*, Summary graph of the effects of DA (20 μ M) in saline ($n = 9$ cells, 7 mice) and cocaine-treated ($n = 10$ cells, 5 mice) mice. *D*, Magnitude of inhibition of AMPAR EPSCs by DA in saline and cocaine-treated mice (* $p < 0.05$).

the cocaine-treated group could be explained by some modification of the D1-like DA receptors (e.g., increase in receptor number and/or function) or by a change in the DA transporters (DATs) that might influence the effective concentration of DA when it is applied to the slices (e.g., decrease in DAT number and/or function). To help distinguish between these possibilities, we examined whether the selective DAT inhibitor GBR-12909 (300 nM) enhanced the synaptic actions of DA. If it did, it would suggest that the level of DAT activity in our slices could limit the effective concentration of DA. However, in saline-treated mice, GBR-12909 (300 nM) did not significantly affect the synaptic depression elicited by DA (30 μ M; $n = 4$; data not shown). These results indicate that DATs do not influence the effective concentration of exogenous DA achieved in the slices. Therefore, it is very unlikely that the enhanced inhibition of excitatory synaptic transmission by DA in cocaine-treated mice is caused by a reduction in DAT number and/or function.

Lack of a postsynaptic effect of DA on NMDAR-mediated EPSCs

It has been suggested that the inhibitory effects of D1 receptor activation in the NAc are the consequence of a DA-induced enhancement of NMDAR-mediated responses (Harvey and Lacey, 1997), an action of DA that has also been reported to occur in the dorsal striatum (Cepeda et al., 1993; Levine et al., 1996). To determine whether DA modulation of NMDAR-mediated responses is affected by chronic *in vivo* cocaine treatment, we simultaneously measured the effect of DA on NMDAR-

and AMPAR-mediated EPSCs by holding the cell at +40 mV (Fig. 4*A*) (see Materials and Methods). If DA, via a postsynaptic action, potentiates NMDAR-mediated EPSCs (NMDAR EPSCs) but not AMPAR EPSCs, then the presynaptic DA-induced depression of NMDAR EPSCs should be less than that for AMPAR EPSCs, and the ratio of AMPAR- to NMDAR-mediated synaptic currents should decrease during DA application. If DA has no postsynaptic effect, the AMPAR/NMDAR ratio should remain constant throughout the experiment. In slices from saline-treated mice, DA (75 μ M) depressed AMPAR- and NMDAR-mediated responses to the same degree (Fig. 4*B*) (AMPA, $-33.7 \pm 7.6\%$; NMDAR, $-44.8 \pm 5.4\%$; $n = 8$; $p > 0.05$), as reflected by the lack of change in the AMPAR/NMDAR ratio in the presence of DA (Fig. 4*E*) (control, 2.9 ± 0.56 ; DA, 3.31 ± 0.69 ; $n = 8$; $p > 0.05$). We then repeated the same experiments in cocaine-treated mice to see whether this might reveal an effect of DA on NMDAR-mediated responses. Again, the depressant action of DA on AMPAR- and NMDAR-mediated EPSCs was not significantly different (Fig. 4*B*) (AMPA, $-28.5 \pm 5.4\%$; NMDAR, $-38.1 \pm 3.6\%$; $n = 15$; $p > 0.05$), and no change in the AMPAR/NMDAR ratio was induced by DA (Fig. 4*E*) (control, 3.25 ± 0.47 ; DA, 3.68 ± 0.53 ; $n = 15$; $p > 0.05$).

Although the previous work in the NAc also used standard whole-cell recording techniques (Harvey and Lacey, 1997), we were concerned that the lack of effect of DA on NMDAR EPSCs may be caused by dialysis, so-called washout of some intracellular components that are necessary for the postsynaptic effects of DA.

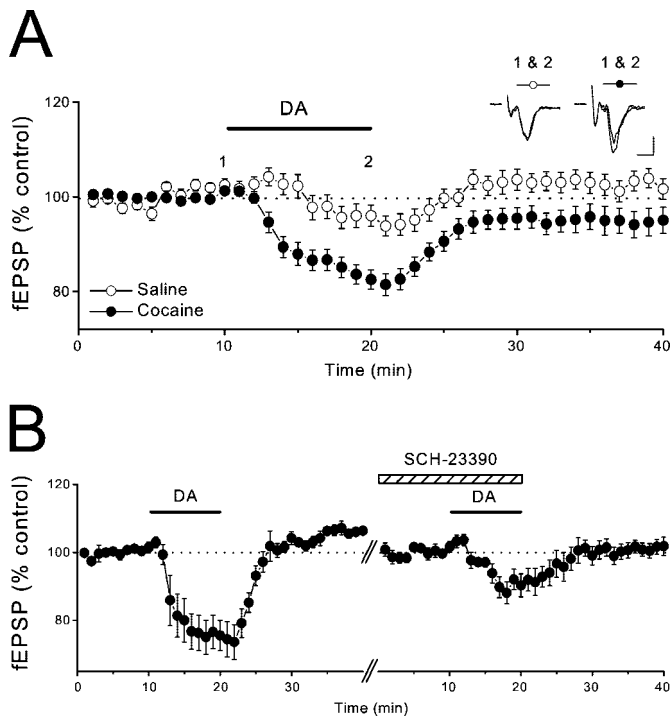


Figure 3. The DA-induced depression of excitatory synaptic transmission in cocaine-treated mice is mediated by D1-like receptors. *A*, Summary graph showing effects of DA (20 μ M) on field EPSPs in saline ($n = 11$ slices, 8 mice) and cocaine-treated ($n = 28$ slices, 20 mice) mice. Sample traces were collected at the times indicated on the graph. Calibration: 4 msec, 0.1 mV. *B*, Summary of experiments in which DA (20 μ M) was applied to slices from cocaine-treated mice first in the absence and then in the presence of SCH-23390 (10 μ M; $n = 6$ slices, 6 mice). fEPSP amplitudes were renormalized when SCH-23390 was applied to minimize possible effects of experimental drift.

Therefore, we repeated the same experiment in slices from control mice using perforated-patch recording techniques. Again, the inhibition of AMPAR- and NMDAR-mediated EPSCs induced by DA (100 μ M) was similar (Fig. 4C) (AMPA, $-26.8 \pm 12.6\%$; NMDAR, $-19.7 \pm 16.3\%$; $n = 5$; $p > 0.05$), and, thus, there was no effect on the AMPAR/NMDAR ratio (Fig. 4E) (control, 2.18 ± 0.2 ; DA, 2.16 ± 0.29 ; $n = 5$; $p > 0.05$). In a final attempt to determine whether DA potentiates NMDAR EPSCs, we tested its effects in the dorsal striatum, an area of the brain in which DA does not have a presynaptic action (Calabresi et al., 1987, 1995; Nicola and Malenka, 1998). Consistent with these previous results, DA (30–75 μ M) did not affect AMPAR EPSCs (Fig. 4D) ($-5.5 \pm 3.8\%$; $n = 4$). However, it also did not affect NMDAR EPSCs (Fig. 4D) ($-5.9 \pm 2.9\%$; $n = 4$) or the AMPAR/NMDAR ratio (Fig. 4E) (control, 1.73 ± 0.35 ; DA, 1.77 ± 0.42 ; $n = 4$; $p > 0.05$). Thus, we were unable to observe any postsynaptic effect of DA on NMDAR-mediated synaptic responses in either the NAc or the dorsal striatum.

DISCUSSION

A prominent rodent model for some key features of addiction is the long-lasting increase in the acute drug-induced locomotor response after repeated exposure to psychostimulants (Robinson and Berridge, 1993; Wolf, 1998; Vanderschuren and Kalivas, 2000). This increased response, termed behavioral sensitization, is thought to reflect modifications in the mesolimbic DA system, especially in dopaminergic and glutama-

tergic synaptic transmission (Wolf, 1998; Vanderschuren and Kalivas, 2000). In a previous study, we examined basal excitatory synaptic transmission in the NAc during behavioral sensitization and found that chronic *in vivo* cocaine exposure caused a long-lasting depression of synaptic strength in the NAc shell (Thomas et al., 2001). Here, we examine whether this same treatment protocol affects the modulation of excitatory synaptic transmission by DA. This is of particular interest because chronic psychostimulant administration appears to enhance DA release in the NAc in response to subsequent challenge injections of drug, an effect that is observed even after relatively long periods of abstinence after the initial psychostimulant administration (Robinson et al., 1988; Kalivas and Duffy, 1993; Pierce and Kalivas, 1995; White and Kalivas, 1998).

We find that the presynaptic inhibitory action of DA is enhanced in cocaine-sensitized animals, and that this effect is mediated by a D1-like receptor, as found previously in control animals (Pennartz et al., 1992; Nicola et al., 1996; but see O'Donnell and Grace, 1994). The lack of effect of GBR-12909, a DAT inhibitor, on the synaptic action of DA indicates that enhancement of the presynaptic effect of DA is probably not attributable to some downregulation of DAT activity. Instead, the change appears to be caused by a modification in the number and/or function of the presynaptic D1-like receptors. Consistent with this hypothesis is the finding that chronic cocaine administration increases the inhibitory action of D1 agonists on the single-unit responses of NAc neurons (Henry and White, 1991), and that an enhancement of the presynaptic effects of DA has also been reported after chronic treatment with methamphetamine (Higashi et al., 1989).

Because DA has been reported to enhance NMDAR-mediated responses in both the NAc (Harvey and Lacey, 1997) and the dorsal striatum (Cepeda et al., 1993; Levine et al., 1996), we also examined whether this action of DA is modified by chronic *in vivo* cocaine exposure. Surprisingly, however, we saw no effect of DA on NMDAR EPSCs in either control or sensitized mice, even when perforated-patch recording techniques were used. Furthermore, we saw no effect of DA on AMPAR or NMDAR EPSCs in the dorsal striatum. In addition to species differences (mice vs rats), one important difference between our experiments and previous ones is that we monitored the NMDAR EPSC at +40 mV, a holding potential at which all voltage-dependent conductances are inactivated. If the enhancement of NMDAR-mediated responses observed in previous work was caused by a modulation of such conductances by DA, under our recording conditions, we would not expect to see any effect. Indeed, DA modulates a number of different voltage-dependent conductances in striatal cells (Nicola et al., 2000), and blockade of L-type Ca^{2+} channels eliminates the DA-induced enhancement of NMDAR-mediated responses in dorsal striatal cells (Cepeda et al., 1998). Therefore, we conclude that DA does not directly modulate NMDAR function in medium spiny neurons in either the NAc or dorsal striatum, although via modulation of voltage-dependent conductances, DA may have important indirect effects on NMDAR-mediated currents. Because we did not examine and compare isolated NMDAR EPSCs, we cannot state whether the cocaine exposure modified the properties of NMDARs, as has been observed with chronic morphine treatment (Martin et al., 1999); e.g., dramatic cocaine-induced changes in the kinetics of the AMPAR EPSC or NMDAR

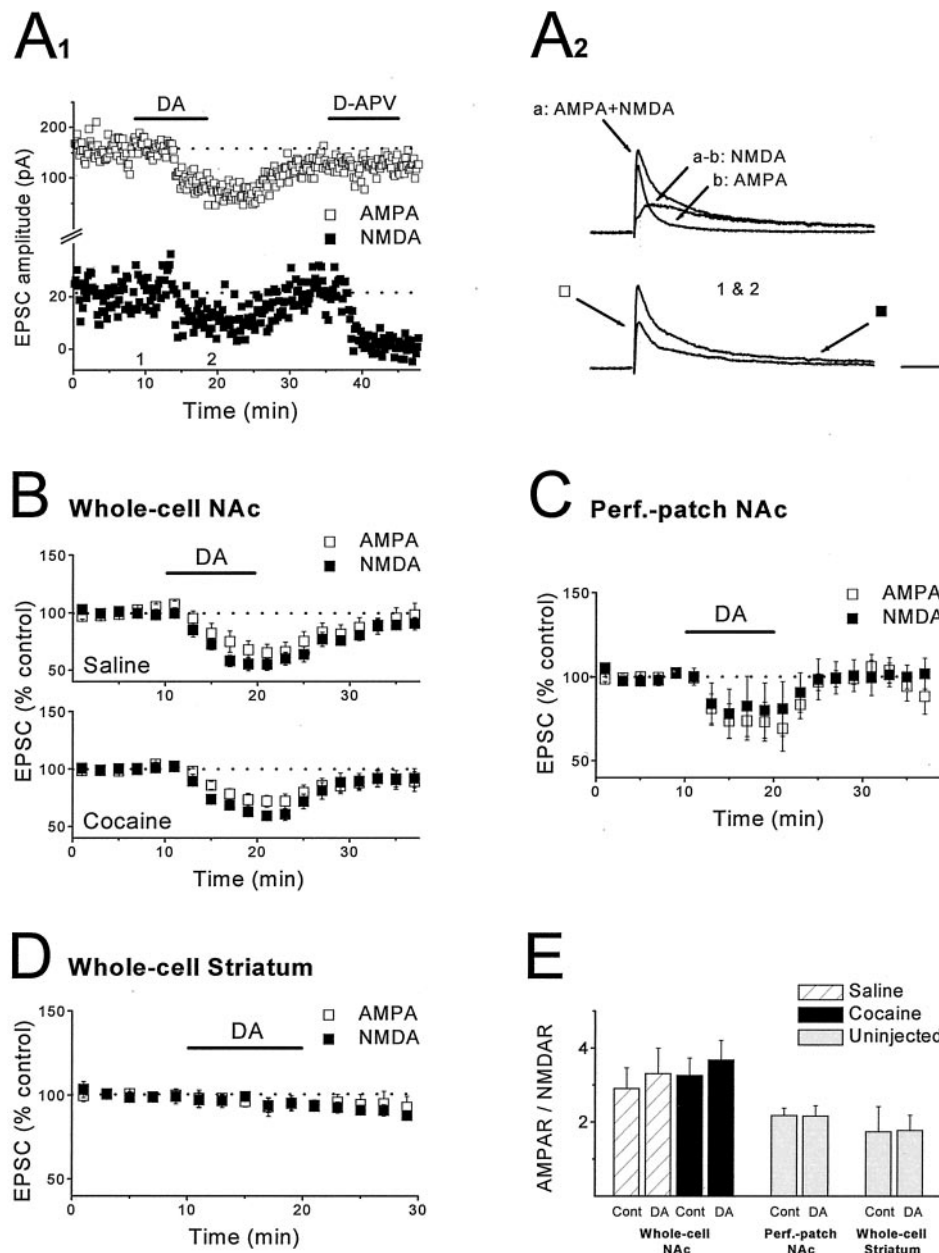


Figure 4. DA does not potentiate NMDAR EPSCs in either the NAc or dorsal striatum. *A1*, Example of an experiment in which DA (75 μM) was applied while simultaneously monitoring AMPAR EPSCs and NMDAR EPSCs at +40 mV. Note that application of D-APV (50 μM) had minimal effect on the measurement of the AMPAR EPSC but eliminated the NMDAR EPSC. *A2*, Top traces show the dual-component EPSC, the AMPAR EPSC obtained after application of D-APV, and the NMDAR EPSC obtained by subtraction of the two traces. Bottom traces show the dual-component EPSC before and after application of DA. Arrows show time points at which measurements were made. Calibration: 50 msec, 100 pA. *B*, Summary graph of the effects of DA (75 μM) on NMDAR EPSCs and AMPAR EPSCs in saline ($n = 8$ cells, 5 mice) and cocaine-treated ($n = 15$ cells, 9 mice) mice. *C*, Summary graph of the effects of DA (100 μM) on NMDAR EPSCs and AMPAR EPSCs recorded in slices from control mice using perforated-patch recording techniques ($n = 5$ cells, 4 mice). *D*, Summary graph of the effects of DA (30–75 μM) on NMDAR EPSCs and AMPAR EPSCs in dorsal striatum slices from control mice ($n = 4$ cells, 4 mice). *E*, Mean AMPAR/NMDAR ratio during baseline and at the end of DA application for experiments shown in *B–D*. In all cases, DA did not affect the AMPAR/NMDAR ratios.

EPSC might obscure a direct postsynaptic effect of DA on NMDAR EPSCs. It is also conceivable that the strong depolarization of the cells caused them to release some substance that obscured this effect of DA. However, to account for our results, such an action must have lasted >10 min, because we routinely obtained a minimum of a 10 min baseline before applying DA.

The functional significance of the enhancement of the inhibitory synaptic actions of DA in the NAc shell after chronic *in vivo* cocaine exposure remains to be determined. We would suggest it is likely one of a number of modifications of synaptic and cellular function in the NAc contributing to behavioral sensitization. Interestingly, many of the reported effects of chronic *in vivo* cocaine exposure would be expected to decrease net excitatory drive to medium spiny neurons (Henry and White, 1991; White et al., 1995; White and Kalivas, 1998; Wolf, 1998; Thomas et al., 2001), an action that might sensitize the rewarding or incentive

value of drugs of abuse (Wise, 1998; Robinson and Berridge, 2000).

REFERENCES

Calabresi P, Mercuri N, Stanzione P, Stefani A, Bernardi G (1987) Intracellular studies on the dopamine-induced firing inhibition of neostriatal neurons *in vitro*: evidence for D1 receptor involvement. *Neuroscience* 20:757–771.

Calabresi P, De Murtas M, Pisani A, Stefani A, Sancesario G, Mercuri NB, Bernardi G (1995) Vulnerability of medium spiny striatal neurons to glutamate: role of Na⁺/K⁺ ATPase. *Eur J Neurosci* 7:1674–1683.

Cepeda C, Buchwald NA, Levine MS (1993) Neuromodulatory actions of dopamine in the neostriatum are dependent upon the excitatory amino acid receptor subtypes activated. *Proc Natl Acad Sci USA* 90:9576–9580.

Cepeda C, Colwell CS, Itri JN, Chandler SH, Levine MS (1998) Dopaminergic modulation of NMDA-induced whole cell currents in neostriatal neurons in slices: contribution of calcium conductances. *J Neurophysiol* 79:82–94.

Civelli O, Bunzow JR, Grandy DK (1993) Molecular diversity of the dopamine receptors. *Annu Rev Pharmacol Toxicol* 33:281–307.

- Groenewegen HJ, Wright CI, Beijer AV, Voorn P (1999) Convergence and segregation of ventral striatal inputs and outputs. *Ann NY Acad Sci* 877:49–63.
- Harvey J, Lacey MG (1996) Endogenous and exogenous dopamine depress EPSCs in rat nucleus accumbens *in vitro* via D1 receptor activation. *J Physiol (Lond)* 492:143–154.
- Harvey J, Lacey MG (1997) A postsynaptic interaction between dopamine D1 and NMDA receptors promotes presynaptic inhibition in the rat nucleus accumbens via adenosine release. *J Neurosci* 17:5271–5280.
- Henry DJ, White FJ (1991) Repeated cocaine administration causes persistent enhancement of D1 dopamine receptor sensitivity within the rat nucleus accumbens. *J Pharmacol Exp Ther* 258:882–890.
- Higashi H, Inanaga K, Nishi S, Uchimura N (1989) Enhancement of dopamine actions on rat nucleus accumbens neurones *in vitro* after methamphetamine pre-treatment. *J Physiol (Lond)* 408:587–603.
- Jarvie KR, Caron MG (1993) Heterogeneity of dopamine receptors. *Adv Neurol* 60:325–333.
- Kalivas PW, Duffy P (1993) Time course of extracellular dopamine and behavioral sensitization to cocaine. I. Dopamine axon terminals. *J Neurosci* 13:266–275.
- Levine MS, Li Z, Cepeda C, Cromwell HC, Altemus KL (1996) Neuro-modulatory actions of dopamine on synaptically-evoked neostriatal responses in slices. *Synapse* 24:65–78.
- Martin G, Ahmed SH, Blank T, Spiess J, Koob GF, Siggins GR (1999) Chronic morphine treatment alters NMDA receptor-mediated synaptic transmission in the nucleus accumbens. *J Neurosci* 19:9081–9089.
- Nicola SM, Malenka RC (1997) Dopamine depresses excitatory and inhibitory synaptic transmission by distinct mechanisms in the nucleus accumbens. *J Neurosci* 17:5697–5710.
- Nicola SM, Malenka RC (1998) Modulation of synaptic transmission by dopamine and norepinephrine in ventral but not dorsal striatum. *J Neurophysiol* 79:1768–1776.
- Nicola SM, Kombian SB, Malenka RC (1996) Psychostimulants depress excitatory synaptic transmission in the nucleus accumbens via presynaptic D1-like dopamine receptors. *J Neurosci* 16:1591–1604.
- Nicola SM, Surmeier J, Malenka RC (2000) Dopaminergic modulation of neuronal excitability in the striatum and nucleus accumbens. *Annu Rev Neurosci* 23:185–215.
- O'Donnell P, Grace AA (1994) Tonic D2-mediated attenuation of cortical excitation in nucleus accumbens neurons recorded *in vitro*. *Brain Res* 634:105–112.
- Pennartz CM, Dolleman-Van der Weel MJ, Kitai ST, Lopes da Silva FH (1992) Presynaptic dopamine D1 receptors attenuate excitatory and inhibitory limbic inputs to the shell region of the rat nucleus accumbens studied *in vitro*. *J Neurophysiol* 67:1325–1334.
- Pierce RC, Kalivas PW (1995) Amphetamine produces sensitized increases in locomotion and extracellular dopamine preferentially in the nucleus accumbens shell of rats administered repeated cocaine. *J Pharmacol Exp Ther* 275:1019–1029.
- Robinson TE, Berridge KC (1993) The neural basis of drug craving: an incentive-sensitization theory of addiction. *Brain Res Brain Res Rev* 18:247–291.
- Robinson TE, Berridge KC (2000) The psychology and neurobiology of addiction: an incentive-sensitization view. *Addiction* 95 [Suppl 2]:S91–S117.
- Robinson TE, Jurson PA, Bennett JA, Bentgen KM (1988) Persistent sensitization of dopamine neurotransmission in ventral striatum (nucleus accumbens) produced by prior experience with (+)-amphetamine: a microdialysis study in freely moving rats. *Brain Res* 462:211–222.
- Sibley DR, Monsma Jr FJ (1992) Molecular biology of dopamine receptors. *Trends Pharmacol Sci* 13:61–69.
- Thomas MJ, Beurrier C, Bonci A, Malenka RC (2001) Long-term depression in the nucleus accumbens: a neural correlate of behavioral sensitization to cocaine. *Nat Neurosci* 4:1217–1223.
- Uchimura N, North RA (1991) Baclofen and adenosine inhibit synaptic potentials mediated by γ -aminobutyric acid and glutamate release in rat nucleus accumbens. *J Pharmacol Exp Ther* 258:663–668.
- Vanderschuren LJ, Kalivas PW (2000) Alterations in dopaminergic and glutamatergic transmission in the induction and expression of behavioral sensitization: a critical review of preclinical studies. *Psychopharmacology (Berl)* 151:99–120.
- White FJ, Kalivas PW (1998) Neuroadaptations involved in amphetamine and cocaine addiction. *Drug Alcohol Depend* 51:141–153.
- White FJ, Hu X-T, Zhang X-F, Wolf ME (1995) Repeated administration of cocaine or amphetamine alters neuronal responses to glutamate in the mesoaccumbens dopamine system. *J Pharmacol Exp Ther* 273:445–454.
- Wise RA (1998) Drug-activation of brain reward pathways. *Drug Alcohol Depend* 51:13–22.
- Wolf ME (1998) The role of excitatory amino acids in behavioral sensitization to psychomotor stimulants. *Prog Neurobiol* 54:679–720.
- Zahm DS (1999) Functional-anatomical implications of the nucleus accumbens core and shell subterritories. *Ann NY Acad Sci* 877:113–128.

Cellular and Behavioral Outcomes of Dorsal Striatonigral Neuron Ablation: New Insights into Striatal Functions

Delphine Révy^{1,5}, Florence Jaouen^{1,5}, Pascal Salin¹, Christophe Melon¹, Dorian Chabbert¹, Elisiana Tafi², Lena Concetta², Francina Langa³, Marianne Amalric⁴, Lydia Kerkerian-Le Goff¹, Hélène Marie^{2,6} and Corinne Beurrier^{*,1}

¹Institut de Biologie du Développement de Marseille (IBDM), Aix-Marseille University (AMU), Centre National de la Recherche Scientifique (CNRS), UMR 7288, Marseille Cedex 9, France; ²The European Brain Research Institute, Roma, Italy; ³Institut Pasteur, Mouse Genetics Engineering Center, Paris Cedex 15, France; ⁴Laboratoire de Neurosciences Cognitives, Aix-Marseille University, Centre National de la Recherche Scientifique (CNRS), UMR 7291, Marseille Cedex 3, France

The striatum is the input structure of the basal ganglia network that contains heterogeneous neuronal populations, including two populations of projecting neurons called the medium spiny neurons (MSNs), and different types of interneurons. We developed a transgenic mouse model enabling inducible ablation of the striatonigral MSNs constituting the direct pathway by expressing the human diphtheria toxin (DT) receptor under the control of the *Slc35d3* gene promoter, a gene enriched in striatonigral MSNs. DT injection into the striatum triggered selective elimination of the majority of striatonigral MSNs. DT-mediated ablation of striatonigral MSNs caused selective loss of cholinergic interneurons in the dorsal striatum but not in the ventral striatum (nucleus accumbens), suggesting a region-specific critical role of the direct pathway in striatal cholinergic neuron homeostasis. Mice with DT injection into the dorsal striatum showed altered basal and cocaine-induced locomotion and dramatic reduction of L-DOPA-induced dyskinesia in the parkinsonian condition. In addition, these mice exhibited reduced anxiety, revealing a role of the dorsal striatum in the modulation of behaviors involving an emotional component, behaviors generally associated with limbic structures. Altogether, these results highlight the implication of the direct striatonigral pathway in the regulation of heterogeneous functions from cell survival to regulation of motor and emotion-associated behaviors.

Neuropsychopharmacology advance online publication, 9 July 2014; doi:10.1038/npp.2014.121

INTRODUCTION

The basal ganglia (BG) are key neural substrates that control motor and reward-associated behaviors. Their dysfunction is associated with several disorders, including Parkinson's disease (PD), schizophrenia, and drug addiction (Cenci, 2007; Graybiel, 2000; Lobo and Nestler, 2011). As the main BG input, the striatum is thought to be an important site for mediating many of the maladaptive processes responsible for these devastating neurological disorders.

The striatum is classically delineated into dorsal (dorsal striatum) and ventral (nucleus accumbens) territories,

involved in cognitive/motor and emotional/motivational functions, respectively. However, interconnections and other crosstalk, in particular involving the dopamine systems, provide an anatomical basis for a multifunctional interface (Haber *et al*, 2000). The dorsal striatum receives heavy dopaminergic input from the substantia nigra pars compacta (SNc), and dysfunction of dopamine signaling is implicated in almost all BG-associated disorders. The major striatal targets of dopamine afferents are the GABAergic medium spiny neurons (MSNs) which constitute 95% of the striatal population. The remaining neurons, comprising approximately 5% of the total number of striatal neurons, are made up of different subtypes of GABAergic interneurons and of cholinergic interneurons. Despite being few in number, cholinergic interneurons are crucial for the tuning of striatal output owing to their dense terminal fields primarily directed to the two populations of MSNs that overlap those of dopaminergic neurons (Bolam *et al*, 1984). The two types of MSNs are distinguished depending on their projections and expression of distinct set of proteins. MSNs that project primarily to the substantia nigra pars reticulata (SNr), so-called direct-pathway or striatonigral MSNs, express the dopamine D₁ receptor, substance P (SP) and dynorphin, whereas MSNs that project to the globus

*Correspondence: Dr C Beurrier, Institut de Biologie du Développement de Marseille (IBDM), Aix-Marseille University (AMU), Centre National de la Recherche Scientifique (CNRS), UMR 7288, Parc Scientifique de Luminy, Case 907, Marseille 13288, France, Tel: +33 491 26 92 48, Fax: +33 491 26 92 44, E-mail: corinne.beurrier@univ-amu.fr

⁵These authors contributed equally to this work.

⁶Current address: Institut de Pharmacologie Moléculaire et Cellulaire (IPMC), Université de Nice Sophia Antipolis, Centre National de la Recherche Scientifique (CNRS), UMR 7275, Valbonne 06560, France. Received 2 December 2013; revised 18 April 2014; accepted 16 May 2014; accepted article preview online 6 June 2014

pallidus (GP), so-called indirect or striatopallidal MSNs, express the dopamine D₂ receptor and enkephalin (Enk) (Gerfen *et al*, 1990; Smith *et al*, 1998). Because of the differential expression of dopamine receptors, the striatonigral and striatopallidal MSNs are thought to have opposing but balancing roles on BG output and behaviors (Albin *et al*, 1989; DeLong, 1990).

Recent advances in cell-type-specific technologies have provided a wealth of data allowing a more comprehensive understanding of MSNs roles in drug addiction (Durieux *et al*, 2009; Durieux *et al*, 2012; Ferguson *et al*, 2011; Lobo *et al*, 2010), cognitive functions (Hikida *et al*, 2010; Hikida *et al*, 2013; Nishizawa *et al*, 2012; Tai *et al*, 2012; Yawata *et al*, 2012), and parkinsonian physiopathology (Kravitz *et al*, 2010). Here, we developed a new inducible model of diphtheria toxin (DT) receptor-mediated ablation to further explore the functional implications of striatonigral MSNs of the dorsal striatum. For behavioral characterization, we first focused on motor function linked to disturbed striatal dopamine tone, cocaine-induced locomotion, and L-DOPA-induced dyskinesia (LID), which are associated with selective and robust molecular changes in striatonigral MSNs, including ERK signaling (Bertran-Gonzalez *et al*, 2008; Santini *et al*, 2009). Acute response to psychostimulant has been investigated using amphetamine in a model of striatonigral MSNs ablation restricted to subterritories of the dorsal striatum (Durieux *et al*, 2012), and direct demonstration of dorsal striatonigral MSNs involvement in LID, a major complication of the most common pharmacotherapy of PD, is still lacking. We next moved to non-motor function as accumulating evidence suggests that, in addition to sensorimotor information processing, the dorsal striatum might also mediate emotional/motivational functions classically ascribed to the ventral striatum (Balleine *et al*, 2007). We focused on anxiety behavior, notably because SP and dynorphin, two molecules released by striatonigral MSNs, have been implicated in the regulation of anxiety (Ebner and Singewald, 2006; Van't Veer and Carlezon, 2013).

The results show that ablation of striatonigral MSNs impacts heterogeneous functions from motor- and emotional-associated behaviors to region-specific regulation of cholinergic homeostasis.

MATERIALS AND METHODS

Generation of Transgenic Mice

The human Diphtheria Toxin Receptor-green fluorescent protein (DTR-GFP) cDNA was inserted in front of the endogenous ATG in exon 1 of the *Slc35d3* gene in a 196-kilobase mouse bacterial artificial chromosome (BAC) (RP23-344M6) by homologous recombination using the recombinase plasmid pL451. DNA from the modified BAC was purified and microinjected into pronuclei of fertilized mouse eggs (B65JL/F1) to generate transgenic founders (Mouse Genetics Engineering Center, Institut Pasteur). A total of five transgene-positive founders were obtained and were bred with C57Bl/6 mice. Offspring consisted of an equal number of DTR-expressing mice (DTR⁺) and of DTR non-expressing mice (DTR⁻).

Stereotaxic Injections

All animal experimental procedures were carried out in strict accordance with local rules concerning the use of laboratory animals (authorization no.B 13-464) and with the recommendations of the EEC (2010/63/UE) for care and use of laboratory animals and conformed to the ethical guidelines of the French Ministry of Agriculture and Forests (Animal Health and Protection Veterinary Service).

Surgery was performed on 8–12 week-old mice under xylazine/ketamine anesthesia (intraperitoneal injections, 10 and 100 mg/kg, respectively). All stereotaxic coordinates are listed in Supplementary Table S1. DT, (Calbiochem, Darmstadt, Germany) was diluted to a concentration of 0.5 ng/ μ l, and 1 μ l was injected at two sites either into the dorsal striatum or into the nucleus accumbens. For retrograde tracing, 1 μ l of fluorescent microbeads (Life Technologies, Saint-Aubin, France) were injected into the SNr. For dopaminergic lesion, mice received one unilateral injection (1.5 μ l) of 6-hydroxydopamine hydrochloride (6-OHDA; 2.7 μ g/ μ l; diluted in 0.9% sterile NaCl containing 0.1% ascorbic acid; Sigma-Aldrich, St Quentin-Fallavier, France) into the SNc.

Quantitative *In Situ* Hybridization and Dopamine Transporter Autoradiography

Radioactive *in situ* hybridization histochemistry was performed as described previously (Salin *et al*, 2002). Probes were 44–56 mer synthetic oligonucleotides selected on the basis of the sequence of *Tac1* (which encodes SP; hereafter called SP), *Penk* (which encodes Enk; hereafter called Enk), *GAD 67*, and tyrosine hydroxylase (*TH*) and were 3'-end-labeled by terminal deoxynucleotide transferase with ³⁵S-dATP. ³H-mazindol was used as a ligand to label dopamine transporter sites. Briefly, after appropriate washes, sections were incubated with 15 nM [³H]-mazindol (DuPont NEN Research Products, Boston, MA; specific activity, 17 Ci/mmol) in a Tris buffer containing 0.3 mM desipramine to block the noradrenalin uptake sites.

Quantitative RT-PCR

The uninjected and injected dorsal striatum of three DTR⁺ mice injected with DT into the dorsal striatum were punched separately. Specific primers for the different genes of interest were designed using the Universal ProbeLibrary (ProbeFinder version 2.5 for mouse, Roche Diagnostics) and chosen intron-spanning when possible (Supplementary Table S2). Total RNA (170 ng) was reverse transcribed for 5 min at 25 °C, 30 min at 42 °C and 5 min at 85 °C using iScript Reverse Transcription Supermix for RT-qPCR (BIO-RAD). A Bio-Rad CFX96 cyler was used with the following cycling parameters: 1 cycle at 95 °C for 8 min, 40 cycles at 95 °C for 15 s followed by 60 °C for 1 min. Samples were run in three replicates for each gene. Relative target gene concentration was calculated using the 2^{- $\Delta\Delta$ Ct} method (Livak and Schmittgen, 2001), which uses normalization to β -actin endogenous reference gene (as described in Lobo *et al*, 2006) and normalization to calibrator sample (here, uninjected dorsal striatum side).

Dual Fluorescence *In Situ* Hybridization

Two-color fluorescent *in situ* hybridization was performed with a mixture of fluorescein-labeled antisense riboprobe for ChAT or SP and a digoxigenin-labeled riboprobe for DTR. After appropriate pretreatments, sections were incubated at 65 °C overnight in the hybridization mix containing 400 ng/ml of both probes. After posthybridization washes, sections were incubated for 5 h with anti-Fluorescein-POD (HRP) (1/300) (Roche-Applied Science), and the fluorescein probe was visualized in green with fluorescein-tyramide reagent (TSA Plus PerkinElmer Life Sciences). After inactivating the HRP conjugate of the anti-Fluorescein-POD antibody (3% H₂O₂), the digoxigenin probe was then visualized in red with anti-digoxigenin-POD antibody (1/300) followed by cyanine-3-tyramide reagent.

Immunohistochemistry

Mice were perfused transcardially with ice-cold 4% paraformaldehyde in 0.1 M phosphate-buffered saline (PBS, pH 7.4). After overnight postfixation, brains were protected in a PBS solution containing 30% sucrose and frozen. Cryostat sections (40 μm) were incubated overnight at 4 °C with primary antibodies and then incubated with the appropriate secondary antibodies (Supplementary Table S3).

Data Analysis

Analysis of DT-mediated effects in the striatum was performed on 4–6 coronal sections per animal extending from AP = +1.54 to 0.14 relative to bregma according to the mouse stereotaxic brain atlas of Paxinos and Franklin (Second edition, 2001).

Single-Cell RT-PCR

Coronal striatal slices (250 μm) from DTR⁺ mice were prepared and recorded as previously described (Beurrier *et al*, 2009). After cell-attached and whole-cell recordings, the cell content was aspirated, expelled into a test tube where the RT reaction was performed overnight at 40 °C. The single-cell RT-PCR protocol used here was adapted from Lena *et al* (1999) to simultaneously detect the expression of *DTR-GFP* and *ChAT* mRNAs. Genomic DNA amplification was systematically assessed using a NMDA receptor gene intron (NR1 subunit, *GRIN1*) as genomic control (Supplementary Table S4). The cDNAs were first amplified by 20 PCR cycles (94 °C, 1 min; 60 °C, 1 min; 72 °C, 1 min) using 5 U of *Taq* polymerase (Qiagen, Hilden, Germany), and 10 pmol of different sets of primers (Supplementary Table S3) were added (final volume, 100 μl). Second rounds of PCR (40 cycles as described above) were then performed using 6 μl of the first PCR product as a template (final volume 50 μl). Each cDNA was amplified individually using its specific primer generating PCR fragments of 406, 323 and 162 bp for *DTR-GFP*, *ChAT* and *GRIN1* introns, respectively.

Behavioral Tests

Mice were group-housed (2–5 mice/cage) and maintained on a 12:12-h light–dark cycle (0700 hours lights on) with *ad libitum* food and water available.

Locomotor activity. Locomotor activity was monitored in individual activity chambers (11.2 cm × 20.7 cm) housed within a sound-attenuating cubicle and under homogenous light illumination (Imetronic, Pessac, France). Each chamber was equipped with four infrared photobeams located 1.5 cm above floor level, two at the rear and two at the front of the chamber. Mice were given i.p. injections of saline (0.9% NaCl) for the first 3 testing days to habituate them to the injections, handling, and activity chambers. On the fourth day, mice of each genotype were divided into two groups receiving either i.p. injections of saline (0.9% NaCl) or cocaine hydrochloride (5 or 15 mg/kg; Sigma-Aldrich). Locomotor activity was monitored immediately afterwards for 60 min. The number of beam breaks was recorded in 5-min bins.

L-DOPA-induced dyskinesia. Mice received unilateral DT injection into the dorsal striatum ipsilateral to the 6-OHDA-injected side. Fifteen days later, they received a single daily injection of L-DOPA (20 mg/kg) and benserazide hydrochloride (10 mg/kg) for 21 days. The abnormal involuntary movements (AIMs) were assessed by two investigators blind of subject genotype for 1 min every 20 min from 20 to 120 min after the last injection on day 21. Axial, limb, and orolingual AIMs were scored using a previously established scale from 0 to 4 for each AIM subtype (Lundblad *et al*, 2004), and the sum of the three scores, defined as dyskinesia score, was determined for each animal (maximal score, 12). Locomotive AIM was expressed as the number of contralateral rotations per minute for each animal.

Open field. The open-field chamber (50 × 50 cm² with a 30 cm-high white plastic wall) was virtually divided into a central field (center, 25 × 25 cm²) and an outer field (periphery). The open-field test consisted of a 5-min session and was conducted under dim lighting conditions (12 Lux). Individual mice were placed in the center of the field, and the paths of the animals were recorded by a video camera. The distance traveled in the different zones was analyzed by a video-tracking software (Viewpoint Life Sciences, Lyon, France).

Elevated plus maze. The apparatus is elevated 50 cm above the floor and consisted of four arms (6 cm × 37 cm), two enclosed by 18 cm-high white plastic walls and two open. Light intensity was 12 Lux in open arms and 4 Lux in closed arms. Each trial began with the placement of the mouse in the maze center, facing an open arm. The paths of the animals were recorded for 5 min by a video camera. The distance traveled and the numbers of entries in the open and closed arms were quantified by a video-tracking software (Viewpoint Life Sciences). Mice were tested in the elevated plus maze 1 day after the open-field test.

Statistical Analysis

Data are presented as mean ± SEM. Statistical analyses (SigmaStat, v3.1) were performed using the unpaired Student's *t*-test. A nonparametric test (test of Mann-Whitney) was used if the normality or equal variance test failed. Two-way repeated-measured ANOVA followed by

Holm–Sidak post tests was used for analyzing time profiles of AIM scores. A significance of $p < 0.05$ was required for rejection of the null hypothesis.

RESULTS

Generation of *Slc35d3*^{DTR-GFP} Transgenic Mice

To ablate striatonigral MSNs, we used the human DTR, the activation of which by DT induces cell apoptosis. We first checked the ability of the fusion DTR-GFP construct to induce cell death *in vitro*. In wild-type cultured hippocampal neurons expressing DTR-GFP fusion, administration of DT triggered apoptosis of GFP-positive cells (Supplementary Figure S1A). To specifically ablate striatonigral MSNs, we chose to drive the expression of the DTR-GFP construct under the control of a highly enriched striatonigral MSNs gene, *Slc35d3* (Heiman *et al*, 2008; Lobo *et al*, 2006), using the BAC-based strategy (Supplementary Figure S1B). Transgenic mice were generated by injecting the recombinant BAC into the pronuclei of hybrid C57Bl/6 × CB1 F1 fertilized oocytes, which were then implanted into pseudopregnant females. The five *Slc35d3*^{DTR-GFP} transgenic founders obtained (hereafter named DTR mice) were outbred with C57Bl/6 mice. One founder did not breed correctly and was discarded from the study. In the four remaining lines, GFP-positive cells were detected in the striatum of DTR⁺ mice (Supplementary Figure S1C) with a virtually indistinguishable expression pattern. Intrastratial DTR-GFP protein levels assessed by western blotting were also similar in all the four lines (data not shown). We next determined in which cell type DTR-GFP was expressed. Retrograde fluorescent microbeads were injected into the SNr (Figure 1a), a main target of striatonigral MSNs. The colocalization of GFP-positive soma in the striatum with microbeads confirmed the expression of DTR-GFP by striatonigral MSNs (Figure 1a). The drastic reduction in GFP fluorescence after DT injection into the dorsal striatum of DTR⁺ mice indicated an efficient ablation of DTR-GFP-positive cells *in vivo* (Figure 1b). The decrease in GFP fluorescence was observed in the rostro-caudal extent of the dorsal striatum while the ventral part (nucleus accumbens) was preserved (Supplementary Figure S2A). Time course analysis showed that the decrease in GFP fluorescence was progressive from day 1 to day 7; over day 7, the ablation was maximal and did not evolve anymore (Supplementary Figure S2B). All the following experiments were performed around 15 days after DT injection after stabilization of the ablation.

Ablation of Striatonigral MSNs by DT Injection

To test the specificity of striatonigral MSNs ablation, we analyzed markers of the different striatal populations using *in situ* hybridization, RT-qPCR, or immunohistochemistry 15 days after unilateral intrastratial DT injection into the dorsal striatum. None of the markers examined was altered in the DT-injected side vs uninjected side in DTR⁻ mice. DTR⁺ mice showed strongly reduced *SP* mRNA, a specific marker of striatonigral MSNs, while *Enk* mRNA, a specific marker of striatopallidal MSNs, was unchanged (Figure 1c and d). Among the four lines, line 4 was selected for

subsequent experiments, because it showed the highest decrease of *SP* mRNA (-66.3% vs uninjected side, $p < 0.001$). RT-qPCR analysis confirmed the significant reduction of *SP* (-0.59 -fold vs uninjected side, $p < 0.01$) and also showed a pronounced decrease in the expression of dopamine D₁ receptor (*Drd1a*: -0.76 -fold vs uninjected side, $p < 0.001$), another gene specifically expressed by striatonigral MSNs. In contrast, three genes enriched in striatopallidal MSNs (dopamine D₂ receptor *Drd2*, *Enk* and Adenosine A_{2A} receptor *Adora2a*) were not affected by DT injection, confirming the specificity of the ablation (Figure 1e). The levels of cAMP-regulated phosphoprotein-32 (DARPP-32), a protein expressed in both populations of MSNs, were also significantly reduced by 39.2% (data not shown).

Knowing that MSNs project to the SNc (Gerfen, 1984), we examined *TH* mRNA levels in the SNc of DT-injected DTR⁺ mice and found that it was not altered by striatonigral MSNs ablation (data not shown). We then sought to determine the effect of intrastratial DT on the two main targets of striatonigral and striatopallidal MSNs, the GABAergic neurons of the SNr and GP, respectively. We examined intraneuronal mRNA levels of the GABA synthesis enzyme *GAD67* as an indirect index of GABA neuron activity. *GAD67* mRNA expression was increased in the SNr of DTR⁺ mice ($+18.2\%$ vs uninjected side, $p < 0.05$), consistent with overactivity of this structure due to removal of the inhibitory control exerted by striatonigral MSNs (Figure 1f). In contrast, there was no change in *GAD67* mRNA expression in the GP. Altogether, these data demonstrate that the DTR⁺ transgenic mice are a reliable and effective model to specifically ablate striatonigral vs striatopallidal MSNs and that this ablation has a functional impact on BG output.

The striatum contains three categories of GABAergic interneurons with specific cytochemical markers, parvalbumin, calretinin, or neuropeptide Y/NADPH-diaphorase, and one population of cholinergic interneurons expressing choline acetyltransferase (ChAT) (Kawaguchi, 1993). The density of neurons stained for parvalbumin, calretinin, or NADPH-diaphorase was unaffected by DT injection, whereas the density of ChAT-expressing neurons was decreased by 42.7% ($p < 0.01$; Figure 2). To exclude down-regulation of ChAT expression, we examined the effect of DT on another protein also specifically expressed by striatal cholinergic interneurons, the type A tyrosine kinase receptor (TrkA) (Holtzman *et al*, 1992). The density of TrkA-positive cells in the DT-injected side of DTR⁺ mice was decreased to a similar level than ChAT-positive cells (-41.2% vs uninjected side, $p < 0.01$; Figure 2). In DTR⁻ mice, DT injection did not affect ChAT-positive cells' density (uninjected side: 44.20 ± 4.11 , injected side: 43.01 ± 3.25 , $n = 4$ DTR⁻, $p = 0.83$), excluding a peculiar sensitivity of this population to DT compared with other striatal populations.

How one can explain the loss of cholinergic interneurons? Two possibilities: (1) DT injection mediates direct ablation of ChAT-positive neurons; and (2) loss of striatonigral MSNs in the dorsal striatum indirectly interferes with the survival of cholinergic interneurons. To distinguish between these two possibilities, we performed a series of control experiments. Using double staining experiments, we

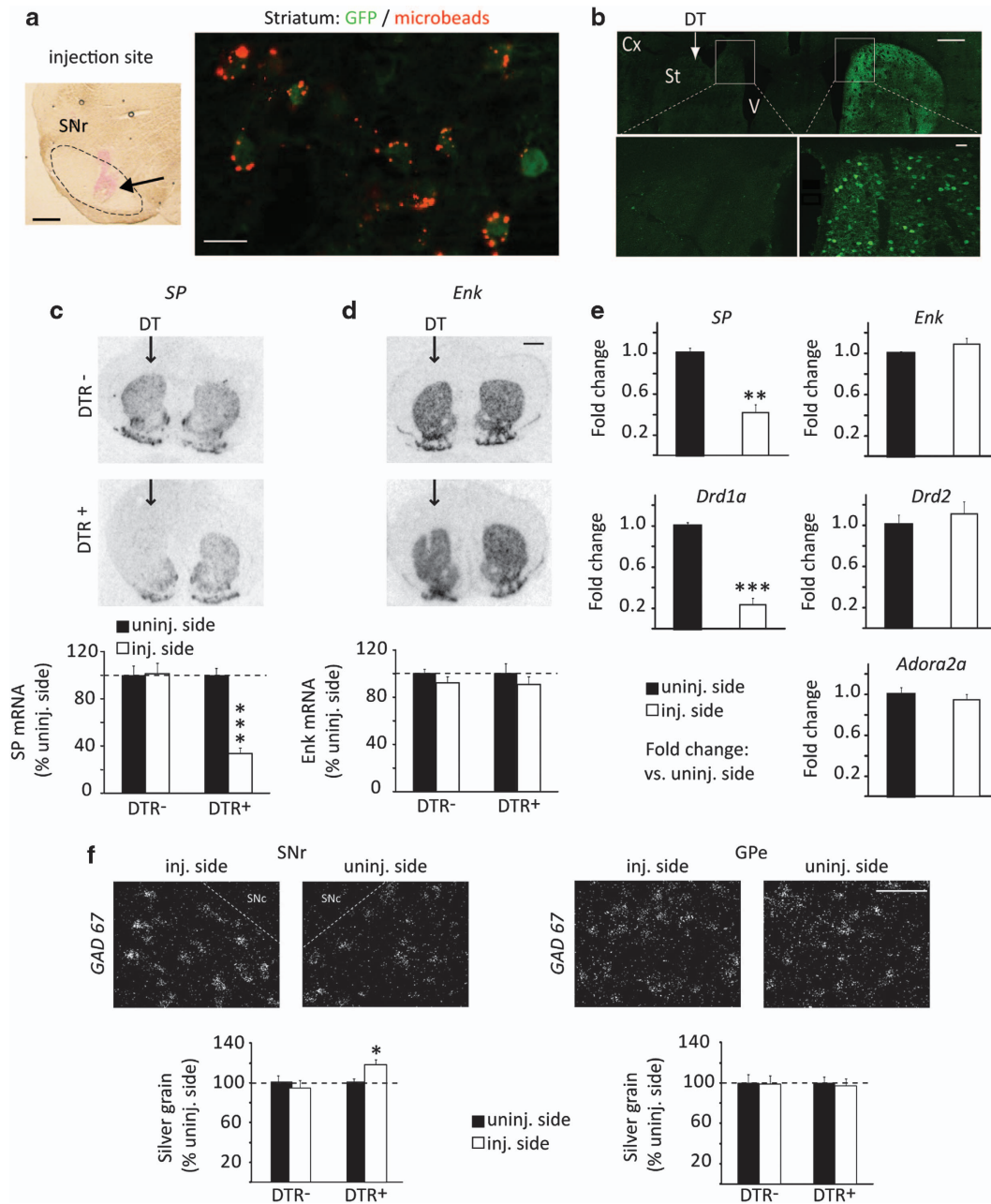


Figure 1 Selective expression of DTR-GFP in striatonigral neurons and impact of DT injection. (a) Left: injection site of fluorescent microbeads indicated by the arrow in the SNr. Scale bar, 200 μ m. SNr: substantia nigra pars reticulata. Right: combined immunofluorescence detection of GFP-expressing striatal neurons and retrograde labeling of striatonigral MSNs 7 days after injection of fluorescent microbeads into the SNr of DTR⁺ mice. The microbeads colocalized with GFP. Scale bar, 10 μ m. (b) Striatal GFP immunodetection on a DTR⁺ coronal brain section 7 days after unilateral DT injection into the striatum showing the loss of GFP expression in the injected side (left) compared with the uninjected side (right). Scale bars, top: 500 μ m and bottom: 20 μ m. Cx: cortex, St: striatum, V: ventricle. (c, d) Radioactive *in situ* hybridizations and quantification of striatal SP (c) and *Enk* (d) mRNA levels 15 days after unilateral DT injections into the striatum of DTR⁻ ($n = 6$) and DTR⁺ ($n = 10$) mice. Arrows indicate the injected side. Scale bar, 1 mm. Data are reported as optical density values and expressed as percentage \pm SEM. Student's *t*-test: *** $p < 0.001$ vs uninjected side. (e) Quantitative RT-qPCR for genes specifically expressed in striatonigral (*SP*, *Drd1a*) or in striatopallidal MSNs (*Enk*, *Drd2*, *Adora2a*). Three DTR⁺ mice were unilaterally injected with DT into the dorsal striatum, and the total RNA samples from this area were collected in the injected and uninjected side. Results were calculated for each sample relative to the expression of the endogenous reference gene, β -actin, and fold change was determined using the $2^{-\Delta\Delta Ct}$ method. Student's *t*-test: ** $p < 0.01$, *** $p < 0.001$ vs uninjected side. (f) Photomicrographs taken under dark-field epi-illumination illustrating intraneuronal GAD 67 mRNA levels in the SNr and GPe of DTR⁺ mice, 15 days after DT injections. Scale bar, 100 μ m. Quantitative analysis of the number of silver grains per neurons in the SNr (left) ($n = 5$ DTR⁻ and 5 DTR⁺) and GPe (right) ($n = 5$ DTR⁻ and 6 DTR⁺). Data are expressed as percentage \pm SEM. Student's *t*-test: * $p < 0.05$ vs uninjected side.

performed a thorough examination of DTR expression in cholinergic interneurons. We found no colocalization between GFP and ChAT proteins in the striatum of DTR⁺

mice (Figure 3a). Using double *in situ* hybridization, we found no expression overlap between *ChAT* and *DTR*, whereas all *SP*-expressing cells were *DTR* positive

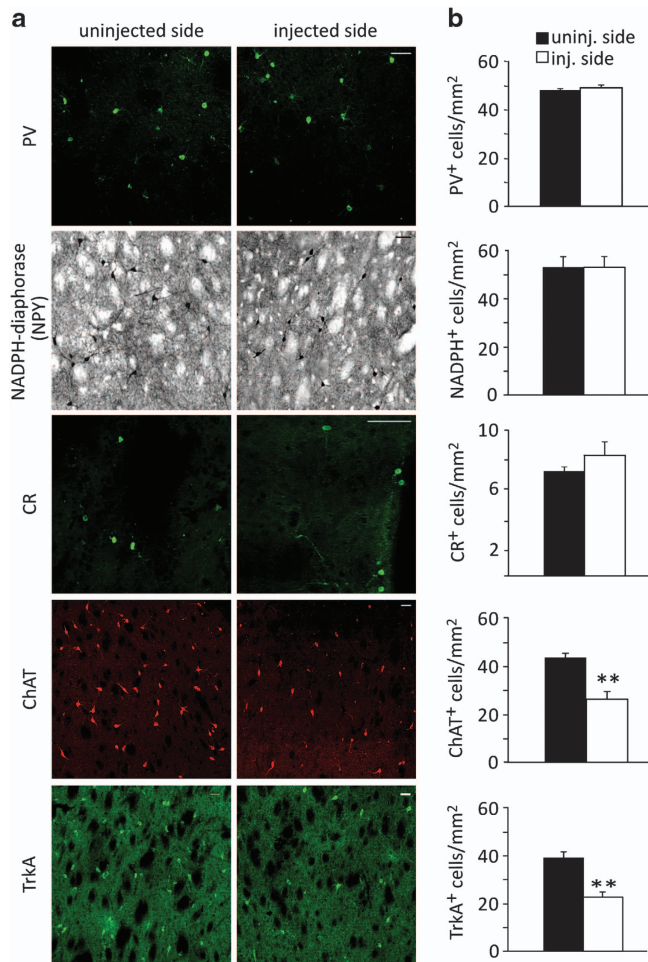


Figure 2 Consequences of striatonigral neuron ablation on striatal interneurons. (a) Coronal sections from DTR⁺ mice unilaterally injected with DT were stained 15 days after injections for specific markers of GABAergic interneuron subpopulations (parvalbumin, PV; NADPH diaphorase to identify NPY interneurons, calretinin, CR) and for two markers of cholinergic interneurons (choline acetyltransferase, ChAT; type A tyrosine kinase receptor, TrkA). Scale bars, 50 μ m. (b) Quantitative analyses illustrate the density of positive cells in the injected and uninjected sides ($n=4$ DTR⁺). Data are expressed as mean \pm SEM. Student's t -test: ** $p<0.01$ vs uninjected side.

(Figure 3b). To further confirm the lack of expression of DTR in cholinergic interneurons, we used single-cell RT-PCR. MSNs and cholinergic interneurons were identified by their distinctive morphological features and firing patterns recorded in cell-attached mode: MSNs have small soma and do not fire action potentials, whereas cholinergic interneurons have large soma and are the only striatal cells in slices that discharge spontaneously. *ChAT* mRNA was never detected in neurons expressing DTR ($n=9$), and *DTR* mRNA was never detected in the neurons expressing ChAT ($n=8$) (Figure 3c). Altogether, these results demonstrate that the loss of cholinergic interneurons is not due to a direct effect of the toxin but is rather an indirect consequence of striatonigral MSNs ablation. This hypothesis is further strengthened by the time course analysis of cell loss we performed from 1 up to 22 days post-DT injection. We found that the loss of ChAT-positive cells

was positively correlated to the loss of GFP fluorescence (reflecting MSNs ablation) and that a critical threshold of striatonigral MSNs ablation ($>40\%$) is required to impact cholinergic interneurons' viability (Figure 3d). Finally, as the nucleus accumbens is very similar to the dorsal striatum in terms of cellular composition, we examined the effect of a full ablation of striatonigral MSNs by injecting DT into both regions in the same mouse. Cholinergic interneurons in the dorsal striatum were significantly decreased ($p<0.001$) while those located in the nucleus accumbens were not affected ($p=0.12$), showing that cholinergic interneurons dependence on striatonigral MSNs is territory specific (Figure 3e).

Behavioral Characterization

Behavioral experiments were conducted on G3 mice 15 ± 3 days after intrastriatal DT injection in the dorsal striatum. Injections were made bilaterally except for LID (unilateral injection in the dopamine lesioned side). Animals included in the behavioral analyses were selected *a posteriori* based on marked reduction of *SP* mRNAs determined by *in situ* hybridization in the dorsal striatum ($-63.27 \pm 2.78\%$, $n=27$ DTR⁺ mice, $p<0.001$). In addition, we also quantified the level of *SP* mRNAs in the nucleus accumbens in animals used in the open-field and elevated plus maze tests and found no significant change ($-11.10 \pm 4.91\%$, $n=10$ DTR⁺ mice, $p=0.07$). Performances of DTR⁺ mice were compared with their control DTR⁻ littermates.

Basal and cocaine-induced locomotion is altered in DT-injected DTR⁺ mice. The dorsal striatum is involved in the regulation of motor activity and motor response to psychostimulants. We therefore examined basal locomotor activity and drug-induced locomotion after cocaine injection, a drug of abuse that increases locomotion by potentiating dopamine signaling. DTR⁺ mice exhibited significantly reduced basal locomotion during the 60-min test duration compared with DTR⁻ mice ($p<0.05$) (Figure 4a). When acutely challenged with 15 mg/kg cocaine, both DTR⁻ and DTR⁺ mice showed an increased activity compared with their respective saline-injected group (DTR⁻ cocaine: $+134.90\%$ vs DTR⁻ saline, $p<0.001$; DTR⁺ cocaine: $+302.24\%$ vs DTR⁺ saline, $p<0.001$) (Figure 4a). To be unbiased by the hypolocomotion of DTR⁺ mice, the cocaine-induced locomotor activity was normalized for each genotype to the respective basal activity recorded in saline-injected mice. The locomotor response to cocaine observed in DTR⁺ mice greatly exceeded the one observed in DTR⁻ mice ($+71.83\%$ vs DTR⁻ mice, $p<0.01$). To further confirm the hypersensitivity of DTR⁺ mice to cocaine, we tested the effect of a lower dose of cocaine in another two groups of mice. A similar enhancement of the locomotor response to cocaine 5 mg/kg was found in DTR⁺ mice ($+72.90\%$ vs DTR⁻ mice, $p<0.05$; Figure 4b).

L-DOPA induced dyskinesia are strongly reduced in DT-injected DTR⁺ mice. Dyskinesia is a common complication of L-DOPA pharmacotherapy in PD, affecting a large majority of patients within a few years from treatment onset. LID are associated with biochemical

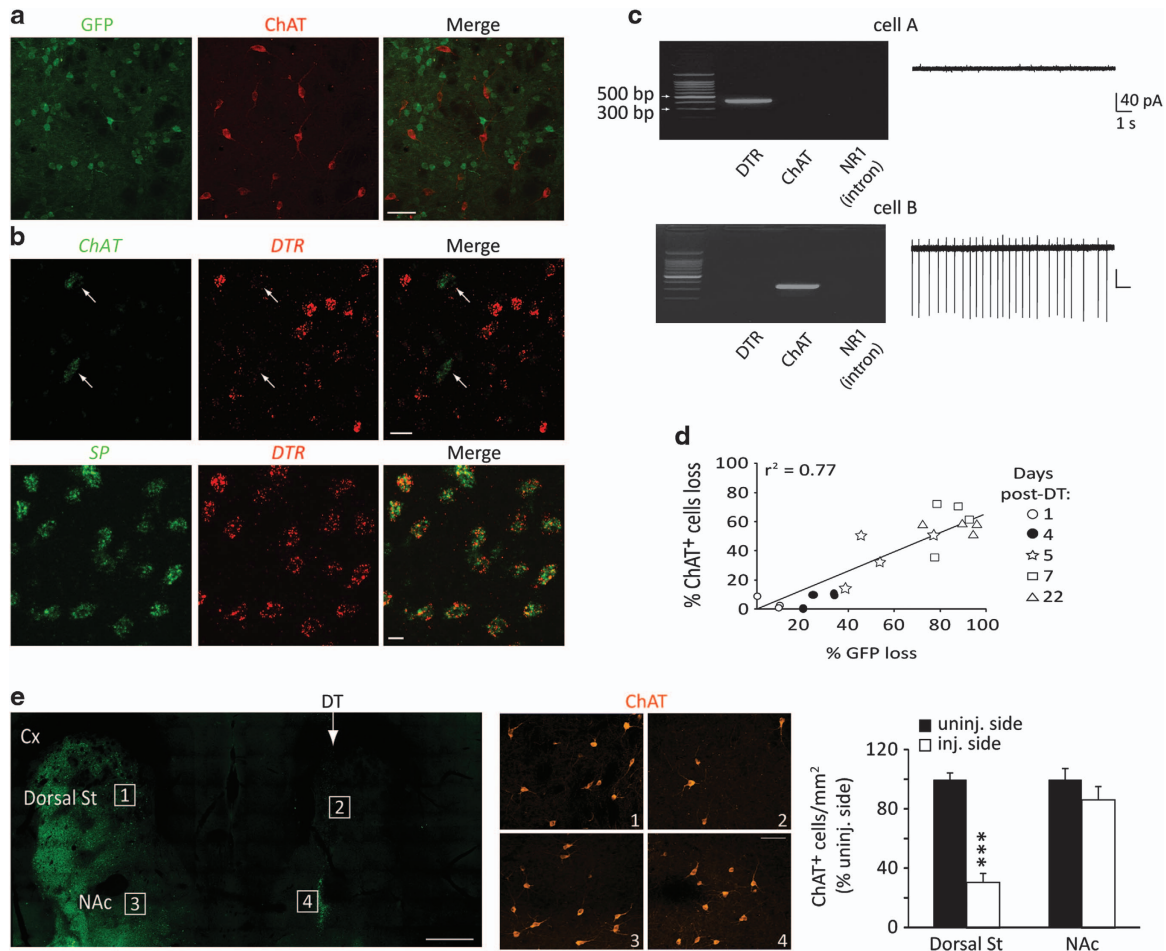


Figure 3 Absence of DTR expression in cholinergic interneurons and characteristics of cholinergic interneuron loss. (a) Double immunofluorescence labeling demonstrated that DTR, revealed by GFP expression (green), does not colocalize with choline acetyltransferase (ChAT) which labels the cholinergic interneurons (red). Scale bar, 50 μ m. (b) Dual *in situ* hybridization showing that DTR (red) is not expressed in ChAT⁺ cells (green, top, arrows) but colocalized with SP (green, bottom). Scale bars, 25 μ m (top) and 10 μ m (bottom). (c) Agarose gels of the single-cell RT-PCR products from two individual neurons whose electrical activity, recorded in cell-attached mode, is illustrated on the right. DTR-GFP mRNA (406 bp) is detected in a silent cell identified as MSN (top) but not in a spontaneous firing cell identified as cholinergic interneuron (bottom) that indeed expresses ChAT mRNA (323 bp). Cells are negative for the NR1 gene intron showing no contamination of the cytoplasm by genomic DNA. (d) The percentage of cholinergic interneurons' (revealed by GFP staining) and striatonigral MSNs' (revealed by GFP staining) loss, quantified at different time points after unilateral DT injection, is highly correlated. (e) GFP (left) and ChAT (right) immunodetection on a DTR⁺ coronal brain section 15 days after unilateral DT injection into the dorsal striatum and the nucleus accumbens. Scale bars, left: 500 μ m; right: 50 μ m. Quantitative analyses illustrate the density of ChAT-positive cells in the dorsal striatum and the nucleus accumbens ($n = 6$ DTR⁺). Cx: cortex, St: striatum, NAc: nucleus accumbens. Data are expressed as percentage \pm SEM. Student's *t*-test: *** $p < 0.001$ vs uninjected side.

alterations of the striatonigral pathway. We therefore examined whether LID expression was affected in DT-injected DTR⁺ compared with DTR⁻ mice rendered hemiparkinsonian by unilateral intranigral injection of 6-OHDA (Figure 5a). Strong and equivalent dopaminergic denervation of the striatum ipsilateral to the lesioned side was measured in both DTR⁻ (-95.5% vs uninjected side, $p < 0.001$) and DTR⁺ (-94.9% vs uninjected side, $p < 0.001$) mice (Figure 5b). After a chronic 21 days of treatment with L-DOPA, DTR⁻ mice exhibited robust AIMs, which were strongly reduced in DTR⁺ mice both for dyskinesia (-67.1%, $p < 0.001$) and contralateral rotations (-78.4%, $p < 0.001$) (Figure 5c). The reduction of AIMs was observed at every time points over the 120-min scoring period following the last L-DOPA injection (repeated-measures ANOVA: genotype effect, $F_{(1,26)}$

= 22.32, $p < 0.001$; time effect, $F_{(5,130)} = 50.21$, $p < 0.001$; genotype \times time interaction, $F_{(5,130)} = 18.51$, $p < 0.001$; Figure 5d). These results provide direct evidence that striatonigral MSNs ablation can inhibit the expression of LID.

DT-injected DTR⁺ mice show anxiolytic behavior. The limbic-related connections of the dorsal striatum raise the possibility of its involvement in emotional processing. To test this hypothesis, we assessed our transgenic mice in behavioral paradigms involving an anxiety component: the open field and the elevated plus maze. Mice display anxiety-related behaviors in open spaces; therefore, increased time spent in the central zone of the open field or in the open arms of the elevated plus maze is interpreted

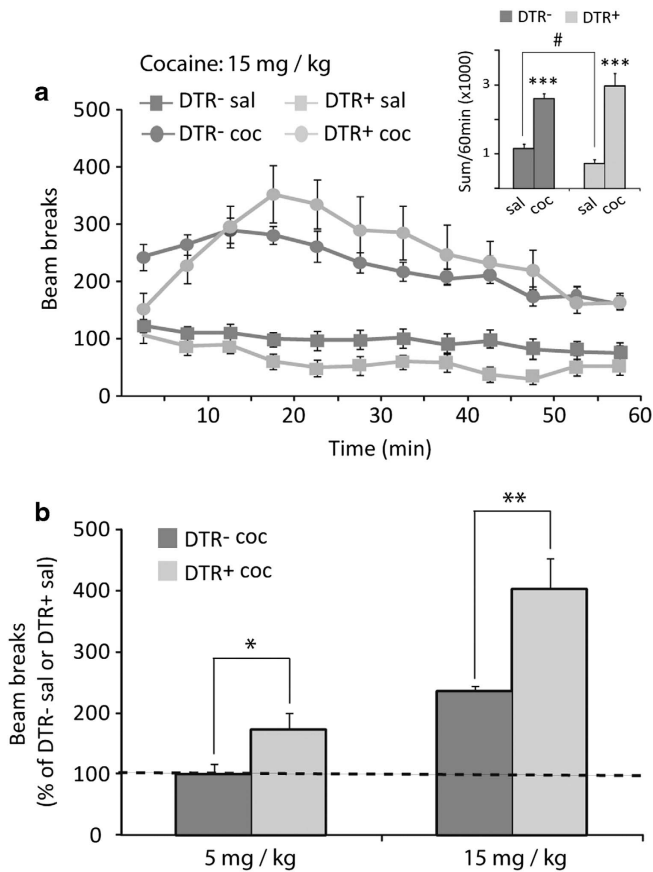


Figure 4 DT injection alters basal and cocaine-induced locomotion. (a) Line graphs illustrate the number of beam breaks in 5-min bins over a 60-min period after saline or cocaine (15 mg/kg) injections for DTR⁻ ($n=14$ saline and 10 cocaine) and DTR⁺ ($n=9$ saline and 6 cocaine) mice. Inset shows the group means \pm SEM of total beam breaks for the 60-min test period. Student's t -test: *** $p<0.001$ vs DTR⁻ sal or DTR⁺ sal, # $p<0.05$ vs DTR⁻ sal. (b) Bar graphs comparing the locomotor response to two different doses of cocaine (5 and 15 mg/kg). Data are the mean number of beam breaks measured during 60 min and are expressed for each genotype as the percentage \pm SEM of respective saline-treated mice (5 mg/kg group: DTR⁻ mice, $n=12$ saline and 12 cocaine and DTR⁺ mice, $n=5$ saline and 5 cocaine; 15 mg/kg group: DTR⁻ mice, $n=14$ saline and 10 cocaine and DTR⁺ mice, $n=9$ saline and 6 cocaine). Student's t -test: * $p<0.05$, ** $p<0.01$ vs DTR⁻ coc.

as reduced anxiety. DT-injected DTR⁺ mice showed marked increase in the time spent in the central zone of the open field ($p<0.05$) as well as in the time spent ($p<0.001$) and number of entries ($p<0.01$) in the elevated plus maze (Figure 6). These changes reflect reduced anxiety and not a motor impairment as the total distance traveled during the 5-min test period was similar for DTR⁻ and DTR⁺ mice in the open-field (DTR⁻: 2958.04 ± 202.53 mm, $n=17$; DTR⁺: 2487.03 ± 264.37 mm, $n=10$; NS) and in the EPM (DTR⁻: 2094.1 ± 96.7 mm, $n=17$; DTR⁺: 2014.8 ± 116.3 mm, $n=10$; NS).

DISCUSSION

In the present study, we achieved inducible striatonigral MSNs' ablation by using cell-type specific expression of DTR and revealed three original results: (i) a region-specific

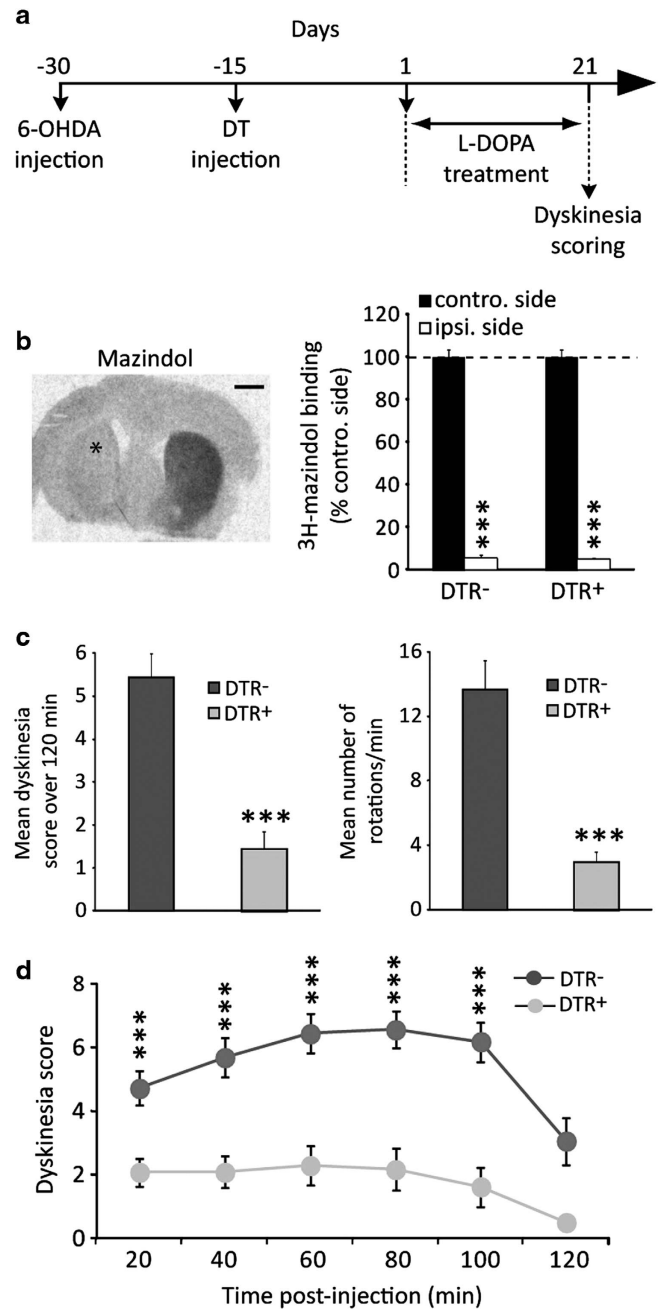


Figure 5 L-DOPA-induced dyskinesia are dramatically reduced after striatonigral neurons ablation. (a) Time course of L-DOPA-induced dyskinesia. (b) Autoradiographic image and quantitative analysis of ³H-mazindol binding showing the extensive loss of dopamine terminals in the striatum ipsilateral to the 6-OHDA injected side (*) ($n=16$ DTR⁻ and 12 DTR⁺). Data are expressed as the percentage \pm SEM. Student's t -test, *** $p<0.001$ vs contralateral side. Scale bar, 1 mm. (c) Dyskinesia score (left; sum of the mean scores for axial, orolingual, and forelimb AIMs over 120 min; maximum 12) and locomotive AIM (right; mean number of contralateral rotations per minute over 120 min) after L-DOPA injection on day 21 of chronic treatment ($n=16$ DTR⁻ and 12 DTR⁺). Data are expressed as mean \pm SEM. Student's t -test, *** $p<0.001$ vs DTR⁻ mice. (d) Time profile of axial, limb and orolingual dyskinesia scored every 20 min over a 120-min period after L-DOPA injection at day 21 in DTR⁻ ($n=16$) and DTR⁺ ($n=12$) mice. Data are reported as mean \pm SEM. Two-way RM ANOVA: Genotype: $F_{(1,26)}=22.32$, $p<0.001$; time: $F_{(5,130)}=50.21$, $p<0.001$; genotype \times time: $F_{(5,130)}=18.51$, $p<0.001$, Holm-Sidak posttest: *** $p<0.001$.

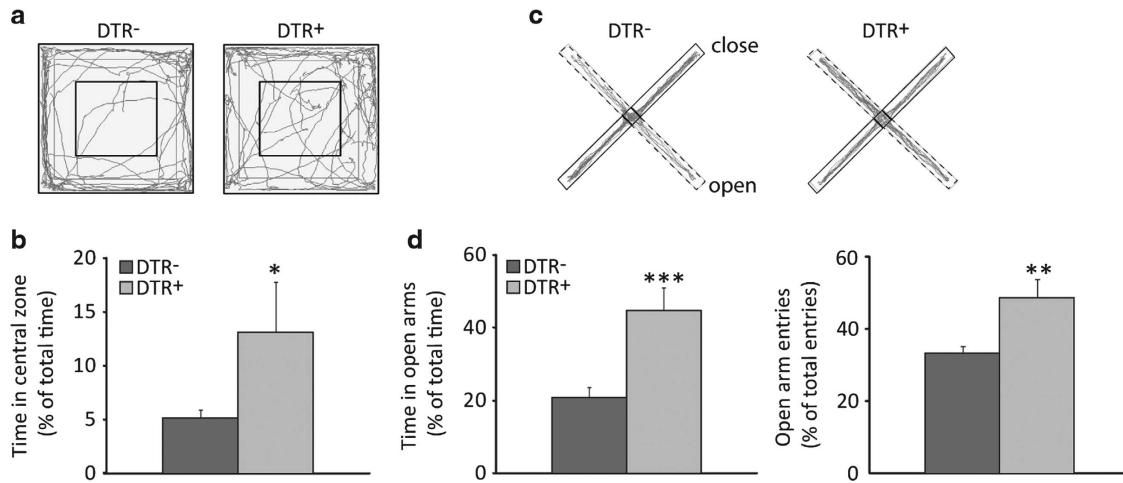


Figure 6 Anxiety is reduced after striatonigral MSNs' ablation. Representative paths (a, c) and quantification showing the time spent in the central zone of the open field (b) as well as the time and the number of entries in the open arms of the elevated plus maze (d) for DTR⁻ ($n = 17$) and DTR⁺ ($n = 10$) mice. Data are expressed as the percentage \pm SEM of the total time. Student's *t*-test: * $p < 0.05$, ** $p < 0.01$, *** $p < 0.001$ vs DTR⁻ mice.

regulation of cholinergic interneurons homeostasis by striatonigral MSNs, (ii) a causal implication of striatonigral MSNs in L-DOPA-induced dyskinesia, and (iii) the involvement of the dorsal striatum in the regulation of anxiety behavior.

We chose to express DTR under the control of the *Slc35d3* gene promoter based on two studies using FACS (fluorescence-activated cell sorting) and TRAP (translating ribosome affinity purification) that identified *Slc35d3* as the most striatonigral-enriched gene with a restricted expression to the striatum (Heiman *et al*, 2008; Lobo *et al*, 2006). Accordingly, intra-striatal injection of DT into the dorsal striatum triggered not only the elimination of a majority of striatonigral MSNs but also of a portion of cholinergic interneurons. We performed a series of experiments suggesting that the cholinergic loss, which occurred specifically in the dorsal but not in the ventral striatum, is the consequence of striatonigral MSNs' ablation. Another study, in which ablation of striatonigral MSNs is also obtained by DTR activation, reported no change in the number of striatal cholinergic interneurons after DT injection (Durieux *et al*, 2012). In this study, DTR expression in striatonigral MSNs is achieved by crossing iDTR mice (in which DTR expression is under the control of the ubiquitous Rosa26 promoter but is prevented by a loxP-flanked STOP cassette) with D₁-Cre mice. Knowing that transgene expression level is highly dependent on the promoter used to drive its expression, we can assume that DTR level is quite different in the two models. This might also explain the difference in the efficient DT dose between the two studies (0.5 ng/ μ l vs 0.1 ng/ μ l in Durieux *et al*, 2012); indeed 0.1 ng/ μ l did not produce significant ablation in our model (not shown). Level of DTR expression might impact the degenerative process, as for instance the kinetics of striatonigral MSNs death and glial reactivity, and differently affect cholinergic interneurons. Reliance of striatal cholinergic survival on non-cell autonomous processes, involving for instance sonic hedgehog signaling from dopaminergic projections, was recently demonstrated in the adult brain (Gonzalez-Reyes *et al*, 2012). In our case, SP

released by striatonigral MSNs might be a good candidate to support such pro-survival function as: (i) the presence of numerous SP positive axonal terminals making synaptic contact with dendrites of cholinergic neurons suggests an intimate relationship between these two populations (Bolam *et al*, 1986), (ii) SP biological functions are mediated by the NK1 receptor, which is almost exclusively expressed by cholinergic interneurons in the striatum (Elde *et al*, 1990; Gerfen, 1991), and (iii) NK1 receptor activation triggers pro-survival pathways crucial for the maintenance of some neuronal populations (Chu *et al*, 2011). The differential effects of DT in the striatum and nucleus accumbens open interesting questions and suggest that the cholinergic interneurons have distinct properties in each territory. Further experiments, which are beyond the scope of this study, will be necessary to investigate this region-specific interaction between striatonigral MSNs and cholinergic interneurons.

Our behavioral data showing reduced locomotion in DT-injected DTR⁺ mice confirm the BG model of the direct pathway promoting movement and are consistent with recent studies reporting that optogenetic activation or specific ablation of striatonigral MSNs enhances and reduces locomotion, respectively (Durieux *et al*, 2012; Kravitz *et al*, 2010). The increase in *GAD 67* mRNA level in the SNr of DT-injected mice further supports the view that hypolocomotion results from overactive BG outflow subsequent to removal of the inhibitory influence exerted by striatonigral MSNs. In contrast to basal locomotion, our transgenic mice unexpectedly displayed an increase in cocaine-induced activity. Indeed, previous studies reported decreased locomotor response to acute injection of psychostimulants after specifically inhibiting synaptic transmission in striatonigral MSNs (Hikida *et al*, 2010) or ablating these neurons in the striatum (Durieux *et al*, 2012). Differences in the psychostimulant used or the area of the striatum targeted is unlikely to account for such a discrepancy, suggesting that our phenotype might not be the direct consequence of striatonigral damage. Interestingly, an increased sensitivity to acute cocaine has been

reported after elimination of cholinergic cells in the dorsal striatum or the nucleus accumbens (Hikida *et al*, 2001; Sano *et al*, 2003), suggesting that the loss of striatal cholinergic interneurons rather than ablation of striatonigral MSNs might be responsible for the potentiation of cocaine-induced locomotor response.

LID, a major side effect of chronic L-DOPA treatment in PD, are associated with molecular changes occurring specifically in striatonigral MSNs (Santini *et al*, 2009). Our data, showing that striatonigral MSNs ablation prevents the development of LID, provide direct evidence for the causal role of these neurons in LID. This antidyskinetic effect is in agreement with the one obtained after genetic inactivation of DARPP-32 in striatonigral MSNs (Bateup *et al*, 2010). The shift in ERK activation from MSNs to cholinergic interneurons described after long-term exposure to L-DOPA (7 weeks) suggests that the cholinergic interneurons might also be involved in LID expression (Ding *et al*, 2011). Here the beneficial effect of striatonigral MSNs ablation on LID was observed as early as 7 days post-L-DOPA treatment (not shown), a time where ERK activation in cholinergic interneurons is not yet turned on (Ding *et al*, 2011). Thus our results support a primary role of striatonigral MSNs in the development of dyskinesia and also suggest that therapeutic strategies based on manipulation of dopamine-dependent signaling in the striatum should target the striatonigral MSNs for an efficient clinical approach to prevent LID.

Accumulating evidence suggest that the dorsal striatum might also be involved in emotional and motivational processing (Balleine *et al*, 2007). Here we found that DT-injected DTR⁺ mice exhibited reduced anxiety in the open-field and elevated plus maze tests. Considering that SP is of relevance in the regulation of emotional states, including anxiety-related behavior (Ebner and Singewald, 2006), and that striatonigral MSNs are the main source of SP in the striatum, our result suggest a role for striatal SP in the regulation of anxiety. Consistent with the anxiolytic effect of striatonigral MSNs ablation, pharmacological blockade or genetic deletion of NK1 receptors produced anxiolytic-like effects (File, 1997; Santarelli *et al*, 2001). As NK1 receptors expressed by cholinergic interneurons are important mediators of SP action in the striatum, the loss of this striatal population in our model is likely to accentuate the anxiolytic effect. SP is widely distributed in the brain and the SP-sensitive areas commonly implicated in the control of anxious states are part of the limbic system (Davis *et al*, 2010). Although the dorsal striatum has limbic connections through the dopamine system (Haber *et al*, 2000), its involvement in anxiety behavior is quite novel and highlights the plurality of neuronal substrates underlying this behavior. Interestingly, dynorphin, another peptide specifically expressed by striatonigral MSNs, has been implicated in anxiety and might thus participate to the reduced anxiety exhibited by the DT-injected transgenic mice (Schwarzer, 2009; Van't Veer and Carlezon, 2013).

Altogether, our data reveal an intimate relationship between striatonigral MSNs and cholinergic interneurons in the dorsal striatum and provide experimental evidence for the implication of these populations not only in dopamine-dependent motor behaviors but also in the

control of anxiety, emphasizing the functional overlap between the dorsal striatum and the nucleus accumbens.

FUNDING AND DISCLOSURE

The authors declare no conflict of interest.

ACKNOWLEDGEMENTS

This work was supported by CNRS, Aix-Marseille Université, Fondation de France, Fédération pour la Recherche sur le Cerveau. D.R. was supported by a grant from the Ministry of Education and Research and France Parkinson. We thank A. de Kerchove d'Exaerde for his help in the BAC transgenesis and single-cell RT-PCR experiments, A. Moqrigh for helpful discussion and comments on the manuscript, and A. Reynders for her critical comments on the manuscript. We also thank the animal and imaging facilities of the IBDM.

REFERENCES

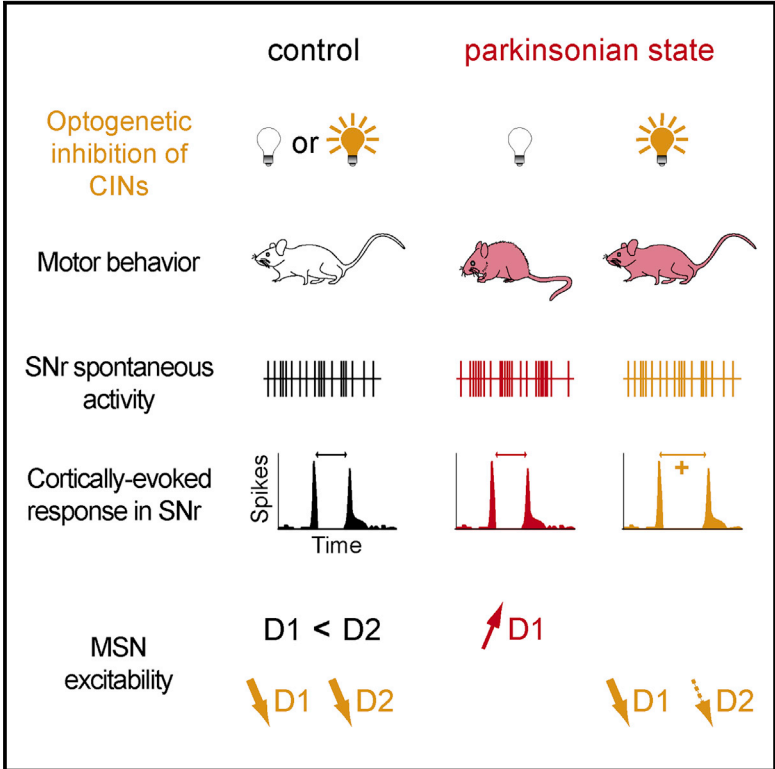
- Albin RL, Young AB, Penney JB (1989). The functional anatomy of basal ganglia disorders. *Trends Neurosci* 12: 366–375.
- Balleine BW, Delgado MR, Hikosaka O (2007). The role of the dorsal striatum in reward and decision-making. *J Neurosci* 27: 8161–8165.
- Bateup HS, Santini E, Shen W, Birnbaum S, Valjent E, Surmeier DJ *et al* (2010). Distinct subclasses of medium spiny neurons differentially regulate striatal motor behaviors. *Proc Natl Acad Sci USA* 107: 14845–14850.
- Bertran-Gonzalez J, Bosch C, Maroteaux M, Matamalas M, Herve D, Valjent E *et al* (2008). Opposing patterns of signaling activation in dopamine D1 and D2 receptor-expressing striatal neurons in response to cocaine and haloperidol. *J Neurosci* 28: 5671–5685.
- Beurrier C, Lopez S, Revy D, Selvam C, Goudet C, Lherondel M *et al* (2009). Electrophysiological and behavioral evidence that modulation of metabotropic glutamate receptor 4 with a new agonist reverses experimental parkinsonism. *FASEB J* 23: 3619–3628.
- Bolam JP, Ingham CA, Izzo PN, Levey AI, Rye DB, Smith AD *et al* (1986). Substance P-containing terminals in synaptic contact with cholinergic neurons in the neostriatum and basal forebrain: a double immunocytochemical study in the rat. *Brain Res* 397: 279–289.
- Bolam JP, Wainer BH, Smith AD (1984). Characterization of cholinergic neurons in the rat neostriatum. A combination of choline acetyltransferase immunocytochemistry, Golgi-impregnation and electron microscopy. *Neuroscience* 12: 711–718.
- Cenci MA (2007). Dopamine dysregulation of movement control in L-DOPA-induced dyskinesia. *Trends Neurosci* 30: 236–243.
- Chu JM, Chen LW, Chan YS, Yung KK (2011). Neuroprotective effects of neurokinin receptor one in dopaminergic neurons are mediated through Akt/PKB cell signaling pathway. *Neuropharmacology* 61: 1389–1398.
- Davis M, Walker DL, Miles L, Grillon C (2010). Phasic vs sustained fear in rats and humans: role of the extended amygdala in fear vs anxiety. *Neuropsychopharmacology* 35: 105–135.
- DeLong MR (1990). Primate models of movement disorders of basal ganglia origin. *Trends Neurosci* 13: 281–285.
- Ding Y, Won L, Britt JP, Lim SA, McGehee DS, Kang UJ (2011). Enhanced striatal cholinergic neuronal activity mediates L-DOPA-induced dyskinesia in parkinsonian mice. *Proc Natl Acad Sci USA* 108: 840–845.

- Durieux PF, Bearzatto B, Guiducci S, Buch T, Waisman A, Zoli M *et al* (2009). D2R striatopallidal neurons inhibit both locomotor and drug reward processes. *Nat Neurosci* 12: 393–395.
- Durieux PF, Schiffmann SN, de Kerchove dA (2012). Differential regulation of motor control and response to dopaminergic drugs by D1R and D2R neurons in distinct dorsal striatum subregions. *EMBO J* 31: 640–653.
- Ebner K, Singewald N (2006). The role of substance P in stress and anxiety responses. *Amino Acids* 31: 251–272.
- Elde R, Schalling M, Ceccatelli S, Nakanishi S, Hokfelt T (1990). Localization of neuropeptide receptor mRNA in rat brain: initial observations using probes for neurotensin and substance P receptors. *Neurosci Lett* 120: 134–138.
- Ferguson SM, Eskenazi D, Ishikawa M, Wanat MJ, Phillips PE, Dong Y *et al* (2011). Transient neuronal inhibition reveals opposing roles of indirect and direct pathways in sensitization. *Nat Neurosci* 14: 22–24.
- File SE (1997). Anxiolytic action of a neurokinin1 receptor antagonist in the social interaction test. *Pharmacol Biochem Behav* 58: 747–752.
- Gerfen CR (1984). The neostriatal mosaic: compartmentalization of corticostriatal input and striatonigral output systems. *Nature* 311: 461–464.
- Gerfen CR (1991). Substance P (neurokinin-1) receptor mRNA is selectively expressed in cholinergic neurons in the striatum and basal forebrain. *Brain Res* 556: 165–170.
- Gerfen CR, Engber TM, Mahan LC, Susel Z, Chase TN, Monsma FJ Jr *et al* (1990). D1 and D2 dopamine receptor-regulated gene expression of striatonigral and striatopallidal neurons. *Science* 250: 1429–1432.
- Gonzalez-Reyes LE, Verbitsky M, Blesa J, Jackson-Lewis V, Paredes D, Tillack K *et al* (2012). Sonic hedgehog maintains cellular and neurochemical homeostasis in the adult nigrostriatal circuit. *Neuron* 75: 306–319.
- Graybiel AM (2000). The basal ganglia. *Curr Biol* 10: R509–R511.
- Haber SN, Fudge JL, McFarland NR (2000). Striatonigrostriatal pathways in primates form an ascending spiral from the shell to the dorsolateral striatum. *J Neurosci* 20: 2369–2382.
- Heiman M, Schaefer A, Gong S, Peterson JD, Day M, Ramsey KE *et al* (2008). A translational profiling approach for the molecular characterization of CNS cell types. *Cell* 135: 738–748.
- Hikida T, Kaneko S, Isobe T, Kitabatake Y, Watanabe D, Pastan I *et al* (2001). Increased sensitivity to cocaine by cholinergic cell ablation in nucleus accumbens. *Proc Natl Acad Sci USA* 98: 13351–13354.
- Hikida T, Kimura K, Wada N, Funabiki K, Nakanishi S (2010). Distinct roles of synaptic transmission in direct and indirect striatal pathways to reward and aversive behavior. *Neuron* 66: 896–907.
- Hikida T, Yawata S, Yamaguchi T, Danjo T, Sasaoka T, Wang Y *et al* (2013). Pathway-specific modulation of nucleus accumbens in reward and aversive behavior via selective transmitter receptors. *Proc Natl Acad Sci USA* 110: 342–347.
- Holtzman DM, Li Y, Parada LF, Kinsman S, Chen CK, Valletta JS *et al* (1992). p140trk mRNA marks NGF-responsive forebrain neurons: evidence that trk gene expression is induced by NGF. *Neuron* 9: 465–478.
- Kawaguchi Y (1993). Physiological, morphological, and histochemical characterization of three classes of interneurons in rat neostriatum. *J Neurosci* 13: 4908–4923.
- Kravitz AV, Freeze BS, Parker PR, Kay K, Thwin MT, Deisseroth K *et al* (2010). Regulation of parkinsonian motor behaviours by optogenetic control of basal ganglia circuitry. *Nature* 466: 622–626.
- Lena C, de Kerchove D'E, Cordero-Erausquin M, le NN, del MA-J, Changeux JP (1999). Diversity and distribution of nicotinic acetylcholine receptors in the locus ceruleus neurons. *Proc Natl Acad Sci USA* 96: 12126–12131.
- Livak KJ, Schmittgen TD (2001). Analysis of relative gene expression data using real-time quantitative PCR and the 2⁻(Delta Delta C(T)) method. *Methods* 25: 402–408.
- Lobo MK, Covington HE III, Chaudhury D, Friedman AK, Sun H, mez-Werno D *et al* (2010). Cell type-specific loss of BDNF signaling mimics optogenetic control of cocaine reward. *Science* 330: 385–390.
- Lobo MK, Nestler EJ (2011). The striatal balancing act in drug addiction: distinct roles of direct and indirect pathway medium spiny neurons. *Front Neuroanat* 5: 41.
- Lobo MK, Karsten SL, Gray M, Geschwind DH, Yang XW (2006). FACS-array profiling of striatal projection neuron subtypes in juvenile and adult mouse brains. *Nat Neurosci* 9: 443–452.
- Lundblad M, Picconi B, Lindgren H, Cenci MA (2004). A model of L-DOPA-induced dyskinesia in 6-hydroxydopamine lesioned mice: relation to motor and cellular parameters of nigrostriatal function. *Neurobiol Dis* 16: 110–123.
- Nishizawa K, Fukabori R, Okada K, Kai N, Uchigashima M, Watanabe M *et al* (2012). Striatal indirect pathway contributes to selection accuracy of learned motor actions. *J Neurosci* 32: 13421–13432.
- Paxinos G, Franklin KBJ (2001). *The Mouse Brain in Stereotaxic Coordinates*, 2nd edn. Academic Press: San Diego.
- Salin P, Manrique C, Forni C, Kerkerian-Le GL (2002). High-frequency stimulation of the subthalamic nucleus selectively reverses dopamine denervation-induced cellular defects in the output structures of the basal ganglia in the rat. *J Neurosci* 22: 5137–5148.
- Sano H, Yasoshima Y, Matsushita N, Kaneko T, Kohno K, Pastan I *et al* (2003). Conditional ablation of striatal neuronal types containing dopamine D2 receptor disturbs coordination of basal ganglia function. *J Neurosci* 23: 9078–9088.
- Santarelli L, Gobbi G, Debs PC, Sibille ET, Blier P, Hen R *et al* (2001). Genetic and pharmacological disruption of neurokinin 1 receptor function decreases anxiety-related behaviors and increases serotonergic function. *Proc Natl Acad Sci USA* 98: 1912–1917.
- Santini E, Alcaccer C, Cacciatore S, Heiman M, Herve D, Greengard P *et al* (2009). L-DOPA activates ERK signaling and phosphorylates histone H3 in the striatonigral medium spiny neurons of hemiparkinsonian mice. *J Neurochem* 108: 621–633.
- Schwarzer C (2009). 30 years of dynorphins—new insights on their functions in neuropsychiatric diseases. *Pharmacol Ther* 123: 353–370.
- Smith Y, Bevan MD, Shink E, Bolam JP (1998). Microcircuitry of the direct and indirect pathways of the basal ganglia. *Neuroscience* 86: 353–387.
- Tai LH, Lee AM, Benavidez N, Bonci A, Willbrecht L (2012). Transient stimulation of distinct subpopulations of striatal neurons mimics changes in action value. *Nat Neurosci* 15: 1281–1289.
- Van't Veer A, Carlezon WA (2013). Role of kappa-opioid receptors in stress and anxiety-related behavior. *Psychopharmacology (Berl)* 229: 435–452.
- Yawata S, Yamaguchi T, Danjo T, Hikida T, Nakanishi S (2012). Pathway-specific control of reward learning and its flexibility via selective dopamine receptors in the nucleus accumbens. *Proc Natl Acad Sci USA* 109: 12764–12769.

Supplementary Information accompanies the paper on the Neuropsychopharmacology website (<http://www.nature.com/npp>)

Striatal Cholinergic Interneurons Control Motor Behavior and Basal Ganglia Function in Experimental Parkinsonism

Graphical Abstract



Authors

Nicolas Maurice, Martine Liberge, Florence Jaouen, ..., Marianne Amalric, Lydia Kerkerian-Le Goff, Corinne Beurrier

Correspondence

corinne.beurrier@univ-amu.fr

In Brief

By combining optogenetics with behavioral and electrophysiological approaches in mice, Maurice et al. provide evidence for a causal role of striatal cholinergic interneurons in parkinsonian symptomatology and identify underlying neural substrates in the basal ganglia network.

Highlights

- CIN activity impacts motor function and basal ganglia output in parkinsonian state
- CIN inhibition alleviates parkinsonian symptoms, while activation has no effect
- CIN inhibition corrects burst firing and enhances cortically evoked inhibition in SNr
- CIN's control of D2-, but not D1-MSN, excitability is reduced in parkinsonian state



Striatal Cholinergic Interneurons Control Motor Behavior and Basal Ganglia Function in Experimental Parkinsonism

Nicolas Maurice,^{1,4} Martine Liberge,^{2,4} Florence Jaouen,¹ Samira Ztaou,² Marwa Hanini,¹ Jeremy Camon,² Karl Deisseroth,³ Marianne Amalric,^{2,5} Lydia Kerkerian-Le Goff,^{1,5} and Corinne Beurrier^{1,5,*}

¹Aix-Marseille Université (AMU), Centre National de la Recherche Scientifique (CNRS), UMR 7288, Institut de Biologie du Développement de Marseille (IBDM), 13288 Marseille cedex 9, France

²Aix-Marseille Université (AMU), Centre National de la Recherche Scientifique (CNRS), UMR 7291, FR3C 3512, Laboratoire de Neurosciences Cognitives, 13331 Marseille cedex 3, France

³Departments of Bioengineering and Psychiatry and Howard Hughes Medical Institute, Stanford University, Palo Alto, CA 94305, USA

⁴Co-first author

⁵Co-senior author

*Correspondence: corinne.beurrier@univ-amu.fr

<http://dx.doi.org/10.1016/j.celrep.2015.09.034>

This is an open access article under the CC BY-NC-ND license (<http://creativecommons.org/licenses/by-nc-nd/4.0/>).

SUMMARY

Despite evidence showing that anticholinergic drugs are of clinical relevance in Parkinson's disease (PD), the causal role of striatal cholinergic interneurons (CINs) in PD pathophysiology remains elusive. Here, we show that optogenetic inhibition of CINs alleviates motor deficits in PD mouse models, providing direct demonstration for their implication in parkinsonian motor dysfunctions. As neural correlates, CIN inhibition in parkinsonian mice differentially impacts the excitability of striatal D1 and D2 medium spiny neurons, normalizes pathological bursting activity in the main basal ganglia output structure, and increases the functional weight of the direct striatonigral pathway in cortical information processing. By contrast, CIN inhibition in non-lesioned mice does not affect locomotor activity, equally modulates medium spiny neuron excitability, and does not modify spontaneous or cortically driven activity in the basal ganglia output, suggesting that the role of these interneurons in motor function is highly dependent on dopamine tone.

INTRODUCTION

Parkinson's disease (PD) is a debilitating neurodegenerative movement disorder resulting from the loss of nigral dopaminergic (DA) neurons that project massively to the striatum, the main basal ganglia input structure. The hypokinetic parkinsonian syndrome is thought to be the consequence of opposite changes in the activity of the two populations of GABAergic striatal projection neurons, also called medium spiny neurons (MSNs), which control the basal ganglia output nuclei, mainly the substantia nigra pars reticulata (SNr) in rodent. Dopamine D1 receptor-expressing MSNs (D1 or direct MSNs), giving rise

to a monosynaptic inhibitory projection (direct pathway) onto SNr, become hypoactive, whereas dopamine D2 receptor-expressing MSNs (D2 or indirect MSNs), at the origin of a polysynaptic projection with excitatory influence onto SNr (indirect pathway), become hyperactive (Albin et al., 1989; Mallet et al., 2006). This imbalance leads to pathological activation of SNr, reinforcing its inhibitory tone onto the thalamocortical circuit and, hence, on motor cortical outflow. The pathological changes in the activity of the two striatal pathways, whose functional relationship with movement control is still debated (Calabresi et al., 2014; Cui et al., 2013), may involve profound reorganizations within the striatal circuitry.

Striatal cholinergic interneurons (CINs), which correspond to the tonically active neurons recorded in vivo, constitute 1%–3% of all striatal neurons. Despite being few in numbers, they are the main source of acetylcholine (ACh) within the striatum, and their dense terminal fields are primarily directed to MSNs (Phelps et al., 1985). The improvement of parkinsonian tremor by both DA agonists and anticholinergic drugs led to the DA-ACh balance hypothesis, where DA and ACh are believed to play opposite roles in the striatum (Barbeau, 1962). This clinical observation particularly underlines the functional impact of ACh as DA levels fall. There is indeed compelling evidence showing that DA depletion triggers complex alterations in striatal cholinergic signaling and activity (Aosaki et al., 1994; Ding et al., 2006), leading, among other things, to morphofunctional alterations of striatal output neurons (Pisani et al., 2007; Shen et al., 2007). However, whether and how this cholinergic-dependent disruption of striatal properties contributes to motor symptoms in PD and affects basal ganglia circuitry remain an open question.

The diversity of cholinergic receptors expressed in the striatum, located both at the presynaptic and postsynaptic levels (Goldberg et al., 2012), suggests that CINs exert complex and powerful influence on striatal functioning and, hence, on basal ganglia outflow. An additional level of complexity in understanding cholinergic regulation of striatal function comes from recent studies showing the following: (1) CINs co-release glutamate able to evoke fast glutamatergic responses in MSNs (Higley

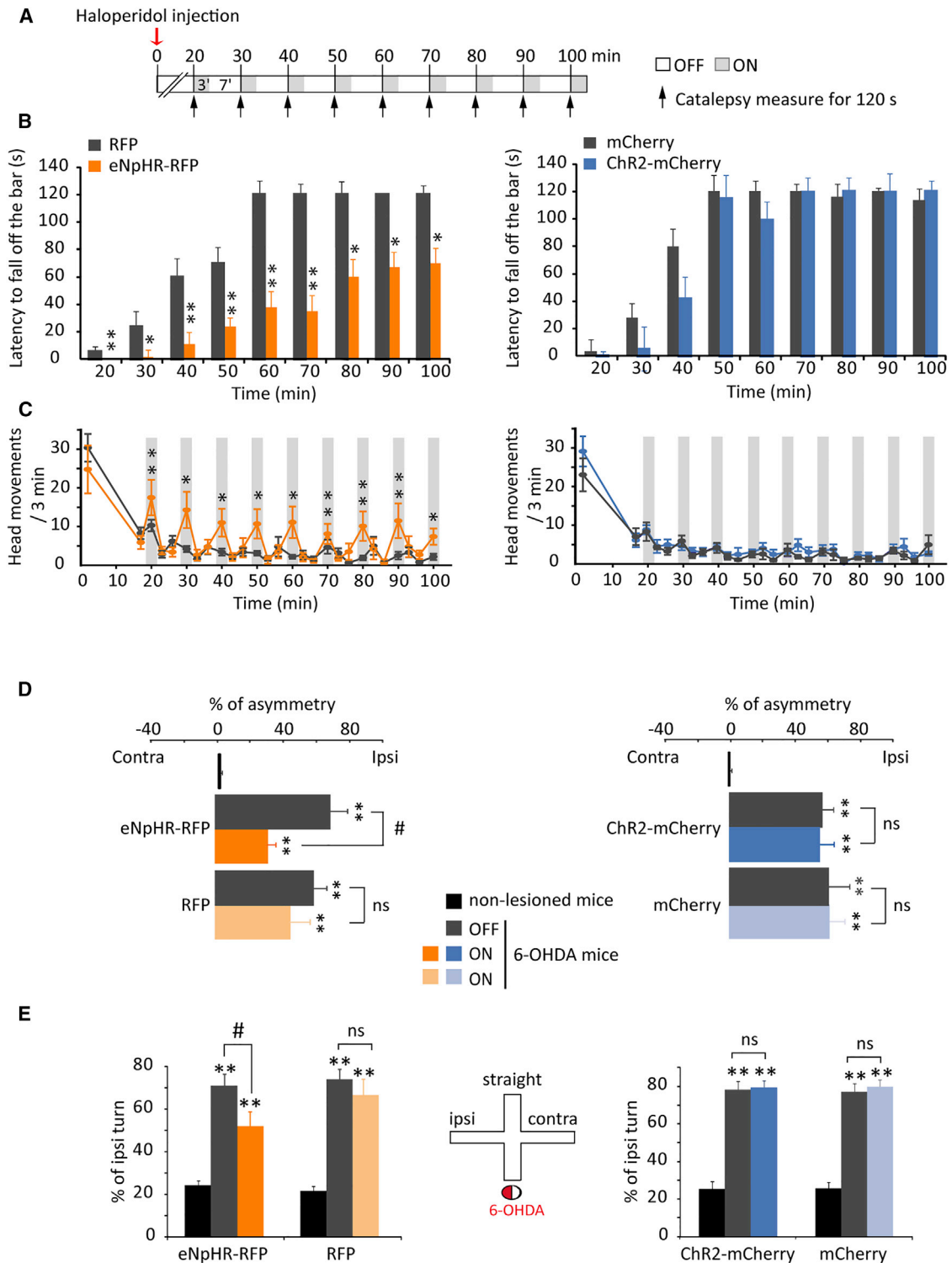


Figure 1. Photoinhibition of CINs rReduces Haloperidol-Induced Catalepsy and Relieves Parkinsonian-like Motor Deficits

(A) Experimental design. Mice received haloperidol (0.25 mg/kg) and the latency to step down the bar was measured 20 min later, then every 10 min, with a 120-s cutoff. Light was turned on (blue light: 10 Hz, 25-ms pulse width; yellow light: continuous illumination) for 3 min when placing the mice on the bar and was turned off afterward for 7 min, until next measure.

(B) Yellow light reduced haloperidol-induced catalepsy in eNpHR-RFP mice versus RFP mice (* $p < 0.05$, ** $p < 0.01$, U-Mann-Whitney after significant Kruskal-Wallis test), whereas blue light illumination in Chr2-mCherry mice had no effect versus mCherry mice ($p = 0.3$).

(legend continued on next page)

et al., 2011), (2) CIN activation can drive GABA release from dopaminergic terminals (Nelson et al., 2014; Tritsch et al., 2014) and neuropeptide Y-expressing interneurons (English et al., 2011), and (3) their synchronous activation triggers striatal DA release (Threlfell et al., 2012). While we do not know yet how these different actions are coordinated in vivo, these results suggest that DA/ACh interactions are more complex than the traditional antagonistic model would predict. Therefore, the contribution of CINs to basal ganglia function cannot be fully understood unless an approach mimicking the diversity of their actions is used. Optogenetics that allows precise control of circuit function, was, for example, used successfully to demonstrate the role of CINs in the nucleus accumbens during cocaine conditioning (Witten et al., 2010).

Here, using a combination of optogenetic, behavioral, and electrophysiological approaches, we demonstrate a major role of CINs in PD pathophysiology. We show that selective inhibition of CINs alleviates motor deficits and corrects dysfunctions at the main input and output stages of the basal ganglia network in PD mouse models, with a preferential action on the direct striatonigral pathway.

RESULTS

Inhibition of Striatal Cholinergic Interneurons Reduces Parkinsonian-like Motor Deficits

We expressed ChR2-mCherry or eNpHR-RFP in choline acetyltransferase (ChAT)-expressing neurons by injecting a Cre-dependent adeno-associated virus (AAV) carrying the opsins or their reporter genes into the dorsal striatum of ChAT^{cre/cre} mice (subsequently referred to as ChR2-mCherry and eNpHR-RFP mice). Quantifying the proportion of neurons expressing opsins that were also ChAT positive and vice versa demonstrated the specificity and efficiency of the targeting strategy (Figure S1). Recordings of optogenetically identified CINs in striatal slices and anesthetized mice showed that opsins were functional (Figure S2).

CIN photoinhibition or photoactivation had no significant effect on locomotor activity of non-lesioned RFP, eNpHR-RFP, mCherry, and ChR2-mCherry mice in an open field (Figure S3A). To determine whether CINs affect parkinsonian akinesia, the effects of CIN modulation were examined in the haloperidol-induced catalepsy model (Figure 1A). The eNpHR-RFP haloperidol-treated mice removed their forepaws from the bar significantly faster under yellow illumination than did the RFP-treated mice (Figure 1B). Consistently, yellow light restored head move-

ments in a light-locked manner in haloperidol-injected eNpHR-RFP mice, demonstrating a robust anti-akinetic action of CIN inhibition (Figure 1C). In contrast, ChR2-mCherry mice under blue illumination exhibited a long-lasting cataleptic state, similar to mCherry mice (Figures 1B and 1C).

We next tested whether CIN inhibition could alleviate motor dysfunction in the 6-hydroxydopamine (6-OHDA) lesion model of PD. Unilateral 6-OHDA injection into the substantia nigra pars compacta (SNc) resulted in a near-total loss of DA cells after 2 weeks. In the cylinder test (Figure 1D), RFP and mCherry non-lesioned mice used their two forepaws indifferently during exploratory rearing (asymmetry score close to zero). The 6-OHDA lesions produced a significant shift toward ipsilateral forepaw use due to contralateral forelimb akinesia. Photoinhibition of CINs ipsilateral to the lesioned side in eNpHR-RFP mice induced a significant reduction in the asymmetry score. In contrast, CIN photoactivation in ChR2-mCherry 6-OHDA mice did not affect asymmetry (Figure 1D). In the cross maze test (Figure 1E), the 6-OHDA-induced bias toward ipsilateral turns, which reflects sensorimotor neglect, was significantly reduced by CIN inhibition in eNpHR-RFP mice, while CIN activation had no effect in ChR2-mCherry mice. The non-selective muscarinic receptor antagonist scopolamine (1 mg/kg) also reduced the asymmetry in the cylinder and cross maze tests in 6-OHDA mice (Figures S3B and S3C). Finally, we examined the effect of CIN photoinhibition on L-DOPA-induced dyskinesia, a main side effect of long-term DA treatment. CIN inhibition in eNpHR-RFP mice failed to affect the severity of dyskinesia once expressed (Figure S4). Taken together, these data show that CIN inhibition has no effect on spontaneous locomotion and L-DOPA-induced dyskinesia in our lesion and treatment conditions, but significantly alleviates parkinsonian-like motor deficits.

Inhibition of Striatal CINs Regulates the Basal Ganglia Output Structure in Parkinsonian Condition Only

A leading hypothesis on the origin of motor dysfunction in PD is that DA loss induces abnormal bursting activity in basal ganglia output nuclei, leading to pathological inhibitory tone onto the thalamocortical circuit that disrupts motor planning and execution. We tested whether striatal CIN inhibition modifies the activity of SNr neurons recorded in vivo in anesthetized transgenic eNpHR mice. CIN photoinhibition in non-lesioned animals did not affect spontaneous activity of SNr neurons (Table S1). The 6-OHDA mice showed altered burst firing, with significant increases in burst duration and number of spikes per burst (Figure 2A). CIN photoinhibition normalized these changes, without

(C) Light partially restored head movements in eNpHR-RFP mice (ON versus OFF preceding light: * $p < 0.05$, ** $p < 0.01$, paired Student's *t* test after significant two-way ANOVA), but not in ChR2-mCherry mice or in control RFP and mCherry mice ($n = 10$ – 13 per group).

(D) In the cylinder test, 6-OHDA mice showed marked forelimb asymmetry compared to non-lesioned mice (** $p < 0.01$, Fisher's least significant difference [LSD] test after significant ANOVA). (Left) This asymmetry was significantly improved by yellow light in eNpHR-RFP mice (ON versus OFF: # $p < 0.05$, Student's *t* test). Light did not affect asymmetry in RFP control mice ($n = 7$ – 8 per group). (Right) The significant forelimb asymmetry measured in 6-OHDA versus non-lesioned mice (** $p < 0.01$, Fisher's LSD test after significant ANOVA) was not affected by blue light illumination in ChR2-mCherry (ON versus OFF: ns, Student's *t* test) and mCherry (ON versus OFF: ns, Student's *t* test) mice ($n = 7$ – 8 per group).

(E) (Left) Ipsilateral turn bias induced by 6-OHDA lesion in the cross maze (6-OHDA versus non-lesioned: ** $p < 0.01$, one-way ANOVA) was partially corrected by photoinhibition in eNpHR-RFP mice (ON versus OFF: # $p < 0.05$, paired Student's *t* test), but not in RFP control mice ($n = 14$ per group). (Right) Photoactivation did not affect the ipsilateral turn bias induced by 6-OHDA lesion (6-OHDA versus non-lesioned: ** $p < 0.01$, one-way ANOVA) in ChR2-mCherry mice nor in mCherry mice (ON versus OFF: ns, Student's *t* test, $n = 12$ per group). In (D) and (E), continuous illumination was for 5 min with yellow light and 25-ms pulse width was at 10 Hz for blue light. Circle under the cross maze symbolizes a mouse with the 6-OHDA-injected side in red. Errors bars, SEM.

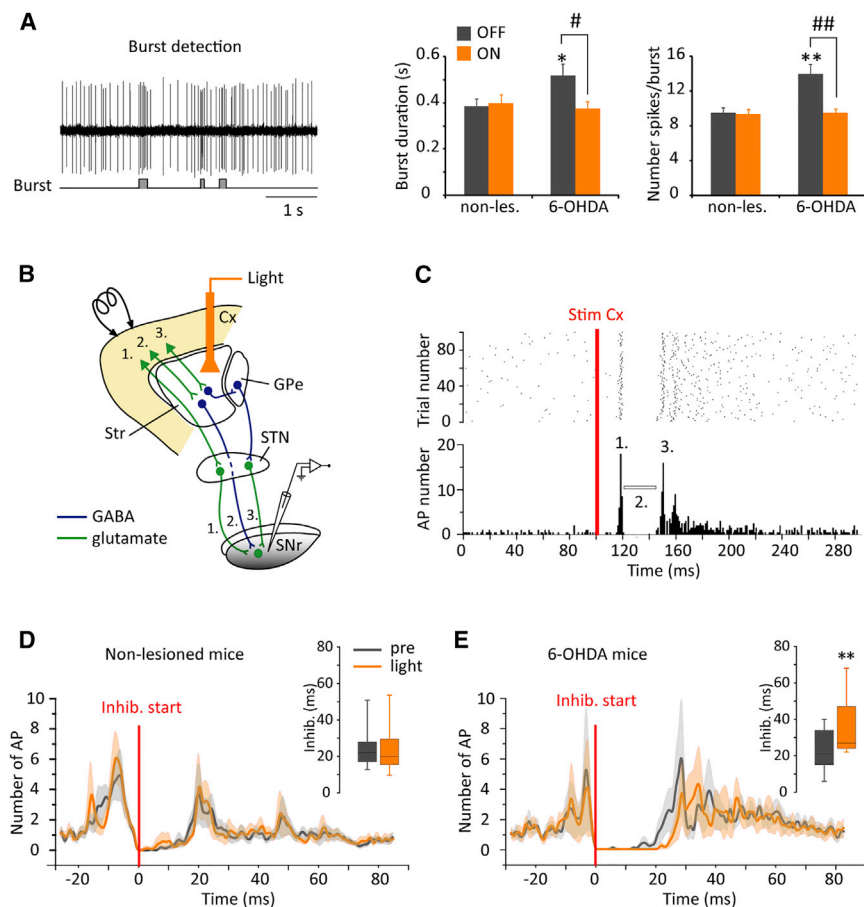


Figure 2. Photoinhibition of CINs Normalizes SNr Burst Firing and Strengthens the Inhibitory Influence of the Striatonigral Direct Pathway in 6-OHDA Mice

(A) Detection of bursts according to Poisson Surprise analysis in a spontaneously firing SNr neuron recorded in 6-OHDA transgenic eNpHR mice. The histograms show that the 6-OHDA induced increases in burst duration and number of spikes per burst (6-OHDA versus non-lesioned: * $p < 0.05$, ** $p < 0.01$, Student's *t* test) were normalized by CIN photoinhibition (light was delivered for 1 min; 6-OHDA ON versus OFF: # $p < 0.05$, ## $p < 0.01$, Holm-Sidak test after significant one-way ANOVA). Non-lesioned mice, $n = 18$ cells from six mice; 6-OHDA mice, $n = 13$ cells from six mice.

(B) Schematic representation shows pathways activated by cortical stimulation that project to SNr neurons. Cx, cortex; Str, striatum; GPe, external globus pallidus; STN, subthalamic nucleus.

(C) Raster plot and peristimulus time histogram (PSTH) show the typical triphasic response evoked by motor cortex stimulation in one SNr neuron recorded from a 6-OHDA transgenic eNpHR mouse.

(D and E) Population PSTHs of the cortically evoked responses recorded in SNr neurons in non-lesioned (D, $n = 17$ cells from six mice) and 6-OHDA (E, $n = 7$ cells from five mice) mice. The same neuron was recorded before (pre, gray line) and during (light, orange line) CIN photoinhibition. Light was delivered for 1 s at the beginning of each trial. PSTHs are aligned on the beginning of the inhibitory component (red lines) and the light-shaded colors represent (red lines) and the light-shaded colors represent

SEM. CIN photoinhibition induced a significant increase of the inhibitory component duration only in 6-OHDA mice, as illustrated by the box plots (insets) (** $p < 0.01$, Holm-Sidak test after significant one-way RM ANOVA). Errors bars, SEM.

modifying the parameters unaltered by the lesion (firing frequency and burst recurrence) (Table S1).

Next, to examine whether CINs influence the processing of cortical information through the trans-striatal pathways, we recorded the responses of individual SNr neurons to cortical stimulation (Figures 2B and 2C). As previously reported, such stimulation triggers a complex response composed, in most cases, of an early excitation followed by an inhibition and a late excitation, which has been attributed to the respective activation of the hyperdirect corticosubthalamic, the direct and indirect striatonigral pathways (Maurice et al., 1999; Ryan and Sanders, 1994; Sano et al., 2013; Tachibana et al., 2008). Because the characteristics of the evoked responses greatly vary among cells depending on the stimulation (e.g., location and number of stimulated fibers) but remain stable in a given cell over time, comparisons were made for a same cell under successive light conditions and not between cells from 6-OHDA versus non-lesioned mice. CIN photoinhibition had no effect on cortical information transfer in non-lesioned mice, whereas, in 6-OHDA mice, it increased the duration of the inhibitory component of the triphasic response without significantly affecting the excitatory components (Figures 2D and 2E; Table S2). Since parkinsonian akinesia is classically associated with overactive indirect pathway

and hypoactive direct pathway, our results suggest that CIN inhibition might partially restore balance in striatal outputs by increasing the functional impact of the direct pathway. In contrast, CIN photoinhibition had no effect on SNr spontaneous activity and cortical information transfer in non-lesioned transgenic eNpHR mice.

Dopamine Depletion Affects the Intrinsic Excitability of D1 MSNs

We first determined whether CINs themselves were affected by 6-OHDA lesion, as there is no consensus on whether CIN activity or striatal ACh release increases in PD models. Optogenetically identified CINs recorded either in slices or in anesthetized mice exhibited similar firing frequency in non-lesioned and 6-OHDA conditions (Figure 3), showing that they are not hyperactive in our experimental conditions. However, CINs were more excitable in slices from 6-OHDA mice, as illustrated by a lower rheobase current (non-lesioned: 137.7 ± 16.7 pA, $n = 17$; 6-OHDA: 87.1 ± 16.5 pA, $n = 17$; $p < 0.05$, Mann-Whitney test).

We then tested whether CIN modulation of striatal functions could be altered in PD state, by examining its impact on identified D1 and D2 MSNs that form the direct and indirect striatal projection systems, 2–3 weeks after 6-OHDA lesion. The

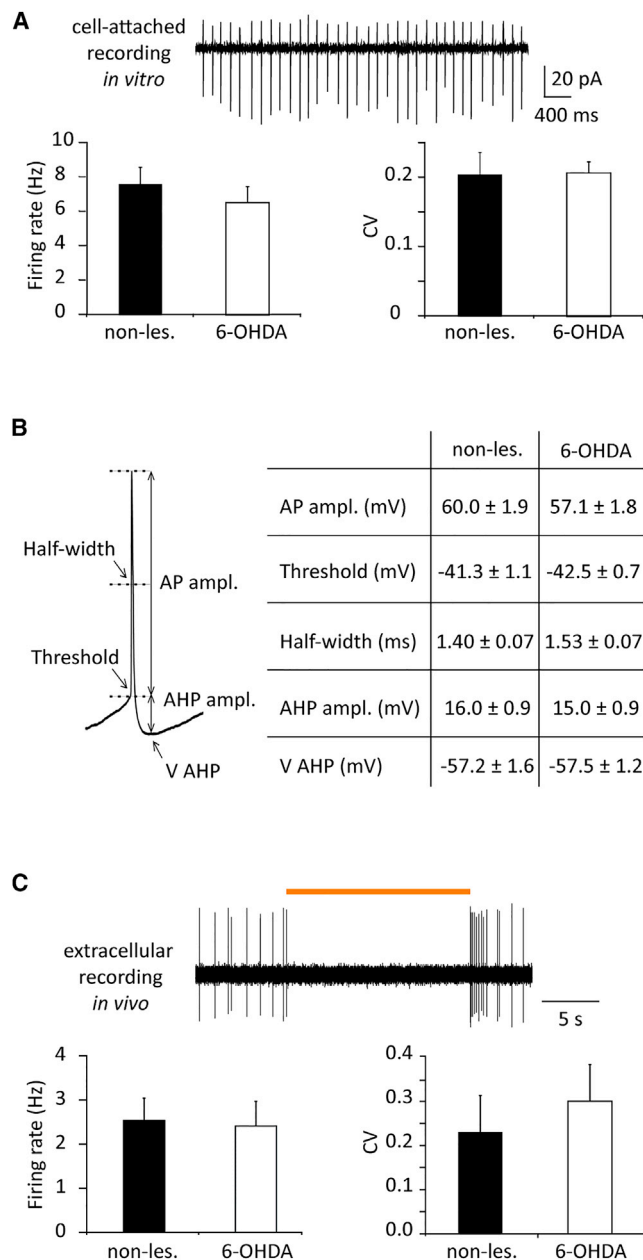


Figure 3. Impact of 6-OHDA Lesion on CIN Electrophysiological Properties

(A) Spontaneous activity from a CIN recorded in cell-attached configuration. Histograms show the mean firing rate and coefficients of variation (CV = firing rate SD/firing rate mean) in non-lesioned (n = 12 cells) and 6-OHDA (n = 20 cells) transgenic eNpHR mice (ns, Mann-Whitney test).

(B) Action potential characteristics of CINs recorded in non-lesioned (n = 13 cells) and 6-OHDA (n = 22 cells) mice. No significant differences were observed between the two groups (ns, Student's t test).

(C) Spontaneous activity and optogenetic identification of a CIN recorded *in vivo*. Histograms show the mean frequency rate and CVs (firing rate SD/firing rate mean) in non-lesioned (n = 8 cells) and 6-OHDA (n = 7 cells) transgenic eNpHR mice (ns, Mann-Whitney test). Errors bars, SEM.

resting membrane potentials of D1 and D2 MSNs were similar in non-lesioned and 6-OHDA mice (data not shown). However, in non-lesioned mice, D2 MSNs were more excitable than D1 MSNs, in agreement with previous reports (Gertler et al., 2008; Kreitzer and Malenka, 2007; Figure 4A). After DA depletion, D2 MSN excitability was not changed, while that of D1 MSNs greatly increased. D1 MSNs fired at higher frequency at each depolarizing current step, and the rheobase current was significantly lower in 6-OHDA versus non-lesioned mice (Figure 4). These results show that DA depletion reduces the dichotomy between D1 and D2 MSN excitability by increasing D1 MSN excitability.

Striatal CINs Differentially Modulate the Excitability of D1 and D2 MSNs in Parkinsonian Condition

Changes in intrinsic membrane excitability can occur either independently or in concert with changes in synaptic inputs. As cortical inputs strongly drive MSN activity and are modulated by presynaptic muscarinic receptors (Hernández-Echeagaray et al., 1998; Malenka and Kocsis, 1988; Pakhotin and Bracci, 2007), we investigated whether CIN inhibition affects corticostriatal transmission. Recordings were made 2–3 weeks after 6-OHDA lesion in transgenic eNpHR/D1 mice expressing both eNpHR in CINs and the fluorescent reporter tdTomato in DA D1 receptor-containing neurons (Figure S5A). In non-lesioned mice, excitatory postsynaptic currents (EPSCs) were not significantly altered by CIN inhibition, both in D1 and D2 MSNs (D1 MSNs, light versus pre-light: 325.99 ± 57.92 pA versus 311.16 ± 53.47 pA, not significant [ns], paired Student's t test, n = 14 cells; D2 MSNs, light versus pre-light: 214.98 ± 30.07 pA versus 214.59 ± 26.44 pA, ns, paired Student's t test, n = 11 cells) (Figure S5B). In contrast, CIN inhibition in 6-OHDA mice significantly potentiated EPSCs in both D1 and D2 MSNs (D1 MSNs, light versus pre-light: 262.22 ± 24.93 pA versus 240.76 ± 23.84 pA, p < 0.05, Wilcoxon test, n = 15 cells; D2 MSNs, light versus pre-light: 231.06 ± 34.00 pA versus 198.06 ± 24.07 pA, p < 0.05, Wilcoxon test, n = 9 cells) (Figure S5B). This potentiation was blocked by scopolamine (10 μM) (data pooled for D1 and D2 MSNs: light versus pre-light: 181.24 ± 35.92 pA versus 178.31 ± 33.35 pA, ns, paired Student's t test, n = 8 cells, data not shown). These results show that CIN inhibition potentiates corticostriatal transmission onto both D1 and D2 MSNs in parkinsonian condition. Therefore, corticostriatal transmission is unlikely to contribute to a differential impact of CIN inhibition on D1 and D2 MSNs.

In the healthy striatum, cholinergic modulation facilitates the firing of MSNs through M1 receptors (Galarraga et al., 1999; Goldberg et al., 2012; Pisani et al., 2007). What happens after chronic DA depletion is still unclear. We therefore examined whether and how CIN photoinhibition impacts MSN excitability in non-lesioned and 6-OHDA mice. D1 and D2 MSNs fired significantly less action potential during light illumination in both non-lesioned and 6-OHDA mice (Figures 5A and 5B). However, while the magnitude of firing inhibition was similar in D2 and D1 MSNs in non-lesioned mice, firing inhibition was weaker in D2 MSNs compared to D1 MSNs in 6-OHDA mice (Figure 5C). This result shows that D2 MSNs are less sensitive to CIN inhibition than D1 MSNs after DA depletion.

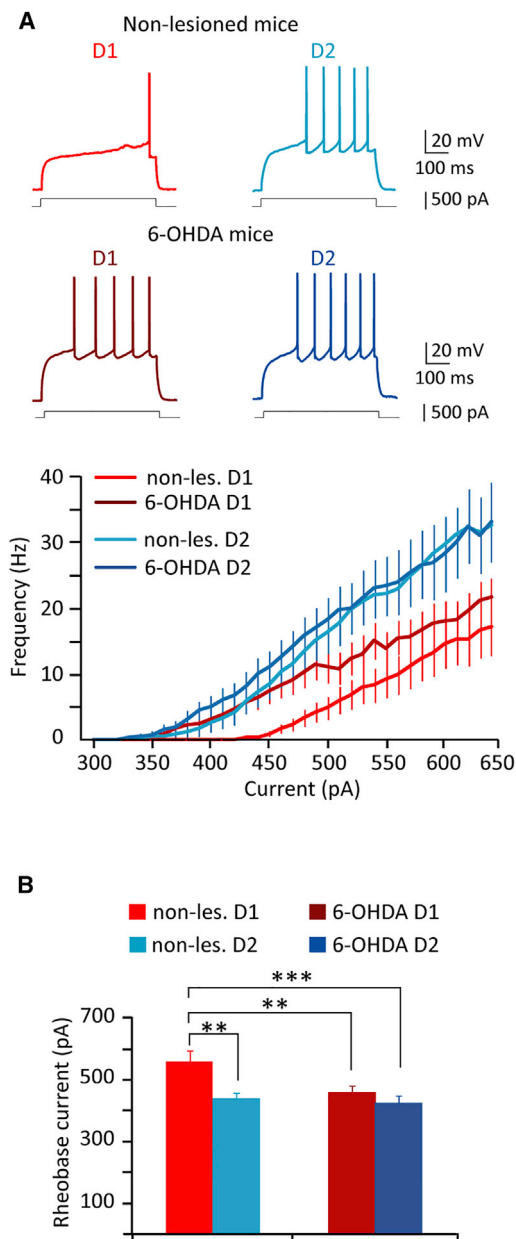


Figure 4. Impact of 6-OHDA Lesion on D1 and D2 MSN Excitability

(A) Current-clamp recordings showing the responses of D1 and D2 MSNs to depolarizing current pulses in non-lesioned (+450 pA) and 6-OHDA (+400 pA) mice. Summary graph illustrates the number of action potentials as a function of injected current in D1 MSNs (non-lesioned mice, n = 14 cells; 6-OHDA mice, n = 23 cells) and D2 MSNs (non-lesioned mice, n = 13 cells; 6-OHDA mice, n = 13 cells).

(B) Bars graph shows the mean rheobase current in D1 MSNs (non-lesioned mice, n = 14 cells; 6-OHDA mice, n = 23 cells) and D2 MSNs (non-lesioned mice, n = 13 cells; 6-OHDA mice, n = 13 cells) (**p < 0.01, ***p < 0.001, Holm-Sidak test after significant one-way ANOVA). Error bars, SEM.

DISCUSSION

Although ACh is undeniably a critical player in striatal functioning, the role of CINs in PD pathophysiology has remained un-

solved. We tackled this issue by combining optogenetics with in vitro and in vivo electrophysiology and behavioral analyses. We first showed that selective inhibition of CINs in the dorsal striatum reduces parkinsonian motor dysfunction in pharmacological and lesional PD models, attesting to their causal involvement in PD symptomatology. This provides a functional support for the long-standing hypothesis that poses PD as a striatal cholinergic disorder. Second, we identified several physiological parameters affected by CIN inhibition in the parkinsonian condition at both the input (striatum) and output (SNr) levels of the basal ganglia network. In addition, we found that CIN inhibition does not significantly impact basic motor function nor the spontaneous and cortically driven activity of SNr neurons in non-lesioned mice. This lack of effect in SNr is consistent with previous results from selective CIN ablation (Sano et al., 2013). Also, CIN inhibition does not modify the severity of dyskinesia in 6-OHDA mice. Altogether, these data suggest that CIN actions are highly dependent on DA tone.

CIN inhibition in vivo efficiently alleviates parkinsonian deficits measured after 6-OHDA lesions and neuroleptic-induced catalepsy, two different models widely used to assess motor symptoms reminiscent of parkinsonian akinesia. As neural correlates of PD symptoms' improvement by CIN inhibition, our in vivo recordings showed that it normalized the 6-OHDA-induced changes in SNr burst firing. Over the last few years, an abundant literature has clearly reported that parkinsonism is associated with increased bursting activity in the basal ganglia, including SNr (Lobb, 2014; Rivlin-Etzion et al., 2006; Wichmann et al., 1999). Even though the mechanisms leading to this abnormal activity are still elusive, its normalization by efficient antiparkinsonian treatments, such as dopaminy or subthalamic nucleus deep brain stimulation (Brown, 2003; Degos et al., 2005; Eusebio et al., 2011), suggests that such change may contribute importantly to the development of the behavioral manifestations of the disease. Thus, it is likely that the decrease in burst activity of SNr neurons elicited by CIN inhibition contributes to the improvement of parkinsonian symptoms that we observed in 6-OHDA mice. Future studies will be required to understand fully how CINs influence SNr burst firing in PD.

The second effect of CIN inhibition revealed by our in vivo recordings in 6-OHDA mice was an increase in the inhibitory component of the cortically evoked triphasic response in SNr neurons, suggesting that CIN silencing strengthens the inhibitory influence of the direct striatonigral pathway in parkinsonian condition. Although the relationship between the activity of the direct and indirect pathways and movement generation is still under debate, it has been demonstrated that specific activation of D1 MSNs by optogenetics efficiently relieves parkinsonian deficits (Kravitz et al., 2010). In this context, it is likely that the increased duration of the cortically evoked inhibition induced by CIN inhibition contributes importantly to the improvement of parkinsonian-like motor symptoms induced by DA depletion.

What are the striatal targets modulated by CINs that could mediate their preponderant action on basal ganglia function in PD state? We showed that CIN inhibition in 6-OHDA mice potentiates corticostriatal transmission onto both types of MSNs. However, our recordings in the SNr of 6-OHDA mice clearly showed that CIN inhibition increases the cortically evoked

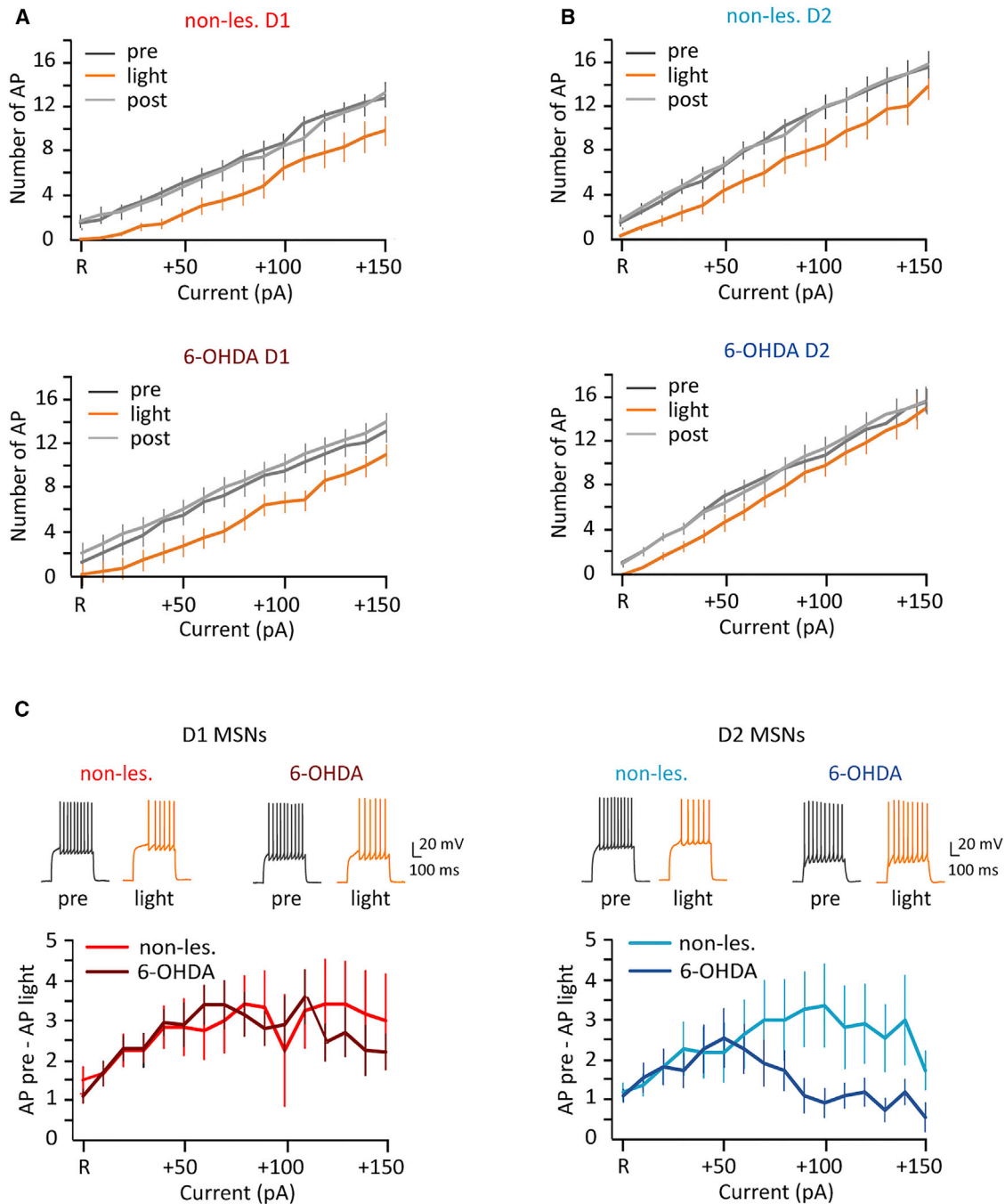


Figure 5. Photoinhibition of CINs Differentially Decreases D1 and D2 MSN Excitability in 6-OHDA Mice

(A and B) The graphs illustrate the decreased excitability of MSNs during light illumination versus pre and post conditions in non-lesioned (A, top; D1 MSNs: $F(2, 572) = 55.26$, $p < 0.0001$, $n = 12$; B, top; D2 MSNs: $F(2, 524) = 37.97$, $p < 0.0001$, $n = 11$, linear regression analysis) and 6-OHDA (A, bottom; D1 MSNs: $F(2, 953) = 209.72$, $p < 0.0001$, $n = 20$; B, bottom; D2 MSNs: $F(2, 524) = 17.09$, $p < 0.0001$, $n = 11$, linear regression analysis) mice. R is the minimal current intensity to trigger a spike in pre-light condition. From R, current intensity increased by +10-pA increment.

(C) (Top) Representative traces showing the responses to 500-ms depolarizing current steps (R+80 for D1 MSN non-les., D2 MSN non-les., and D2 MSN 6-OHDA) and R+110 (D1 MSN 6-OHDA). Light was delivered 200 ms before and continued 200 ms after the 500-ms depolarizing current step. (Bottom) The graphs show the difference in the number of action potentials evoked in pre versus light conditions in D1 MSNs (left; non-les., $n = 12$; 6-OHDA, $n = 20$) and D2 MSNs (right; non-les., $n = 11$; 6-OHDA, $n = 11$). There is a significant effect of current intensity in D1 MSNs ($F[15,450] = 3.67$, $p < 0.005$) and D2 MSNs ($F[15,300] = 2.02$, $p < 0.01$). From R+80 pA, D2 MSNs in 6-OHDA mice are less inhibited during light illumination, as shown by a significant interaction between lesion \times current intensity for D2 MSNs ($F[15,300] = 2.39$, $p < 0.05$), but not for D1 MSNs. Errors bars, SEM.

inhibition linked to the activation of the direct (D1) pathway, but not the late excitation linked to the activation of the indirect (D2) pathway. The high degree of convergence of the direct pathway at the level of the SNr (48 striatal neurons converge into one SNr cell; [Smith et al., 1998](#)) may explain how a modest increase in corticostriatal transmission onto D1 MSNs impacts the cortically evoked inhibition in the SNr. In contrast, complex information processing at each stage of the polysynaptic indirect pathway might minimize the outcome of EPSC potentiation on D2 MSNs.

Another interesting result of our study is that DA depletion tends to erase the dichotomy in MSN excitability by inducing a specific increase in D1 MSN excitability. A recent study also reported increased D1 MSN excitability after DA lesion, but associated with a slight decrease in D2 MSN excitability ([Fieblinger et al., 2014](#)), whereas we failed to detect any change for D2 MSNs. This apparent discrepancy might be due to different lesion models or post-lesion delay, since opposite changes in D2 MSN excitability have been described after acute or chronic DA depletion ([Day et al., 2006](#); [Fieblinger et al., 2014](#); [Shen et al., 2007](#)). Elevated excitability in D1 MSNs might be considered as a homeostatic response counteracting the decreased activity triggered by the loss of dopaminergic excitatory drive on these neurons. However, if we assume that the dichotomy between D1 and D2 MSN excitability is a fundamental process for normal striatal function, making both MSNs more alike after DA depletion might be more harmful than beneficial. In favor of this hypothesis, we showed that CIN inhibition decreases the excitability more in D1 than in D2 MSNs after DA depletion, whereas it has similar impact on the two populations in control condition. Thus, restoring the dichotomy between D1 and D2 MSN excitability might be one component of the anti-parkinsonian effect of CIN inhibition. What happens following DA depletion to explain the reduced sensitivity of D2 MSNs to CIN inhibition remains an open and challenging question. It will be also interesting to investigate whether the cholinergic projection from the brainstem to the striatum ([Dautan et al., 2014](#)) cooperates with CINs to modulate striatal output.

Our results show that CINs are critical players in the host of cellular and synaptic changes induced in MSNs by DA depletion. Without excluding indirect pathway contributions, our findings point to CIN control of the direct striatonigral pathway as a critical component involved in the control of striatal output and motor dysfunction in PD state. These results should stimulate the development of therapeutic strategies targeting striatal CIN activity in PD.

EXPERIMENTAL PROCEDURES

Mice

All procedures were approved by the French National Ethical Committee (45-29102012) and were in accordance with the recommendations of the European Commission (2010/63/EU) for care and use of laboratory animals. See the [Supplemental Experimental Procedures](#) for a detailed description of the mice used.

Stereotaxic Surgery

All coordinates were adapted from the mouse stereotaxic atlas by [Paxinos and Franklin \(2001\)](#) with bregma and dura as references. See the [Supplemental Experimental Procedures](#) for details.

In Vitro Electrophysiology

Patch-clamp recordings on brain slices and data analysis were performed as described in the [Supplemental Experimental Procedures](#). Excitation of opsins was achieved with a light-emitting diode source (Spectra light engine, Lumen-cor) connected to a 3-mm liquid core fiber. Statistical analyses were performed using paired or unpaired Student's *t* test. Nonparametric tests (Mann-Whitney test for unpaired data or Wilcoxon test for paired data) were used if the normality or equal variance test failed. For multiple group comparisons, one- or two-way ANOVA was used. We applied the log₂ transformation to make the data normal if necessary. Linear regression analysis was used to compare the effect of CIN inhibition on MSN excitability. A significance of $p < 0.05$ was required for rejection of the null hypothesis.

Behavioral Testing

All behavioral analyses were conducted on littermates that entered the study at around 3–5 months of age. See the [Supplemental Experimental Procedures](#) for a detailed description of the behavioral tests. For open field, data were analyzed using two-way ANOVA followed by paired Student's *t* test, when appropriate. For haloperidol-induced catalepsy, median latencies (\pm semi-quartile) were compared among groups over time using the nonparametric Kruskal-Wallis test, followed by U-Mann-Whitney for pairwise comparisons at each time. Head movements were summed for the 3-min ON periods and compared to those measured 3-min OFF periods, using a two-way ANOVA. For cylinder and cross maze tests, data were analyzed using one-way ANOVA, followed by Student's *t* test. For L-DOPA-induced dyskinesia, data were analyzed by two-way repeated-measures (RM) ANOVA with opsins (eNpHR-RFP versus RFP) as between factor and time as within factor.

In Vivo Recordings in Anesthetized Mice

Extracellular recordings in the striatum and the SNr were performed as described in the [Supplemental Experimental Procedures](#). The patterns of cortically evoked discharges in the same SNr neuron were analyzed before, during, and after CIN photoinhibition in the striatum. Results are given as means \pm SEM of the individual responses per condition. Spontaneous activity in the three conditions was compared using one-way ANOVA followed by comparison versus pre-light condition (Holm-Sidak method). Cortically evoked responses of the same SNr neurons in the three light conditions were compared using one-way RM ANOVA, followed by comparison versus pre-light condition (Holm-Sidak method).

Histology and Immunohistochemistry

For primary antibody exposure, brain sections were incubated overnight at 4°C in rabbit anti-RFP (1/1,000, tebu-bio, 600-401-379) and goat anti-ChAT (1/100, Millipore, AB144P) for colocalization experiments and in mouse anti-tyrosine hydroxylase (1/1,000, Millipore, MAB318) to control DA lesion. Sections were then incubated, respectively, in Alexa Fluor 555 donkey anti-rabbit (1/500, Invitrogen, A31572), Alexa Fluor 488 donkey anti-goat (1/500, Invitrogen, A11055), and Alexa Fluor 555 donkey anti-mouse (1/500, Invitrogen, A31570) for 1 hr 30 min at room temperature. Rabbit anti-GFP (1/500, Invitrogen, A11122) and Alexa fluor 488 donkey anti-rabbit (1/500, Invitrogen, A21206) were used the same way to reveal eNpHR expression in transgenic mice.

SUPPLEMENTAL INFORMATION

Supplemental Information includes Supplemental Experimental Procedures, five figures, and two tables and can be found with this article online at <http://dx.doi.org/10.1016/j.celrep.2015.09.034>.

AUTHOR CONTRIBUTIONS

N.M., M.L., M.A., L.K.-L., and C.B. designed the study. N.M., M.L., F.J., S.Z., M.H., J.C., and C.B. performed experiments. K.D. provided reagents and critical feedback. N.M., M.L., F.J., S.Z., J.C., L.K.-L., M.A., and C.B. analyzed the results. N.M., M.L., M.A., L.K.-L., and C.B. wrote the paper.

ACKNOWLEDGMENTS

This work was supported by CNRS, Aix-Marseille Université, Fondation de France (2013 00043175), France Parkinson Association, and Agence Nationale de la Recherche (ANR-2010-1416). We thank C. Melon, C. Marra, and D. Paleressompoulle for their excellent technical assistance. Microscopy was performed at PiCSL-FBI core facility, member of the France-Biomed national research infrastructure. We thank R. Ragheb, B. Burle, and P. Gubellini for statistical analysis; and A. Moqrich and P. Marcaggi for their critical comments on the manuscript.

Received: October 23, 2014

Revised: August 25, 2015

Accepted: September 10, 2015

Published: October 15, 2015

REFERENCES

- Albin, R.L., Young, A.B., and Penney, J.B. (1989). The functional anatomy of basal ganglia disorders. *Trends Neurosci.* *12*, 366–375.
- Aosaki, T., Graybiel, A.M., and Kimura, M. (1994). Effect of the nigrostriatal dopamine system on acquired neural responses in the striatum of behaving monkeys. *Science* *265*, 412–415.
- Barbeau, A. (1962). The pathogenesis of Parkinson's disease: a new hypothesis. *Can. Med. Assoc. J.* *87*, 802–807.
- Brown, P. (2003). Oscillatory nature of human basal ganglia activity: relationship to the pathophysiology of Parkinson's disease. *Mov. Disord.* *18*, 357–363.
- Calabresi, P., Picconi, B., Tozzi, A., Ghiglieri, V., and Di Filippo, M. (2014). Direct and indirect pathways of basal ganglia: a critical reappraisal. *Nat. Neurosci.* *17*, 1022–1030.
- Cui, G., Jun, S.B., Jin, X., Pham, M.D., Vogel, S.S., Lovinger, D.M., and Costa, R.M. (2013). Concurrent activation of striatal direct and indirect pathways during action initiation. *Nature* *494*, 238–242.
- Dautan, D., Huerta-Ocampo, I., Witten, I.B., Deisseroth, K., Bolam, J.P., Gerdjikov, T., and Mena-Segovia, J. (2014). A major external source of cholinergic innervation of the striatum and nucleus accumbens originates in the brainstem. *J. Neurosci.* *34*, 4509–4518.
- Day, M., Wang, Z., Ding, J., An, X., Ingham, C.A., Shering, A.F., Wokosin, D., Iljic, E., Sun, Z., Sampson, A.R., et al. (2006). Selective elimination of glutamatergic synapses on striatopallidal neurons in Parkinson disease models. *Nat. Neurosci.* *9*, 251–259.
- Degos, B., Deniau, J.M., Thierry, A.M., Glowinski, J., Pezard, L., and Maurice, N. (2005). Neuroleptic-induced catalepsy: electrophysiological mechanisms of functional recovery induced by high-frequency stimulation of the subthalamic nucleus. *J. Neurosci.* *25*, 7687–7696.
- Ding, J., Guzman, J.N., Tkatch, T., Chen, S., Goldberg, J.A., Ebert, P.J., Levitt, P., Wilson, C.J., Hamm, H.E., and Surmeier, D.J. (2006). RGS4-dependent attenuation of M4 autoreceptor function in striatal cholinergic interneurons following dopamine depletion. *Nat. Neurosci.* *9*, 832–842.
- English, D.F., Ibanez-Sandoval, O., Stark, E., Tecuapetla, F., Buzsáki, G., Deisseroth, K., Tepper, J.M., and Koos, T. (2011). GABAergic circuits mediate the reinforcement-related signals of striatal cholinergic interneurons. *Nat. Neurosci.* *15*, 123–130.
- Eusebio, A., Thevathasan, W., Doyle Gaynor, L., Pogosyan, A., Bye, E., Foltynie, T., Zrinzo, L., Ashkan, K., Aziz, T., and Brown, P. (2011). Deep brain stimulation can suppress pathological synchronisation in parkinsonian patients. *J. Neurol. Neurosurg. Psychiatry* *82*, 569–573.
- Fieblinger, T., Graves, S.M., Sebel, L.E., Alcacer, C., Plotkin, J.L., Gertler, T.S., Chan, C.S., Heiman, M., Greengard, P., Cenci, M.A., and Surmeier, D.J. (2014). Cell type-specific plasticity of striatal projection neurons in parkinsonism and L-DOPA-induced dyskinesia. *Nat. Commun.* *5*, 5316.
- Galarraga, E., Hernández-López, S., Reyes, A., Miranda, I., Bermudez-Rattoni, F., Vilchis, C., and Vargas, J. (1999). Cholinergic modulation of neostriatal output: a functional antagonism between different types of muscarinic receptors. *J. Neurosci.* *19*, 3629–3638.
- Gertler, T.S., Chan, C.S., and Surmeier, D.J. (2008). Dichotomous anatomical properties of adult striatal medium spiny neurons. *J. Neurosci.* *28*, 10814–10824.
- Goldberg, J.A., Ding, J.B., and Surmeier, D.J. (2012). Muscarinic modulation of striatal function and circuitry. *Handb. Exp. Pharmacol.* *208*, 223–241.
- Hernández-Echeagaray, E., Galarraga, E., and Vargas, J. (1998). 3-Alpha-chloro-imperialine, a potent blocker of cholinergic presynaptic modulation of glutamatergic afferents in the rat neostriatum. *Neuropharmacology* *37*, 1493–1502.
- Higley, M.J., Gittis, A.H., Oldenburg, I.A., Balthasar, N., Seal, R.P., Edwards, R.H., Lowell, B.B., Kreitzer, A.C., and Sabatini, B.L. (2011). Cholinergic interneurons mediate fast VGluT3-dependent glutamatergic transmission in the striatum. *PLoS ONE* *6*, e19155.
- Kravitz, A.V., Freeze, B.S., Parker, P.R., Kay, K., Thwin, M.T., Deisseroth, K., and Kreitzer, A.C. (2010). Regulation of parkinsonian motor behaviours by optogenetic control of basal ganglia circuitry. *Nature* *466*, 622–626.
- Kreitzer, A.C., and Malenka, R.C. (2007). Endocannabinoid-mediated rescue of striatal LTD and motor deficits in Parkinson's disease models. *Nature* *445*, 643–647.
- Lobb, C. (2014). Abnormal Bursting as a Pathophysiological Mechanism in Parkinson's Disease. *Basal Ganglia* *3*, 187–195.
- Malenka, R.C., and Kocsis, J.D. (1988). Presynaptic actions of carbachol and adenosine on corticostriatal synaptic transmission studied in vitro. *J. Neurosci.* *8*, 3750–3756.
- Mallet, N., Ballion, B., Le Moine, C., and Gonon, F. (2006). Cortical inputs and GABA interneurons imbalance projection neurons in the striatum of parkinsonian rats. *J. Neurosci.* *26*, 3875–3884.
- Maurice, N., Deniau, J.M., Glowinski, J., and Thierry, A.M. (1999). Relationships between the prefrontal cortex and the basal ganglia in the rat: physiology of the cortico-nigral circuits. *J. Neurosci.* *19*, 4674–4681.
- Nelson, A.B., Hammack, N., Yang, C.F., Shah, N.M., Seal, R.P., and Kreitzer, A.C. (2014). Striatal cholinergic interneurons Drive GABA release from dopamine terminals. *Neuron* *82*, 63–70.
- Pakhotin, P., and Bracci, E. (2007). Cholinergic interneurons control the excitatory input to the striatum. *J. Neurosci.* *27*, 391–400.
- Paxinos, G., and Franklin, K.B.J. (2001). *The Mouse Brain in Stereotaxic Coordinates*, Second Edition (San Diego: Academic Press).
- Phelps, P.E., Houser, C.R., and Vaughn, J.E. (1985). Immunocytochemical localization of choline acetyltransferase within the rat neostriatum: a correlated light and electron microscopic study of cholinergic neurons and synapses. *J. Comp. Neurol.* *238*, 286–307.
- Pisani, A., Bernardi, G., Ding, J., and Surmeier, D.J. (2007). Re-emergence of striatal cholinergic interneurons in movement disorders. *Trends Neurosci.* *30*, 545–553.
- Rivlin-Etzion, M., Marmor, O., Heimer, G., Raz, A., Nini, A., and Bergman, H. (2006). Basal ganglia oscillations and pathophysiology of movement disorders. *Curr. Opin. Neurobiol.* *16*, 629–637.
- Ryan, L.J., and Sanders, D.J. (1994). Subthalamic nucleus and globus pallidus lesions alter activity in nigrothalamic neurons in rats. *Brain Res. Bull.* *34*, 19–26.
- Sano, H., Chiken, S., Hikida, T., Kobayashi, K., and Nambu, A. (2013). Signals through the striatopallidal indirect pathway stop movements by phasic excitation in the substantia nigra. *J. Neurosci.* *33*, 7583–7594.
- Shen, W., Tian, X., Day, M., Ulrich, S., Tkatch, T., Nathanson, N.M., and Surmeier, D.J. (2007). Cholinergic modulation of Kir2 channels selectively elevates dendritic excitability in striatopallidal neurons. *Nat. Neurosci.* *10*, 1458–1466.
- Smith, Y., Bevan, M.D., Shink, E., and Bolam, J.P. (1998). Microcircuitry of the direct and indirect pathways of the basal ganglia. *Neuroscience* *86*, 353–387.

- Tachibana, Y., Kita, H., Chiken, S., Takada, M., and Nambu, A. (2008). Motor cortical control of internal pallidal activity through glutamatergic and GABAergic inputs in awake monkeys. *Eur. J. Neurosci.* 27, 238–253.
- Threlfell, S., Lalic, T., Platt, N.J., Jennings, K.A., Deisseroth, K., and Cragg, S.J. (2012). Striatal dopamine release is triggered by synchronized activity in cholinergic interneurons. *Neuron* 75, 58–64.
- Tritsch, N.X., Oh, W.J., Gu, C., and Sabatini, B.L. (2014). Midbrain dopamine neurons sustain inhibitory transmission using plasma membrane uptake of GABA, not synthesis. *eLife* 3, e01936.
- Wichmann, T., Bergman, H., Starr, P.A., Subramanian, T., Watts, R.L., and DeLong, M.R. (1999). Comparison of MPTP-induced changes in spontaneous neuronal discharge in the internal pallidal segment and in the substantia nigra pars reticulata in primates. *Exp. Brain Res.* 125, 397–409.
- Witten, I.B., Lin, S.-C., Brodsky, M., Prakash, R., Diester, I., Anikeeva, P., Gradinaru, V., Ramakrishnan, C., and Deisseroth, K. (2010). Cholinergic interneurons control local circuit activity and cocaine conditioning. *Science* 330, 1677–1681.

Cell Reports

Supplemental Information

**Striatal Cholinergic Interneurons Control
Motor Behavior and Basal Ganglia Function
in Experimental Parkinsonism**

Nicolas Maurice, Martine Liberge, Florence Jaouen, Samira Ztaou, Marwa Hanini,
Jeremy Camon, Karl Deisseroth, Marianne Amalric, Lydia Kerkerian-Le Goff, and
Corinne Beurrier

SUPPLEMENTAL DATA

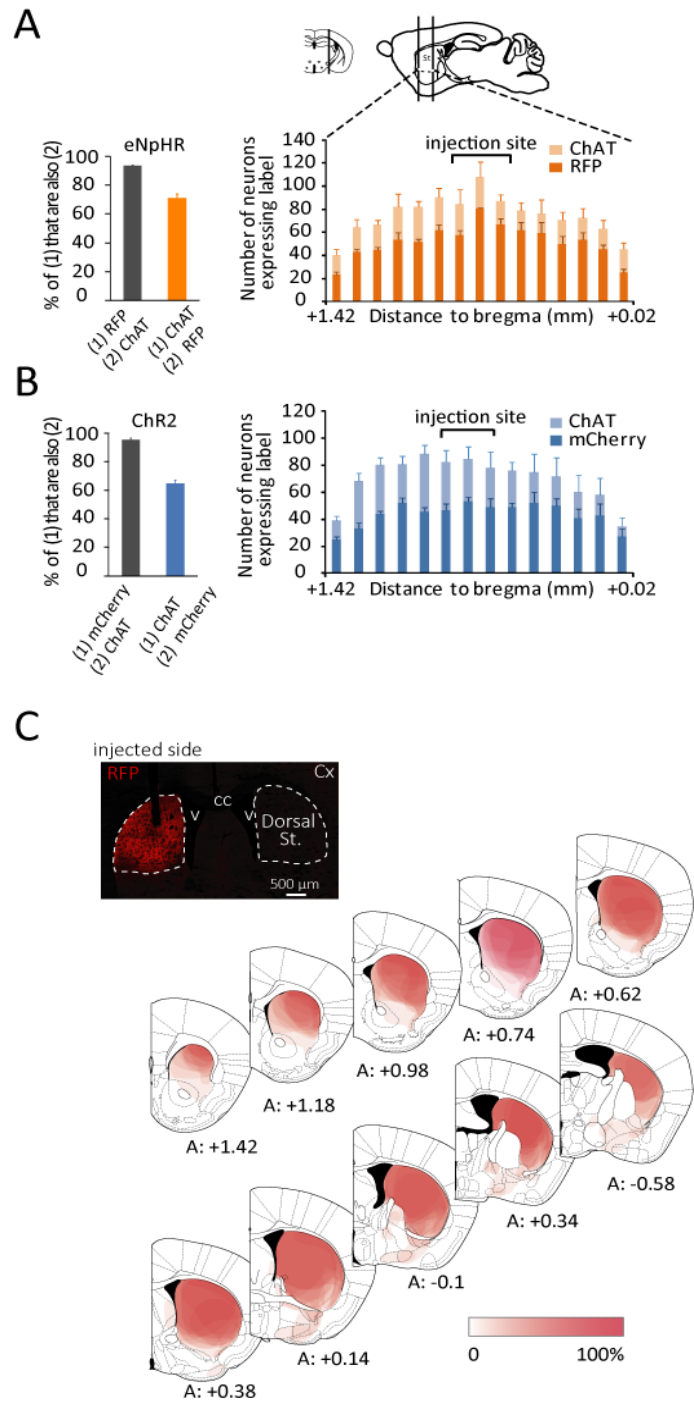


Figure S1, Related to Supplemental Experimental Procedures: Specific expression of opsins in CINs (A and B) and topography of RFP staining in eNpHR-RFP-injected mice (C).

(A, B) Left, histograms represent the mean coexpression in the whole dorsal striatum in eNpHR-RFP (n=2) or Chr2-mCherry (n=2) mice. Virtually all opsin-expressing neurons were ChAT-positive. The majority of neurons that expressed ChAT also expressed eNpHR-RFP ($71.0 \pm 2.9\%$) or Chr2-mCherry ($64.7 \pm 2.6\%$). Right, quantification of co-expression of RFP and mCherry and ChAT

immunofluorescence from two bilaterally eNpHR-RFP-injected and Chr2-mCherry-injected mice, from the rostral-to-caudal ends of the dorsal striatum (from +1.42 to +0.02 mm). Error bars, SEM. (C) Top, coronal section showing a representative RFP staining from an eNpHR-RFP-injected mouse. The track shows the location at which viral injection, followed by implantation of optical fiber, was made. Note the large diffusion of eNpHR-RFP in nearly the whole dorsal striatum. Cx: cortex, cc: corpus callosum, v: ventricle, St: striatum. Bottom, coronal schematic sections from the stereotaxic atlas of Paxinos and Watson showing the topography of RFP staining in eNpHR-RFP mice (from +1.42 to -0.58 mm with bregma as reference, n=14 mice). The intensity of the gradient of color (white to red) corresponds to the measured RFP positive area in the different brain structures studied for each injection performed. The highest intensity of red (100%) indicates that all animals had signal in the corresponding area, whereas the lowest color intensity (white, 0%) corresponds to non-stained areas. RFP labeling outside the striatum was very scarce and localized ventrally in the nucleus accumbens or caudally in the ventral pallidum and the bed nucleus of the stria terminalis.

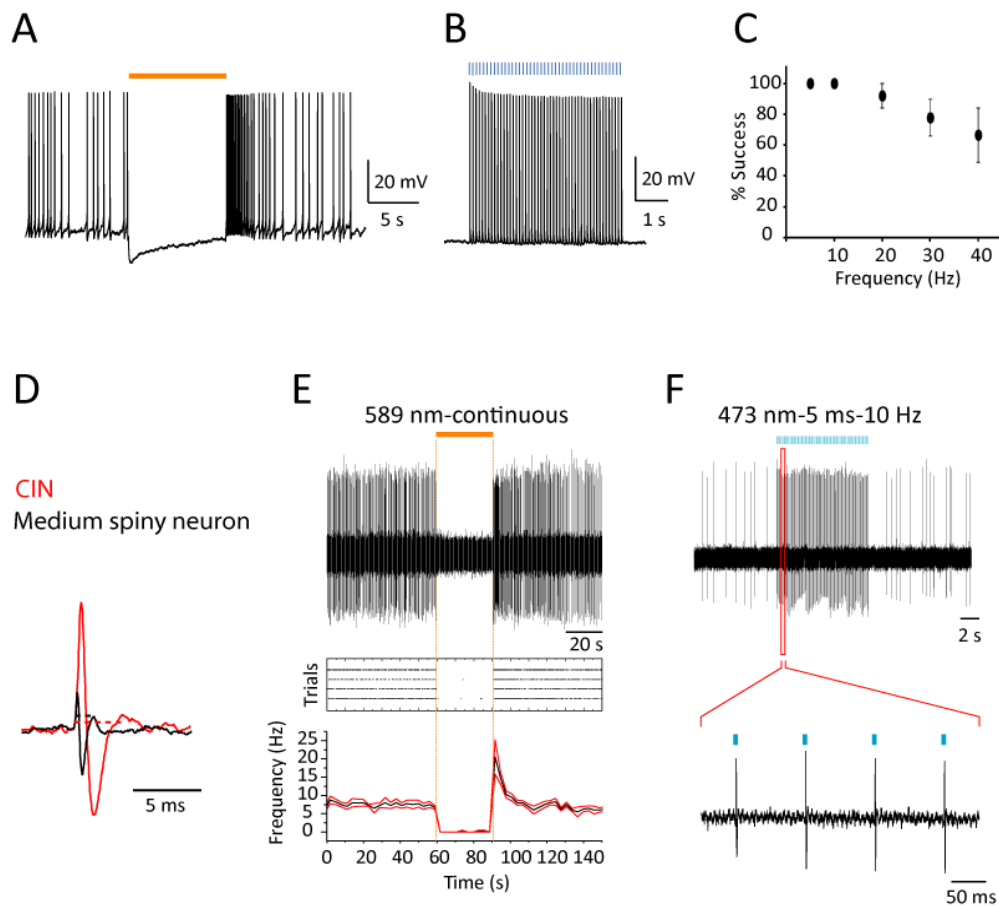


Figure S2: Functional expression of ChR2-mCherry and eNpHR-RFP in CINs both *in vitro* (A, B and C) and *in vivo* (D, E and F).

(A) Action potential inhibition induced by 10 s yellow light illumination in a eNpHR-RFP-expressing neuron. (B) Action potentials in a ChR2-mCherry-expressing neuron evoked by 5-ms blue light pulses (10 Hz). (C) Average success probability for generating action potentials in neurons expressing ChR2-mCherry at different stimulation frequencies (n=4-5, 5-ms pulse width). (D) Superimposed recordings of a CIN and a medium spiny neuron. CINs were distinguished from medium size spiny neurons by their typical tonic activity and spike duration. Dotted lines indicate spike duration. (E) Raw trace (top) of an isolated unit, identified as a CIN, inhibited by yellow light continuous stimulation. Raster plot (middle) displaying the response of the same unit to four repetitions of the light stimulation, with each action potential represented as a dot. Average and SEM of the firing rate over time (bottom) for the same unit. (F) Raw trace (top) of another putative CIN that is excited by 5ms-blue light pulses (10 Hz). Note at higher magnification that every light pulse drives a spike (bottom). Errors bars, SEM.

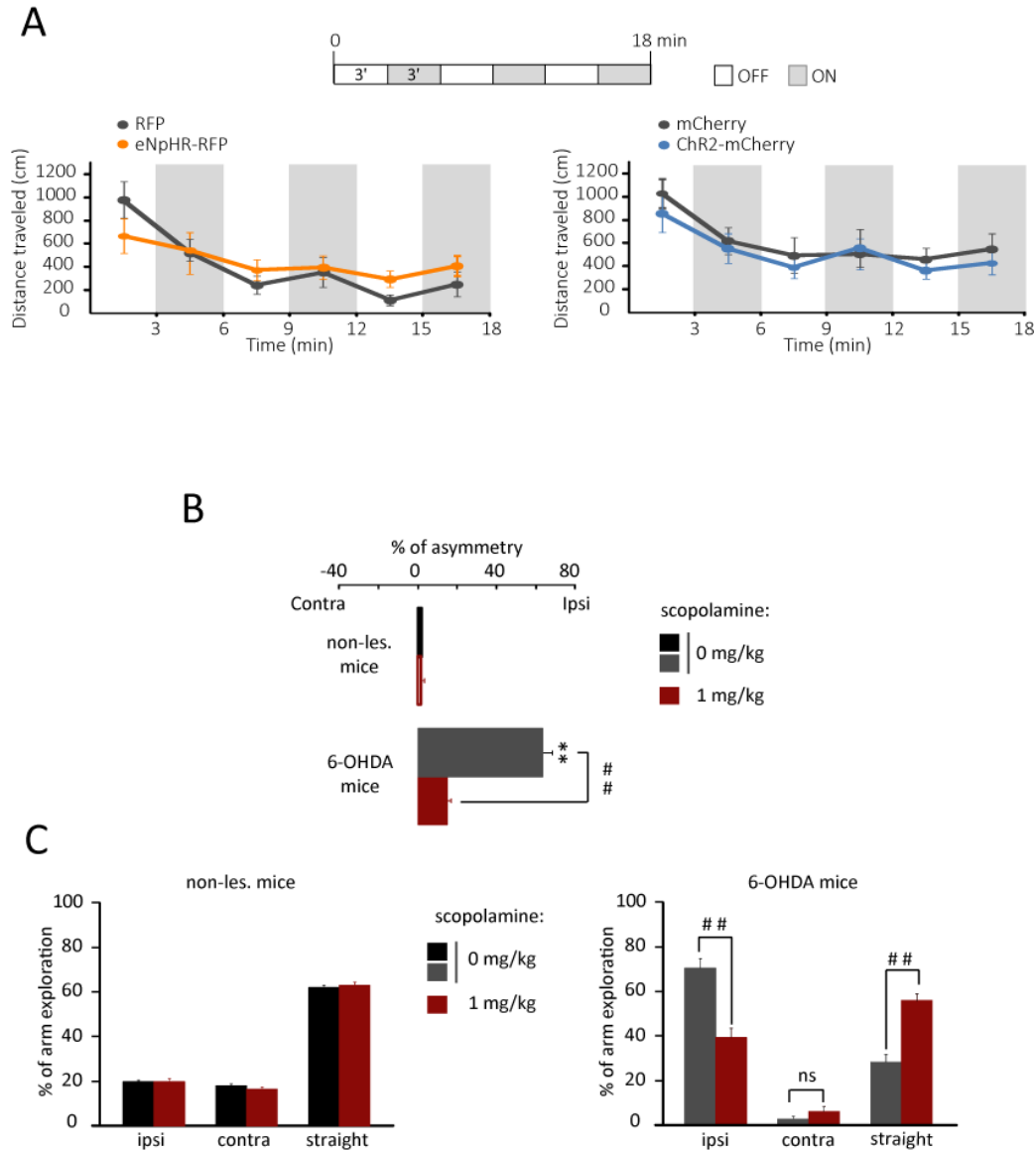


Figure S3, related to Figure 1: (A) Effects of CIN manipulation on the spontaneous locomotor activity in non-lesioned mice. Top, experimental design. Graphs show the locomotor activity before (OFF) and during (ON) bilateral striatal illumination in RFP, eNpHR-RFP, mCherry and Chr2-mCherry mice, in 3-min period. No change in ambulation was observed in response to photoinhibition or photoactivation of CINs in either group (two-way ANOVA, ns), $n=6-9$ per group. (B, C) Muscarinic receptors blockade with scopolamine relieves parkinsonian-like motor deficits. B, in the cylinder test, 6-OHDA mice ($n=14$) showed a marked forelimb asymmetry compared to non-lesioned mice ($*p<0.01$, Fisher PLSD test after significant ANOVA $F_{3,40}=76.66$). This asymmetry was significantly improved by intraperitoneal (i.p.) scopolamine injection (scopolamine 1 mg/kg vs. 0 mg/kg; # $p<0.01$, Student's t test). Scopolamine did not affect asymmetry in non-lesioned mice ($n=8$). C, non-lesioned mice ($n=8$) placed in the cross-maze perform mainly straight-arm exploration with equivalent percentage of ipsi- or contralateral arms

exploration (* $p < 0.01$, Fisher PLSD test after significant ANOVA $F_{5,35}=402.9$). 6-OHDA lesion induced a bias in arms exploration with a dramatic increase in ipsilateral turns and decrease in contralateral and straight exploration. Scopolamine significantly modified the performance of 6-OHDA mice ($n=14$) in the cross-maze (significant one-way ANOVA $F_{5,65}=48.58$, $p < 0.01$). It significantly decreased ipsilateral arm exploration ($\# p < 0.01$, Student's t test) and increased straight exploration ($\# p < 0.01$, Student's t test) while not affecting contralateral bias (ns, Student's t test). Errors bars, SEM.

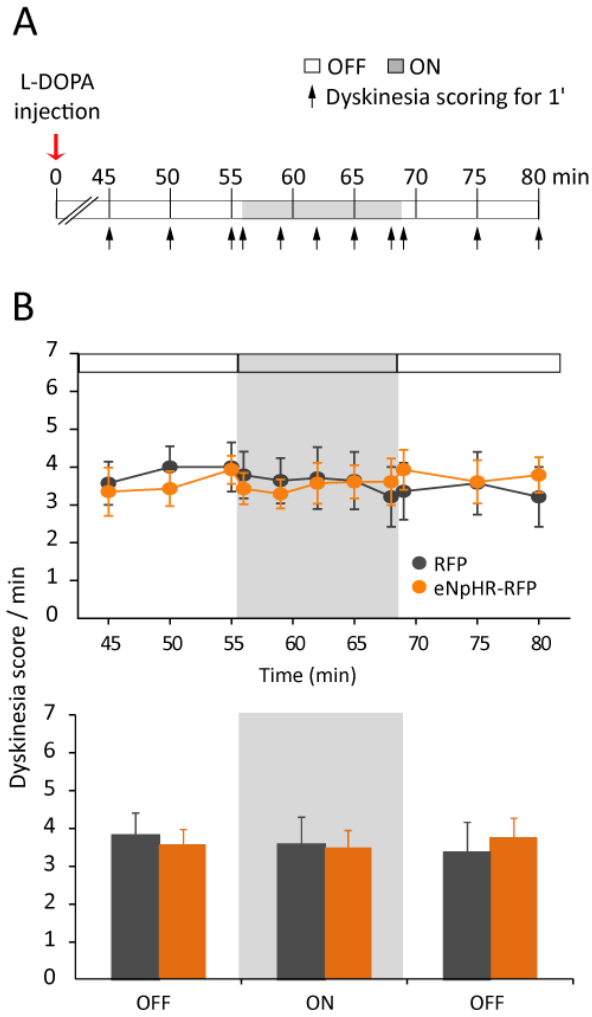


Figure S4: Photoinhibition of CINs does not affect L-DOPA-induced dyskinesia.

(A) Experimental design. Two weeks after intranigral injection of 6-OHDA, RFP and eNpHR-RFP mice received a chronic L-DOPA treatment for 21 days and dyskinesia were quantified at day 21. (B) Time profile of dyskinesia score (sum of the mean scores for axial and forelimb dyskinesia over 35 min; maximum score 8) after L-DOPA injection on day 21 of chronic treatment. Light did not produce a significant difference in dyskinesia score (two-way repeated measure ANOVA, ns, $n = 7$ per group). Errors bars, SEM.

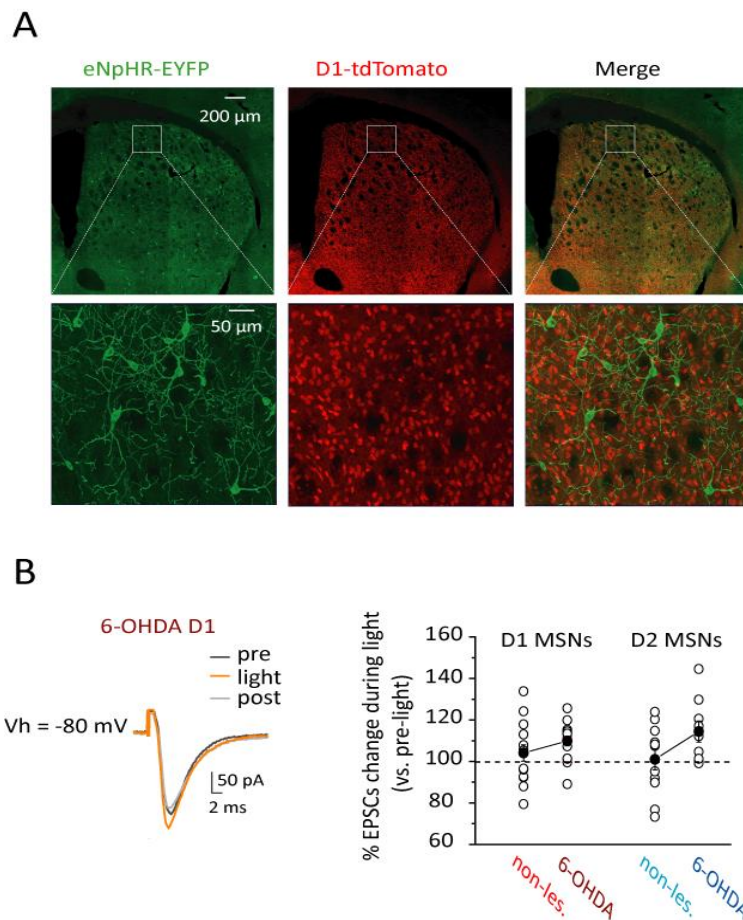


Figure S5, related to Figures 4 and 5: (A) Representative photomicrographs of a transgenic eNpHR/D1 mouse. Dorsal striatum sections showing eNpHR-EYFP expressing cells that are immunostained with antibodies against GFP (green) and D1-MSNs which are visualized by the direct fluorescence of tdTomato (red). Merge image shows no colocalization. (B) Photoinhibition of CINs potentiates corticostriatal transmission onto both populations of MSNs in 6-OHDA mice. EPSCs traces from a D1 MSN recorded in a 6-OHDA mouse before, during and after light illumination. Light was sent 50 ms before cortical stimulation and continue 250 ms after. Graph illustrates the value of EPSCs change during light illumination compared to pre-light condition in all cells. Black circles represent the mean. Errors bars, SEM.

	Frequency of discharge (Hz)		Burst recurrence (burst/s)		Burst duration (s)		Number of spikes/burst	
	Non-lesioned (n = 18)	6-OHDA (n = 13)	Non-lesioned	6-OHDA	Non-lesioned	6-OHDA	Non-lesioned	6-OHDA
Pre	14.4 ± 1.7	12.3 ± 1.4	0.218 ± 0.057	0.258 ± 0.070	0.384 ± 0.033	0.517 ± 0.052*	9.5 ± 0.6	14.0 ± 1.1**
Light	13.2 ± 1.8	11.1 ± 1.5	0.247 ± 0.053	0.315 ± 0.068	0.398 ± 0.036	0.374 ± 0.031#	9.4 ± 0.5	9.5 ± 0.5##
Post	13.0 ± 1.7	11.9 ± 2.1	0.255 ± 0.046	0.290 ± 0.075	0.460 ± 0.030	0.404 ± 0.028	10.6 ± 0.5	11.9 ± 0.6

Table S1, related to Figure 2: Effect of 6-OHDA lesion and impact of CIN photoinhibition on spontaneous activity of SNr neurons in transgenic eNpHR mice.

* p<0.05, ** p<0.01, unpaired Student's *t* test, 6-OHDA vs. non-lesioned mice. #p<0.05, ##p<0.01, one-way ANOVA followed by Holm-Sidak post-hoc test, vs. pre-light condition.

		Early excitation			Inhibition		Late excitation		
		L (ms)	D (ms)	Nb Sp	L (ms)	D (ms)	L (ms)	D (ms)	Nb Sp
Non-lesioned	Pre-Light	11.0 ± 0.9 (n = 13)	7.5 ± 0.7	45.5 ± 8.3	22.8 ± 1.2 (n = 18)	25.4 ± 3.2	45.1 ± 3.4 (n = 13)	8.5 ± 1.0	44.0 ± 6.3
	Light	10.9 ± 0.9	8.1 ± 1.2	47.6 ± 7.7	21.8 ± 1.1	25.4 ± 3.9	43.9 ± 3.4	9.2 ± 1.2	44.9 ± 7.1
	Post-Light	11.5 ± 0.8	8.7 ± 0.8	54.0 ± 8.8	22.0 ± 1.2	25.3 ± 2.4	44.0 ± 2.3	9.6 ± 1.0	47.5 ± 8.6
6-OHDA	Pre-Light	11.0 ± 2.5 (n = 6)	9.0 ± 2.9	60.3 ± 13.4	22.3 ± 1.5 (n = 9)	23.0 ± 4.3	58.0 ± 7.1 (n = 10)	33.8 ± 5.9	133.4 ± 32.1
	Light	10.0 ± 3.0	8.0 ± 2.5	55.0 ± 17.1	19.3 ± 1.7	36.3 ± 6.4**	62.2 ± 10.2	35.8 ± 9.2	137.6 ± 26.7
	Post-Light	10.0 ± 2.6	9.3 ± 2.1	50.0 ± 23.3	20.0 ± 2.6	32.4 ± 4.8	61.2 ± 8.5	38.2 ± 4.8	119.2 ± 32.4

Table S2, related to Figure 2: Characteristics of the responses evoked on the same SNr cells by electrical stimulation of the motor cortex in non-lesioned and 6-OHDA transgenic eNpHR mice, before, during and following CINs photoinhibition.

The latency (L) and duration (D) of the different components of the cortically evoked response were measured on the basis of post-stimulus time histograms generated from 100 cortical stimulations. Nb Sp: number of spikes of the excitatory component.

**p≤0.01, one-way repeated measure ANOVA followed by Holm-Sidak post-hoc test, vs. pre-light condition.

SUPPLEMENTAL EXPERIMENTAL PROCEDURES

Mice. All mice strains used in this study were purchased from Jackson Laboratory. We used Choline acetyltransferase ChAT-IRES-Cre knock-in mice (ChAT^{cre/cre} mice, stock number: 006410), LoxP-stop-eNpHR3.0-EYFP mice (Ai39 mice, stock number: 014539) and BAC Drd1a-tdTomato mice (Tg^{D1-tdTomato} mice, stock number: 016204). Ai39 mice were crossed with ChAT^{cre/cre} mice to induce eNpHR3.0 expression in cholinergic neurons and were used for *in vivo* electrophysiology (Rosa^{eNpHR/+::ChAT^{cre/+}} mice that were called transgenic eNpHR mice in this study). For *in vitro* electrophysiological experiments requiring distinguishing D1 and D2 MSNs, Rosa^{eNpHR/+::ChAT^{cre/+}} mice were crossed with Tg^{D1-tdTomato} mice to obtain both eNpHR expression in the cholinergic neurons and dtTomato expression in the direct(D1)-MSNs (Rosa^{eNpHR/+::ChAT^{cre/+}}::Tg^{D1-tdTomato} mice that were called transgenic eNpHR/D1 mice in this study) (Figure S5).

Stereotaxic surgery. Mice were anaesthetized with intraperitoneal (i.p.) injections of ketamine and xylazine (100 and 10 mg/kg, respectively) and mounted on a stereotaxic apparatus (Kopf Instruments). Injections were made with a 10- μ l syringe, connected to the injector by a polyethylene tubing, and controlled by an injection pump at 0.3 μ l/min.

Viral expression of opsins in CINs. pAAV vectors containing opsins transgenes (ChR2: pAAV-Ef1a-DIO-hChR2(H134R)-mCherry and eNpHR: pAAV-Ef1a-DIO-eNpHR3.0-EYFP) were provided by Dr. Deisseroth (Stanford University). For practical consideration, we switched EYFP by TagRFP by overlap extension PCR cloning method. The recombinant AAV vectors were serotyped with AAV5 coat proteins and packaged by the viral vector core at the University of North Carolina. To achieve Cre-dependent expression of opsins in CINs, we microinjected 1 μ l of AAV at two dorso-ventral sites into the dorsal striatum of ChAT^{cre/cre} mice (+1.0 mm AP, \pm 1.5 mm ML, -2.7 and -2.1 mm DV). Opsin-expressing neurons were largely confined to the dorsal striatum (Figure S1B). Mice that were used in behavioral experiments were then implanted with a bilateral guide cannula (+1.0 mm AP, \pm 1.5 mm ML, 26 gauge, positioned 2.5-mm below skull; PlasticsOne). All viral injections were made unilaterally except for *in vitro* recordings and haloperidol-induced catalepsy.

6-OHDA lesions. Mice received one unilateral injection of 6-OHDA hydrochloride (1.5 μ l at 2.7 μ g/ μ l diluted in 0.9% sterile NaCl containing 0.1% ascorbic acid, Sigma-Aldrich) into the substantia nigra pars compacta: -3.0 mm AP, \pm 1.3 mm ML, -4.3 mm DV. 6-OHDA injection was immediately followed by unilateral intrastriatal viral injection and experiments were performed at least two weeks later. DA lesion extent was systematically assessed by anti-tyrosine hydroxylase immunohistochemistry.

Optic fiber implantation. For L-DOPA-induced dyskinesia experiments that required long-term treatment, we used implantable optical fibers consisting of a zirconia ferrule with a 200- μ m diameter

and 3.3 mm-long cleaved bare optic fibers (0.22 N.A., Doric Lenses). Fibers were implanted ipsilaterally to the lesioned side at the following coordinates: +1.0 mm AP, \pm 1.5 mm ML, -2.0 mm DV.

***In vitro* electrophysiology.** Coronal striatal slices (250 μ m) from 7 to 10-week-old bilaterally AAV-injected or transgenic mice were cut in ice-cold high-choline artificial cerebro-spinal fluid (ACSF) with a vibratome (Leica) as previously described (Beurrier et al., 2009). Recordings from 6-OHDA mice were performed 2 to 3 weeks after 6-OHDA injection and the extent of DA lesion was systematically assessed a posteriori by anti-tyrosine hydroxylase immunocytochemistry in the striatum. Only mice exhibiting >70% of DA depletion compared to the non-injected hemisphere were kept for the analysis. Slices were then transferred to oxygenated ACSF and maintained at room temperature until recording. Neurons were visualized on an upright microscope (Nikon Eclipse FN1) equipped with DIC optic and filters set to visualize mCherry, TagRFP, tdTomato and EYFP using a x40 water-immersion objective. Combination of electrophysiological properties and expression of fluorophore was used to identify CINs and D1 MSNs while unlabeled MSNs were considered as D2 MSNs. Recordings were interleaved in labeled D1 MSNs and unlabeled putative D2 MSNs from the same mice. Patch-clamp recordings were performed in cell-attached and whole-cell configurations in current- or voltage-clamp mode in oxygenated ACSF warmed to 33°C. Patch-clamp electrodes (4-6 M Ω) were filled with an intracellular solution containing 126 mM KMeSO₄, 14 mM KCl, 3 mM MgCl₂, 0.5 mM CaCl₂, 5 mM EGTA, 10 mM HEPES, 2 mM NaATP and 0.5 mM NaGTP, pH adjusted to 7.25 with NaOH and osmolarity adjusted to 270-280 mOsm/L. To activate opsins, light was delivered under control of the acquisition software from a Spectra Light Engine (Lumencor, Optoprim) and was focused onto the back aperture of the microscope objective, producing a wide-field exposure around the recorded cell.

MSN excitability was tested at least 5 min after seal rupture by sending a series of 500 ms depolarizing current steps with an increment of 10 pA. For trials in which CINs were photoinhibited, light was ON 200 ms before and continues 200 ms after the 500 ms depolarizing current step, making the total illumination time equal to 900 ms. The time interval between each current step was 3 s. EPSCs were elicited by current pulses (0.1-ms width every 10 s) using a bipolar tungsten electrode placed preferentially at the motor cortex-dorsal striatum border to stimulate afferents from the motor cortex. For trials in which CINs were photoinhibited, light was ON 50 ms before cortical stimulation and continues 250 ms after. EPSCs amplitudes were calculated on at least 10 averaged traces by taking a mean of a 1-ms window around the peak and comparing this with the mean of a 3-ms window immediately before the stimulation artifact. Series resistances were monitored with a 5-mV negative step given with every afferent stimulus. Data were collected with a MultiClamp 700B amplifier (Molecular Devices), analyzed and plotted in clampfit (Molecular Devices, v 10.2) and Origin (v 7.5).

Behavioral testing. *Open-field.* Spontaneous locomotor activity was evaluated in an open field placed in a dim lighted room. Before testing, mice were acclimated to the testing room for at least 1 h. RFP, eNpHR-RFP, mCherry and Chr2-mCherry mice were tested for 18 min in a square chamber (50 x 50 cm) with a 30 cm-high white plastic wall. CINs were photoactivated (25-ms pulse width, 10 Hz) or photoinhibited (continuous illumination) during 3-min ON periods interspersed with 7-min OFF periods. Ambulation was defined as the total distance (in cm) covered by each mouse measured by 3-min bin for 18 min and recorded by a video track system (Viewpoint Life sciences Inc.).

Haloperidol-induced catalepsy. Optical fibers were inserted into the bilateral cannula just before haloperidol injection. Mice received 0.25 mg/kg haloperidol i.p. After 20 min, mice forepaws were placed on an horizontal bar 4 cm above the floor and the latency to step down was measured (with a cut-off of 120 s) every 10 min during the 80-min test (Figure 1A). Head movements were also measured continuously for the whole test duration. Mice received either blue (25-ms pulse width, 10 Hz) or yellow (continuous illumination) light 20 min after haloperidol injection. Light was ON for 3-min during which catalepsy was measured and then turned OFF for 7 min until the next measurement started.

Cylinder test. Mice were put into Plexiglas cylinders (20 cm height, 9 cm diameter) in order to evaluate motor asymmetry induced by 6-OHDA lesion. The number of contacts against the cylinder wall with the forepaws (weight-bearing contacts with fully extended digits) was monitored continuously for 5 min by two investigators blind of experimental conditions. A double contact was defined as simultaneous or closely performed ipsilateral and contralateral forepaws touches. Mice failing to reach 10 contacts were excluded from the analyses. Data are expressed as side bias calculated as % ipsilateral minus % contralateral contacts to the 6-OHDA lesioned side. All mice were tested only once to prevent habituation to the apparatus. Two groups of eNpHR-RFP or Chr2-mCherry 6-OHDA-lesioned mice were tested either in ON or OFF condition (yellow light: continuous illumination for 5 min, blue light: 25-ms pulse width, 10 Hz) and compared to the non-lesioned group. The same experiment was performed in two groups of RFP or mCherry 6-OHDA mice.

Cross maze test. Mice were placed into a cross maze consisting of 4 identical arms (45 cm x 7 cm x 15 cm) at 90° to each other and made with clear Plexiglas. The acquisition sessions started with the mouse placed in the middle, facing one arm. The number of ipsilateral and contralateral turns as well as the number of time the mouse went straight was monitored for 5 min. Pre-6-OHDA data were collected and then, 2 weeks after 6-OHDA lesions, mice were tested twice: one to collect post-6-OHDA data without light and the day after with the light ON (yellow light: continuous illumination for 5 min, blue light: 25-ms pulse width, 10 Hz).

L-DOPA-induced dyskinesia. Fifteen to eighteen days after 6-OHDA injections, mice received a single daily injection of L-DOPA (20 mg/kg) and benserazide hydrochloride (10 mg/kg) for 21 days. The abnormal involuntary movements (AIMs) were assessed by two investigators blind of subject viral

infections (eNpHR-RFP or RFP). Peak-dose dyskinesia scoring was performed for 1 min at different time points, 45 to 80 min after the last L-DOPA injection on day 21 (Figure S4). Axial and limb AIMs were scored using a previously established scale from 0 to 4 for each AIM subtype (Lundblad et al., 2004) and the sum of the 2 scores, defined as dyskinesia score, was determined for each animal (maximal score, 8). Yellow light was delivered during 13 min, starting 56 min after L-DOPA injections.

For experiments involving scopolamine injection (scopolamine hydrobromide, Sigma-Aldrich), scopolamine was dissolved with NaCl and administered by i.p. injection at a dose of 1 mg/kg in ChAT^{cre/cre} mice.

Optogenetic photostimulation and photoinhibition in awake mice. Optical fiber (200 μm - diameter, 0.22 N.A., Doric Lenses) was inserted without anesthesia through the implanted cannula (tip protruding 0.3 mm). For bilateral illumination, optical fibers were connected to the laser through a rotary joint (FRJ_1x2i_FC-2FC, Doric Lenses) that sent half of the light coming from the laser into each of the two optical fibers inserted in the mouse brain and enabled the mouse to move freely during behavioral assessments. Light was provided by a yellow- (589 nm, 75.2 mW) and blue- (473 nm, 118.5 mW) laser (Combined Dual Wavelength DPSS Laser System, Laserglow). Optical-fiber light power was measured using a light sensor and intensity calculated using the model based on direct measurements in mammalian brain tissue for predicting irradiance values developed in K. Deisseroth's lab and available at <http://www.stanford.edu/group/dlab/cgi-bin/graph/chart.php>. Light intensity at 0.2 mm from fiber tip was calculated to be 11.3 and 20.0 mW/mm² for blue and yellow light, respectively (corresponding to 200 and 140 mW/mm² at the fiber tip).

In vivo recordings in anaesthetized mice. Non-lesioned and 6-OHDA lesioned (at least two weeks post-lesion) transgenic eNpHR mice were anesthetized with a mixture of ketamine and xylazine (100 and 10 mg/kg i.p., respectively, supplemented as needed by i.p. injection during the course of the experiment) and fixed in a stereotaxic head frame (Horsley-Clarke apparatus; Unimécanique). Body temperature was monitored by a rectal thermometer and maintained at 36.5°C with a homeothermic blanket (Harvard Apparatus). Single-unit activity of SNr cells was recorded extracellularly using glass micropipettes (25-35 M Ω) filled with a 0.5 M sodium chloride solution containing 1.5 % neurobiotin (Vectors Laboratories Inc.). Single neuron action potentials were recorded using the active bridge mode of an Axoclamp-2B amplifier (Molecular Devices), amplified, and filtered with an AC/DC amplifier (DAM 50; World Precision Instruments). Nigral neurons were identified as non-dopaminergic by their classically defined electrophysiological characteristics: narrow spikes (width \leq 2 ms) and ability to present relatively high frequency discharges ($>$ 10 Hz) without decrease in spike amplitude (Deniau et al., 1978). The optical fiber (core 200 μm , N.A. 0.22, Dorics Lenses) was positioned in the striatum (+1.0

mm AP, ± 1.5 mm ML, -2.0 mm DV). The cortical and SNr areas to stimulate and record, respectively, were precisely defined by anterograde and retrograde tracing methods consisting in an iontophoretic deposit, at these striatal coordinates, of wheat germ agglutinin horseradish peroxidase (Vector Laboratories). This striatal territory receives inputs from the motor cortical area stimulated ($+2.1$ mm AP, ± 0.5 mm ML, -0.7 mm DV) and sends projections to the recording site in the SNr (-3.3 mm AP, ± 1.5 mm ML, $-4.0/-4.8$ mm DV). The patterns of cortically-evoked responses in the same SNr neuron were analyzed before, during and after CIN photoinhibition in the striatum. Yellow light was delivered for 5 min (589 nm, power at the tip of optical fiber: 140 mW/mm²). Only SNr cells presenting an inhibitory component in response to cortical stimulation were recorded as they were the only ones to receive direct inputs from the striatal area activated by cortical stimulation meaning they belonged to the basal ganglia channel in register with the cortical area stimulated. This inhibitory component was preceded and/or followed by excitations due to the activation of the two trans-subthalamic pathways. Population post-stimulus time histograms (PSTHs) were generated by aligning the evoked responses on the onset of the inhibitory component. Results are given as means \pm SEM of the individual responses per condition.

Spontaneous activity of SNr neurons was analyzed before, during and after CIN photoinhibition in the striatum by sampling a period of 60 s in each condition. Yellow light was delivered for 5 min (589 nm, power at the tip of optical fiber: 140 mW/mm²). Epochs of elevated discharge rate were classified as bursts using a Poisson Surprise analysis (Legendy and Salcman, 1985). This was done using a script written for the Spike2 software. Briefly, this analysis evaluates how improbable any given burst, that contains n spikes in a time interval T , occurred by chance and computed as follows: $S = -\log p$, where p is the probability that, in a random (Poisson) spike train having the same average spikes rate r as the spike train studied, a given time interval of length T contains n or more spikes. p is given by Poisson's formula, as follows:

$$p = e^{-rT} \sum_{i=n}^{\infty} (rT)^i / i!$$

where S refers to the Poisson Surprise of the burst (the degree to which the burst surprises a person who expects the spike train to be a Poisson process). In this study, only spike trains with $S \geq 2$ were considered to be bursts. At the end of electrophysiological experiments, the tip of the stimulating electrodes was marked by an electrical deposit of iron (5 μ A anodal, 20 s) and the tip of the recording electrodes was marked by iontophoretic ejection of Chicago Sky Blue (Sigma, 4% in NaCl 0,6 M; 8 μ A cathodal, 20 min). Brains were removed and fixed in a 10% formalin solution after a ferri-ferrocyanide reaction. The localization of the blue points and iron deposits were observed on serial frozen sections (70 μ m) counterstained with safranin O (Sigma). All the recorded cells kept in the analysis were localized in the SNr.

Histology, immunohistochemistry and microscopy. Animals were deeply anesthetized with a mixture of ketamine/xylazine and then transcardially perfused with an ice-cold solution of paraformaldehyde 4% in PBS. After dissection, brains were post-fixed overnight in the same fixative at 4 °C, cryoprotected in 30% sucrose dissolved in 1X PBS for an additional 36 h at 4 °C, and frozen. Coronal cryostat sections (40 µm) covering the antero-posterior extent of the striatum or the substantia nigra pars compacta were used for labeling. Brain sections were permeabilized in PBS with 0.4% Triton X-100 (PBST) for 30 min at room temperature. Sections were then incubated in a blocking solution composed of PBST with 3% bovine serum albumin and 10% normal goat serum for 1h at room temperature. Immunostaining was done on free-floating sections, which were then mounted onto SuperFrost Plus glass slides (VWR) and coverslipped with FluorSave mounting media (Merck Chemicals). Quantification of colocalization was performed from approximately bregma +1.42 to +0.02 mm (around 14 sections per mouse) using Mercator System (Explora Nova) combined with a DMR Leica microscope coupled to a DXC-990P color video camera (Sony). Images were collected using Axio Imager Z1 with the Apotome system (Zeiss) with a Plan-Apochromat 20×/0.8 or a Plan-Neofluar x40/1.3 objective (Zeiss) for the high magnification or with a Plan-Apochromat 10×/0.45 objective (Zeiss) to acquire whole-brain images.

SUPPLEMENTAL REFERENCES

Beurrier, C., Lopez, S., Révy, D., Selvam, C., Goudet, C., Lhérondel, M., Gubellini, P., Kerkerian-LeGoff, L., Acher, F., Pin, J.-P., et al. (2009). Electrophysiological and behavioral evidence that modulation of metabotropic glutamate receptor 4 with a new agonist reverses experimental parkinsonism. *FASEB J.* *23*, 3619–3628.

Deniau, J.M., Hammond, C., Risz, A., and Feger, J. (1978). Electrophysiological properties of identified output neurons of the rat substantia nigra (pars compacta and pars reticulata): evidences for the existence of branched neurons. *Exp. BRAIN Res.* *32*, 409–422.

Kolomiets, B.P., Deniau, J.M., Glowinski, J., and Thierry, A.M. (2003). Basal ganglia and processing of cortical information: functional interactions between trans-striatal and trans-subthalamic circuits in the substantia nigra pars reticulata. *Neuroscience* *117*, 931–938.

Legendy, C.R., and Salzman, M. (1985). Bursts and recurrences of bursts in the spike trains of spontaneously active striate cortex neurons. *J. Neurophysiol.* *53*, 926–939.

Lundblad, M., Picconi, B., Lindgren, H., and Cenci, M.A. (2004). A model of L-DOPA-induced dyskinesia in 6-hydroxydopamine lesioned mice: relation to motor and cellular parameters of nigrostriatal function. *Neurobiol. Dis.* *16*, 110–123.